



Universitat de València

Facultat de Física

Department de Física Teòrica

Programa de Doctorat en Física

**Dynamical Hadrons:
Case Studies of Meson-Meson
and Meson-Baryon Molecules
and Triangle Singularities**

Vinícius Rodrigues Debastiani

Doctoral Thesis, june 2020

Supervisor:
Eulogio Oset Báuena

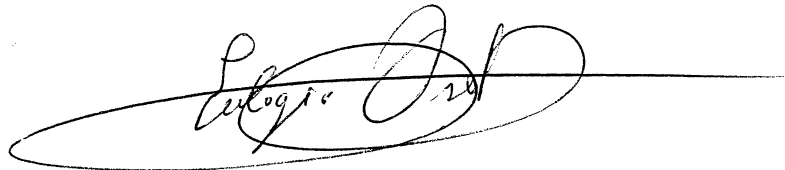
Dr. Eulogio Oset Báguena, Catedrático del Departamento de Física Teórica de la Universidad de Valencia,

Certifica:

Que la presente memoria, “*Dynamical Hadrons: Case Studies of Meson-Meson and Meson-Baryon Molecules and Triangle Singularities*”, ha sido realizada bajo su dirección en el Departamento de Física Teórica de la Universidad de Valencia por Vinícius Rodrigues Debastiani como Tesis para obtener el grado de Doctor.

Y para que así conste, en cumplimiento con la legislación vigente, presenta ante el Departamento de Física Teórica de la Universidad de Valencia la referida memoria, y firmando el presente certificado.

Valencia, 18 de junio de 2020.

A handwritten signature in black ink, appearing to read 'Eulogio Oset', is written over a horizontal line. The signature is stylized and cursive.

Fdo.: Eulogio Oset Báguena

Contents

Table of Contents	iii
List of Publications	v
Abstract	vii
I Introduction	1
A brief introduction	3
Resumen en Español	5
Bibliografía	13
II Scientific Research	15
1 Meson-Meson Interactions	17
1.1 Introduction	17
1.1.1 Chiral Unitary Approach	17
1.1.2 $c\bar{c} \rightarrow$ light pseudoscalars	19
1.2 Predictions for $\eta_c \rightarrow \eta\pi^+\pi^-$ producing $f_0(500)$, $f_0(980)$ and $a_0(980)$.	25
1.2.1 Introduction	25
1.2.2 Formalism	26
1.2.3 Results	29
1.2.4 Conclusions	32
1.3 $a_0(980) - f_0(980)$ mixing in $\chi_{c1} \rightarrow \pi^0 f_0(980) \rightarrow \pi^0\pi^+\pi^-$ and $\chi_{c1} \rightarrow$ $\pi^0 a_0(980) \rightarrow \pi^0\pi^0\eta$	33
1.3.1 Introduction	33
1.3.2 Formalism	36
1.3.3 Results	40
1.3.4 Conclusions	46
Bibliography	47
2 Meson-Baryon Interactions	53
2.1 Introduction	53
2.1.1 Chiral Lagrangians	53

2.1.2	Local Hidden Gauge approach	54
2.1.3	Poles and couplings	59
2.2	Molecular Ω_c states	60
2.2.1	Introduction	61
2.2.2	Formalism	62
2.2.3	Results	70
2.2.4	Conclusions	73
2.3	The $\Omega_b \rightarrow \Omega_c$ decay and the molecular Ω_c states	73
2.3.1	Introduction	74
2.3.2	The $\Omega_c(3050)$ and $\Omega_c(3090)$ in the molecular picture	75
2.3.3	The $\Omega_b^- \rightarrow (\Xi_c \bar{K} / \Xi'_c \bar{K} / \Xi D) \pi^-$ decays	75
2.3.4	Results	80
2.3.5	Conclusions	84
2.4	Predictions for molecular Ω_b states	85
2.4.1	Introduction	85
2.4.2	Formalism	86
2.4.3	Results	89
2.4.4	Conclusions	91
	Bibliography	92
3	Triangle Singularities	101
3.1	Introduction	101
3.2	Revising the $f_1(1420)$	109
3.2.1	Introduction	109
3.2.2	Formalism	111
3.2.3	The $K^* \bar{K}$ channel	112
3.2.4	The $\pi a_0(980)$ decay mode of the $f_1(1285)$	115
3.2.5	The singularity of the triangle diagram	119
3.2.6	Detailed evaluation with the $I = 0$ and $C = +$ parity of the $f_1(1285)$	120
3.2.7	Conclusions	122
3.3	Role of a triangle singularity in the $\pi N(1535)$ contribution to $\gamma p \rightarrow p \pi^0 \eta$	124
3.3.1	Introduction	124
3.3.2	Formalism	126
3.3.3	Results	131
3.3.4	Conclusions	134
3.4	Considerations on the Schmid theorem	135
3.4.1	Introduction	135
3.4.2	Formulation	137
3.4.3	Study of the singular behavior	147
3.4.4	Considerations on the Dalitz plot	150
3.4.5	Results	151
3.4.6	Conclusions	156
	Bibliography	158
4	Final Remarks	167

List of Publications

This thesis is based on the following articles:

Meson-Meson interactions (Chapter 1):

- V. R. Debastiani, W. H. Liang, J. J. Xie and E. Oset,
“Predictions for $\eta_c \rightarrow \eta\pi^+\pi^-$ producing $f_0(500)$, $f_0(980)$ and $a_0(980)$,”
Phys. Lett. B **766**, 59 (2017).
doi:10.1016/j.physletb.2016.12.054
arXiv:1609.09201 [hep-ph]
- M. Bayar and V. R. Debastiani,
“ $a_0(980)-f_0(980)$ mixing in $\chi_{c1} \rightarrow \pi^0 f_0(980) \rightarrow \pi^0\pi^+\pi^-$ and $\chi_{c1} \rightarrow \pi^0 a_0(980) \rightarrow \pi^0\pi^0\eta$,”
Phys. Lett. B **775**, 94 (2017).
doi:10.1016/j.physletb.2017.10.061
arXiv:1708.02764 [hep-ph]

Meson-Baryon interactions (Chapter 2):

- V. R. Debastiani, J. M. Dias, W. H. Liang and E. Oset,
“Molecular Ω_c states generated from coupled meson-baryon channels,”
Phys. Rev. D **97**, 094035 (2018).
doi:10.1103/PhysRevD.97.094035
arXiv:1710.04231 [hep-ph]
- V. R. Debastiani, J. M. Dias, W. H. Liang and E. Oset,
“ $\Omega_b^- \rightarrow (\Xi_c^+ K^-)\pi^-$ and the Ω_c states,”
Phys. Rev. D **98**, 094022 (2018).
doi:10.1103/PhysRevD.98.094022
arXiv:1803.03268 [hep-ph]

- W. H. Liang, J. M. Dias, V. R. Debastiani and E. Oset,
“*Molecular Ω_b states,*”
Nucl. Phys. B **930**, 524 (2018).
doi:10.1016/j.nuclphysb.2018.03.008
arXiv:1711.10623 [hep-ph]

Triangle singularities (Chapter 3):

- V. R. Debastiani, F. Aceti, W. H. Liang and E. Oset,
“*Revising the $f_1(1420)$ resonance,*”
Phys. Rev. D **95**, 034015 (2017).
doi:10.1103/PhysRevD.95.034015
arXiv:1611.05383 [hep-ph]
- V. R. Debastiani, S. Sakai and E. Oset,
“*Role of a triangle singularity in the $\pi N(1535)$ contribution to $\gamma p \rightarrow p\pi^0\eta$,*”
Phys. Rev. C **96**, 025201 (2017).
doi:10.1103/PhysRevC.96.025201
arXiv:1703.01254 [hep-ph]
- V. R. Debastiani, S. Sakai and E. Oset,
“*Considerations on the Schmid theorem for triangle singularities,*”
Eur. Phys. J. C **79**, 69 (2019).
doi:10.1140/epjc/s10052-019-6558-1
arXiv:1809.06890 [hep-ph]

Abstract

In this thesis we used various methods based on Effective Quantum Field Theories to study the interaction of hadrons. In particular, we focused on problems related to what is known as *exotic* hadrons, which are hadronic states that have different configurations from the standard of baryons or mesons, which are made of three quarks or a quark-antiquark pair, respectively. The meson-meson interaction, for example, can form hadronic molecules with four quarks, also known as *tetraquarks*; the same is true of the meson-baryon interaction, which can generate states with five quarks, known as *pentaquarks*. Evidence of the existence of these states has been accumulating in recent decades, due to new data from high-energy particle accelerators such as the Large Hadron Collider, LHC, at CERN.

Here we show the results of various research works that we have produced in recent years, contributing to the development of our understanding of hadronic states. Our approach is based on the picture of the hadronic molecule, where these states emerge from the dynamical interaction of meson-meson (or meson-baryon) coupled channels, sometimes called dynamically generated. We also use this same framework to study what is known as triangular singularities, which are kinematic effects that arise from hadronic interactions that can be misinterpreted as real physical states.

By showing how experimental data can be explained with our theoretical models, and making predictions that can then be compared with future experiments, we add a little more to the bulk of knowledge of hadronic physics, contributing to our understanding of the fundamental properties of matter.

This thesis is structured around three chapters: 1) *Meson-meson interactions*, 2) *Meson-baryon interactions* and 3) *Triangular singularities*. Each chapter contains a selection of published articles that share a similar framework.

First we briefly discuss the main characteristics of the method we use to describe meson-meson interactions, in particular the interaction that generates the well-known scalar mesons $f_0(500)$, $f_0(980)$ and $a_0(980)$. These states appear in the two articles discussed in the first chapter: that of the $\eta_c \rightarrow \eta\pi^+\pi^-$ decay, and that of the $a_0(980) - f_0(980)$ mixing in the reactions $\chi_{c1} \rightarrow \pi^0\pi^0\eta$ and $\chi_{c1} \rightarrow \pi^0\pi^+\pi^-$. Both works share common characteristics of a method also used in an earlier study on the $\chi_{c1} \rightarrow \eta\pi^+\pi^-$ decay.

The method we use is known as *chiral unitary approach*. In essence, these states are described as meson-meson molecules, emerging from the interaction of pairs of light pseudoscalar mesons. Its main ingredient comes from chiral perturbation theory which is an effective field theory that uses chiral symmetry to describe the meson

interaction. In this framework, pseudoscalar mesons are the degrees of freedom that act as Goldstone bosons.

In our approach, the interaction of the mesons is described by the lowest order chiral Lagrangian, from which we extract the interaction between channels, which in this case are given by: 1) $\pi^+\pi^-$, 2) $\pi^0\pi^0$, 3) K^+K^- , 4) $K^0\bar{K}^0$, 5) $\eta\eta$, 6) $\pi^0\eta$. Next, we unitarize the amplitude using the Bethe-Salpeter equations for the coupled channels, which implements the sum of loop diagrams in infinite order. Factorizing the V (interactions) and T (amplitudes) matrices on-shell out of the internal integrals, the solution of the Bethe-Salpeter equation is purely algebraic, and we can rearrange the sum as follows: $T = (1 - VG)^{-1}V$, where G is the matrix of the integral of the propagators of meson pairs, which we regularize with a cutoff. The T matrix gives us all the dispersion amplitudes, including the transitions between each coupled channel, and the resonances appear as poles in the dispersion amplitudes of the channels to which they are coupled. From the position of the pole in the complex energy plane, the mass and width of each resonance can be obtained.

In chapter one we also presented an approach of using elements of $SU(3)$ symmetry to see the weight of different trios of pseudoscalars produced in the charmonium decay $c\bar{c} \rightarrow 123$. The pseudoscalars then can undergo the final state interaction of pairs of mesons that generate the scalar mesons $f_0(500)$, $f_0(980)$ and $a_0(980)$. The combination of three mesons that behaves like a scalar of $SU(3)$ is given by $SU(3)[\text{scalar}] \equiv \text{Trace}(\phi\phi\phi)$, where ϕ is the matrix of pseudoscalar mesons, as the dominant term. We start discussing an example of using that method in the study of the reaction $\chi_{c1} \rightarrow \eta\pi^+\pi^-$. Using $SU(3)$ symmetry we can obtain the initial proportion of the pairs of mesons created at the moment that the χ_{c1} decays. Next, we can for example calculate the main contribution for the invariant mass distribution of $\pi^+\pi^-$, which can be calculated assuming that η goes in P wave and then $\pi^+\pi^-$, $\pi^0\pi^0$ or $\eta\eta$ that occur in the primary step, go through the final state interaction to produce a $\pi^+\pi^-$ pair, which gives rise to the resonances $f_0(500)$ and $f_0(980)$ that are seen in the experimental measurement.

After that we present our first work on the $\eta_c \rightarrow \eta\pi^+\pi^-$ decay, where we have also explored the contribution of other possible structures of $SU(3)$, and complemented the information for the case of $\chi_{c1} \rightarrow \eta\pi^+\pi^-$, where only $\text{Trace}(\phi\phi\phi)$ was used. We have concluded that this is the best way to describe these decays, based on the symmetry of the structure and the conformity of the results in relation to the experimental data. In our first work, we performed calculations for the decay $\eta_c \rightarrow \eta\pi^+\pi^-$. After finding the initial pseudoscalar trios using $SU(3)$ symmetry, we used the chiral unitary approach to describe the meson pair interaction leading to $\eta\pi^+\pi^-$ in the final state. We have evaluated the invariant mass distributions of $\pi^+\pi^-$ and $\pi\eta$ and we have found large and clear signals for the resonances $f_0(500)$, $f_0(980)$ and $a_0(980)$. The experimental implementation of this reaction and comparison with our predictions is of great value in shedding light on the nature of the light scalar mesons.

We also use the chiral unitary approach and $SU(3)$ symmetry to study isospin breaking in the reactions $\chi_{c1} \rightarrow \pi^0\pi^+\pi^-$ and $\chi_{c1} \rightarrow \pi^0\pi^0\eta$ and its relation to the $a_0(980) - f_0(980)$ mixing. We have shown that the same theoretical model previously developed could also be used successfully in this study. The isospin violation was

introduced by using different masses for the charged and neutral kaons, either in the meson pair propagators created in the decay of χ_{c1} , or in the propagators within the matrix T . We have found that violating isospin inside the T matrix makes the amplitude of the transition $\pi^0\eta \rightarrow \pi^+\pi^-$ non-zero, which generates a significant contribution, and it also increases the effect of the contribution of $K\bar{K}$. We also find that the most important effect on the total amplitude is the isospin breaking within the T matrix, due to the constructive sum of $\pi^0\eta \rightarrow \pi^+\pi^-$ and $K\bar{K} \rightarrow \pi^+\pi^-$, which is essential to achieve a good agreement with the experimental measurement of the mixing.

In chapter two we saw a method for studying meson-baryon interactions and looking for new states as poles in the scattering amplitude. In this chapter we present three papers on meson-baryon interactions: the one on the five new Ω_c states recently discovered by the LHCb collaboration, the following article on how to observe these states in the weak decay of Ω_b baryons and a third article with predictions for Ω_b molecular states.

At the beginning of chapter two we discussed two frameworks that are useful for describing meson-baryon states, either using the lowest-order chiral Lagrangian that describes the meson-baryon interaction in the $SU(3)$ sector (octet of pseudoscalar mesons with octet of baryons $1/2^+$), and the *local hidden gauge approach*, describing the interaction through the exchange of vector mesons. We briefly discuss the relationship of the two methods, with an emphasis on the particular case where certain simplifications can be made and the interactions can be obtained at the quark level.

In particular, we discussed how to extend the local hidden gauge approach to the charm sector, which is particularly complicated in the case of the chiral Lagrangians. Using the local hidden gauge approach and singling out the heavy quark, we can assume $SU(3)$ symmetry and obtain the interaction in a very simple way through the wave function of the baryons, looking at their quark content. We have shown that the dominant terms come from the exchange of light vectors, where the heavy quarks are spectators. This has the consequence that the heavy quark symmetry is conserved for the dominant terms in the expansion in powers of $(1/m_Q)$, and also that the interaction in this case is equivalent to what can be obtained from the chiral Lagrangians in $SU(3)$.

In the first work on this topic we have investigated the Ω_c states, which can be generated dynamically from the meson-baryon interaction, looking for poles in the dispersion matrix that correspond to physical states. We show that for a standard value for the cutoff, we get two states with $J^P = 1/2^-$ and two more states with $J^P = 3/2^-$, three of them in remarkable agreement with three experimental states, $\Omega_c(3050)$, $\Omega_c(3090)$ and $\Omega_c(3119)$, of the five recently measured by the LHCb collaboration, in mass and width. We also made predictions at higher energies for states of vector-baryon nature, which could be further explored in future experiments.

After this work we have studied the weak decay $\Omega_b^- \rightarrow (\Xi_c^+ K^-) \pi^-$, using our method to describe how the Ω_c states arise from the final state interaction. We analyze the particular case in which the states $\Omega_c(3050)$ and $\Omega_c(3090)$ can be generated from the pseudoscalar-baryon($1/2$) interaction. We investigated the invariant mass distributions ΞD , $\Xi_c \bar{K}$, and $\Xi'_c \bar{K}$, making predictions that could be confronted with future experiments.

Finally, we have extended our approach and made predictions for the meson-baryon interaction in the Beauty sector, with bottom quarks instead of charm quarks. We have found several Ω_b states: two states with masses 6405 MeV and 6465 MeV with $J^P = 1/2^-$; two more states with masses 6427 MeV and 6665 MeV with $J^P = 3/2^-$; and three states between 6500 and 6820 MeV, degenerate with $J^P = 1/2^-, 3/2^-$, derived from the vector-baryon interaction, analogous to what we had for the Ω_c states. Future experiments could also search for these states. Indeed, after the production of this work, a new article from the LHCb collaboration appeared, announcing the discovery of new Ω_b states. As discussed in a recent article, at higher energies, between 6400 MeV and 6500 MeV, four peaks appear in the experiment that are consistent with our predictions.

In chapter three we see how triangular singularities can be formed in the decay $A \rightarrow 1 + R$, followed by $R \rightarrow 2 + 3$ and the rescattering $1 + 2 \rightarrow 1' + 2'$. We show our method of explicitly making the loop integral of the triangle to find the amplitude and how, by studying its poles, we find the conditions and position of the singularity. We have seen that especially in the case when there is a resonance from the rescattering $(1, 2)$, at the same energy corresponding to the singularity of the triangle, its effect can be seen in the experiment and can even be misinterpreted by a new state.

In our first work on triangular singularities we studied the production and decay of $f_1(1285)$ in $\pi a_0(980)$ and $K^* \bar{K}$ as a function of the resonance mass. In particular, we found an enhancement in the mass distribution around 1400 MeV in the $\pi a_0(980)$ decay mode tied to a triangular singularity, which explains the peak in the experimental data, and we also found a peak around 1420 MeV with approximately 60 MeV of width for the $K^* \bar{K}$ mode. Both characteristics are in agreement with the experimental information on which the resonance $f_1(1420)$ is based. Furthermore, we find that if the $f_1(1420)$ is a genuine resonance, coupling primarily to $K^* \bar{K}$ as seen experimentally, a fraction of 20% is inevitably found for the decay mode $\pi a_0(980)$ of this resonance, in drastic contradiction with all experiments. In total, we have concluded that the $f_1(1420)$ is not a genuine resonance, but the manifestation of the decay modes $\pi a_0(980)$ and $K^* \bar{K}$ of $f_1(1285)$ at energies higher than the nominal one.

Next, we have studied the reaction $\gamma p \rightarrow p \pi^0 \eta$ paying attention to the two main mechanisms at low energies, $\gamma p \rightarrow \Delta(1700) \rightarrow \eta \Delta(1232)$ and $\gamma p \rightarrow \Delta(1700) \rightarrow \pi N(1535)$. Both are generated by the photoexcitation of the $\Delta(1700)$ and the second involves a mechanism that leads to a triangular singularity. We can quantitatively evaluate the cross section of this process and show that it agrees with the experimental determination. However, there are some differences from the standard partial wave analysis that does not explicitly include the triangular singularity. The exercise also shows the value of exploring possible triangular singularities in other reactions and how a standard partial wave analysis can be extended to accommodate them.

Finally, we have investigated the Schmid theorem that states that if one has a tree-level mechanism with a particle A that decays into two particles 1 and R , with a subsequent decay of R into particles 2 and 3, the possible singularity of the triangle developed by the elastic rescattering mechanism of two of the three particles does

not change the cross section provided by the tree level. We have investigated the process in terms of the width of the unstable particle produced in the first decay and determined the violation and the limits for validity of the theorem. One of the conclusions is that the theorem remains valid at the strict limit of the zero width of that resonance, in which case the weight of the triangular diagram becomes insignificant compared to the tree level. Another conclusion, from a practical point of view, is that for realistic width values, the triangular singularity can provide a contribution comparable to or even bigger than the tree level, indicating that invoking the Schmid theorem to omit the triangular diagram derived from the elastic rescattering from the tree level should not be done. Furthermore, we note that the realistic case keeps some memory of the Schmid theorem, which is visible in a peculiar interference pattern with the tree level.

Overall we have seen many examples of the dynamical nature of states emerging from the hadron-hadron interaction, either in the case of the light scalar mesons emerging from meson-meson interactions, or new heavy baryon states from the meson-baryon interaction, or even cases where peaks can be misunderstood as genuine states due to the effects of triangle singularities. In the big picture we have shown, through a series of examples and applications, the importance of the dynamically generated states, and how this description should be part of our understanding of the fundamental interactions of matter.

Part I
Introduction

A brief introduction

Hadron Physics is in the intersection of Nuclear and Particle Physics. Hadrons are the bulk of all matter as we know it, and they are composed of smaller particles, the *quarks*. Quantum Chromodynamics is the theory of the Standard Model that describes the interactions of quarks due to the *strong force*, which are mediated by the *gluons*, just like the photon is the mediator of the electromagnetic force. In a simplified description, we can say that quarks are always bound together in two main configurations: the *baryons*, which are composed of three quarks, and the *mesons*, which are composed of a quark and an antiquark. These states composed by quarks, such as baryons and mesons are what we call *hadrons*, which is the domain of knowledge we focus on this thesis. Known examples of baryons are protons and neutrons, which can bind together to form the nuclei of atoms; whereas a good example of a meson is the meson π , which is responsible for the residual force that binds protons and neutrons together and can also be found in cosmic rays entering the atmosphere.

Quarks come with many different properties such as color, flavor and mass, and can be combined in many different configurations, giving rise to a huge number of composite states with many mechanisms of decay. Just as in atomic and molecular physics one can study an infinity of different configurations and interactions, or all the possible nuclei studied in nuclear physics, their binding and decays, in hadron physics one can study all the possible hadron configurations, interactions and decays. Most of them are unstable and live for just a tiny fraction of a second after being created in experiments on particle accelerators. Through the effort of huge collaborations of scientists, today we can study the complex world of these subatomic particles and the fundamental structure of matter as we known it.

These subjects of study are very rich and complex. The state of the art of these theories are based on a framework called Quantum Field Theory, which takes into account the relativistic and quantum nature of the subatomic world. In this framework particles are described as excitations of the field they generate. In theories such as Quantum Chromodynamics, properties such as asymptotic freedom and color confinement make the exact solution of the equations virtually unsolvable, therefore creating the necessity of certain simplifications in order to extract information about the physical objects the theory predicts. Approaches known as Effective Quantum Field Theories use symmetries of the theory to extract information by means of approximations valid in certain domains, such as at low energies, heavy particles, and so on.

In this thesis we will be using several methods based on Effective Quantum Field Theories to study the interaction of hadrons. In particular, we will focus on problems related to what is known as *exotic* hadrons, which are hadronic states that have different configurations from the standard baryons and mesons. The meson-meson interaction, for instance, can form hadronic molecules with four quarks, also known as *tetraquarks*; the same can be said about the meson-baryon interaction, which can generate states with five quarks, known as *pentaquarks*. The existence of these states were already a possibility in the past, since they could in principle fit in the framework of Quantum Chromodynamics. In the past decades evidence of their existence has been accumulating, due to new data from high energy particle accelerators such as the Large Hadron Collider in CERN.

Specifically, we will show the results of several research papers we produced during the past years contributing to the development of our understanding of these states. Our approach is based on the hadronic molecule picture, where these states emerge from the dynamical interaction of meson-meson (or meson-baryon) coupled channels, sometimes referred to as *dynamically generated*. We also used this same framework to study what is known as *triangle singularities*, which are kinematic effects that emerge from hadronic interactions that can be misunderstood as real physical states.

Our contribution to this field has the objective of increasing the knowledge on the topic of hadron interactions. By showing how experimental data can be explained with our theoretical models, and by making predictions that can later be confronted with future experiments, we add a bit more to the bulk of knowledge that has been generated over the years, contributing towards a deeper understanding of the fundamental properties of matter.

This thesis is structured around three core chapters: 1) *Meson-Meson Interactions*, 2) *Meson-Baryon Interactions* and 3) *Triangle Singularities*. Each chapter contains a selection of published articles which share some common features and references, being somewhat complementary.

Therefore, we have combined the general features from the formalism of these articles into an introductory section at the beginning of each chapter, leaving only the specific framework of each article into its own section later on. The references of each article have also been combined into one common bibliography per chapter. Note that each chapter has its own bibliography, instead of one long bibliography for the whole thesis. To avoid any misreading we have used the following notation for reference numbering: [(chapter#) (dot) (reference#)]. This way, each chapter is self-contained and can in principle be read in any order, although it is advisable to read at least the first section *Chiral Unitary Approach* to start.

Next we present a summary of the whole thesis in Spanish.

Resumen en Español

A continuación presentamos un resumen de toda la tesis, con una pequeña introducción acerca de la motivación y objetivos del trabajo, los puntos principales de cada capítulo (de la metodología y de los resultados con sus respectivas conclusiones) y la conclusión final.

Introducción y Objetivos

La Física Hadrónica está en la intersección de la Física Nuclear y de Partículas. Los hadrones son la mayor parte de toda la materia tal como la conocemos, y están compuestos de partículas más pequeñas, los *quarks*. La Cromodinámica Cuántica es la teoría del modelo estándar que describe las interacciones de los quarks debido a la *fuerza fuerte*, que está mediada por los *gluones*, al igual que el fotón es el mediador de la fuerza electromagnética. En una descripción simplificada, podemos decir que los quarks siempre están unidos en dos configuraciones principales: *bariones*, que están compuestos por tres quarks, y *mesones*, que están compuestos por un quark y un antiquark. Los estados compuestos por quarks, como bariones y mesones, son lo que llamamos *hadrones*, que es el dominio del conocimiento en el que nos centramos en esta tesis. Ejemplos conocidos de bariones son los protones y los neutrones, que pueden unirse para formar los núcleos de los átomos; mientras que un buen ejemplo de un mesón es el mesón π , que es responsable de la fuerza residual que une protones y neutrones y también se puede encontrar en los rayos cósmicos que ingresan en la atmósfera.

Los quarks tienen muchas propiedades diferentes, como color, sabor y masa, y se pueden combinar en muchas configuraciones diferentes, dando lugar a una gran cantidad de estados diferentes con muchos mecanismos de desintegración. Al igual que en física atómica y molecular se puede estudiar una infinidad de átomos y moléculas diferentes y sus interacciones, o todos los núcleos posibles estudiados en física nuclear, su ligadura y desintegraciones, en física de hadrones se pueden estudiar todas las configuraciones, interacciones y desintegraciones posibles de hadrones. La mayoría de ellos son inestables y viven solo una pequeña fracción de segundo después de haber sido creados en experimentos con aceleradores de partículas. Gracias al esfuerzo de grandes colaboraciones de científicos, hoy podemos estudiar el complejo mundo de las partículas subatómicas y la estructura fundamental de la materia tal como la conocemos.

Estos temas de estudio son muy ricos y complejos. El estado del arte de estas teorías se basa en un marco llamado Teoría Cuántica de Campos, que tiene en cuenta la naturaleza relativista y cuántica del mundo subatómico. En este marco, las partículas se describen como excitaciones del campo que generan. En teorías como la cromodinámica cuántica, propiedades como la libertad asintótica y el confinamiento del color hacen que la solución exacta de las ecuaciones sea prácticamente imposible, creando así la necesidad de ciertas simplificaciones para extraer información sobre los objetos físicos que la teoría predice. Un enfoque conocido como teorías de campo cuántico efectivas utiliza simetrías de la teoría para extraer información por medio de aproximaciones válidas en ciertos dominios, como a bajas energías, partículas pesadas, etc.

En esta tesis usaremos varios métodos basados en teorías de campo cuántico efectivas para estudiar la interacción de los hadrones. En particular, nos centraremos en los problemas relacionados con lo que se conoce como hadrones *exóticos*, que son estados hadrónicos que tienen configuraciones diferentes de la configuración estándar de los bariones o mesones. La interacción mesón-mesón, por ejemplo, puede formar moléculas hadrónicas con cuatro quarks, también conocidas como *tetraquarks*; lo mismo puede decirse de la interacción mesón-barión, que puede generar estados con cinco quarks, conocidos como *pentaquarks*. La existencia de estos estados ya parecía una posibilidad en el pasado, ya que podrían encajar en el marco de la cromodinámica cuántica. En las últimas décadas, la evidencia de su existencia se ha ido acumulando, debido a los nuevos datos de aceleradores de partículas de alta energía como el Gran Colisionador de Hadrones, LHC, en el CERN.

Específicamente, mostraremos los resultados de varios trabajos de investigación que produjimos durante los últimos años contribuyendo al desarrollo de nuestra comprensión de estos estados. Nuestro enfoque se basa en la imagen de la molécula hadrónica, donde estos estados emergen de la interacción dinámica de los canales acoplados mesón-mesón (o mesón-barión), a veces denominados como *generados dinámicamente*. También usamos este mismo marco para estudiar lo que se conoce como *singularidades triangulares*, que son efectos cinemáticos que surgen de las interacciones hadrónicas que pueden malinterpretarse como estados físicos reales.

Nuestra contribución a este campo tiene el objetivo de aumentar el conocimiento sobre el tema de las interacciones de hadrones. Al mostrar cómo se pueden explicar los datos experimentales con nuestros modelos teóricos, y al hacer predicciones que luego se pueden confrontar con futuros experimentos, agregamos un poco más al conjunto de conocimiento que se ha generado a lo largo de los años, contribuyendo a una comprensión más profunda de las propiedades fundamentales de la materia.

Metodología, Resultados y Conclusiones

Esta tesis está estructurada en torno a tres capítulos: 1) *Interacciones mesón-mesón*, 2) *Interacciones mesón-barión* y 3) *Singularidades triangulares*. Cada capítulo contiene una selección de artículos publicados que comparten un marco similar.

Interacciones Mesón-Mesón

En esta sección discutimos brevemente las características principales del método que utilizamos para describir las interacciones mesón-mesón, en particular la interacción de mesones que genera los conocidos mesones escalares $f_0(500)$, $a_0(980)$ y $f_0(980)$. Estos estados aparecen en los dos artículos discutidos en el primer capítulo: el de la desintegración $\eta_c \rightarrow \eta\pi^+\pi^-$ de la Ref. [1], y el de la mezcla $a_0(980) - f_0(980)$ en las reacciones $\chi_{c1} \rightarrow \pi^0\pi^0\eta$ y $\chi_{c1} \rightarrow \pi^0\pi^+\pi^-$ de la Ref. [2]. Ambos trabajos comparten características comunes de un método también empleado en un estudio anterior sobre la desintegración $\chi_{c1} \rightarrow \eta\pi^+\pi^-$ de la Ref. [3].

Nuestros dos trabajos, el de la desintegración $\eta_c \rightarrow \eta\pi^+\pi^-$ y el de la mezcla $a_0(980) - f_0(980)$, fueron citados en los artículos de BESIII y en otros trabajos posteriores relacionados.

Teoría quiral unitaria

El método que empleamos para describir las resonancias escalares $f_0(500)$, $a_0(980)$ y $f_0(980)$ es conocido como *teoría quiral unitaria*. En esencia, estos estados se describen como moléculas mesón-mesón, que emergen de la interacción de pares de mesones pseudoescalares ligeros.

El ingrediente principal proviene de la teoría de perturbación quiral que es una teoría de campo efectiva que utiliza la simetría quiral para describir la interacción de los mesones. En este marco, los mesones pseudoescalares son los grados de libertad que actúan como bosones de Goldstone.

El marco que adoptamos en esta sección para describir las resonancias escalares está en la misma línea que la Ref. [4]. En nuestro enfoque, la interacción de los mesones es descrita por el Lagrangiano quiral de orden más bajo, de donde extraemos la interacción entre canales, que en este caso vienen dados por: 1) $\pi^+\pi^-$, 2) $\pi^0\pi^0$, 3) K^+K^- , 4) $K^0\bar{K}^0$, 5) $\eta\eta$, 6) $\pi^0\eta$. A continuación, unitarizamos la amplitud utilizando las ecuaciones de Bethe-Salpeter para los canales acoplados que implementan la suma de diagramas de bucle en orden infinito. Al factorizar sobre la capa máxima las matrices V y T (de interacciones y amplitudes, respectivamente) la solución de la ecuación de Bethe-Salpeter es puramente algebraica, y podemos reorganizar la suma de la siguiente forma: $T = (1 - VG)^{-1}V$, donde G es la matriz de la integral de los propagadores de pares de mesones, que regularizamos con un *cutoff*.

Finalmente, la matriz T nos dará todas las amplitudes de dispersión, incluidas las transiciones entre cada canal acoplado, y las resonancias aparecerán como polos en las amplitudes de dispersión de los canales a que se acoplan. Desde la posición del polo en el plano complejo se puede obtener la masa y la anchura de cada resonancia.

$c\bar{c} \rightarrow$ pseudoescalares ligeros

En el capítulo uno también estudiamos cómo usar elementos de simetría $SU(3)$ para ver el peso de diferentes tríos de pseudoescalares producidos en la desintegración del charmonio $c\bar{c} \rightarrow 123$. Los pseudoescalares experimentan luego la interacción del estado final de pares de mesones que generan los mesones escalares

$f_0(500)$, $f_0(980)$ y $a_0(980)$, para lo cual utilizamos la *teoría chiral unitaria*. La combinación de tres mesones que se comporta como un escalar de $SU(3)$ viene dada por $SU(3)[\text{scalar}] \equiv \text{Trace}(\phi\phi\phi)$, donde ϕ es la matriz de mesones pseudoescalares, como término dominante.

Un ejemplo del uso de ese método se discutió en la Ref. [3] acerca de la reacción $\chi_{c1} \rightarrow \eta\pi^+\pi^-$. Utilizando la simetría $SU(3)$ se puede obtener la proporción inicial de los pares de mesones creados en el momento que χ_{c1} se desintegra. En seguida, podemos por ejemplo, calcular la contribución principal para la distribución de masa invariante $\pi^+\pi^-$, que se puede calcular asumiendo que η se va en onda P y luego $\pi^+\pi^-$, $\pi^0\pi^0$ or $\eta\eta$ que se producen en el paso primario, pasan por la interacción de estado final para producir un par $\pi^+\pi^-$, el que dá lugar a las resonancias $f_0(500)$, $f_0(980)$ que se ve experimentalmente en la medida de la distribución de masa invariante $\pi^+\pi^-$.

Se ha demostrado que este enfoque es muy fiable a bajas energías, y en el trabajo de Ref. [3] los datos de estadísticas altas de BESIII [5] de la reacción $\chi_{c1} \rightarrow \eta\pi^+\pi^-$ podrían reproducirse bien, explicando los picos de $f_0(500)$, $f_0(980)$ en la distribución de masa invariante $\pi^+\pi^-$, y también en el pico de $a_0(980)$ en la distribución de masa invariante $\pi\eta$.

En el trabajo de la desintegración de η_c de la Ref. [1] también hemos explorado la contribución de otras posibles estructuras de $SU(3)$, y complementamos la información dada en la Ref. [3] para $\chi_{c1} \rightarrow \eta\pi^+\pi^-$, donde solo se usó $\text{Trace}(\phi\phi\phi)$. Hemos concluído que esta es la mejor manera describir las desintegraciones investigadas, basándonos en la simetría de la estructura y la conformidad de los resultados en relación a los datos experimentales.

En vista de estos resultados, las predicciones para la desintegración $\eta_c \rightarrow \eta\pi^+\pi^-$ y el estudio de la mezcla $a_0(980) - f_0(980)$ en las reacciones $\chi_{c1} \rightarrow \pi^0 f_0(980) \rightarrow \pi^0\pi^+\pi^-$ y $\chi_{c1} \rightarrow \pi^0 a_0(980) \rightarrow \pi^0\pi^0\eta$ se realizaron solo con el término $\text{Trace}(\phi\phi\phi)$.

Predicciones para $\eta_c \rightarrow \eta\pi^+\pi^-$ produciendo $f_0(500)$, $f_0(980)$ y $a_0(980)$

En nuestro primer trabajo, en la Ref. [1], realizamos cálculos para la desintegración $\eta_c \rightarrow \eta\pi^+\pi^-$. Después de encontrar los tríos de pseudoescalares utilizando la simetría $SU(3)$, utilizamos la teoría quiral unitaria para describir la interacción de pares de mesones que conduce a $\eta\pi^+\pi^-$ en el estado final. Hemos evaluado las distribuciones de masa invariante de $\pi^+\pi^-$ y $\pi\eta$ y hemos encontrado señales grandes y claras para las resonancias $f_0(500)$, $f_0(980)$ y $a_0(980)$. La implementación experimental de esta reacción y comparación con nuestras predicciones tiene mucho valor para arrojar luz sobre la naturaleza de los mesones escalares ligeros.

La mezcla $a_0(980) - f_0(980)$ en $\chi_{c1} \rightarrow \pi^0 f_0(980) \rightarrow \pi^0\pi^+\pi^-$ y $\chi_{c1} \rightarrow \pi^0 a_0(980) \rightarrow \pi^0\pi^0\eta$

En la Ref. [2] también usamos la teoría quiral unitaria y la simetría $SU(3)$ para estudiar la ruptura de isospin en las reacciones $\chi_{c1} \rightarrow \pi^0\pi^+\pi^-$ y $\chi_{c1} \rightarrow \pi^0\pi^0\eta$ y su relación con la mezcla $a_0(980) - f_0(980)$, que también fue medida por la colaboración BESIII, antes y después de nuestro trabajo [6, 7]. Hemos demostrado que el mismo modelo teórico desarrollado previamente para estudiar la reacción $\chi_{c1} \rightarrow \eta\pi^+\pi^-$, y

explorado más a fondo en las predicciones de $\eta_c \rightarrow \eta\pi^+\pi^-$, podría también emplearse con éxito en este estudio. La violación de isospin se introdujo mediante el uso de diferentes masas para los kaones cargados y neutros, ya sea en los propagadores de pares de mesones creados en la desintegración de χ_{c1} , o en los propagadores dentro de la matriz T , construida a través de la unitarización de las amplitudes de dispersión y transición de pares de mesones pseudoescalares. Hemos encontrado que violar isospin dentro de la matriz T hace que la amplitud de la transición $\pi^0\eta \rightarrow \pi^+\pi^-$ sea no nula, lo que genera una contribución importante y también aumenta el efecto de la contribución de $K\bar{K}$. También encontramos que el efecto más importante en la amplitud total es la ruptura de isospin dentro de la matriz T , debido a la suma constructiva de $\pi^0\eta \rightarrow \pi^+\pi^-$ y $K\bar{K} \rightarrow \pi^+\pi^-$, que es esencial para lograr un buen acuerdo con la medición experimental de la mezcla.

Interacciones Mesón-Barión

En el capítulo dos vimos un método para estudiar las interacciones mesón-barión y buscar nuevos estados como polos en la amplitud de dispersión.

En este capítulo presentamos tres trabajos sobre las interacciones mesón-barión: el de la Ref. [8] sobre los cinco nuevos estados Ω_c recientemente descubiertos por la colaboración LHCb [9], el siguiente artículo de la Ref. [10] sobre cómo observar estos estados en la desintegración de bariones Ω_b y el de la Ref. [11] con predicciones para estados moleculares Ω_b .¹

Nuestro trabajo en los estados Ω_c fue citado muchas veces, y la predicción sobre los estados Ω_b también ha sido citada en el informe del LHC para las perspectivas futuras en la próxima ejecución después del *upgrade* actual.

Lagrangianos quirales y la teoría de calibre local oculto

Al principio del capítulo dos comentamos dos marcos que son útiles para describir los estados meson-barión, ya sea utilizando el Lagrangiano quiral de orden más bajo que describe la interacción mesón-barión en el sector $SU(3)$ (octete de mesones pseudoescalares con el octete de bariones $1/2^+$), y la teoría de calibre local oculto, basando la interacción en el cambio de mesones vectoriales. Discutimos brevemente la relación de los dos métodos, con énfasis en el caso particular donde se pueden hacer ciertas simplificaciones y las interacciones se pueden obtener a nivel de quarks.

En particular, discutimos cómo estender el método de la teoría de calibre local oculto para el sector de *charm*, que es particularmente complicado en el caso de los Lagrangianos quirales. Utilizando la teoría de calibre local oculto y destacando el quark pesado, podemos asumir la simetría $SU(3)$ en la interacción, y obtener la interacción de manera muy sencilla a través de la función de onda de los bariones mirando su contenido de quarks. Hemos demostrado que los términos dominantes provienen del intercambio de vectores ligeros, donde los quarks pesados son espectadores. Esto tiene como consecuencia que la simetría de quark pesados se conserva

¹ Después de la producción de este trabajo, apareció un nuevo artículo de la colaboración LHCb [12], que anuncia el descubrimiento de nuevos estados Ω_b . Tal como se discute en un reciente artículo [13], a energías más altas, entre 6400 MeV y 6500 MeV, aparecen en el experimento cuatro picos que son compatibles con nuestras predicciones.

para los términos dominantes en el desarrollo en potencias de $(1/m_Q)$, y también que la interacción en este caso es equivalente a lo que se puede obtener de los Lagrangianos quirales en $SU(3)$.

Estados Moleculares Ω_c

En el primer trabajo [8] sobre este tema hemos investigado los estados Ω_c , que se generan dinámicamente a partir de la interacción mesón-barión, buscando polos en la matriz de dispersión que corresponden a estados físicos. Mostramos que para un valor estándar para el *cutoff*, obtenemos dos estados con $J^P = 1/2^-$ y dos más con $J^P = 3/2^-$, tres de ellos en notable acuerdo con tres estados experimentales, $\Omega_c(3050)$, $\Omega_c(3090)$ y $\Omega_c(3119)$ de los cinco recientemente medidos por la colaboración LHCb, en masa y anchura. También hicimos predicciones a energías más altas para estados de naturaleza vector-barión, que podrían explorarse más a fondo en experimentos en el futuro.

La desintegración $\Omega_b \rightarrow \Omega_c$ y los estados moleculares Ω_c

Después del trabajo sobre los estados Ω_c hemos estudiado en la Ref. [10] la desintegración débil $\Omega_b^- \rightarrow (\Xi_c^+ K^-) \pi^-$, utilizando nuestro método para describir los estados Ω_c [8] que surgen de la interacción del estado final. Analizamos el caso particular en el que se pueden generar los estados $\Omega_c(3050)$ y $\Omega_c(3090)$ a partir de la interacción pseudoscalar-barión(1/2). Investigamos las distribuciones de masa invariantes ΞD , $\Xi_c \bar{K}$ y $\Xi'_c \bar{K}$ haciendo predicciones que podrían confrontarse con futuros experimentos, proporcionando información útil que podría ayudar a determinar los números cuánticos y naturaleza de estos estados.

Predicciones para estados moleculares Ω_b

Finalmente, en la Ref. [11] hemos extendido nuestro enfoque sobre los estados Ω_c [8] e hicimos predicciones para la interacción de mesón-barión en el sector de la Belleza (*Beauty / bottom*). Hemos encontrado varios estados Ω_b : dos estados con masas 6405 MeV y 6465 MeV con $J^P = 1/2^-$; dos estados más con masas 6427 MeV y 6665 MeV con $J^P = 3/2^-$; y tres estados entre 6500 y 6820 MeV, degenerados con $J^P = 1/2^-, 3/2^-$, derivados de la interacción del vector-barión en el sector de la Belleza, análogo a lo que teníamos para los estados Ω_c . Experimentos futuros también podrían buscar estos estados.

Singularidades Triangulares

En el capítulo tres vimos cómo se pueden formar singularidades triangulares en la desintegración $A \rightarrow 1+R$, seguida por $R \rightarrow 2+3$ y por el *rescattering* (dispersión) $1+2 \rightarrow 1'+2'$. Vimos nuestro método de hacer explícitamente la integral del bucle del triángulo para encontrar la amplitud [14] y cómo, estudiando sus polos, encontramos las condiciones y la posición de la singularidad. Hemos visto que especialmente en el caso cuando hay una resonancia proveniente del *rescattering* (1, 2), a la misma

energía correspondiente a la singularidad del triángulo, su efecto puede verse en el experimento e incluso puede ser malinterpretado por un nuevo estado.

Revisando la $f_1(1420)$

En nuestro primer trabajo sobre singularidades triangulares en la Ref. [15] estudiamos la producción y la desintegración de la $f_1(1285)$ en $\pi a_0(980)$ y $K^* \bar{K}$ en función de la masa de la resonancia. En particular, encontramos un aumento en la distribución de masa alrededor de 1400 MeV en el modo de desintegración $\pi a_0(980)$ atado a una singularidad triangular, lo que explica los datos de la Ref. [16], y encontramos también un pico alrededor de 1420 MeV con aproximadamente 60 MeV de anchura para el modo $K^* \bar{K}$. Ambas características están de acuerdo con la información experimental en la que se basa la resonancia $f_1(1420)$. Además, encontramos que si la $f_1(1420)$ es una resonancia genuina, acoplándose principalmente a $K^* \bar{K}$ como se ve experimentalmente, se encuentra inevitablemente una fracción de 20 % para el modo de desintegración $\pi a_0(980)$ de esta resonancia, en contradicción drástica con todos los experimentos. En total, hemos concluido que la $f_1(1420)$ no es una resonancia genuina, sino la manifestación de los modos de desintegración $\pi a_0(980)$ y $K^* \bar{K}$ de la $f_1(1285)$ a energías más altas que la nominal.

Rol de una singularidad triangular en la contribución $\pi N(1535)$ a $\gamma p \rightarrow p \pi^0 \eta$

A continuación, hemos estudiado en la Ref. [17] la reacción $\gamma p \rightarrow p \pi^0 \eta$ prestando atención a los dos mecanismos principales a bajas energías, $\gamma p \rightarrow \Delta(1700) \rightarrow \eta \Delta(1232)$ y $\gamma p \rightarrow \Delta(1700) \rightarrow \pi N(1535)$. Ambos son generados por la fotoexcitación de la $\Delta(1700)$ y el segundo involucra un mecanismo que conduce a una singularidad triangular. Podemos evaluar cuantitativamente la sección eficaz de este proceso y demostrar que está de acuerdo con la determinación experimental [18]. Sin embargo, hay algunas diferencias con el análisis de onda parcial estándar que no incluye explícitamente la singularidad triangular. El ejercicio también muestra la conveniencia de explorar posibles singularidades triangulares en otras reacciones y cómo se puede extender el análisis parcial estándar para acomodarlas.

Consideraciones sobre el teorema de Schmid

Finalmente, en la Ref. [19] hemos investigado el teorema de Schmid [20], que establece que si uno tiene un mecanismo a nivel de árbol con una partícula A que se desintegra en dos partículas 1 y R , con una desintegración posterior de R en partículas 2 y 3, la posible singularidad del triángulo desarrollada por el mecanismo de *re scattering* elástico de dos de las tres partículas no cambia la sección transversal proporcionada por el nivel del árbol. Hemos investigado el proceso en términos de la anchura de la partícula inestable producida en la primera desintegración y determinamos los límites de validez y violación del teorema. Una de las conclusiones es que el teorema se mantiene en el límite estricto de la anchura cero de esa resonancia, en cuyo caso el peso del diagrama triangular se vuelve insignificante en comparación con el nivel del árbol. Otra conclusión, desde el punto de vista práctico, es que

para valores realistas de la anchura, la singularidad triangular puede proporcionar una contribución comparable o incluso mayor que el nivel del árbol, lo que indica que invocar el teorema de Schmid para omitir el diagrama triangular derivado del *reescattering* elástico del nivel del árbol no debe hacerse. Además, observamos que el caso realista guarda algo de memoria del teorema de Schmid, que es visible en un patrón de interferencia peculiar con el nivel del árbol.

Conclusiones Finales

En general, hemos visto muchos ejemplos de la naturaleza dinámica de los estados que emergen de la interacción hadron-hadron, ya sea en el caso de los mesones escalares ligeros que emergen de las interacciones mesón-mesón, o nuevos estados bariónicos pesados de la interacción mesón-barión, o incluso casos en los que los picos pueden malinterpretarse como estados genuinos debido a los efectos de las singularidades triangulares. En el panorama general, hemos demostrado, a través de una serie de ejemplos y aplicaciones, la importancia de los estados generados dinámicamente y cómo esta descripción debería ser parte de nuestra comprensión de las interacciones fundamentales de la materia.

Bibliografia

- [1] V. R. Debastiani, W. H. Liang, J. J. Xie and E. Oset, “Predictions for $\eta_c \rightarrow \eta\pi^+\pi^-$ producing $f_0(500)$, $f_0(980)$ and $a_0(980)$,” Phys. Lett. B **766**, 59 (2017).
- [2] M. Bayar and V. R. Debastiani, “ $a_0(980) - f_0(980)$ mixing in $\chi_{c1} \rightarrow \pi^0 f_0(980) \rightarrow \pi^0\pi^+\pi^-$ and $\chi_{c1} \rightarrow \pi^0 a_0(980) \rightarrow \pi^0\pi^0\eta$,” Phys. Lett. B **775**, 94 (2017).
- [3] W. H. Liang, J. J. Xie and E. Oset, “ $f_0(500)$, $f_0(980)$ and $a_0(980)$ production in the $\chi_{c1} \rightarrow \eta\pi^+\pi^-$ reaction,” Eur. Phys. J. C **76**, 700 (2016).
- [4] J. A. Oller and E. Oset, “Chiral symmetry amplitudes in the S wave isoscalar and isovector channels and the sigma, $f_0(980)$, $a_0(980)$ scalar mesons,” Nucl. Phys. A **620**, 438 (1997) [Erratum-ibid. A **652**, 407 (1999)].
- [5] M. Ablikim *et al.* [BESIII Collaboration], “Amplitude analysis of the $\chi_{c1} \rightarrow \eta\pi^+\pi^-$ decays,” Phys. Rev. D **95**, 032002 (2017).
- [6] M. Ablikim *et al.* [BESIII Collaboration], “Study of $a_0^0(980) - f_0(980)$ mixing,” Phys. Rev. D **83**, 032003 (2011).
- [7] M. Ablikim *et al.* [BESIII Collaboration], “Observation of $a_0^0(980)$ - $f_0(980)$ Mixing,” Phys. Rev. Lett. **121**, 022001 (2018).
- [8] V. R. Debastiani, J. M. Dias, W. H. Liang and E. Oset, “Molecular Ω_c states generated from coupled meson-baryon channels,” Phys. Rev. D **97**, 094035 (2018).
- [9] R. Aaij *et al.* [LHCb Collaboration], “Observation of five new narrow Ω_c^0 states decaying to $\Xi_c^+ K^-$,” Phys. Rev. Lett. **118**, 182001 (2017).
- [10] V. R. Debastiani, J. M. Dias, W. H. Liang and E. Oset, “ $\Omega_b^- \rightarrow (\Xi_c^+ K^-) \pi^-$ and the Ω_c states,” Phys. Rev. D **98**, 094022 (2018).
- [11] W. H. Liang, J. M. Dias, V. R. Debastiani and E. Oset, “Molecular Ω_b states,” Nucl. Phys. B **930**, 524 (2018).
- [12] R. Aaij *et al.* [LHCb Collaboration], “First observation of excited Ω_b^- states,” Phys. Rev. Lett. **124**, 082002 (2020).
- [13] W. H. Liang and E. Oset, “Observed Ω_b spectrum and meson-baryon molecular states,” arXiv:2001.02929 [hep-ph].
- [14] M. Bayar, F. Aceti, F. K. Guo and E. Oset, “A Discussion on Triangle Singularities in the $\Lambda_b \rightarrow J/\psi K^- p$ Reaction,” Phys. Rev. D **94**, 074039 (2016).
- [15] V. R. Debastiani, F. Aceti, W. H. Liang and E. Oset, “Revising the $f_1(1420)$ resonance,” Phys. Rev. D **95**, 034015 (2017).

- [16] D. Barberis *et al.* [WA102 Collaboration], “A Measurement of the branching fractions of the $f(1)(1285)$ and $f(1)(1420)$ produced in central $p p$ interactions at 450-GeV/c,” Phys. Lett. B **440**, 225 (1998).
- [17] V. R. Debastiani, S. Sakai and E. Oset, “Role of a triangle singularity in the $\pi N(1535)$ contribution to $\gamma p \rightarrow p\pi^0\eta$,” Phys. Rev. C **96**, 025201 (2017).
- [18] E. Gutz *et al.* [CBELSA/TAPS Collaboration], “High statistics study of the reaction $\gamma p \rightarrow p\pi^0\eta$,” Eur. Phys. J. A **50**, 74 (2014).
- [19] V. R. Debastiani, S. Sakai and E. Oset, “Considerations on the Schmid theorem for triangle singularities,” Eur. Phys. J. C **79**, 69 (2019).
- [20] C. Schmid, “Final-State Interactions and the Simulation of Resonances,” Phys. Rev. **154**, 1363 (1967).

Part II
Scientific Research

1.1 Introduction

Throughout this thesis we will use a method known as the *chiral unitary approach*. In the following section 1.1.1 we will briefly discuss its main features in describing meson-meson interactions, in particular the light pseudoscalar-pseudoscalar interaction that generates the well-known scalar mesons $f_0(500)$, $a_0(980)$ and $f_0(980)$, which will appear in the two articles discussed in this chapter: the one about the decay $\eta_c \rightarrow \eta\pi^+\pi^-$ of Ref. [1.1], which will be discussed in section 1.2, and the one about the $a_0(980) - f_0(980)$ mixing in the reactions $\chi_{c1} \rightarrow \pi^0\pi^0\eta$ and $\chi_{c1} \rightarrow \pi^0\pi^+\pi^-$ of Ref. [1.2], which will be discussed in section 1.3. Both works share common features from an approach also employed in a previous study about the decay $\chi_{c1} \rightarrow \eta\pi^+\pi^-$ of Ref. [1.3], on which we will also comment throughout this chapter. The general aspects of this approach will be outlined in section 1.1.2.

1.1.1 Chiral Unitary Approach

In this section we will present the basic features of the method we employ to describe the $f_0(500)$ (previously denoted as the σ meson), the $a_0(980)$ and $f_0(980)$ resonances. In essence, these states are described as meson-meson molecules, which emerge from the interaction of pairs of pseudoscalar mesons.

The main ingredient comes from chiral perturbation theory [1.4–1.6], which is an effective field theory that uses chiral symmetry to describe the interaction of mesons. In this framework the pseudoscalar mesons are the degrees of freedom which act as Goldstone bosons, and a series expansion is made as a function of the energy of the mesons. Since this is a perturbative approach, one can go to higher orders at the expense of introducing new parameters, which later have to be adjusted with experimental data, therefore increasing both accuracy and uncertainty. Due to this compromise and the need of experimental data to fit the increasing number of parameters, the predictive power of the theory may also decrease at higher orders.

The framework we adopt in this chapter to describe the scalar resonances is in the same line as Ref. [1.7], where more details can be found. In our approach the interaction of mesons will be described by the lowest order chiral Lagrangian

$$\mathcal{L}_2 = \frac{1}{12 f_\pi^2} \text{Trace} [(\partial_\mu \phi \phi - \phi \partial_\mu \phi)^2 + M \phi^4], \quad (1.1)$$

where $f_\pi = 93$ MeV is the pion decay constant and ϕ is the pseudoscalar matrix

$$\phi_8 \equiv \begin{pmatrix} \frac{1}{\sqrt{2}}\pi^0 + \frac{1}{\sqrt{6}}\eta_8 & \pi^+ & K^+ \\ \pi^- & -\frac{1}{\sqrt{2}}\pi^0 + \frac{1}{\sqrt{6}}\eta_8 & K^0 \\ K^- & \bar{K}^0 & -\frac{2}{\sqrt{6}}\eta_8 \end{pmatrix}, \quad (1.2)$$

whereas M is given by

$$M = \begin{pmatrix} m_\pi^2 & 0 & 0 \\ 0 & m_\pi^2 & 0 \\ 0 & 0 & 2m_K^2 - m_\pi^2 \end{pmatrix}. \quad (1.3)$$

Next, we unitarize the amplitude using the Bethe-Salpeter equations in coupled channels which implements the resummation of loop diagrams to infinite order, as depicted in Fig. 1.1.

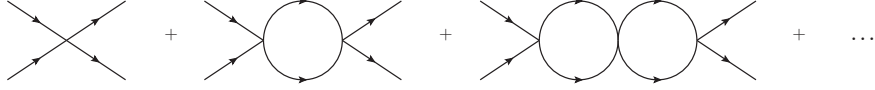


Figure 1.1: Diagrams representing meson-meson loops.

As seen in the diagrams, the amplitude goes like

$$T = V + VGV + VGVG + \dots \quad (1.4)$$

which can be written as

$$T_{ij} = V_{ij} + V_{il}G_l T_{lj} \quad (1.5)$$

where T_{ij} stands for the matrix elements of the scattering amplitude corresponding to the transition between channel i to j . Analogously, V corresponds to the matrix describing the tree level interaction in each vertex and G_l is the diagonal matrix of the propagators describing the meson-meson loops of channel l .

The term VGT actually means

$$VGT = \int \frac{d^4q}{(2\pi)^4} V(k, p; q) G(P, q) T(q; k', p'). \quad (1.6)$$

where P, q, k, p, k', p' are the energy-momentum quadrivectors of the center-of-mass, the internal loop, and incoming and outgoing meson pairs.

Factorizing the V and T matrices on-shell out of the internal integrals, which is justified in Refs. [1.7] and [1.8], the solution of the former equation is purely algebraic, and we can rearrange the sum in the following form

$$T = (1 - VG)^{-1} V, \quad (1.7)$$

From the Lagrangian in Eq. (1.1) we extract the kernel of each channel, which in charge basis are: 1) $\pi^+\pi^-$, 2) $\pi^0\pi^0$, 3) K^+K^- , 4) $K^0\bar{K}^0$, 5) $\eta\eta$, 6) $\pi^0\eta$ and can be found in Refs. [1.7, 1.9, 1.10]. These kernels are used to build the V matrix which is then inserted into the Bethe-Salpeter equation. Each kernel is projected in S -wave

and a normalization factor is included when identical particles are present, which later needs to be restored.

The individual amplitudes can be plugged into a specific case of study, as we will do in the following sections 1.2 and 1.3, or be combined in isospin basis to obtain each resonance. One could as well write the V and T matrix in isospin basis from the beginning, as done in Ref. [1.7].

The functions G_l are given by

$$G_l = i \int \frac{d^4q}{(2\pi)^4} \frac{1}{q^2 - m_1^2 + i\epsilon} \frac{1}{(P - q)^2 - m_2^2 + i\epsilon}, \quad (1.8)$$

where m_1 and m_2 are the masses of the two mesons of the l -channel. This function diverges and it must be regularized with a proper scheme. We will use a cutoff regularization method, which consists in replacing the infinite upper limit of the integral by a large enough cutoff q_{max} for the modulus of the three-momentum. We will take $q_{max} \sim 600$ MeV, the value used in Refs. [1.1–1.3] which we will discuss in this chapter. After the integration in q^0 and $\cos\theta$ we have

$$G = \int_0^{q_{max}} \frac{\mathbf{q}^2 d\mathbf{q}}{(2\pi)^2} \frac{\omega_1 + \omega_2}{\omega_1 \omega_2 [(P^0)^2 - (\omega_1 + \omega_2)^2 + i\epsilon]}, \quad (1.9)$$

$$\omega_i = \sqrt{\mathbf{q}^2 + m_i^2}, \quad (P^0)^2 = s.$$

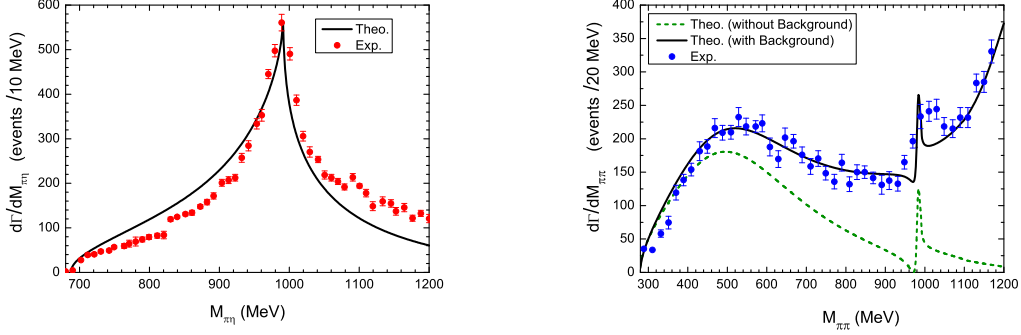
Finally, the T matrix will give us all the scattering amplitudes, including transitions between each coupled channel, and the resonances will appear as poles in the scattering amplitudes of the channels that couple to them. From the pole position in the complex plane the mass and width of the resonance can be obtained.

To illustrate this, we show in Figs. 1.2a and 1.2b the results from Ref. [1.3] on the study of the $\chi_{c1} \rightarrow \eta\pi^+\pi^-$ where one can see the three scalar resonances: the $f_0(500)$ which is dominated by $\pi\pi$ scattering in isospin 0, the $f_0(980)$ which is dominated by $K\bar{K}$ scattering in isospin 0 and also couples to $\pi\pi$, and the $a_0(980)$ which is dominated by $K\bar{K}$ scattering in isospin 1 and also couples to $\pi\eta$.

1.1.2 $c\bar{c} \rightarrow$ light pseudoscalars

As mentioned at the beginning of this chapter, we will present two works that share some general features, the first point being that both study the decay of a charmonium state into a trio of pseudoscalar mesons. The first one will be a particular η_c decay and the second one will be a particular χ_{c1} decay. Both initial states are composed of a $c\bar{c}$ pair, the only difference being their quantum numbers. The η_c has $J^{PC} = 0^{-+}$, and in quark models it can be described as an $L = 0$, $S = 0$ ground state, whereas the χ_{c1} has $J^{PC} = 1^{++}$ and can be described as an orbitally-excited state with $L = 1$, $S = 1$ such that $J = 1$.

Since we will study the decay of these charmonium mesons into trios of light pseudoscalars, it is reasonable to assume that they behave as an $SU(3)$ scalar, that is, we will assume that once the $c\bar{c}$ pair annihilates, trios of light pseudoscalars are created respecting $SU(3)$ symmetry, then the final state interaction of these



(a) $\pi\eta$ invariant mass distribution showing the huge $a_0(980)$ peak.

(b) $\pi\pi$ invariant mass distribution showing the broad shape of the $f_0(500)$ and the sharp $f_0(980)$ peak. The solid line adds an empirical background (see Ref. [1.3] for details).

Figure 1.2: Results from Ref. [1.3] (before publication) using preliminary BESIII data from Ref. [1.11] on the $\chi_{c1} \rightarrow \eta\pi^+\pi^-$ decay.

pseudoscalars will dynamically generate the scalars resonances $f_0(500)$, $f_0(980)$ and $a_0(980)$, which will be observed in the decay channels measured in the experiment.

The assumption that $c\bar{c}$ is an $SU(3)$ singlet stems from the fact that it does not contain any of the u , d , s quarks that are the elements of $SU(3)$. This is in total analogy to the case where $s\bar{s}$ has isospin 0.

This is our starting point, then the first thing we need is to construct a structure containing trios of pseudoscalar mesons which is an $SU(3)$ scalar in terms of the flavor content, that is, being symmetrical in the amount of u , d , s quarks it contains.

An intuitive argument can be drawn based on the following $q\bar{q}$ matrix:

$$M = \begin{pmatrix} u\bar{u} & u\bar{d} & u\bar{s} \\ d\bar{u} & d\bar{d} & d\bar{s} \\ s\bar{u} & s\bar{d} & s\bar{s} \end{pmatrix} = \begin{pmatrix} u \\ d \\ s \end{pmatrix} (\bar{u} \quad \bar{d} \quad \bar{s}). \quad (1.10)$$

This matrix has the property

$$\begin{aligned} & MMM \\ &= \begin{pmatrix} u \\ d \\ s \end{pmatrix} (\bar{u} \quad \bar{d} \quad \bar{s}) \begin{pmatrix} u \\ d \\ s \end{pmatrix} (\bar{u} \quad \bar{d} \quad \bar{s}) \begin{pmatrix} u \\ d \\ s \end{pmatrix} (\bar{u} \quad \bar{d} \quad \bar{s}) \\ &= \begin{pmatrix} u \\ d \\ s \end{pmatrix} (\bar{u} \quad \bar{d} \quad \bar{s}) (\bar{u}u + \bar{d}d + \bar{s}s)^2 \\ &= M(\bar{u}u + \bar{d}d + \bar{s}s)^2. \end{aligned} \quad (1.11)$$

Since $(\bar{u}u + \bar{d}d + \bar{s}s)$ is an $SU(3)$ scalar, then the scalar that we form with the combination of Eq. (1.11) is

$$\text{Trace}[M(\bar{u}u + \bar{d}d + \bar{s}s)^2] = (\bar{u}u + \bar{d}d + \bar{s}s)^3 = \text{Trace}[MMM].$$

This matrix M can be related to the ϕ matrix of the light pseudoscalars meson octet we saw in Eq. (1.2). If we write the light pseudoscalar mesons in terms of their quark content, we see that we need to include the η_1 singlet to match the ϕ matrix with the $q\bar{q}$ matrix M . This can be done by simply making the approximation of $\eta = \eta_8$ and adding a diagonal term of $\eta_1/\sqrt{3} \text{diag}(1, 1, 1)$, with $\eta' = \eta_1$.

Then, the combination of three mesons that behaves as an $SU(3)$ scalar is given by

$$SU(3)[\text{scalar}] \equiv \text{Trace}(\phi\phi\phi). \quad (1.12)$$

For better accuracy one can also consider the $\eta - \eta'$ mixing, in better agreement with the actual physical meson states η and η' , which are defined as

$$\begin{aligned} \eta &= \cos\theta_P \eta_8 - \sin\theta_P \eta_1, \\ \eta' &= \sin\theta_P \eta_8 + \cos\theta_P \eta_1, \end{aligned} \quad (1.13)$$

where θ_P is the mixing angle. In terms of quarks we have

$$\begin{aligned} \eta_8 &= (u\bar{u} + d\bar{d} - 2s\bar{s})/\sqrt{6} \\ \eta_1 &= (u\bar{u} + d\bar{d} + s\bar{s})/\sqrt{3} \end{aligned} \quad (1.14)$$

We will take $\sin\theta_P = -1/3$, which is a standard choice [1.12]. Then

$$\begin{aligned} \eta &\sim \frac{1}{\sqrt{3}}(u\bar{u} + d\bar{d} - s\bar{s}) \\ \eta' &\sim \frac{1}{\sqrt{6}}(u\bar{u} + d\bar{d} + 2s\bar{s}) \end{aligned} \quad (1.15)$$

A more recent determination of this mixing angle from fits to world data is done in Ref. [1.13] with $\theta_P = -14.34^\circ$. Since the dominant η component going with $\cos\theta_P$ only changes by 3% by taking $\theta_P = -14.34^\circ$ or $\sin\theta_P = -1/3$, we choose $\sin\theta_P = -1/3$ ($\cos\theta_P = 2\sqrt{2}/3$), which leads to the following convenient form of the ϕ matrix

$$\phi \equiv \begin{pmatrix} \frac{1}{\sqrt{2}}\pi^0 + \frac{1}{\sqrt{3}}\eta + \frac{1}{\sqrt{6}}\eta' & \pi^+ & K^+ \\ \pi^- & -\frac{1}{\sqrt{2}}\pi^0 + \frac{1}{\sqrt{3}}\eta + \frac{1}{\sqrt{6}}\eta' & K^0 \\ K^- & \bar{K}^0 & -\frac{1}{\sqrt{3}}\eta + \sqrt{\frac{2}{3}}\eta' \end{pmatrix}, \quad (1.16)$$

which is the parametrization we will use throughout this thesis.

As we will discuss in detail in the following sections, using this $SU(3)$ scalar structure we can figure out the weights in which trios of pseudoscalars are created, and then let them undergo final state interaction (using the method described in the previous section 1.1.1) to obtain the final trio of pseudoscalars observed experimentally. We also must take into account the mass and quantum numbers of the initial charmonium state, to properly evaluate the relevant dynamics and resonances that can be present. Since the use of the chiral unitary approach already takes into account the dynamical generation of the scalar resonances in coupled channels, we

can use the amplitudes obtained with such method to calculate the invariant mass distributions of each reaction.

Let us show one example from the work of Ref. [1.3] on the decay $\chi_{c1} \rightarrow \eta\pi^+\pi^-$, when looking at the $\pi^+\pi^-$ invariant mass distribution. By performing the algebra involved in Eq. (1.12) and isolating the η term we find the combination

$$\eta \left(2\sqrt{3}\pi^+\pi^- + \frac{3}{\sqrt{3}}\pi^0\pi^0 + \frac{1}{3\sqrt{3}}\eta\eta \right). \quad (1.17)$$

As discussed in Ref. [1.3], the leading contribution for the $\pi^+\pi^-$ invariant mass distribution can be calculated assuming the η leaves in P -wave and then, according to Eq. (1.17), $\pi^+\pi^-$, $\pi^0\pi^0$ or $\eta\eta$ are produced in the primary step which will undergo final state interaction to produce a $\pi^+\pi^-$ pair, which will give rise to the $f_0(500)$, $f_0(980)$ resonances. The main contribution comes from the diagrams shown in Fig. 1.3.

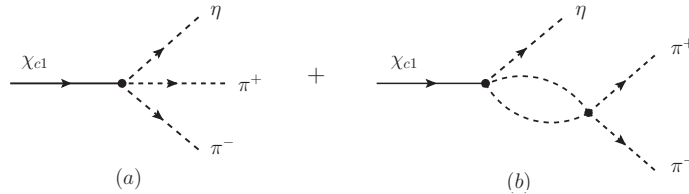


Figure 1.3: Main contribution for the $\pi^+\pi^-$ invariant mass distribution in the $\chi_{c1} \rightarrow \eta\pi^+\pi^-$ decay: tree level (a) or rescattering (b) of $\pi\pi$ or $\eta\eta$ pair, which generate the scalar mesons $f_0(500)$ and $f_0(980)$.

This approach has been shown to be very reliable at low energies, and in the work of Ref. [1.3] the high statistics data from BESIII [1.14] of the $\chi_{c1} \rightarrow \eta\pi^+\pi^-$ reaction could be well reproduced, explaining the $f_0(500)$, $f_0(980)$ peaks in the $\pi^+\pi^-$ invariant mass distribution and the huge $a_0(980)$ peak in the $\pi\eta$ invariant mass distribution, as seen in Figs. 1.2a and 1.2b of the previous section 1.1.1.

Before we dive into the details of the works we will present in this chapter, there is yet another interesting point to discuss regarding the $SU(3)$ structure $\text{Trace}(\phi\phi\phi)$. Although the argumentation using the $q\bar{q}$ matrix to create the $SU(3)$ scalar structure $\text{Trace}(\phi\phi\phi)$ is intuitive, we should note that there are other possibilities. Formally, the quantity $\text{Trace}(\phi\phi\phi)$ is an $SU(3)$ scalar by construction, since the light pseudoscalar matrix ϕ transforms as $\phi \rightarrow U\phi U^{-1}$ under flavor transformations U in $SU(3)$. In fact, even using the $q\bar{q}$ formulation one can get other structures changing the order of rearrangement of the quarks.

That being said we should note that we can construct three independent $SU(3)$ scalars using the ϕ matrix: $\text{Trace}(\phi\phi\phi)$, $\text{Trace}(\phi)\text{Trace}(\phi\phi)$ and $[\text{Trace}(\phi)]^3$. In principle one could use any linear combination of these scalars, however, that would result in a less symmetrical structure and would only introduce more arbitrary parameters and uncertainties. To see that, let us first show all the terms of each one. Using the parametrization of the ϕ matrix with the $\eta - \eta'$ mixing of Eq. (1.16) we obtain

$$\begin{aligned}
\text{Trace}(\phi\phi\phi) &= \frac{\eta\eta\eta}{3\sqrt{3}} + 2\sqrt{3}\eta\pi^+\pi^- + 3\pi^+K^0K^- + 3\pi^-K^+\bar{K}^0 \\
&+ \sqrt{3}\eta\pi^0\pi^0 + \frac{3}{\sqrt{2}}\pi^0K^+K^- - \frac{3}{\sqrt{2}}\pi^0K^0\bar{K}^0 \\
&+ \eta' \left(2\sqrt{\frac{2}{3}}\eta\eta + 3\sqrt{\frac{3}{2}}K^+K^- + 3\sqrt{\frac{3}{2}}K^0\bar{K}^0 + \sqrt{\frac{3}{2}}\pi^0\pi^0 + \sqrt{6}\pi^+\pi^- \right) \\
&+ \frac{\eta'\eta'\eta}{\sqrt{3}} + \frac{5}{3\sqrt{6}}\eta'\eta'\eta', \tag{1.18}
\end{aligned}$$

$$\begin{aligned}
\text{Trace}(\phi)\text{Trace}(\phi\phi) &= \frac{\eta}{\sqrt{3}} (\eta\eta + \pi^0\pi^0 + 2\pi^+\pi^- + 2K^+K^- + 2K^0\bar{K}^0) \\
&+ 2\sqrt{\frac{2}{3}}\eta' (\eta\eta + \pi^0\pi^0 + 2\pi^+\pi^- + 2K^+K^- + 2K^0\bar{K}^0) \\
&+ \frac{\eta\eta'\eta'}{\sqrt{3}} + 2\sqrt{\frac{2}{3}}\eta'\eta'\eta', \tag{1.19}
\end{aligned}$$

$$[\text{Trace}(\phi)]^3 = \frac{\eta\eta\eta}{3\sqrt{3}} + 2\sqrt{\frac{2}{3}}\eta\eta\eta' + 8\frac{\eta\eta'\eta'}{\sqrt{3}} + \frac{16}{3}\sqrt{\frac{2}{3}}\eta'\eta'\eta' \tag{1.20}$$

Here we show all the terms obtained for future reference, however, one should be aware that depending on the final state of each reaction, not every term can contribute since it must be possible that a transition to such final state can actually occur using the coupled channels approach discussed in section 1.1.1. Also, since we are interested in the scalar mesons $f_0(500)$, $f_0(980)$ and $a_0(980)$, we will neglect the η' terms, which play only a marginal role in the building of these resonances, because of its large mass and small couplings.

Now let us discuss the different possible structures. First of all we should mention that were the η_1 not included, (which we do through the inclusion of the $\eta - \eta'$ mixing), but instead we had taken $\eta \rightarrow \eta_8$ and no η' , then $\text{Trace}(\phi) = 0$, so the terms $[\text{Trace}(\phi)]^3$ and $\text{Trace}(\phi)\text{Trace}(\phi\phi)$ would vanish. We include the $\eta - \eta'$ mixing to fine tune it to the physical η state, which then allow us to consider these other structures.

However, as we can see in Eqs. (1.20) and (1.19), these terms are not very symmetrical since the η (or η') have a prominent role in all of them, as expected. We will show in a moment that this asymmetry causes an unbalanced contribution from the channels that have transitions to $\pi\pi$ with respect to the channels with transitions to $\pi\eta$.

We have explored the contribution of these terms and in the work of the η_c decay in Ref. [1.1] we complemented the information given in Ref. [1.3] for the $\chi_{c1} \rightarrow \eta\pi^+\pi^-$ reaction, where only the $\text{Trace}(\phi\phi\phi)$ was used. We show in Figs. 1.4 and 1.5, the results of Ref. [1.3] using only $\text{Trace}(\phi\phi\phi)$ or $\text{Trace}(\phi)\text{Trace}(\phi\phi)$, presented in Ref. [1.1]. The results have been normalized in both cases to the peak of the $\pi\eta$ invariant mass distribution in Fig. 1.4.

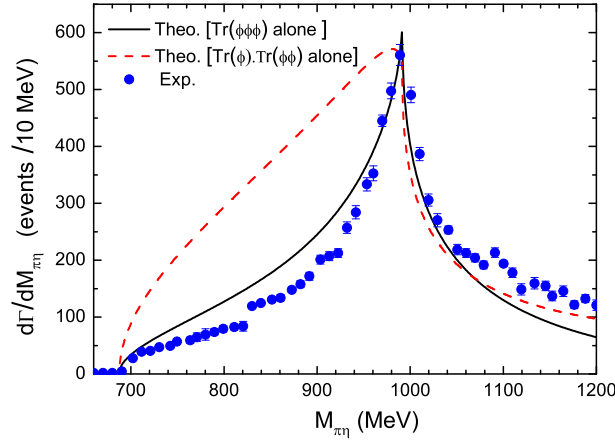


Figure 1.4: Results for the $\pi\eta$ mass distribution in the $\chi_{c1} \rightarrow \eta\pi^+\pi^-$ reaction. Data from Ref. [1.14]. Solid curve: results from Ref. [1.3] using $\text{Trace}(\phi\phi\phi)$. Dashed line: results using $\text{Trace}(\phi)\text{Trace}(\phi\phi)$ normalized to the peak of the distribution.

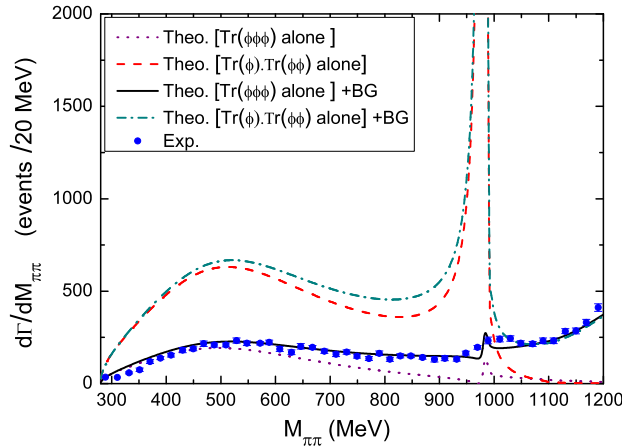


Figure 1.5: Results for the $\pi^+\pi^-$ distribution in the $\chi_{c1} \rightarrow \eta\pi^+\pi^-$ reaction. Data from Ref. [1.14]. Dotted and solid lines: results from Ref. [1.3] using $\text{Trace}(\phi\phi\phi)$, with and without background contribution. Dash-dotted and dashed lines: results using $\text{Trace}(\phi)\text{Trace}(\phi\phi)$, with and without background.

We observe that the shape for the case of $\text{Trace}(\phi)\text{Trace}(\phi\phi)$ is completely off from experiment [1.14]. Similarly, the strength of the $\pi^+\pi^-$ distribution is also much bigger than experiment and it produces a huge $f_0(980)$ peak, in total disagreement with experiment. We have also tried different linear combinations of $\text{Trace}(\phi\phi\phi)$, $\text{Trace}(\phi)\text{Trace}(\phi\phi)$ and $[\text{Trace}(\phi)]^3$, concluding that the best reproduction of the data is obtained with the term $\text{Trace}(\phi\phi\phi)$ alone, which is also more symmetrical in the three mesons. The functional role of the term $[\text{Trace}(\phi)]^3$, involving only η mesons, is negligible since it cannot alone contribute to the $\pi\eta$ invariant mass.

In view of these results, the predictions for the $\eta_c \rightarrow \eta\pi^+\pi^-$ decay that will be presented in section 1.2 and the study of the $a_0(980) - f_0(980)$ mixing in $\chi_{c1} \rightarrow \pi^0 f_0(980) \rightarrow \pi^0\pi^+\pi^-$ and $\chi_{c1} \rightarrow \pi^0 a_0(980) \rightarrow \pi^0\pi^0\eta$ reactions that will be presented in section 1.3, were done with the term $\text{Trace}(\phi\phi\phi)$ alone.

1.2 Predictions for $\eta_c \rightarrow \eta\pi^+\pi^-$ producing $f_0(500)$, $f_0(980)$ and $a_0(980)$

In this section we will present the work of Ref. [1.1] with the predictions for the $\eta_c \rightarrow \eta\pi^+\pi^-$ reaction.

1.2.1 Introduction

The sector of light scalar mesons has been a topic of intense discussions for years [1.15–1.19]. Early discussions on their nature as $q\bar{q}$ or more complex objects have converged to accept that these states cannot be $q\bar{q}$ objects. An extensive updated discussion on the issue can be seen in the report [1.20]. The discussions in Ref. [1.20] reveal the large amount of empirical information favoring a dynamical picture in which the interaction of pseudoscalar mesons in coupled channels and constraints of unitarity generate scalar mesons, which would qualify as multichannel pseudoscalar-pseudoscalar molecular states. The successful picture incorporating the constraints of unitarity in coupled channels and the dynamics of the chiral Lagrangians [1.21–1.23] is known as the chiral unitary approach, and either using the inverse amplitude method [1.24–1.26] or the coupled channels Bethe-Salpeter equations [1.7, 1.27–1.29], the success in providing an accurate description in the different reactions where these resonances are produced is remarkable. Detailed reviews of such reactions can be seen in Ref. [1.30] and more recently in Ref. [1.31], in relation to B , D , Λ_b and Λ_c decays involving these resonances as dynamically generated. We note in passing that the chiral unitary approach does not implement crossing symmetry, which means that it cannot be used to obtain $\pi K \rightarrow \pi K$ from the $\pi\pi \rightarrow K\bar{K}$ amplitudes. In practice what one does is to unitarize $\pi\pi \rightarrow K\bar{K}$ and $\pi K \rightarrow \pi K$ in the physical region as independent reactions. This procedure leads to amplitudes in remarkable agreement with semiempirical studies using the Roy equation, where crossing is also implemented [1.32, 1.33].

Tetraquark pictures have also been invoked [1.18, 1.34], but the standard configurations chosen to account for the masses run into one or another problem in different reactions. A detailed discussion on this issue can be seen in section IV of Ref. [1.35].

What ultimately sets the balance in favor of one or another theoretical picture is the power to provide an accurate explanation of multiple reactions, and in this sense there is nothing more convincing than making predictions for reactions not yet measured and having the predictions realized a posteriori by experiment. This is the aim of the present work where we make predictions for the decay $\eta_c \rightarrow \eta\pi^+\pi^-$ looking into the invariant mass distributions of $\pi\pi$ and $\pi\eta$. In the distributions we find a very clear and strong signal for the $a_0(980)$, and also clearly seen but weaker

signals for $f_0(500)$ and $f_0(980)$ excitation. We are confident on the results up to invariant masses of about 1200 MeV and propose the measurement of this reaction.

There is a precedent for the $\eta_c \rightarrow \eta\pi^+\pi^-$ reaction in the $\chi_{c1} \rightarrow \eta\pi^+\pi^-$ decay, which has been measured at BESIII [1.14]. As discussed previously, in this reaction one can see a neat $a_0(980)$ signal in the $\pi\eta$ mass distribution with its typical cusp shape and with very little background. On the other hand, in the $\pi^+\pi^-$ mass spectrum one sees a very clear peak for the $f_0(500)$ and a smaller, but visible peak for the $f_0(980)$. The $\pi^+\pi^-$ spectrum also shows a pronounced signal for the $f_2(1270)$ excitation. A theoretical study for this reaction using the chiral unitary approach was done in Ref. [1.3] and a good reproduction of the shapes and relative strengths of the invariant mass distributions was obtained up to about 1200 MeV, the present limit of applicability of the chiral unitary approach in the interaction of pseudoscalar mesons.

The $\eta_c \rightarrow \eta\pi^+\pi^-$ reaction has many things in common to the $\chi_{c1} \rightarrow \eta\pi^+\pi^-$ one, but also differences. The χ_{c1} has quantum numbers $I^G(J^{PC}) = 0^+(1^{++})$, the η_c has $0^+(0^{-+})$. In the $\chi_{c1} \rightarrow \eta\pi^+\pi^-$, if the $\pi^+\pi^-$ is in S -wave to create the $f_0(500)$ and $f_0(980)$, the η must be in P -wave to conserve angular momentum and parity. In the η_c decay the process can proceed in S -wave. Concerning the $f_2(1270)$ excitation, in the $\chi_{c1} \rightarrow \eta\pi^+\pi^-$ reaction, the same process with η in P -wave, and the $\pi^+\pi^-$ in D -wave, can produce the resonance. In the $\eta_c \rightarrow \eta\pi^+\pi^-$ we will need a D -wave for η in the production vertex, in addition to the internal D -wave of $\pi^+\pi^-$. This mechanism should be suppressed versus the one of $f_0(500)$ or $f_0(980)$ production and then the signals for the scalar mesons would be cleaner than those in the $\chi_{c1} \rightarrow \eta\pi^+\pi^-$ reaction. With this perspective we perform the calculations and make predictions for the reaction. In the absence of the $f_2(1270)$ excitation we also make predictions for the background. Our limitations to the range below 1200 MeV for the energies of the interacting meson pairs induce uncertainties on the background, but we can show that these uncertainties are small in the region of $\pi^+\pi^-$ or $\pi\eta$ invariant masses below 1200 MeV, thus making our predictions really solid. With these results and clear predictions, we can only encourage the performance of the experiment which is easily implementable at BESIII.

1.2.2 Formalism

As discussed in the previous section, we will assume that trios of light pseudoscalars are created after the $c\bar{c}$ decay respecting $SU(3)$ symmetry, which can be described by the structure $\text{Trace}(\phi\phi\phi)$ that was shown to reproduce well the data of the analogous reaction $\chi_{c1} \rightarrow \eta\pi^+\pi^-$. So, the first step is to select the terms from Eq. (1.18) that can go to the final state $\eta\pi^+\pi^-$ through the coupled channels interactions of pairs of pseudoscalar using the chiral unitary approach from section 1.1.1. As in the $\chi_{c1} \rightarrow \eta\pi^+\pi^-$ decay [1.3], these terms are:

$$\begin{aligned} \text{Trace}(\phi\phi\phi) = & 2\sqrt{3}\eta\pi^+\pi^- + \sqrt{3}\eta\pi^0\pi^0 + \frac{\sqrt{3}}{9}\eta\eta\eta \\ & + 3\pi^+K^0K^- + 3\pi^-K^+K^0. \end{aligned} \quad (1.21)$$

We have eliminated the terms $\pi^0 K^+ K^-$ and $\pi^0 K^0 \bar{K}^0$ because upon final state interaction of any pair, as we do here, we never have the $\eta\pi^+\pi^-$ combination which is measured experimentally. In order to have $\eta\pi^+\pi^-$ at the end, at least one of the mesons has to be the η , π^+ or π^- . The η' terms were also removed because they play a negligible role in the formation of the $f_0(500)$, $f_0(980)$ and $a_0(980)$ states.

This expression gives us the relative weights in which trios of pseudoscalars are produced from η_c decay in a first step, prior to the final state interaction of these mesons. The next step is to allow them to interact. By letting all possible pairs to interact and make transitions, and isolating the final $\eta\pi^+\pi^-$ channel, the diagrams to be considered are given in Fig. 1.6.

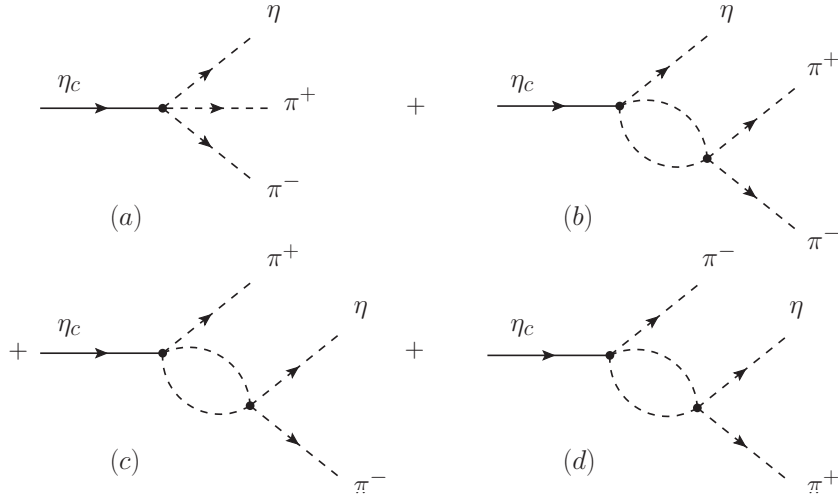


Figure 1.6: Diagrams involved in the $\eta_c \rightarrow \eta\pi^+\pi^-$ reaction including final state interaction of pairs of mesons.

In the loops of Fig. 1.6 we show all pairs allowed by Eq. (1.21) that can give rise to the considered final state. Then the amplitude that sums all terms is given by

$$t = t_{tree} + t_\eta + t_{\pi^+} + t_{\pi^-}, \quad (1.22)$$

where the tree level amplitude is

$$t_{tree} = V_p h_{\eta\pi^+\pi^-}, \quad (1.23)$$

and the first transition amplitude is

$$t_\eta = V_p \sum_i h_i S_i G_i(M_{\text{inv}}(\pi^+\pi^-)) t_{i,\pi^+\pi^-}(M_{\text{inv}}(\pi^+\pi^-)), \quad (1.24)$$

where V_p is a constant coefficient, common to all four terms, that accounts for the matrix element of the tree level $\eta_c \rightarrow 3$ mesons transition, up to h_i coefficients, which are the factors multiplying each combination of three mesons in Eq. (1.21):

$$\begin{aligned} h_{\eta\pi^+\pi^-} &= 2\sqrt{3}, & h_{\eta\pi^0\pi^0} &= \sqrt{3}, \\ h_{\eta\eta\eta} &= \frac{\sqrt{3}}{9}, & h_{\pi^+K^0K^-} &= h_{\pi^-K^+\bar{K}^0} = 3. \end{aligned} \quad (1.25)$$

In Eq. (1.24) only $h_{\eta\pi^+\pi^-}$, $h_{\eta\pi^0\pi^0}$ and $h_{\eta\eta\eta}$ contribute. The function G_i is the loop function of the two intermediate mesons and $t_{i,\pi^+\pi^-}$ is the transition matrix element from the state i to $\pi^+\pi^-$. The G_i and $t_{i,\pi^+\pi^-}$ functions, depending on the invariant masses of $\pi^+\pi^-$, $M_{\text{inv}}(\pi^+\pi^-)$, are taken from the chiral unitary approach, and we follow Refs. [1.7, 1.9, 1.10, 1.37], as presented in section 1.1.1. The factor S_i is a symmetry factor to account for identical particles,

$$S_{\pi^0\pi^0} = 2! \frac{1}{2} \quad (\text{for } \pi^0\pi^0), \quad S_{\eta\eta} = 3! \frac{1}{2} \quad (\text{for } \eta\eta). \quad (1.26)$$

Here we also need the charged components, which can easily be obtained using isospin symmetry and we find [1.36]

$$\begin{aligned} t_{K^0K^-,\pi^-\eta} &= \sqrt{2}t_{K^+K^-,\pi^0\eta}, \\ t_{K^+\bar{K}^0,\pi^+\eta} &= \sqrt{2}t_{K^+K^-,\pi^0\eta}, \\ t_{\pi^+\eta,\pi^+\eta} &= t_{\pi^-\eta,\pi^-\eta} = t_{\pi^0\eta,\pi^0\eta}. \end{aligned} \quad (1.27)$$

Similarly, we have

$$t_{\pi^+} = V_p \sum_i h_i S_i G_i(M_{\text{inv}}(\pi^-\eta)) t_{i,\pi^-\eta}(M_{\text{inv}}(\pi^-\eta)), \quad (1.28)$$

where in the sum over i we have the states $\pi^-\eta$ and K^0K^- , and

$$t_{\pi^-} = V_p \sum_i h_i S_i G_i(M_{\text{inv}}(\pi^+\eta)) t_{i,\pi^+\eta}(M_{\text{inv}}(\pi^+\eta)), \quad (1.29)$$

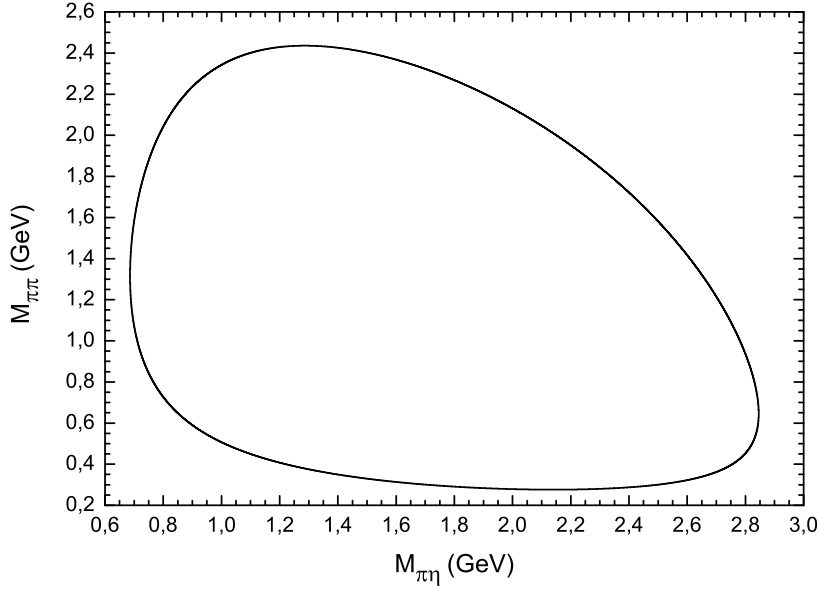
where now in i we have $\pi^+\eta$ and $K^+\bar{K}^0$.

We take as reference the $\pi^+\pi^-$ and $\pi^+\eta$ invariant masses and write the double differential mass distribution for three-body decays [1.38]

$$\begin{aligned} & \frac{d^2\Gamma}{dM_{\text{inv}}(\pi^+\pi^-)dM_{\text{inv}}(\pi^+\eta)} \\ &= \frac{1}{(2\pi)^3} \frac{1}{8M_{\eta c}^3} M_{\text{inv}}(\pi^+\pi^-) M_{\text{inv}}(\pi^+\eta) |t|^2. \end{aligned} \quad (1.30)$$

From this formula we obtain $\frac{d\Gamma}{dM_{\text{inv}}(\pi^+\pi^-)}$ and $\frac{d\Gamma}{dM_{\text{inv}}(\pi^+\eta)}$ by integrating over the other invariant mass. By labeling 1, 2, 3 to the η , π^+ , π^- particles, respectively, if we integrate over M_{23} , the limits of integration are given in Ref. [1.38] (alternative, equivalent, expressions can be obtained from Ref. [1.39]). These limits are

$$\begin{aligned} (M_{23}^2)_{\text{max}} &= (E_2^* + E_3^*)^2 \\ &\quad - \left(\sqrt{E_2^{*2} - m_2^2} - \sqrt{E_3^{*2} - m_3^2} \right)^2, \\ (M_{23}^2)_{\text{min}} &= (E_2^* + E_3^*)^2 \\ &\quad - \left(\sqrt{E_2^{*2} - m_2^2} + \sqrt{E_3^{*2} - m_3^2} \right)^2, \end{aligned} \quad (1.31)$$

Figure 1.7: Dalitz Plot for $\eta_c \rightarrow \eta\pi^+\pi^-$, in the $\pi\eta$ and $\pi\pi$ masses.

where

$$\begin{aligned} E_2^* &= (M_{12}^2 - m_1^2 + m_2^2)/2M_{12}, \\ E_3^* &= (M_{\eta_c}^2 - M_{12}^2 - m_3^2)/2M_{12}. \end{aligned} \quad (1.32)$$

If we integrate over M_{12} , the limits of integration are

$$\begin{aligned} (M_{12}^2)_{max} &= (E_2^{*'} + E_1^{*'})^2 \\ &\quad - \left(\sqrt{E_2^{*'}^2 - m_2^2} - \sqrt{E_1^{*'}^2 - m_1^2} \right)^2, \\ (M_{12}^2)_{min} &= (E_2^{*'} + E_1^{*'})^2 \\ &\quad - \left(\sqrt{E_2^{*'}^2 - m_2^2} + \sqrt{E_1^{*'}^2 - m_1^2} \right)^2, \end{aligned} \quad (1.33)$$

where

$$\begin{aligned} E_2^{*'} &= (M_{23}^2 - m_3^2 + m_2^2)/2M_{23}, \\ E_1^{*'} &= (M_{\eta_c}^2 - M_{23}^2 - m_1^2)/2M_{23}. \end{aligned} \quad (1.34)$$

Since we take the $\pi^+\pi^-$ and $\pi^+\eta$ invariant masses as variables, we must note that t_{π^+} depends on the $\pi^-\eta$ invariant mass, M_{13} . However, this mass is given in terms of the other two variables since one has [1.38]

$$M_{13}^2 = M_{\eta_c}^2 + 2m_\pi^2 + m_\eta^2 - M_{12}^2 - M_{23}^2. \quad (1.35)$$

1.2.3 Results

For simplicity, we will refer to $M_{\text{inv}}(\pi^+\pi^-)$ and $M_{\text{inv}}(\pi^+\eta)$ as $M_{\pi\pi}$ and $M_{\pi\eta}$ respectively. In Fig. 1.7 we show the Dalitz plot for $M_{\pi\pi}$ and $M_{\pi\eta}$ in the $\eta_c \rightarrow \eta\pi^+\pi^-$

decay. We are interested in $\frac{d\Gamma}{dM_{\text{inv}}(\pi^+\pi^-)}$ and $\frac{d\Gamma}{dM_{\text{inv}}(\pi^+\eta)}$ in the region of $f_0(500)$, $f_0(980)$ and $a_0(980)$. If we take $M_{\pi\eta} \sim 1000$ MeV we see that $M_{\pi\pi}$ goes from 500-2300 MeV, but the range is similar for values of $M_{\pi\eta}$ up to 2200 MeV. This means that the strength of the $\pi\pi$ distribution will be spread along a wide range of $M_{\pi\eta}$ and we expect roughly a background following phase space. At $M_{\pi\eta} \sim 750$ MeV the range of $M_{\pi\pi}$ is reduced to 800-1700 MeV and we can expect to obtain contribution from the $M_{\pi\pi} \sim 980$ MeV region, which we have under control. Altogether we might anticipate that the background below the $a_0(980)$ peak will be moderate and controllable.

If we now fix $M_{\pi\pi}$ in 500-1000 MeV, the range of $M_{\pi\eta}$ is large and we should expect a background evenly distributed according to phase space. However, for $M_{\pi\pi} \sim 400$ MeV the range of $M_{\pi\eta}$ begins at 1200 MeV, thus for these energies we will not have contribution from the large peak of the $a_0(980)$ and the background will be small.

In order to evaluate the differential mass distributions we must bear in mind that the chiral unitary approach that we use only makes reliable predictions up to 1100-1200 MeV. One should not use the model for higher invariant masses. With this perspective we will have to admit uncertainties in the mass distributions, particularly at invariant masses higher than 1200 MeV which are a large part of the Dalitz plot. Yet, we are only interested in the region of invariant masses below 1200 MeV both in $M_{\pi\pi}$ and $M_{\pi\eta}$ and it is just there where we would like to know uncertainties of our model. For that purpose we take the following prescription: we evaluate $Gt(M_{\text{inv}})$ combinations up to $M_{\text{inv}} = M_{\text{cut}}$. From there on, we multiply Gt by a smooth factor to make it gradually decrease at large M_{inv} . Thus we take

$$Gt(M_{\text{inv}}) = Gt(M_{\text{cut}})e^{-\alpha(M_{\text{inv}}-M_{\text{cut}})}, \quad \text{for } M_{\text{inv}} > M_{\text{cut}}. \quad (1.36)$$

We take the value $M_{\text{cut}} = 1100$ MeV, with $\alpha = 0.0037$ MeV⁻¹, 0.0054 MeV⁻¹ and 0.0077 MeV⁻¹, which reduce Gt by about a factor 3, 5 and 10, respectively, at $M_{\text{cut}} + 300$ MeV. We show the results in Fig. 1.8 for $\frac{d\Gamma}{dM_{\text{inv}}(\pi^+\eta)}$ and Fig. 1.9 for $\frac{d\Gamma}{dM_{\text{inv}}(\pi^+\pi^-)}$. The results taking $M_{\text{cut}} = 1150$ MeV are practically identical below 1200 MeV.

In Fig. 1.8 we show our results for $\frac{d\Gamma}{dM_{\text{inv}}(\pi^+\eta)}$ (the $\frac{d\Gamma}{dM_{\text{inv}}(\pi^-\eta)}$ is identical). We see that below 1200 MeV, in the region of the $a_0(980)$, the uncertainties are very small, what makes the predictions in that region rather reliable. Since the amplitude t of Eq. (1.22) sums coherently all terms, it is interesting to see what is mostly responsible for the peak. For this we keep in t only the tree level amplitude t_{tree} and t_{π^-} , since t_{π^-} is the term that contains the direct $M_{\text{inv}}(\pi^+\eta)$ dependence in $t_{i,\pi^+\eta}(M_{\text{inv}}(\pi^+\eta))$. The result obtained with these two terms are shown in Fig. 1.8 by the solid line. This is what we call in the figure, “no background”. We can see that the “background” created in that region by the other two terms, t_{π^+} and t_η is rather small. Yet, in the region from $M_{\pi\eta} = 700$ MeV to 990 MeV, this “background” reduces a bit the contribution obtained by $t_{\text{tree}} + t_{\pi^-}$ only.

It is interesting to note that the “no background” prescription was taken in Ref. [1.3], and a smooth background was added incoherently to the $\pi\pi$ mass distribution in the $\chi_{c1} \rightarrow \eta\pi^+\pi^-$, but not to the $\pi\eta$ mass distribution. The $a_0(980)$ mass distribution was in quite good agreement with experiment [1.14], but was a bit

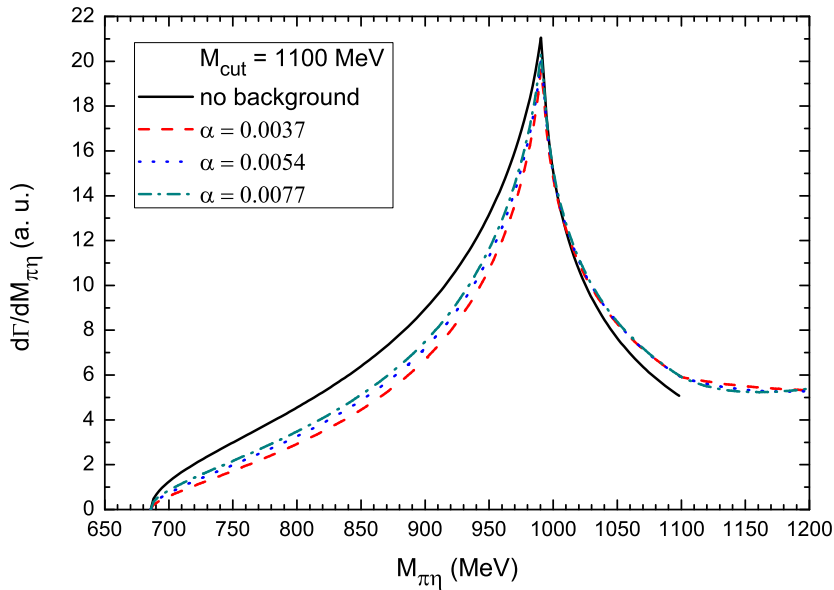


Figure 1.8: $\frac{d\Gamma}{dM_{\pi\eta}}$ as a function of $M_{\pi\eta}$ for $M_{\text{cut}} = 1100$ MeV and three different values of α . See text for explanations.

higher in the $M_{\pi\eta} = 700 - 990$ MeV region, by an amount similar to the difference seen in Fig. 1.8 between the solid and other curves. The results obtained here could be easily translated there, with the consequent improvement of the agreement with the data. Similarly, at energies above 1000 MeV the “background” increases the “no background” curve, and this could also help the results of Ref. [1.3], as seen in Fig. 1.2a of section 1.1.1, to get in better agreement with the data of Ref. [1.14].

The strong cusp shape of the $a_0(980)$ and the small background, qualify this reaction, together with the $\chi_{c1} \rightarrow \eta\pi^+\pi^-$, as the reaction where $a_0(980)$ shows up more strongly and more neatly.

In Fig. 1.9 we show the analogous results of Fig. 1.8 but for the $\frac{d\Gamma}{dM_{\text{inv}}(\pi^+\pi^-)}$ mass distribution. We see that taking $M_{\text{cut}} = 1100$ MeV, there are uncertainties in the region of $M_{\pi\pi} > 1200$ MeV for the different values of α chosen, but the uncertainties are much smaller in the region below 1200 MeV, what makes the predictions more solid. It is more interesting to see that we observe a neat signal for the $f_0(500)$ and a much smaller, but clearly visible, signal for the $f_0(980)$. We also show the results with “no background” obtained taking for t the sum $t_{\text{tree}} + t_\eta$, since in t_η we have the terms $t_{i,\pi^+\pi^-}(M_{\text{inv}}(\pi^+\pi^-))$. We can see that the “background” does not affect the mass distribution below 450 MeV, but gives a sizeable contribution from 550 MeV to 1200 MeV. Once more, in the $\chi_{c1} \rightarrow \eta\pi^+\pi^-$ reaction studied in Ref. [1.3], where only the “no background” terms were considered, it was found that an “empirical” background of this size was needed to reproduce the data of Ref. [1.14], as seen in Fig. 1.2b of section 1.1.1. Again, all these facts reinforce the reliability of the predictions made here.

The results obtained are shown in arbitrary units (the calculations are done taking a value of $V_p = 100$), however, the relative weights for the $M_{\pi\pi}$ and $M_{\pi\eta}$ mass distributions of the figures are also predictions that can be tested in actual

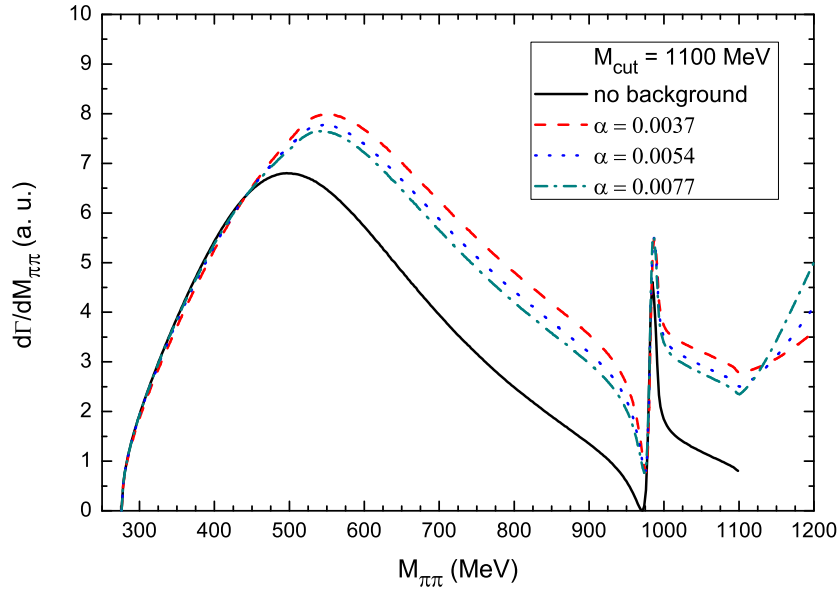


Figure 1.9: $\frac{d\Gamma}{dM_{\pi\pi}}$ as a function of $M_{\pi\pi}$ for $M_{\text{cut}} = 1100$ MeV and three different values of α . See text for explanations.

experiment. As we can see, the strength of the peak of the $a_0(980)\pi$ is about three times the strength of the $f_0(500)$ peak.

We should note that in the region of $M_{\pi\pi}$ or $M_{\pi\eta}$ above 1200 MeV one should expect contribution from other resonances, not accounted for here. However, the small uncertainties of the spectrum below 1200 MeV due to the uncertainties above 1200 MeV, indicate that the corrections below 1200 MeV due to the contribution of higher energy resonances would still be small.

We can be more quantitative about this by looking at the amplitude analysis done in Ref. [1.14]. In Fig. 6 of that work, one can see contributions of $a_0(980)\pi$, $a_2(1320)\pi$, $a_2(1700)\pi$, $S_{K\bar{K}\rightarrow\pi\pi\eta}$, $S_{\pi\pi\rightarrow\pi\pi\eta}$, $f_2(1270)\eta$, $f_4(2050)\eta$. What is seen there is that all these terms (except for the $a_0(980)\pi$ itself) give a negligible background in the $a_0(980)\pi$ peak below 1200 MeV. On the other hand, the $\pi\pi$ distribution is dominated by the $S_{\pi\pi\rightarrow\pi\pi\eta}$ term (leading to the $f_0(500)$ peak) and the $S_{K\bar{K}\rightarrow\pi\pi\eta}$ term (leading to the $f_0(980)$ peak). All the other terms, except for the replica of the $a_0(980)\pi$ peak, give also negligible contribution in the $\pi\pi$ mass distribution below 1200 MeV. Only the $f_2(1270)\eta$ gives some small contribution around 1200 MeV, but we argued that here it should be suppressed. The replica of the $a_0(980)\pi$ peak in the $\pi\pi$ mass distribution we have here, and it is basically responsible for the differences that we have in Fig. 1.9 between the “no background” and the total contributions, similarly as to what is found in Ref. [1.3], as seen in Fig. 1.2b of section 1.1.1.

1.2.4 Conclusions

We have done a theoretical study of the $\eta_c \rightarrow \eta\pi^+\pi^-$ decay paying attention to the final state interaction of the pairs of mesons. We evaluate $\frac{d\Gamma}{dM_{\text{inv}}(\pi^+\pi^-)}$ and $\frac{d\Gamma}{dM_{\text{inv}}(\pi^+\eta)}$ and make predictions that should be confronted by a future experiment. The first step is to see the weight of the possible trios of mesons coming from the η_c

decay, prior to any final state interaction, which is done assuming that the η_c is an $SU(3)$ singlet and then using $SU(3)$ symmetry in the trios of pseudoscalar mesons. We relied upon the results of the $\chi_{c1} \rightarrow \eta \pi^+ \pi^-$ reaction to support the fact that the $\text{Trace}(\phi\phi\phi)$, most symmetric in the three fields, is the appropriate invariant to be used in the present reaction, as discussed in section 1.1.2. After that, all possible pairs in the trios are allowed to interact (not only $\eta \pi^+ \pi^-$) leading to the final $\eta \pi^+ \pi^-$. The calculations are done using the chiral unitary approach for the interaction of mesons, which has a limit of applicability up to $M_{\text{inv}} = 1200$ MeV. We observe a large and clean signal for the $a_0(980)$ in the $\pi\eta$ mass distribution, and a relatively large signal for $f_0(500)$ and a smaller one for $f_0(980)$ in the $\pi^+ \pi^-$ mass distribution.

Given our ignorance above 1200 MeV, we gradually decrease the loop functions and amplitudes beyond M_{cut} around 1200 MeV and, with different options, we estimate uncertainties. What we observe is that, while uncertainties indeed appear in the region of $M_{\text{inv}} > 1200$ MeV, they are very small below that energy, rendering our predictions rather solid. The shape and strength of the mass distributions, up to a global factor (the same for all of them), are predictions of the theory which could be confronted with experiment. The ultimate aim would be to provide support to the picture in which the $f_0(500)$, $f_0(980)$ and $a_0(980)$ resonances are dynamically generated from the pseudoscalar-pseudoscalar interaction. Since neat predictions, more than reproduction of measured data, have a higher value to support one or another picture for the scalar mesons, we encourage both, calculations of the reaction in different models, as well as the performance of the reaction, which in analogy to the $\chi_{c1} \rightarrow \eta \pi^+ \pi^-$ already measured at BESIII, could be measured in this or other facilities.

1.3 $a_0(980) - f_0(980)$ mixing in $\chi_{c1} \rightarrow \pi^0 f_0(980) \rightarrow \pi^0 \pi^+ \pi^-$ and $\chi_{c1} \rightarrow \pi^0 a_0(980) \rightarrow \pi^0 \pi^0 \eta$

In this section we will present the work of Ref. [1.2], where the same framework discussed in the previous sections was employed. In this case we also introduce isospin violation in the reaction $\chi_{c1} \rightarrow \pi^0 f_0(980) \rightarrow \pi^0 \pi^+ \pi^-$ and study its connection with $\chi_{c1} \rightarrow \pi^0 a_0(980) \rightarrow \pi^0 \pi^0 \eta$ and the $a_0(980) - f_0(980)$ mixing.

After this work was published new measurements from BES were published in Ref. [1.40], confirming the previous measurements with higher statistics.

1.3.1 Introduction

The nature of the scalar mesons $a_0(980)$ and $f_0(980)$ has been a topic of much discussion since their discovery decades ago. Several models have been proposed, from regular $q\bar{q}$ to more exotic configurations like tetraquarks $qq\bar{q}\bar{q}$, hybrids $q\bar{q}g$ and meson molecules [1.7, 1.34, 1.41–1.45]. In this context, the isospin-violating mixing of $f_0(980)$ and $a_0^0(980)$ presents an opportunity to filter different proposals and constrain parameters in the models.

In Ref. [1.46], the possibility of observing these scalar mesons in the reaction $e^+ e^- \rightarrow \gamma \pi^0 \pi^0(\eta)$ was already discussed along with their different interpretations

as $s\bar{s}$ states, tetraquarks or $K\bar{K}$ molecules. Their mixing was first suggested in Ref. [1.47] and its connection to the difference in the mass of the charged and neutral kaons was already seen as the main source of the isospin symmetry violation. Also, in Ref. [1.48] the scattering amplitudes of $\pi\pi$ and $\pi\eta$ were studied with the Jülich meson exchange model and it was found that the cross sections for $\pi\pi \rightarrow \pi\eta$ would be nonzero, indicating again the possibility of $a_0(980) - f_0(980)$ mixing.

There are several reactions where this isospin-breaking mixing appears, for instance, in the decay $\eta(1405) \rightarrow \pi^0 f_0(980)$ and $\eta(1405) \rightarrow \pi^0 a_0(980)$ [1.49], which was studied in Ref. [1.50] using the chiral unitary approach. The same puzzle seemed to be present in the decay of the $\eta(1475)$ and both problems were discussed in Refs. [1.51, 1.52], where the interesting role of the triangular singularities in enhancing the isospin violation was shown. This reaction was also discussed in Ref. [1.53], and in Refs. [1.54, 1.55] the reaction $f_1(1285) \rightarrow \pi^0 f_0(980)$ was studied along the same lines.

Recently, another case where a triangular singularity reinforces the isospin breaking in the $a_0(980) - f_0(980)$ mixing was studied in Ref. [1.56], indicating that the reaction $D_s^+ \rightarrow \pi^+ \pi^0 a_0(980) (f_0(980))$ could bring further information on this subject.

Also recently, the role of the $a_0(980) - f_0(980)$ mixing was investigated in the $D^0 \rightarrow K_S^0 \pi^+ \pi^-$ and $D^0 \rightarrow K_S^0 \eta \pi^0$ decays [1.57]; and also in the $D_s^+ \rightarrow \eta \pi^0 \pi^+$ decay [1.58], showing new possible reactions to investigate this topic. In Ref. [1.59] several possibilities of D_s and B_s decays have been proposed and it is argued that the $a_0(980) - f_0(980)$ mixing could be experimentally determined with high precision.

One of the first attempts to quantitatively relate the $a_0(980) - f_0(980)$ mixing with experimental data was made in Ref. [1.60], through the analysis of an enhancement in the production rate of the $a_0(980)$ relative to the $a_2(1320)$ in $pp \rightarrow p_s(\eta \pi^0) p_f$. However, questions about other secondary effects related to G -parity were raised in Ref. [1.61], which could affect the assumptions made in Ref. [1.60].

The mixing of these scalar mesons in the radiative ϕ decay was discussed in Refs. [1.62, 1.63], while the photoproduction of $f_0(980)$ and $a_0(980)$ was studied in Ref. [1.64], with emphasis on the isospin-violating mixing due to the mass difference of kaons and the role of polarized photons and protons.

The decay of η' has also been a topic where this mixing was investigated. For instance, in Ref. [1.65] the reaction $\eta' \rightarrow \eta \pi^0 \pi^0$ was studied in the framework of the isobar model, where the $f_0(500)$ was also included in the analysis. Similarly, the decays $\eta' \rightarrow 3\pi^0$ and $\eta' \rightarrow \pi^0 \pi^+ \pi^-$ were considered in Ref. [1.66], both recently measured by the BESIII Collaboration [1.67]. After this measurement, the decay $\eta \rightarrow 3\pi$ was studied in Ref. [1.68] with an extended chiral Khuri–Treiman formalism, where the $a_0(980)$ and $f_0(980)$ are taken into account in the dispersive integrals.

Other reactions have been proposed to search for the $f_0(980)$ and $a_0(980)$ mixing, like the $pn \rightarrow da_0$ in Ref. [1.69]. This reaction was also studied in Ref. [1.70], where two more reactions were proposed: the $pd \rightarrow {}^3\text{He}/{}^3\text{H} a_0$ and the $dd \rightarrow {}^4\text{He} a_0$. Also, in Ref. [1.71] it was suggested performing polarized target experiments on the reaction $\pi^- p \rightarrow \eta \pi^0 n$, where the mixing would be detected through the presence of a jump in the azimuthal asymmetry in the $\pi^0 \eta$ S -wave production cross section around the $K\bar{K}$ threshold.

Searching for a reaction where the isospin breaking could be measured unambiguously, the decay $J/\psi \rightarrow \phi f_0(980) \rightarrow \phi a_0(980) \rightarrow \phi \pi^0 \eta$ was proposed in Ref. [1.61], where it was assumed that first there would be the formation of the $f_0(980)$, which then would make a transition to $a_0(980)$ violating isospin conservation and finally the latter would decay into $\pi^0 \eta$. The background of other reactions was analysed and the conclusion was that one should expect a narrow peak in the $\pi^0 \eta$ invariant mass with a width of about 8 MeV in the region of the $K\bar{K}$ threshold, which would come from the difference in the mass of the charged and neutral kaons, and would be clearly distinguishable from the broad structure of other background process.

The reaction $J/\psi \rightarrow \phi \pi^0 \eta$ was also investigated in Ref. [1.72], where the chiral unitary approach was used to study the $a_0(980) - f_0(980)$ mixing, considering the difference in quark masses and also one-photon exchange between charged mesons. It was shown that this mixing was indeed the most important isospin-breaking effect and could be extracted from experiment through that reaction.

Next, the question whether there would be a difference in the inverse isospin-breaking process, where the $a_0(980)$ would make a transition to the $f_0(980)$, the complementary reaction $\chi_{c1} \rightarrow \pi^0 a_0(980) \rightarrow \pi^0 f_0(980) \rightarrow \pi^0 \pi^+ \pi^-$ was proposed in Ref. [1.73], and it was found that one could indeed expect different rates of mixing. The uncertainty of these calculations were attributed essentially to the different parameters extracted from different theoretical models or experimental measurements of these two scalar mesons.

Some time later, the two reactions proposed in Refs. [1.61, 1.72, 1.73] were measured by the BESIII Collaboration [1.74], the isospin-forbidden production of $a_0(980)$ in the decay $J/\psi \rightarrow \phi \pi^0 \eta$ and the isospin-forbidden production of $f_0(980)$ in the decay $\chi_{c1} \rightarrow \pi^0 \pi^+ \pi^-$. The mixing in both reactions was determined through the fraction of the branching ratios with their corresponding isospin-allowed process [1.74], respectively the $J/\psi \rightarrow \phi \pi^+ \pi^-$ (where the $f_0(980)$ shows up) measured by the BES Collaboration [1.75], and the $\chi_{c1} \rightarrow \pi^0 \pi^0 \eta$ (where the $a_0^0(980)$ shows up). As argued in Ref. [1.73], the latter reaction could be compared to the $\chi_{c1} \rightarrow \eta \pi^+ \pi^-$ (where the $a_0^\pm(980)$ shows up clearly), since by isospin symmetry the same production rate is expected for $\chi_{c1} \rightarrow \pi^0 a_0^0(980)$ as in $\chi_{c1} \rightarrow \pi^\pm a_0^\mp(980)$ (with $a_0^\mp(980) \rightarrow \eta \pi^\mp$). The $\chi_{c1} \rightarrow \eta \pi^+ \pi^-$ was measured by the CLOE Collaboration [1.76] and recently by BESIII [1.14] with high statistics.

After the BESIII experiment [1.74], the reaction $J/\psi \rightarrow \phi \pi^0 \eta$ was studied in Ref. [1.77] using the chiral unitary approach, where the importance of other mechanisms was also shown, like the sequential exchange of vector and axial-vector mesons to obtain a good agreement with the data. Also based on this experiment, a study of the amount of $K\bar{K}$ in the $a_0(980)$ and $f_0(980)$ was developed in Ref. [1.78] using the chiral unitary approach and the Flatté parametrization, where the mixing of these scalar mesons, formulated in a similar manner of Refs. [1.61, 1.73], was used to constrain their parameters and compositeness.

Not much theoretical work has been done to describe the other isospin-breaking reaction also measured by BESIII, the $\chi_{c1} \rightarrow \pi^0 \pi^+ \pi^-$, in which we focus. There is one more reason to tackle this reaction at this stage, since the recent experiment by BESIII [1.14] on the $\chi_{c1} \rightarrow \eta \pi^+ \pi^-$ reaction has brought new light into this problem. Indeed, the process was studied theoretically in Ref. [1.3] (see Figs. 1.2a

and 1.2b) with the basic assumption that the χ_{c1} is an $SU(3)$ singlet due to its $c\bar{c}$ structure. The different $SU(3)$ scalar structures with three mesons were discussed in Refs. [1.1, 1.79] in the study of the $\eta_c \rightarrow \eta\pi^+\pi^-$ reaction (see section 1.1.2) supporting the structure used in Ref. [1.3] by means of which a good agreement with the experimental data of $\chi_{c1} \rightarrow \eta\pi^+\pi^-$ [1.14] was found (see Figs. 1.4 and 1.5). This information is important for the $\chi_{c1} \rightarrow \pi^0\pi^+\pi^-$ reaction since it provides the weights of different trios of pseudoscalar mesons that can be formed, prior to their final state interaction from where the $f_0(980)$ and $a_0(980)$ resonances emerge. The use of this information and of the chiral unitary approach to deal with the interaction of pairs of pseudoscalars allows a thorough investigation of this process, clarifying the mechanisms that lead to isospin breaking, and providing for the first time a quantitative description of the $f_0(980)$ and $a_0(980)$ production with a ratio of strengths in agreement with the BESIII [1.74] experimental data.

1.3.2 Formalism

In this work we are interested in two reactions: $\chi_{c1} \rightarrow \pi^0 f_0(980) \rightarrow \pi^0\pi^+\pi^-$ and $\chi_{c1} \rightarrow \pi^0 a_0(980) \rightarrow \pi^0\pi^0\eta$, from which we wish to calculate the invariant mass distribution of $\pi^+\pi^-$ and $\pi^0\eta$, respectively. We follow a similar approach to the one of Refs. [1.1, 1.3], assuming that the χ_{c1} behaves as a flavor $SU(3)$ scalar since it is a $c\bar{c}$ state. Therefore, in the present work we also adopt $\text{Trace}(\phi\phi\phi)$ as the $SU(3)$ scalar. Since we are interested in observing the $f_0(980)$ in the $\pi^+\pi^-$ channel when the final state is $\pi^0\pi^+\pi^-$ and the $a_0(980)$ in the $\pi^0\eta$ channel when the final state is $\pi^0\pi^0\eta$, we need trios of pseudoscalars that have at least one π^0 , and such that the remaining pairs couple to these channels, directly or indirectly. Looking back to Eq. (1.18) for the $\text{Trace}(\phi\phi\phi)$ we obtain the combinations $\pi^0\pi^0\eta$ and $\pi^0 K\bar{K}$, as follows

$$\text{Trace}(\phi\phi\phi) = \sqrt{3}\pi^0\pi^0\eta + \frac{\pi^0}{\sqrt{2}}(3K^+K^- - 3K^0\bar{K}^0), \quad (1.37)$$

Then Eq. (1.37) tells us the weight by which trios of pseudoscalars are produced in the first step of the χ_{c1} decay. The next step consists of letting these mesons interact in coupled channels such that the final state is $\pi^0\pi^0\eta$ or $\pi^0\pi^+\pi^-$. In this case, the diagrams for $a_0(980)$ and $f_0(980)$ production are shown in Fig. 1.10 and 1.11, respectively.

Here we have a different situation from the η_c ($J = 0$) decay of the previous section 1.2 and Ref. [1.1], where every main contribution would proceed in S -wave, such that all diagrams could in principle interfere. In the present case, since the χ_{c1} ($J = 1$) has an orbital excitation, we need to take into account the different combination of quantum numbers.

In the study of the $\chi_{c1} \rightarrow \eta\pi^+\pi^-$ reaction in Ref. [1.3], to conserve the J^P quantum numbers, we needed a P -wave in either any of the three mesons η , π^+ or π^- , such that the remaining pair $\pi^+\pi^-$ or $\eta\pi^\pm$ could interact in S -wave to generate the $f_0(980)$ or $a_0^\pm(980)$, respectively.

In that case the possible structures were

$$V_1 = A\vec{\epsilon}_{\chi_{c1}} \cdot \vec{p}_\eta,$$

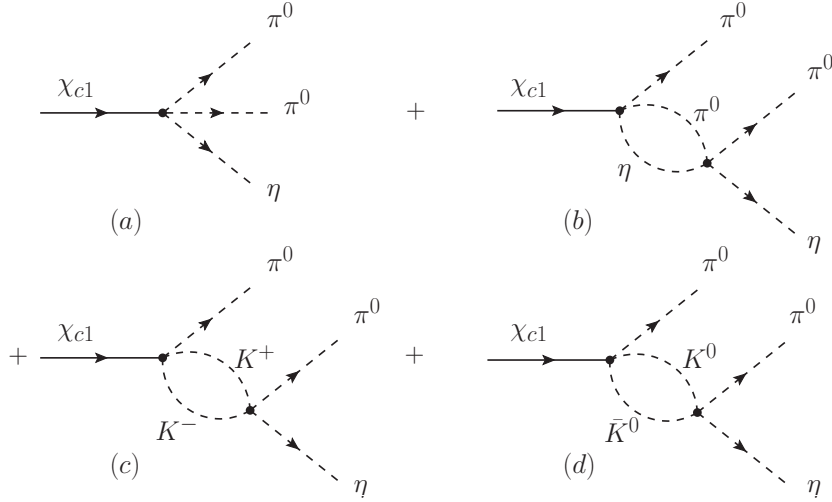


Figure 1.10: Diagrams involved in the $a_0(980)$ production in the $\chi_{c1} \rightarrow \pi^0 a_0(980) \rightarrow \pi^0 \pi^0 \eta$ reaction: (a) tree level; and rescattering of (b) $\pi^0 \eta$, (c) $K^+ K^-$, (d) $K^0 \bar{K}^0$.

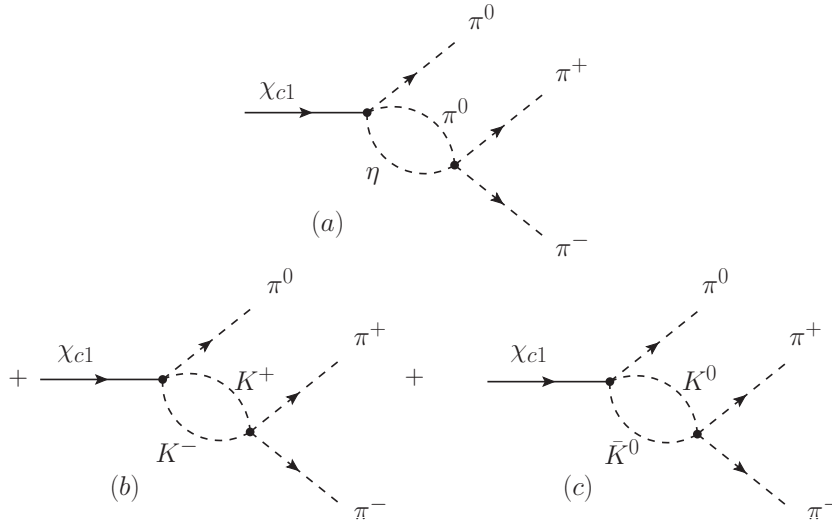


Figure 1.11: Diagrams involved in the $f_0(980)$ production in the $\chi_{c1} \rightarrow \pi^0 f_0(980) \rightarrow \pi^0 \pi^+ \pi^-$ reaction: rescattering of (a) $\pi^0 \eta$, (b) $K^+ K^-$, (c) $K^0 \bar{K}^0$.

$$\begin{aligned} V_2 &= B \vec{\epsilon}_{\chi_{c1}} \cdot \vec{p}_{\pi^+}, \\ V_3 &= C \vec{\epsilon}_{\chi_{c1}} \cdot \vec{p}_{\pi^-}. \end{aligned} \quad (1.38)$$

If, for instance, we take the first structure of V_1 , the \vec{p}_η coupling introduces $L = 1$ and forces the $\pi^+ \pi^-$ pair to also have positive parity. With these quantum numbers, the $\pi^+ \pi^-$ pair can be in $I^G(J^{PC}) = 0^+(0^{++})$ and then produce the resonance $f_0(980)$.

Then we would have a combination of the three structures of Eq. (1.38) and then the primary amplitude would be of the type

$$t = A \vec{\epsilon}_{\chi_{c1}} \cdot \vec{p}_\eta + B \vec{\epsilon}_{\chi_{c1}} \cdot \vec{p}_{\pi^+} + C \vec{\epsilon}_{\chi_{c1}} \cdot \vec{p}_{\pi^-}. \quad (1.39)$$

However, as discussed in Ref. [1.3], there is no interference between these terms. Indeed, the crossed terms in $|t|^2$ after averaging over the polarization of the massive

χ_{c1} state go as

$$\begin{aligned} & \overline{\sum} 2\text{Re}(AB^*) \vec{\epsilon}_{\chi_{c1}} \cdot \vec{p}_\eta \vec{\epsilon}_{\chi_{c1}} \cdot \vec{p}_{\pi^+} \\ & = 2\text{Re}(AB^*) \frac{1}{3} \delta_{ij} p_{\eta i} p_{\pi^+ j} = \frac{2}{3} \text{Re}(AB^*) \vec{p}_\eta \cdot \vec{p}_{\pi^+}, \end{aligned} \quad (1.40)$$

which vanish upon integration over angles in phase space. Thus, for $|t|^2$ we have the sum of the squares of each amplitude in Eq. (1.39), in which the tree level and rescattering of a pair is contained in each one.

For symmetry reasons, the probability that the P -wave is in either of the mesons should be the same, then $A = B = C$ at tree level (up to the factor of the weight of each trio under $SU(3)$ symmetry), then we will use a common normalization factor V_P that stands for the dynamics of $\chi_{c1} \rightarrow$ three mesons, as in the case of the η_c decay.

Also, as argued in Ref. [1.3], the interaction of the meson that comes in the P -wave with any of the other two should proceed in P -wave, which is negligible for $\pi\eta$ and zero for $\pi\pi$ which have been created in $I = 0$. That made the interpretation of the signals in Ref. [1.3] particularly easy, since they came from either the $\pi\pi$ or $\eta\pi$ interaction in S -wave. Under this condition, one can avoid using the double differential mass distribution as in the η_c decay of section 1.2, which forced us to introduce a cut in the amplitudes at high energies, and instead use directly a simple invariant mass distribution with just the dominant contribution when one meson leaves in P -wave and the remaining pair interact in S -wave. Since the same argumentation is valid in the reactions we will present in this work, the $\chi_{c1} \rightarrow \pi^0 a_0(980) \rightarrow \pi^0 \pi^0 \eta$ and the $\chi_{c1} \rightarrow \pi^0 f_0(980) \rightarrow \pi^0 \pi^+ \pi^-$, we will follow the same approach.

That being said, let us analyse the specific case of the present work. The quantum numbers of the χ_{c1} are $I^G(J^{PC}) = 0^+(1^{++})$, while the quantum numbers of the $a_0(980)$ and $f_0(980)$ are $1^-(0^{++})$ and $0^+(0^{++})$, respectively. If the $\pi^0 \eta$ and $\pi^+ \pi^-$ are in S -wave to create the $a_0(980)$ and $f_0(980)$, the remaining π^0 must be in P -wave to conserve angular momentum and parity. Then the structure of the amplitude at tree level will be

$$t = V_p \vec{\epsilon}_{\chi_{c1}} \cdot \vec{p}_{\pi^0}, \quad (1.41)$$

where, for comparison purposes, we will take the same value of V_p that was used in Ref. [1.3].

The full amplitude for the isospin-allowed $a_0(980)$ production (with final state $\pi^0 \pi^0 \eta$) is obtained considering also the rescattering of the pairs of mesons as indicated in Fig. 1.10, then

$$t = \vec{\epsilon}_{\chi_{c1}} \cdot \vec{p}_{\pi^0} \tilde{t}_{\pi^0 \eta}, \quad (1.42)$$

with

$$\begin{aligned} \tilde{t}_{\pi^0 \eta} &= V_p (h_{\pi^0 \eta} + h_{\pi^0 \eta} G_{\pi^0 \eta} t_{\pi^0 \eta \rightarrow \pi^0 \eta} \\ &+ h_{K^+ K^-} G_{K^+ K^-} t_{K^+ K^- \rightarrow \pi^0 \eta} \\ &+ h_{K^0 \bar{K}^0} G_{K^0 \bar{K}^0} t_{K^0 \bar{K}^0 \rightarrow \pi^0 \eta}), \end{aligned} \quad (1.43)$$

where the weights h_i are obtained from Eq. (1.37): $h_{\pi^0 \eta} = 2\sqrt{3}$, $h_{K^+ K^-} = 3/\sqrt{2}$ and $h_{K^0 \bar{K}^0} = -3/\sqrt{2}$. Note that $h_{\pi^0 \eta}$ has an extra factor 2 with respect to the

coefficient $\sqrt{3}$ for the $\pi^0 \pi^0 \eta$ field in Eq. (1.37), since with the production of two π^0 we will have the terms $\partial_i \pi^0 \pi^0 + \pi^0 \partial_i \pi^0$. The functions G_{ij} are the same used in the Bethe-Salpeter equation, from which we also obtain the rescattering amplitudes, as we saw in section 1.1.1.

Now for the isospin-forbidden $f_0(980)$ production (with final state $\pi^0 \pi^+ \pi^-$) we have no tree level, and we consider only the rescattering diagrams, as indicated in Fig. 1.11, then

$$t = \vec{\epsilon}_{\chi_{c1}} \cdot \vec{p}_{\pi^0} \tilde{t}_{\pi^+ \pi^-}, \quad (1.44)$$

where

$$\begin{aligned} \tilde{t}_{\pi^+ \pi^-} &= V_p (h_{\pi^0 \eta} G_{\pi^0 \eta} t_{\pi^0 \eta \rightarrow \pi^+ \pi^-} \\ &+ h_{K^+ K^-} G_{K^+ K^-} t_{K^+ K^- \rightarrow \pi^+ \pi^-} \\ &+ h_{K^0 \bar{K}^0} G_{K^0 \bar{K}^0} t_{K^0 \bar{K}^0 \rightarrow \pi^+ \pi^-}). \end{aligned} \quad (1.45)$$

As we will discuss in a moment, the isospin symmetry breaking will be introduced through the use of different masses for the charged and neutral kaons. We note that the difference between the $K^+ K^-$ and $K^0 \bar{K}^0$ loops is convergent, and useful to investigate the $f_0(980)$ production, but in order to deal with the $a_0(980)$ production and study the whole problem quantitatively, one must face the divergent behaviour of all the propagators. For that we have a simple solution of employing in Eqs. (1.43) and (1.45) the same cutoff used to regularize the loops inside the T matrix, which yields results in good agreement with the $\chi_{c1} \rightarrow \eta \pi^+ \pi^-$ decay, as shown in Ref. [1.3].

We note that our approach is in the same line of Ref. [1.77], but it is different from the approach of Ref. [1.73], where it was assumed that the isospin-forbidden production of $f_0(980)$ comes from a transition $a_0(980) \rightarrow f_0(980)$, related to the phase space available in the propagators of pairs of mesons. On the other hand, we assume that the $f_0(980)$ emerges from the χ_{c1} decay, stemming from the meson-meson loops, without going first through the $a_0(980)$ production. As we will show next, our method has some interesting features, providing an intuitive explanation of the mechanism behind the isospin symmetry violation.

Note that if we consider isospin symmetry the amplitude in Eq. (1.45) would be identically zero, because $\pi^0 \eta \rightarrow \pi^+ \pi^-$ would not conserve isospin – since we consider $\pi^+ \pi^-$ in $I = 0$ to create the $f_0(980)$ – and the terms with kaons would cancel due to the minus sign in $h_{K^0 \bar{K}^0}$. Indeed, we can interpret the last two terms as $K \bar{K}$ in isospin 1 basis, which again, would not go to $\pi^+ \pi^-$ in $I = 0$.

Therefore, the only way to have $f_0(980)$ production is by introducing isospin breaking, which we implement using different kaon masses. We introduce isospin violation from two sources, one comes from $G_{K^+ K^-}$ and $G_{K^0 \bar{K}^0}$, the first loops of rescattering with $K^+ K^-$ and $K^0 \bar{K}^0$ pairs in Eqs. (1.43) and (1.45). In the case of $\pi^0 \eta$ production the $K^+ K^-$ and $K^0 \bar{K}^0$ terms add, but in the case of the $\pi^+ \pi^-$ production they subtract, and would cancel if the masses of the kaons were equal.

The other source comes from the T matrix that we construct with different kaon masses in the propagators inside the Bethe-Salpeter equation $T = (1 - VG)^{-1} V$ [1.7], which we use to obtain the scattering and transition amplitudes $t_{i \rightarrow \pi^0 \eta}$ and $t_{i \rightarrow \pi^+ \pi^-}$. This way, the $t_{\pi^0 \eta \rightarrow \pi^+ \pi^-}$ transition will also be nonzero – because of the coupled channels interaction – when we introduce isospin breaking inside the T matrix.

Finally, for the case of $a_0(980)$ production we can write the invariant mass distribution as

$$\frac{d\Gamma}{dM_{\text{inv}}(\pi^0\eta)} = \frac{1}{(2\pi)^3} \frac{1}{4M_{\chi_{c1}}^2} \frac{1}{3} p_{\pi^0}^2 p_{\pi^0} \tilde{p}_\eta |\tilde{t}_{\pi^0\eta}|^2, \quad (1.46)$$

where

$$p_{\pi^0} = \frac{\lambda^{1/2}(M_{\chi_{c1}}^2, m_{\pi^0}^2, M_{\text{inv}}^2(\pi^0\eta))}{2M_{\chi_{c1}}}, \quad (1.47)$$

and

$$\tilde{p}_\eta = \frac{\lambda^{1/2}(M_{\text{inv}}^2(\pi^0\eta), m_{\pi^0}^2, m_\eta^2)}{2M_{\text{inv}}(\pi^0\eta)}. \quad (1.48)$$

On the other hand, for the case of $f_0(980)$ production, the invariant mass distribution reads

$$\frac{d\Gamma}{dM_{\text{inv}}(\pi^+\pi^-)} = \frac{1}{(2\pi)^3} \frac{1}{4M_{\chi_{c1}}^2} \frac{1}{3} p_{\pi^0}^2 p_{\pi^0} \tilde{p}_{\pi^+} |\tilde{t}_{\pi^+\pi^-}|^2, \quad (1.49)$$

with

$$p_{\pi^0} = \frac{\lambda^{1/2}(M_{\chi_{c1}}^2, m_{\pi^0}^2, M_{\text{inv}}^2(\pi^+\pi^-))}{2M_{\chi_{c1}}}, \quad (1.50)$$

and

$$\tilde{p}_{\pi^+} = \frac{\lambda^{1/2}(M_{\text{inv}}^2(\pi^+\pi^-), m_{\pi^+}^2, m_{\pi^-}^2)}{2M_{\text{inv}}(\pi^+\pi^-)}. \quad (1.51)$$

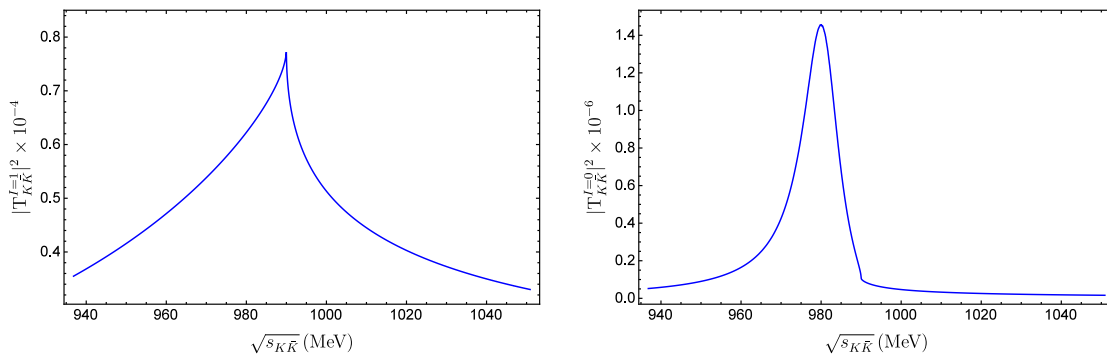
1.3.3 Results

The importance of the kaon mass difference in the $a_0(980) - f_0(980)$ mixing can be appreciated when we look at the $K\bar{K}$ amplitudes obtained with the chiral unitary approach in isospin 0 and 1, as shown in Figs. 1.12a and 1.12b, where isospin symmetry was used. We can see that both resonances appear around the $K\bar{K}$ threshold, and their dynamical nature emerging from coupled channels interactions allows the mixing to occur when isospin symmetry is broken.

The fact that both resonances couple to $K\bar{K}$ and have similar masses around this threshold is what allows the mixing to occur, which takes place in the energy range of about 8 MeV between the charged and neutral kaon pair thresholds, K^+K^- and $K^0\bar{K}^0$.

We should note that all our results are calculated using isospin-average pion masses, but the effect of using different pion masses is completely negligible (as we have checked) in comparison with using different masses for the charged and neutral kaons.

We show in Figs. 1.13 and 1.14 the invariant mass distribution $d\Gamma/dM_{\pi\eta}$ from Eq. (1.46), where the shape of the $a_0(980)$ is clear. The solid line represents the case where different masses for the charged and neutral kaons are used in the propagators inside the T matrix and also in the first rescattering loops $G_{K^+K^-}$ and $G_{K^0\bar{K}^0}$, as discussed in the formalism. The dashed line is the case where the different masses are used only inside the T matrix and the dotted line only in the first rescattering loops $G_{K^+K^-}$ and $G_{K^0\bar{K}^0}$. As we can see in Fig. 1.13, there is only a small difference



(a) $K\bar{K}$ amplitude in $I = 1$; couples to $a_0(980)$, which also couples to $\pi\eta$. (b) $K\bar{K}$ amplitude in $I = 0$; couples to $f_0(980)$, which also couples to $\pi\pi$.

Figure 1.12: Comparison between $K\bar{K} \rightarrow K\bar{K}$ amplitude squared in isospin 1 and 0 (S -wave).

around the $K\bar{K}$ threshold. Looking closer into this region (Fig. 1.14) one can see that in the three curves there is a small cusp effect at $M_{\pi\eta}$ equal to $2m_{K^+}$ and $2m_{K^0}$; whereas in the dashed and dotted line (where the isospin-average kaon mass $\langle m_K \rangle$ is also used) the $a_0(980)$ peak appears at $2\langle m_K \rangle$.

Notice that there is an interesting comparison to be made with the reaction $\chi_{c1} \rightarrow \eta\pi^+\pi^-$. In this case, the $\chi_{c1} \rightarrow \pi^0\pi^0\eta$ has the same isospin content, and we can see for instance in Eq. (7) of Ref. [1.3] that when the π^+ is in P -wave the $\pi^-\eta$ term has the same weight as the $\pi^0\eta$ in Eq. (1.37) – after the inclusion of the statistical factor – while the K^0K^- term has the same weight as the $(K^+K^- - K^0\bar{K}^0)/\sqrt{2}$, and both are $K\bar{K}$ in isospin 1. The same is valid for Eq. (8) of Ref. [1.3], when the π^- is in P -wave. Indeed, if we look at Fig. 6 of Ref. [1.3] (see Fig. 1.2a of section 1.1.1) we see that the intensity of the $a_0(980)$ peak is exactly twice as here (in Figs. 1.13 and 1.14) since there we had the sum of both contributions from $\pi^+\eta$ and $\pi^-\eta$, and here we have only $\pi^0\eta$ (notice the extra factor 2 in Eq. (24) of that reference).

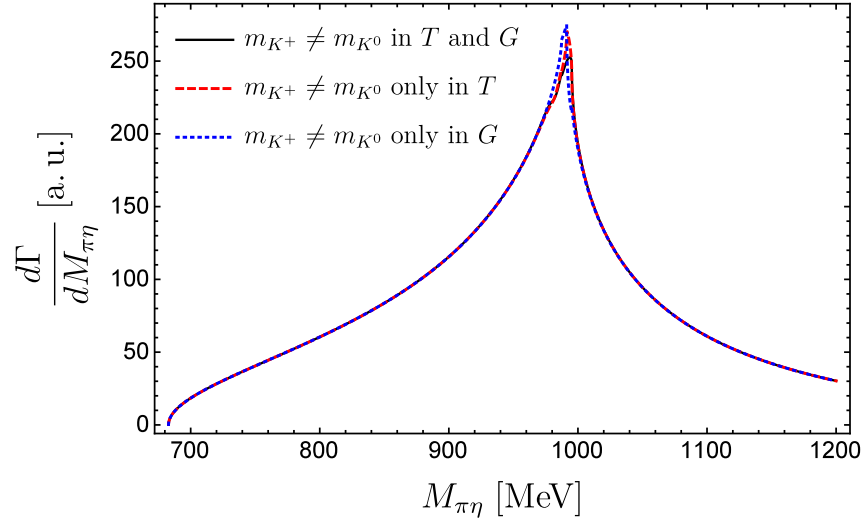


Figure 1.13: Invariant mass distribution of $\pi^0\eta$ in the $\chi_{c1} \rightarrow \pi^0 a_0(980) \rightarrow \pi^0\pi^0\eta$ reaction. (See text for explanations).

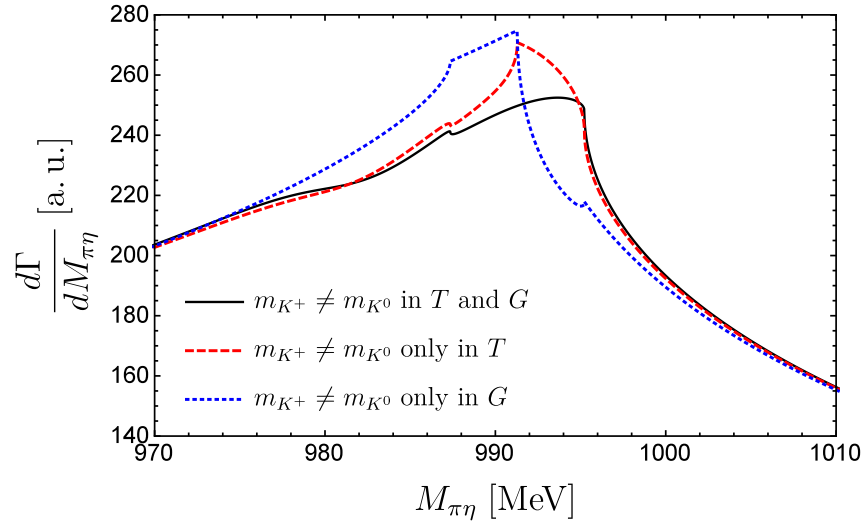


Figure 1.14: Zoom around the $a_0(980)$ peak in the invariant mass distribution of $\pi^0\eta$ in the $\chi_{c1} \rightarrow \pi^0 a_0(980) \rightarrow \pi^0\pi^0\eta$ reaction. (See text for explanations).

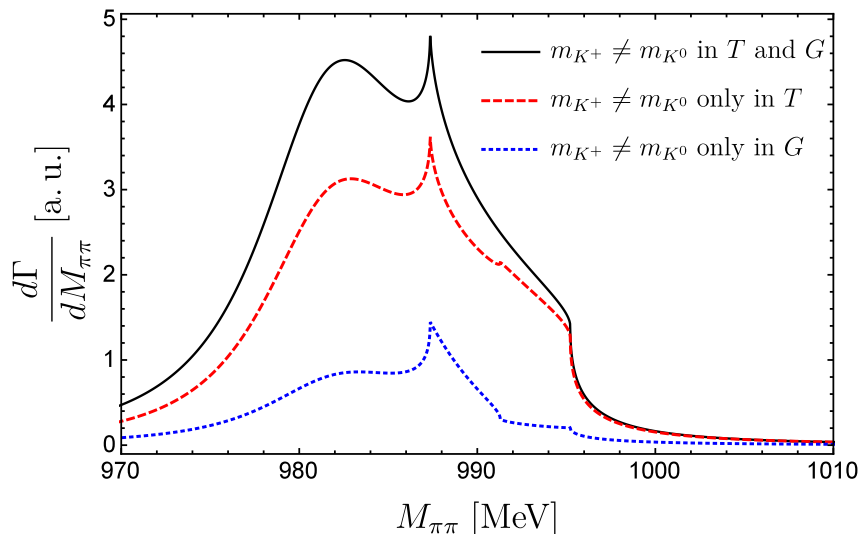


Figure 1.15: Invariant mass distribution of $\pi^+\pi^-$ in the $\chi_{c1} \rightarrow \pi^0 f_0(980) \rightarrow \pi^0 \pi^+ \pi^-$ reaction. (See text for explanations).

For the isospin-breaking production of $f_0(980)$, we show in Fig. 1.15 the invariant mass distribution $d\Gamma/dM_{\pi\pi}$ from Eq. (1.49). We have a narrow peak around the threshold of $K\bar{K}$ similar to the results in the literature [1.73]. We can see clearly the effect of the two different thresholds, at $M_{\pi\pi}$ equal to $2m_{K^+}$ and $2m_{K^0}$, and for the case of the dashed and dotted lines, we also see the cusp effect at $M_{\pi\pi}$ equal to $2\langle m_K \rangle$.

The bump around 980 MeV of $d\Gamma/dM_{\pi\pi}$ is a manifestation of the “good” $f_0(980)$, that can be obtained if one considers the sum of the amplitudes $t_{K^+K^- \rightarrow \pi^+\pi^-}$ and $t_{K^0\bar{K}^0 \rightarrow \pi^+\pi^-}$, with a plus sign, which would be the scattering of $K\bar{K} \rightarrow \pi\pi$ in isospin 0 (similar to the amplitude of Fig. 1.12b). In this work, as in Ref. [1.3], we use a cutoff of 600 MeV to regularize the loops inside and outside the T matrix, which better fits the data and yields the peak position of the $f_0(980)$ in $K\bar{K} \rightarrow \pi\pi$ amplitude at 980 MeV, in agreement with the majority of experimental measurements. This bump can be translated in the direction of the K^+K^- threshold by lowering the cutoff to about 560 MeV, making it less bound and the curve more similar to results of Ref. [1.73], for instance. However, the use of 600 MeV is more appropriate since it is contrasted with the $f_0(980)$ production in isospin-allowed experiments. The shape of Fig. 1.15 also tells us that a very precise measurement of the $\pi^+\pi^-$ invariant mass distribution in the $\chi_{c1} \rightarrow \pi^0 \pi^+ \pi^-$ reaction could help to constrain the model and determine the $f_0(980)$ and $a_0(980)$ parameters precisely.

Another important point to note is that, according to our findings, the isospin breaking inside the T matrix turns out to be more important than from the external kaon loops $G_{K^+K^-}$ and $G_{K^0\bar{K}^0}$, as shown in Fig. 1.15. This seems to go against what one would naturally expect: that regarding the $K\bar{K}$ interaction, the contribution from the external loops would be more significant than the one from the loops inside the T matrix. Actually, this is implicitly assumed in Refs. [1.73, 1.78], since isospin symmetry is assumed for the coupling of the $f_0(980)$ to the K^+K^- and $K^0\bar{K}^0$ components.

To investigate this interesting feature, we look back to Eq. (1.37), where we see that the contribution coming from $\pi^0\eta \rightarrow \pi^+\pi^-$ is:

$$\begin{aligned}\sqrt{3}\pi^0\pi^0\eta &\Rightarrow h_{\pi^0\eta} G_{\pi^0\eta} t_{\pi^0\eta\rightarrow\pi^+\pi^-} \\ &= 2\sqrt{3} G_{\pi^0\eta} t_{\pi^0\eta\rightarrow\pi^+\pi^-},\end{aligned}\tag{1.52}$$

while the contribution coming from $K\bar{K} \rightarrow \pi^+\pi^-$ is:

$$\begin{aligned}3\pi^0\frac{(K^+K^- - K^0\bar{K}^0)}{\sqrt{2}} &\Rightarrow h_{K^+K^-} G_{K^+K^-} t_{K^+K^-\rightarrow\pi^+\pi^-} \\ &\quad + h_{K^0\bar{K}^0} G_{K^0\bar{K}^0} t_{K^0\bar{K}^0\rightarrow\pi^+\pi^-} \\ &= \frac{3}{\sqrt{2}}G_{K^+K^-} t_{K^+K^-\rightarrow\pi^+\pi^-} \\ &\quad - \frac{3}{\sqrt{2}}G_{K^0\bar{K}^0} t_{K^0\bar{K}^0\rightarrow\pi^+\pi^-}.\end{aligned}\tag{1.53}$$

Then we compare in Fig. 1.16 the amplitude square of these two terms. We can see that the $K\bar{K}$ contribution coming from the isospin breaking in $G_{K^+K^-}$ and $G_{K^0\bar{K}^0}$ (blue dotted curve), is indeed greater than the one coming from the isospin breaking inside the T matrix (red dashed curve), and the effect is maximized when isospin symmetry is broken in both (green dash-dotted curve). What happens is that when we violate isospin inside the T matrix, the transition amplitude $t_{\pi^0\eta\rightarrow\pi^+\pi^-}$ becomes nonzero (black solid line), which is even bigger than the contribution of $K\bar{K}$ with isospin breaking only inside the T matrix (red dashed curve), and their combined effect turns out to be greater than the isolated effect from $G_{K^+K^-}$ and $G_{K^0\bar{K}^0}$ (blue dotted curve).

Therefore, we can conclude here that the $K\bar{K}$ contribution is still the dominant term when isospin symmetry is broken both in T and G . However, the effect of isospin-breaking inside the T matrix is of great importance, not just because of the enhancement in the $K\bar{K}$ contribution, but mainly due to the coupled channels interaction that allows the isospin-forbidden $\pi^0\eta \rightarrow \pi^+\pi^-$ transition. This is a novel result which is usually neglected in most of the approaches in the topic of the $a_0(980) - f_0(980)$ mixing.

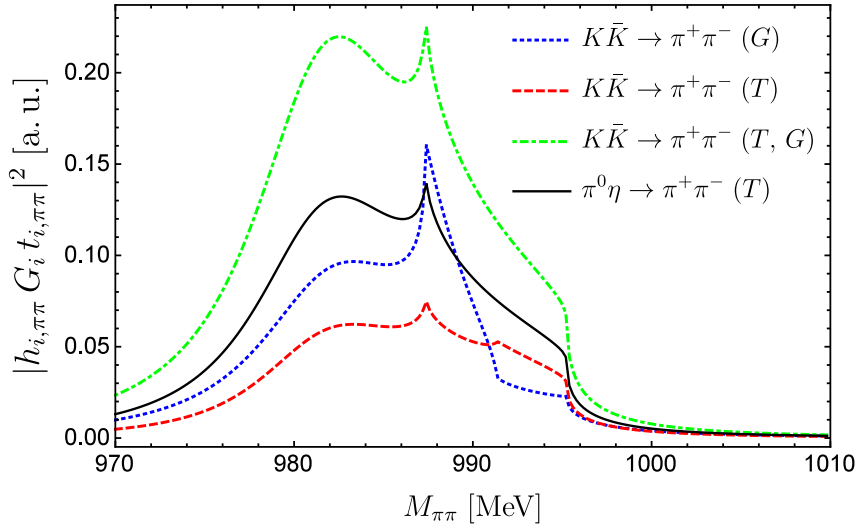


Figure 1.16: Comparison between isolated contribution of $\pi^0\eta \rightarrow \pi^+\pi^-$ and $K\bar{K} \rightarrow \pi^+\pi^-$. (See text for explanations).

Finally, we show in Table 1.1 the results of the $a_0(980) - f_0(980)$ mixing in the $\chi_{c1} \rightarrow \pi^0 \pi^+ \pi^-$ and $\chi_{c1} \rightarrow \pi^0 \pi^0 \eta$ reactions. We calculate it in analogy to Ref. [1.74] (where it is taken as the ratio between the branching ratios of the former to the latter reaction) by integrating the invariant mass distribution $d\Gamma/dM_{\pi\pi}$ and dividing it by the integrated $d\Gamma/dM_{\pi\eta}$, where the latter we calculate in two ways: 1) integrating in the whole mass distribution of the $M_{\pi\eta}$, from $m_\pi + m_\eta$ up to 1200 MeV (around the limit of validity the chiral unitary approach), 2) integrating in the more appropriate range of the $a_0(980)$ resonance, from 885 MeV to 1085 MeV, as done by the BESIII Collaboration in Ref. [1.80] (Section IV.C.2).

Table 1.1: Comparison between experiment and theoretical results for the $a_0(980) - f_0(980)$ mixing in the $\chi_{c1} \rightarrow \pi^0 \pi^+ \pi^-$ and $\chi_{c1} \rightarrow \pi^0 \pi^0 \eta$ reactions.

	$\Gamma(\chi_{c1} \rightarrow \pi^0 \pi^+ \pi^-) / \Gamma(\chi_{c1} \rightarrow \pi^0 \pi^0 \eta)$
BESIII [1.74]	$(0.31 \pm 0.16(\text{stat}) \pm 0.14(\text{sys}) \pm 0.03(\text{para}))\%$
$m_{K^+} \neq m_{K^0}$	$M_{\pi\eta} \in [885, 1085] \text{ MeV}$
in T and G	0.26 %
only in T	0.19 %
only in G	0.05 %
$m_{K^+} \neq m_{K^0}$	$M_{\pi\eta} \in [m_\pi + m_\eta, 1200] \text{ MeV}$
in T and G	0.17 %
only in T	0.12 %
only in G	0.03 %

We can see we get a good agreement with the experimental measurements of BESIII [1.74] only when we introduce isospin breaking inside the T matrix and also in the first external rescattering loops ($G_{K^+K^-}$ and $G_{K^0\bar{K}^0}$). The case where

we use different kaon masses only inside the T matrix is still within the range of the experimental errors, but the one where we consider them only in $G_{K^+K^-}$ and $G_{K^0\bar{K}^0}$ is already outside the range of the experimental errors if they are summed in quadrature, what shows the importance of considering both effects simultaneously. Besides, when we integrate in the more appropriate range of the $a_0(980)$ resonance, from 885 MeV to 1085 MeV as in Ref. [1.80], the results are closer to experiment.

1.3.4 Conclusions

We have shown in the present work that it is possible to use the same theoretical model previously developed to study the $\chi_{c1} \rightarrow \eta\pi^+\pi^-$ reaction [1.3], recently measured by the BESIII Collaboration [1.14], and further explored in the predictions for the $\eta_c \rightarrow \eta\pi^+\pi^-$ reaction [1.1], to study the isospin breaking in the decays $\chi_{c1} \rightarrow \pi^0\pi^+\pi^-$ and $\chi_{c1} \rightarrow \pi^0\pi^0\eta$ and its relation to the $a_0(980) - f_0(980)$ mixing, which was also measured by the BESIII Collaboration [1.74].

We assumed that the χ_{c1} behaves as an $SU(3)$ scalar to find the weight in which trios of pseudoscalars are created, followed by the final state interaction of pairs of mesons to describe how the $a_0(980)$ and $f_0(980)$ are dynamically generated, using the chiral unitary approach in coupled channels. The isospin violation was introduced through the use of different masses for the charged and neutral kaons, either in the propagators of the pairs of mesons created in the χ_{c1} decay, as in the propagators inside the T matrix constructed through the unitarization of the scattering and transition amplitudes of pairs of pseudoscalar mesons.

We have analysed the contribution of each term and found that violating isospin inside the T matrix makes the $\pi^0\eta \rightarrow \pi^+\pi^-$ contribution nonzero, which gives an important contribution to the total amplitude. We also investigated the importance of the isospin breaking from the $K\bar{K}$ term, and found that even though the most important contribution comes from the first rescattering loops, violating isospin inside the T matrix enhances this effect significantly. Also, in the total amplitude the most important effect is the isospin breaking inside the T matrix, due to the constructive sum of $\pi^0\eta \rightarrow \pi^+\pi^-$ and $K\bar{K} \rightarrow \pi^+\pi^-$, which is essential to get a good agreement with the experimental measurement of the mixing [1.74].

Bibliography

- [1.1] V. R. Debastiani, W. H. Liang, J. J. Xie and E. Oset, “Predictions for $\eta_c \rightarrow \eta\pi^+\pi^-$ producing $f_0(500)$, $f_0(980)$ and $a_0(980)$,” Phys. Lett. B **766**, 59 (2017).
- [1.2] M. Bayar and V. R. Debastiani, “ $a_0(980) - f_0(980)$ mixing in $\chi_{c1} \rightarrow \pi^0 f_0(980) \rightarrow \pi^0\pi^+\pi^-$ and $\chi_{c1} \rightarrow \pi^0 a_0(980) \rightarrow \pi^0\pi^0\eta$,” Phys. Lett. B **775**, 94 (2017).
- [1.3] W. H. Liang, J. J. Xie and E. Oset, “ $f_0(500)$, $f_0(980)$ and $a_0(980)$ production in the $\chi_{c1} \rightarrow \eta\pi^+\pi^-$ reaction,” Eur. Phys. J. C **76**, 700 (2016).
- [1.4] S. Scherer and M. R. Schindler, “A Primer for Chiral Perturbation Theory,” Lect. Notes Phys. **830**, pp.1 (2012).
- [1.5] A. Pich, “Effective field theory: Course,” hep-ph/9806303.
- [1.6] A. Pich, “Effective Field Theory with Nambu-Goldstone Modes,” arXiv:1804.05664 [hep-ph].
- [1.7] J. A. Oller and E. Oset, “Chiral symmetry amplitudes in the S wave isoscalar and isovector channels and the sigma, $f_0(980)$, $a_0(980)$ scalar mesons,” Nucl. Phys. A **620**, 438 (1997) [Erratum-ibid. A **652**, 407 (1999)].
- [1.8] J. A. Oller, Ulf-G. Meißner, “Chiral dynamics in the presence of bound states: Kaon nucleon interactions revisited,” Phys. Lett. B **500**, 263 (2001).
- [1.9] W. H. Liang and E. Oset, “ B^0 and B_s^0 decays into $J/\psi f_0(980)$ and $J/\psi f_0(500)$ and the nature of the scalar resonances,” Phys. Lett. B **737**, 70 (2014).
- [1.10] J. J. Xie, L. R. Dai and E. Oset, “The low lying scalar resonances in the D^0 decays into K_s^0 and $f_0(500)$, $f_0(980)$, $a_0(980)$,” Phys. Lett. B **742**, 363 (2015).
- [1.11] M. Kornicer [BESIII Collaboration], “Studying $\chi_{c1} \rightarrow \eta\pi^+\pi^-$ decays at BE-SIII,” AIP Conf. Proc. **1735**, 050011 (2016).
- [1.12] A. Bramon, A. Grau and G. Pancheri, “Intermediate vector meson contributions to $V0 \rightarrow P0 P0$ gamma decays,” Phys. Lett. B **283**, 416 (1992).
- [1.13] F. Ambrosino et al., “A Global fit to determine the pseudoscalar mixing angle and the gluonium content of the eta-prime meson,” JHEP **0907**, 105 (2009).
- [1.14] M. Ablikim et al. [BESIII Collaboration], “Amplitude analysis of the $\chi_{c1} \rightarrow \eta\pi^+\pi^-$ decays,” Phys. Rev. D **95**, 032002 (2017).
- [1.15] E. Klempt and A. Zaitsev, “Glueballs, Hybrids, Multiquarks. Experimental facts versus QCD inspired concepts,” Phys. Rept. **454**, 1 (2007).
- [1.16] E. van Beveren, T. A. Rijken, K. Metzger, C. Dullemond, G. Rupp and J. E. Ribeiro, “A Low Lying Scalar Meson Nonet in a Unitarized Meson Model,” Z. Phys. C **30**, 615 (1986).

- [1.17] N. A. Tornqvist and M. Roos, “*Resurrection of the sigma meson,*” Phys. Rev. Lett. **76**, 1575 (1996).
- [1.18] A. H. Fariborz, R. Jora and J. Schechter, “*Global aspects of the scalar meson puzzle,*” Phys. Rev. D **79**, 074014 (2009).
- [1.19] A. H. Fariborz, N. W. Park, J. Schechter and M. Naeem Shahid, “*Gauged linear sigma model and pion-pion scattering,*” Phys. Rev. D **80**, 113001 (2009).
- [1.20] J. R. Pelaez, “*From controversy to precision on the sigma meson: a review on the status of the non-ordinary $f_0(500)$ resonance,*” Phys. Rept. **658**, 1 (2016).
- [1.21] S. Weinberg, “*Phenomenological Lagrangians,*” Physica A **96**, 327 (1979).
- [1.22] J. Gasser and H. Leutwyler, “*Chiral Perturbation Theory to One Loop,*” Annals Phys. **158**, 142 (1984).
- [1.23] V. Bernard, N. Kaiser and U. G. Meißner, “*Chiral dynamics in nucleons and nuclei,*” Int. J. Mod. Phys. E **4**, 193 (1995).
- [1.24] A. Dobado and J. R. Pelaez, “*The Inverse amplitude method in chiral perturbation theory,*” Phys. Rev. D **56**, 3057 (1997).
- [1.25] J. R. Pelaez and G. Rios, “*Nature of the $f_0(600)$ from its $N(c)$ dependence at two loops in unitarized Chiral Perturbation Theory,*” Phys. Rev. Lett. **97**, 242002 (2006).
- [1.26] J. A. Oller, E. Oset and J. R. Pelaez, “*Meson meson interaction in a nonperturbative chiral approach,*” Phys. Rev. D **59**, 074001 (1999); Erratum: [Phys. Rev. D **60**, 099906 (1999)]; Erratum: [Phys. Rev. D **75**, 099903 (2007)].
- [1.27] N. Kaiser, “ *$\pi\pi S$ wave phase shifts and nonperturbative chiral approach,*” Eur. Phys. J. A **3**, 307 (1998).
- [1.28] M. P. Locher, V. E. Markushin and H. Q. Zheng, “*Structure of $f_0(980)$ from a coupled channel analysis of S wave $\pi\pi$ scattering,*” Eur. Phys. J. C **4**, 317 (1998).
- [1.29] J. Nieves and E. Ruiz Arriola, “*Bethe-Salpeter approach for unitarized chiral perturbation theory,*” Nucl. Phys. A **679**, 57 (2000).
- [1.30] J. A. Oller, E. Oset and A. Ramos, “*Chiral unitary approach to meson meson and meson - baryon interactions and nuclear applications,*” Prog. Part. Nucl. Phys. **45**, 157 (2000).
- [1.31] E. Oset *et al.*, “*Weak decays of heavy hadrons into dynamically generated resonances,*” Int. J. Mod. Phys. E **25**, 1630001 (2016).
- [1.32] B. Ananthanarayan, G. Colangelo, J. Gasser and H. Leutwyler, “*Roy equation analysis of $\pi\pi$ scattering,*” Phys. Rept. **353**, 207 (2001).

- [1.33] R. Garcia-Martin, R. Kaminski, J. R. Pelaez, J. Ruiz de Elvira and F. J. Yndurain, “*The Pion-pion scattering amplitude. IV: Improved analysis with once subtracted Roy-like equations up to 1100 MeV,*” *Phys. Rev. D* **83**, 074004 (2011).
- [1.34] R. L. Jaffe, “*Multi-Quark Hadrons. 1. The Phenomenology of (2 Quark 2 anti-Quark) Mesons,*” *Phys. Rev. D* **15**, 267 (1977); “*Multi-Quark Hadrons. 2. Methods,*” *Phys. Rev. D* **15**, 281 (1977).
- [1.35] J. M. Dias, F. S. Navarra, M. Nielsen and E. Oset, “ *$f_0(980)$ production in $D_s^+ \rightarrow \pi^+ \pi^+ \pi^-$ and $D_s^+ \rightarrow \pi^+ K^+ K^-$ decays,*” *Phys. Rev. D* **94**, 096002 (2016).
- [1.36] J. J. Xie, W. H. Liang and E. Oset, “ *\bar{K} -induced formation of the $f_0(980)$ and $a_0(980)$ resonances on proton targets,*” *Phys. Rev. C* **93**, 035206 (2016).
- [1.37] W. H. Liang, J. J. Xie and E. Oset, “ *\bar{B}^0 decay into D^0 and $f_0(500)$, $f_0(980)$, $a_0(980)$, ρ and \bar{B}_s^0 decay into D^0 and $\kappa(800)$, K^{*0} ,*” *Phys. Rev. D* **92**, 034008 (2015).
- [1.38] M. Tanabashi *et al.* [Particle Data Group], “*Review of Particle Physics,*” *Phys. Rev. D* **98**, 030001 (2018).
- [1.39] E. Byckling and K. Kajantie, “*Particle Kinematics*”, John Wiley and Sons, (1973).
- [1.40] M. Ablikim *et al.* [BESIII Collaboration], “*Observation of $a_0^0(980)$ - $f_0(980)$ Mixing,*” *Phys. Rev. Lett.* **121**, 022001 (2018).
- [1.41] J. D. Weinstein and N. Isgur, “*The $q q$ anti- q anti- q System in a Potential Model,*” *Phys. Rev. D* **27**, 588 (1983).
- [1.42] S. Godfrey and N. Isgur, “*Mesons in a Relativized Quark Model with Chromodynamics,*” *Phys. Rev. D* **32**, 189 (1985).
- [1.43] J. D. Weinstein and N. Isgur, “ *K anti- K Molecules,*” *Phys. Rev. D* **41**, 2236 (1990).
- [1.44] E. van Beveren, D. V. Bugg, F. Kleefeld and G. Rupp, “*The Nature of σ , κ , $a(0)(980)$ and $f(0)(980)$,*” *Phys. Lett. B* **641**, 265 (2006).
- [1.45] F. K. Guo, C. Hanhart, U. G. Meißner, Q. Wang, Q. Zhao and B. S. Zou, “*Hadronic molecules,*” *Rev. Mod. Phys.* **90**, 015004 (2018).
- [1.46] N. N. Achasov and V. V. Gubin, “*Search for the scalar a_0 and f_0 mesons in the reactions $e + e^- \rightarrow \gamma \pi^0 \pi^0$ (η),*” *Phys. Rev. D* **56**, 4084 (1997).
- [1.47] N. N. Achasov, S. A. Devyanin and G. N. Shestakov, “*The S^* Delta0 Mixing as the Threshold Phenomenon,*” *Phys. Lett.* **88B**, 367 (1979).
- [1.48] O. Krehl, R. Rapp and J. Speth, “*Meson meson scattering: K anti- K thresholds and $f_0(980)$ - $a_0(980)$ mixing,*” *Phys. Lett. B* **390**, 23 (1997).

- [1.49] M. Ablikim *et al.* [BESIII Collaboration], “*First observation of $\eta(1405)$ decays into $f_0(980)\pi^0$* ,” Phys. Rev. Lett. **108**, 182001 (2012).
- [1.50] F. Aceti, W. H. Liang, E. Oset, J. J. Wu and B. S. Zou, “*Isospin breaking and $f_0(980)$ - $a_0(980)$ mixing in the $\eta(1405) \rightarrow \pi^0 f_0(980)$ reaction*,” Phys. Rev. D **86**, 114007 (2012).
- [1.51] J. J. Wu, X. H. Liu, Q. Zhao and B. S. Zou, “*The Puzzle of anomalously large isospin violations in $\eta(1405/1475) \rightarrow 3\pi$* ,” Phys. Rev. Lett. **108**, 081803 (2012).
- [1.52] X. G. Wu, J. J. Wu, Q. Zhao and B. S. Zou, “*Understanding the property of $\eta(1405/1475)$ in the J/ψ radiative decay*,” Phys. Rev. D **87**, 014023 (2013).
- [1.53] N. N. Achasov, A. A. Kozhevnikov and G. N. Shestakov, “*Isospin breaking decay $\eta(1405) \rightarrow f_0(980)\pi^0 \rightarrow 3\pi$* ,” Phys. Rev. D **92**, 036003 (2015).
- [1.54] F. Aceti, J. M. Dias and E. Oset, “ *$f_1(1285)$ decays into $a_0(980)\pi^0$, $f_0(980)\pi^0$ and isospin breaking*,” Eur. Phys. J. A **51**, 48 (2015).
- [1.55] N. N. Achasov, A. A. Kozhevnikov and G. N. Shestakov, “*Mechanisms of the isospin-breaking decay $f_1(1285) \rightarrow f_0(980)\pi^0 \rightarrow \pi^+\pi^-\pi^0$* ,” Phys. Rev. D **93**, 114027 (2016).
- [1.56] S. Sakai, E. Oset and W. H. Liang, “*Abnormal isospin violation and $a_0 - f_0$ mixing in the $D_s^+ \rightarrow \pi^+\pi^0 a_0(980)(f_0(980))$ reactions*,” Phys. Rev. D **96**, 074025 (2017).
- [1.57] N. N. Achasov and G. N. Shestakov, “*Manifestations of the $a_0^0(980) - f_0(980)$ mixing in $D^0 \rightarrow K_S^0\pi^+\pi^-$ and $D^0 \rightarrow K_S^0\eta\pi^0$ decays*,” Phys. Rev. D **96**, 016027 (2017).
- [1.58] N. N. Achasov and G. N. Shestakov, “*Interference phenomena in the decay $D_s^+ \rightarrow \eta\pi^0\pi^+$ induced by the $a_0^0(980) - f_0(980)$ mixing*,” Phys. Rev. D **96**, 036013 (2017).
- [1.59] W. Wang, “*Search for the $a_0(980) - f_0(980)$ mixing in weak decays of D_s/B_s mesons*,” Phys. Lett. B **759**, 501 (2016).
- [1.60] F. E. Close and A. Kirk, “*Isospin breaking exposed in $f_0(980) - a_0(980)$ mixing*,” Phys. Lett. B **489**, 24 (2000).
- [1.61] J. J. Wu, Q. Zhao and B. S. Zou, “*Possibility of measuring $a_0(980)$ - $f_0(980)$ mixing from $J/\psi \rightarrow \phi a_0(980)$* ,” Phys. Rev. D **75**, 114012 (2007).
- [1.62] F. E. Close and A. Kirk, “*Large isospin mixing in ϕ radiative decay and the spatial size of the $f_0(980) - a_0(980)$ mesons*,” Phys. Lett. B **515**, 13 (2001).
- [1.63] N. N. Achasov and A. V. Kiselev, “*Once more on mixing of the $a_0(980)$ and $f_0(980)$ mesons*,” Phys. Lett. B **534**, 83 (2002).

- [1.64] B. Kerbikov and F. Tabakin, “*Mixing of the $f(0)$ and $a(0)$ scalar mesons in threshold photoproduction,*” *Phys. Rev. C* **62**, 064601 (2000).
- [1.65] S. V. Donskov, A. K. Likhoded, A. V. Luchinsky and V. D. Samoylenko, “*Scalar mesons in η -prime $\rightarrow \eta \pi^0 \pi^0$ decay,*” *Central Eur. J. Phys.* **8**, 393 (2010).
- [1.66] A. K. Likhoded, A. V. Luchinsky and V. D. Samoylenko, “*Scalar Mesons in $\eta' \rightarrow 3\pi^0, \pi^0\pi^+\pi^-$ Decays,*” *Phys. Atom. Nucl.* **73**, 1789 (2010).
- [1.67] M. Ablikim *et al.* [BESIII Collaboration], “*Amplitude Analysis of the Decays $\eta' \rightarrow \pi^+\pi^-\pi^0$ and $\eta' \rightarrow \pi^0\pi^0\pi^0$,*” *Phys. Rev. Lett.* **118**, 012001 (2017).
- [1.68] M. Albaladejo and B. Moussallam, “*Extended chiral Khuri-Treiman formalism for $\eta \rightarrow 3\pi$ and the role of the $a_0(980)$, $f_0(980)$ resonances,*” *Eur. Phys. J. C* **77**, 508 (2017).
- [1.69] A. E. Kudryavtsev and V. E. Tarasov, “*On the possibility of observation of $a0 - f0$ mixing in the $p n \rightarrow d a0$ reaction,*” *JETP Lett.* **72**, 410 (2000); [*Pisma Zh. Eksp. Teor. Fiz.* **72**, 589 (2000)].
- [1.70] V. Y. Grishina, L. A. Kondratyuk, M. Buescher, W. Cassing and H. Stroher, “ *$A0(980) - f0(980)$ mixing and isospin violation in the reactions $p N \rightarrow d A0$, $p d \rightarrow He-3 / H-3 A0$ and $d d \rightarrow He-4 A0$,*” *Phys. Lett. B* **521**, 217 (2001).
- [1.71] N. N. Achasov and G. N. Shestakov, “*To search for $a0(0)(980) - f0(980)$ mixing in polarization phenomena,*” *Phys. Rev. Lett.* **92**, 182001 (2004).
- [1.72] C. Hanhart, B. Kubis and J. R. Pelaez, “*Investigation of $a0-f0$ mixing,*” *Phys. Rev. D* **76**, 074028 (2007).
- [1.73] J. J. Wu and B. S. Zou, “*Study $a0(0)(980) - f(0)(980)$ mixing from $a0(0)(980) \rightarrow f(0)(980)$ transition,*” *Phys. Rev. D* **78**, 074017 (2008).
- [1.74] M. Ablikim *et al.* [BESIII Collaboration], “*Study of $a_0^0(980) - f_0(980)$ mixing,*” *Phys. Rev. D* **83**, 032003 (2011).
- [1.75] M. Ablikim *et al.* [BES Collaboration], “*Resonances in $J / \psi \rightarrow \phi \pi^+ \pi^-$ and $\phi \pi^+ K^-$,*” *Phys. Lett. B* **607**, 243 (2005).
- [1.76] S. B. Athar *et al.* [CLEO Collaboration], “ *χ_{cJ} Decays to $h^+ h^- h^0$,*” *Phys. Rev. D* **75**, 032002 (2007).
- [1.77] L. Roca, “*Isospin violation in $J/\Psi \rightarrow \phi \pi^0 \eta$ decay and the $f_0 - a_0$ mixing,*” *Phys. Rev. D* **88**, 014045 (2013).
- [1.78] T. Sekihara and S. Kumano, “*Constraint on $K \bar{K}$ compositeness of the $a_0(980)$ and $f_0(980)$ resonances from their mixing intensity,*” *Phys. Rev. D* **92**, 034010 (2015).

- [1.79] V. R. Debastiani, W. H. Liang, J. J. Xie and E. Oset, “Production of $f_0(500)$, $f_0(980)$ and $a_0(980)$ in the $\chi_{c1} \rightarrow \eta\pi^+\pi^-$ and $\eta_c \rightarrow \eta\pi^+\pi^-$ Decay,” Acta Phys. Polon. Supp. **10**, 1067 (2017).
- [1.80] M. Ablikim *et al.*, “Measurements of $\psi(2S)$ decays into gamma K anti- K π and gamma eta π^+ π^- ,” Phys. Rev. D **74**, 072001 (2006).

In this chapter we will present three works on meson-baryon interactions: the one of Ref. [2.1] on the five new Ω_c states recently discovered by the LHCb Collaboration [2.2], the follow-up article of Ref. [2.3] on how to observe these states in the decay of Ω_b baryons and the one of Ref. [2.4] with predictions for molecular Ω_b states.

2.1 Introduction

In this section we will comment on two approaches which are useful to describe the meson-baryon states, either using the chiral Lagrangians or the local hidden gauge, and briefly discuss their relation, with focus on the particular case where certain simplifications can be made and the interactions can be obtained at quark level. Also, in section 2.1.3 we will present how the mass, width and couplings of each state are related to the pole position.

2.1.1 Chiral Lagrangians

The lowest order chiral Lagrangian describing the meson-baryon interaction in the $SU(3)$ sector (pseudoscalar meson octet with the $1/2^+$ baryon octet) is given by [2.5–2.7]

$$\mathcal{L}^B = \langle \bar{B} i \gamma^\mu \nabla_\mu B \rangle - M_B \langle \bar{B} B \rangle + \frac{1}{2} D \langle \bar{B} \gamma^\mu \gamma_5 \{u_\mu, B\} \rangle + \frac{1}{2} F \langle \bar{B} \gamma^\mu \gamma_5 [u_\mu, B] \rangle \quad (2.1)$$

where $\langle \rangle$ stands for trace in $SU(3)$ and

$$\begin{aligned} \nabla_\mu B &= \partial_\mu B + [\Gamma_\mu, B], \\ \Gamma_\mu &= \frac{1}{2} (u^\dagger \partial_\mu u + u \partial_\mu u^\dagger), \\ U &= u^2 = \exp(i\sqrt{2}\Phi/f_\pi), \\ u_\mu &= iu^\dagger \partial_\mu U u^\dagger. \end{aligned} \quad (2.2)$$

Here $f_\pi = 93$ MeV is the pion decay constant, and Φ and B are the $SU(3)$ matrices for the mesons and baryons

$$\Phi = \begin{pmatrix} \frac{1}{\sqrt{2}}\pi^0 + \frac{1}{\sqrt{6}}\eta & & & \\ & \pi^- & & \\ & & -\frac{1}{\sqrt{2}}\pi^0 + \frac{1}{\sqrt{6}}\eta & \\ & & & \bar{K}^0 & \\ & & & & K^+ \\ & & & & & K^0 \\ & & & & & & -\frac{2}{\sqrt{6}}\eta \end{pmatrix}, \quad (2.3)$$

$$B = \begin{pmatrix} \frac{1}{\sqrt{2}}\Sigma^0 + \frac{1}{\sqrt{6}}\Lambda & \Sigma^+ & p \\ \Sigma^- & -\frac{1}{\sqrt{2}}\Sigma^0 + \frac{1}{\sqrt{6}}\Lambda & n \\ \Xi^- & \Xi^0 & -\frac{2}{\sqrt{6}}\Lambda \end{pmatrix}. \quad (2.4)$$

At lowest order in momentum the interaction comes from the Γ_μ term in the covariant derivative, and the Lagrangian reads

$$\mathcal{L}_1^B = \frac{1}{4f_\pi^2} \langle \bar{B}i\gamma^\mu [(\Phi \partial_\mu \Phi - \partial_\mu \Phi \Phi)B - B(\Phi \partial_\mu \Phi - \partial_\mu \Phi \Phi)] \rangle, \quad (2.5)$$

The lowest order amplitudes are of the form

$$V_{ij} = -C_{ij} \frac{1}{4f_\pi^2} \bar{u}(p')\gamma^\mu u(p)(k_\mu + k'_\mu), \quad (2.6)$$

where p, p' are the incoming and outgoing momentum of the baryons and k, k' of the mesons.

At energies close to threshold one can consider only the dominant contribution coming from ∂_0 and γ^0 [2.8], such that the interaction is given by

$$V_{ij} = -C_{ij} \frac{1}{4f_\pi^2} (k^0 + k'^0), \quad (2.7)$$

where k^0, k'^0 are the energies of the incoming and outgoing mesons, respectively,

$$k^0 = \frac{s + m_{m_i}^2 - M_{B_i}^2}{2\sqrt{s}}, \quad k'^0 = \frac{s + m_{m_j}^2 - M_{B_j}^2}{2\sqrt{s}} \quad (2.8)$$

where m_{m_i}, M_{B_i} (m_{m_j}, M_{B_j}) are the masses of the initial (final) meson, baryon, respectively, and C_{ij} are the coefficients one has to calculate, which are tabulated in Ref. [2.6] for the case of K^-p and coupled channels (note that C is a symmetric matrix where C_{ij} corresponds to the transition $(m_i, B_i) \rightarrow (m_j, B_j)$). The extension of Eq. (2.7) to the charm sector is complicated. Yet, using the local hidden gauge approach [2.9–2.13] the task is notably simplified and clarified simultaneously.

2.1.2 Local Hidden Gauge approach

In the hidden gauge approach [2.9–2.13] the meson-baryon interaction in $SU(3)$ is obtained exchanging vector mesons as in Fig. 2.1.

The local hidden gauge approach works with pseudoscalar and vector mesons in the light sector and chiral symmetry is one of its assets, showing up in the limit of small mass of the pseudoscalar mesons (Goldstone bosons). In Refs. [2.9–2.14], and particularly in Refs. [2.9, 2.14], one can see that the terms of the chiral Lagrangians can be obtained from the exchange of vector mesons in the local hidden gauge. Ref. [2.14] also shows that the consideration of vector mesons is necessary to implement vector meson dominance. Both in Ref. [2.14] and Ref. [2.9] it is also shown that the formalisms using antisymmetric tensors for the vector mesons, and the use of ordinary vector fields in the local hidden gauge are equivalent. If one

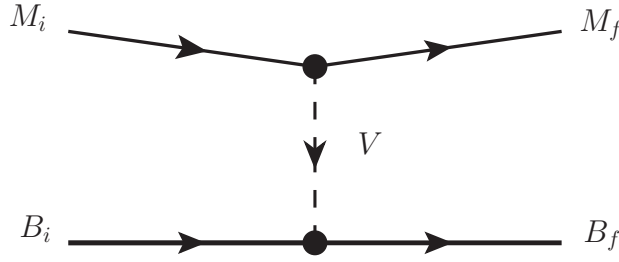


Figure 2.1: Diagram representing the meson-baryon interaction through vector meson exchange. $M_i(M_f)$ and $B_i(B_f)$ are the initial (final) meson and baryon states involved the interaction, while V stands for the vector meson exchanged.

specifies to the meson-baryon Lagrangians [2.5], it is easy to show that the exchange of vector mesons gives rise exactly to the lowest order chiral Lagrangian in the limit of small momentum transfer compared to the vector meson mass. All this occurs within $SU(3)$, involving u, d, s quarks. The local hidden gauge in the unitary gauge in $SU(3)$, can be found in Ref. [2.9] and with more detail in Ref. [2.10].

The ingredients needed are the vector(V)-pseudoscalar(P)-pseudoscalar(P) Lagrangian for the upper vertex on Fig. 2.1

$$\mathcal{L}_{VPP} = -ig \langle [\Phi, \partial_\mu \Phi] V^\mu \rangle, \quad (2.9)$$

with

$$V_\mu = \begin{pmatrix} \frac{1}{\sqrt{2}}\rho^0 + \frac{1}{\sqrt{2}}\omega & \rho^+ & K^{*+} \\ \rho^- & -\frac{1}{\sqrt{2}}\rho^0 + \frac{1}{\sqrt{2}}\omega & K^{*0} \\ K^{*-} & \bar{K}^{*0} & \phi \end{pmatrix}_\mu, \quad (2.10)$$

and the vector(V)-baryon(B)-baryon(B) Lagrangian for the lower vertex on Fig. 2.1

$$\mathcal{L}_{VBB} = g \left(\langle \bar{B} \gamma_\mu [V^\mu, B] \rangle + \langle \bar{B} \gamma_\mu B \rangle \langle V^\mu \rangle \right), \quad (2.11)$$

with $g = m_V/2f_\pi$ and m_V the mass of the vector mesons (we take an average of about 800 MeV).

In Fig. 2.2 we can see three examples of diagrams representing vector meson exchange in $SU(3)$. Note that in diagrams of the type (a) we only exchange light quarks u, d , through ρ and ω exchange while in diagrams of the type (b) a s quark is transferred through K^* exchange (in this case from the K meson to the Σ baryon) and in diagrams of the type (c) u, d and s quarks are exchanged both ways through ρ, ω and ϕ exchange.

It is easy to prove that the picture of the vector meson exchange with the Lagrangians from Eqs. (2.9) and (2.11) gives rise to the same interaction as Eq. (2.7) taking $q^2/m_V^2 \rightarrow 0$ in the propagator of the exchanged vector, which is quite good at low energies. One can even keep this term in the propagator, as done in Ref. [2.15], since in the meson-meson sector this is shown to generate higher order terms of the Lagrangian [2.9, 2.14]. Yet, if one takes a regulator of the loops integrating to a value $|\vec{q}_{max}|$ and fitting this to data, the consideration of the q^2/m_V^2 terms in the vector propagator is unnecessary.

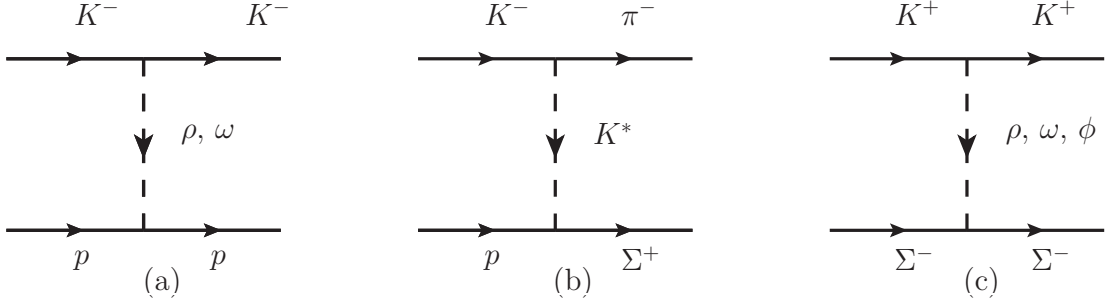


Figure 2.2: Example of diagrams of vector exchange in the meson-baryon interaction.

Extending Eqs. (2.9) and (2.11) to the charm sector is easy for the VPP Lagrangian, as we will discuss in section 2.2.2, but not for the VBB Lagrangian [2.16]. However, we introduce here a procedure that renders it very easy. For this, let us look at the quark structure of the ρ^0 , ω and ϕ (which can be extended to K^* , ρ^\pm)

$$\begin{aligned}\rho^0 &= \frac{1}{\sqrt{2}}(u\bar{u} - d\bar{d}), \\ \omega &= \frac{1}{\sqrt{2}}(u\bar{u} + d\bar{d}), \\ \phi &= s\bar{s}.\end{aligned}\tag{2.12}$$

In the approximation of taking $\gamma^\mu \rightarrow \gamma^0$ the spin dependence disappears, and we can consider an operator at the quark level as in Eq. (2.12).

Let us analyse the vector(V)-baryon(B)-baryon(B) vertex for $p\rho^0p$ at quark level. First we write the proton wave function using $SU(3)$ symmetry:

$$p = \frac{1}{\sqrt{2}}|\phi_{MS}\chi_{MS} + \phi_{MA}\chi_{MA}\rangle,\tag{2.13}$$

where ϕ_{MS} , ϕ_{MA} , χ_{MS} , χ_{MA} are the flavor and spin mixed symmetric and mixed antisymmetric wave functions for the proton [2.17].

Then we take

$$\langle p|g\rho^0|p\rangle \equiv \frac{1}{\sqrt{2}}\frac{1}{\sqrt{2}}\langle\phi_{MS}\chi_{MS} + \phi_{MA}\chi_{MA}|g\frac{1}{\sqrt{2}}(u\bar{u} - d\bar{d})|\phi_{MS}\chi_{MS} + \phi_{MA}\chi_{MA}\rangle,\tag{2.14}$$

where the vector meson ρ^0 will act on the proton wave function as an operator creating and destroying u and d quarks.

The spin 1/2 wave functions, with the symmetric/antisymmetric part on the first two quarks, are given by

$$\chi_{MS} = -\frac{1}{\sqrt{6}}(\uparrow\downarrow\uparrow + \downarrow\uparrow\uparrow - 2\uparrow\uparrow\downarrow), \quad \text{for } S_z = 1/2,\tag{2.15}$$

and

$$\chi_{MA} = \frac{1}{\sqrt{2}}(\uparrow\downarrow - \downarrow\uparrow)\uparrow, \quad \text{for } S_z = 1/2. \quad (2.16)$$

We should note the fact that these wave functions are orthonormal, i. e., $\langle\chi_{MS}|\chi_{MS}\rangle = \langle\chi_{MA}|\chi_{MA}\rangle = 1$ and $\langle\chi_{MA}|\chi_{MS}\rangle = 0$.

Now for the proton we have

$$\Phi_{MS} = \frac{1}{\sqrt{6}}[(ud + du)u - 2uud], \quad (2.17)$$

$$\Phi_{MA} = \frac{1}{\sqrt{2}}[(ud - du)u], \quad (2.18)$$

Taking into account that the mixed-symmetric and mixed-antisymmetric flavor wave functions are also orthonormal, we will get

$$\langle p|\rho^0|p\rangle = \frac{1}{2}\{\langle\Phi_{MS}|\rho^0|\Phi_{MS}\rangle + \langle\Phi_{MA}|\rho^0|\Phi_{MA}\rangle\} \quad (2.19)$$

where we have dropped the coupling g to simplify the notation.

Then

$$\begin{aligned} \langle p|\rho^0|p\rangle = & \frac{1}{2}\left\{\frac{\langle(ud + du)u - 2uud|(u\bar{u} - d\bar{d})|(ud + du)u - 2uud\rangle}{\sqrt{6}\sqrt{2}\sqrt{6}} \right. \\ & \left. + \frac{\langle(ud - du)u|(u\bar{u} - d\bar{d})|(ud - du)u\rangle}{\sqrt{2}\sqrt{2}\sqrt{2}}\right\} \end{aligned} \quad (2.20)$$

We can think of the $q\bar{q}$ of the vector mesons as the operator $a_q^\dagger a_q$ that destroys and creates a q quark. Then we get

$$\begin{aligned} \langle p|\rho^0|p\rangle &= \frac{1}{2}\left\{\langle\Phi_{MS}|\frac{(2-1)}{\sqrt{2}}|\Phi_{MS}\rangle + \langle\Phi_{MA}|\frac{(2-1)}{\sqrt{2}}|\Phi_{MA}\rangle\right\} \\ &= \frac{1}{2}\frac{1}{\sqrt{2}}\left\{\langle\Phi_{MS}|\Phi_{MS}\rangle + \langle\Phi_{MA}|\Phi_{MA}\rangle\right\} \end{aligned} \quad (2.21)$$

So this vertex will be proportional to

$$\langle p|\rho^0|p\rangle = \frac{1}{\sqrt{2}} \quad (2.22)$$

Similarly, for the neutron we would get

$$\Phi_{MS} = -\frac{1}{\sqrt{6}}[(ud + du)d - 2ddu], \quad (2.23)$$

$$\Phi_{MA} = \frac{1}{\sqrt{2}}[(ud - du)d]. \quad (2.24)$$

Then instead of $(2-1)$ we would get $(1-2)$, since now we have one u quark and two d quarks, then we would have

$$\langle n|\rho^0|n\rangle = -\frac{1}{\sqrt{2}} \quad (2.25)$$

We can also have ω exchange. According to Eq. (2.12), we see that we would get $(2 + 1)$ for the $p\omega p$ vertex instead of $(2 - 1)$ that we got for the $p\rho^0 p$ vertex.

$$\langle p | \omega | p \rangle = \frac{3}{\sqrt{2}} \quad (2.26)$$

Since $\phi = s\bar{s}$ and there is no s quarks in the proton wave function, we immediately see there is no contribution from ϕ exchange.

$$\langle p | \phi | p \rangle = 0 \quad (2.27)$$

Now let us calculate the same vertex $\langle p | \rho^0 | p \rangle$ and $\langle p | \omega | p \rangle$ using the Hidden Gauge Lagrangian from Eq. (2.11).

Using the approximation of taking only the γ_0 and δ_0 contribution, and the matrices B and V from Eqs. (2.4) and (2.10), the first term $\langle \bar{B} \gamma_\mu [V^\mu, B] \rangle$ will contribute with

$$\left(\frac{1}{\sqrt{2}} \rho^0 + \frac{1}{\sqrt{2}} \omega \right) - \phi, \quad (2.28)$$

whereas the term $\langle \bar{B} \gamma_\mu B \rangle \langle V^\mu \rangle$ will contribute with

$$\left(\frac{1}{\sqrt{2}} \rho^0 + \frac{1}{\sqrt{2}} \omega \right) + \left(-\frac{1}{\sqrt{2}} \rho^0 + \frac{1}{\sqrt{2}} \omega \right) + \phi = \frac{2}{\sqrt{2}} \omega + \phi. \quad (2.29)$$

So, the total contribution using the Hidden Gauge Lagrangian from Eq. (2.11) will be

$$\frac{1}{\sqrt{2}} \rho^0 + \frac{3}{\sqrt{2}} \omega \quad (2.30)$$

As we had in Eqs. (2.22), (2.26) and (2.27) using the quark operator in the baryon wave functions.

As we have illustrated with this example, one gets the same result using the method at quark level as using the Hidden Gauge Lagrangian from Eq. (2.11), and this is also the case for all transitions in coupled channels.

This artifact can be very useful, in fact, as we will discuss in detail in section 2.2.2, we can also use the operator at quark level to obtain the VBB vertex in the charm sector.

Finally, let us mention that if we have vector mesons instead of pseudoscalars, i.e., for $VB \rightarrow VB$ transitions the only difference is that now we have the VVV vertex instead of VPP one, and it can be evaluated using the following Lagrangian

$$\mathcal{L}_{VVV} = ig \langle [V^\mu, \partial_\nu V_\mu] V^\nu \rangle, \quad (2.31)$$

with the coupling g the same as in Eq. (2.9). In the case where the three-momentum of the vector meson is neglected versus the vector meson mass, as we also do here, only $\nu = 0$ contributes in Eq. (2.31) which forces V^ν to be the exchanged vector, and the structure of the vertex is identical to the one of Eq. (2.9) for pseudoscalars, with the additional factor $\vec{\epsilon} \cdot \vec{\epsilon}'$, with $\vec{\epsilon}$, $\vec{\epsilon}'$ the polarization vectors of the external vector mesons [2.18]. Following this procedure we can calculate all the transition amplitudes.

2.1.3 Poles and couplings

Once we have a method to describe the meson-baryon interaction, which could be of the form of Eq. (2.7) for instance, then we proceed to find the amplitude using the on-shell factorized Bethe-Salpeter equation [2.19, 2.20], as we had in chapter 1 section 1.1.1,

$$T = [1 - VG]^{-1} V, \quad (2.32)$$

with G the meson-baryon loop function.

We choose to regularize it with the cutoff method to avoid potential pathologies of the dimensional regularization in the charm sector, which we will investigate in the next section 2.2, where G can become positive below threshold (and eventually produce bound states with a repulsive potential) [2.21]. There is another reason, because in order to respect rules of heavy quark symmetry in bound states, it was shown in Refs. [2.15, 2.22] that the same cutoff has to be used in all cases. Alternatively one can use a special G function defined in Ref. [2.23].

The G function for meson-baryon with the cutoff method is given by

$$\begin{aligned} G_l &= i \int \frac{d^4 q}{(2\pi)^4} \frac{M_l}{E_l(\mathbf{q})} \frac{1}{k^0 + p^0 - q^0 - E_l(\mathbf{q}) + i\epsilon} \frac{1}{\mathbf{q}^2 - m_l^2 + i\epsilon} \\ &= \int_{|\mathbf{q}| < q_{max}} \frac{d^3 q}{(2\pi)^3} \frac{1}{2\omega_l(\mathbf{q})} \frac{M_l}{E_l(\mathbf{q})} \frac{1}{k^0 + p^0 - \omega_l(\mathbf{q}) - E_l(\mathbf{q}) + i\epsilon}, \end{aligned} \quad (2.33)$$

where $k^0 + p^0 = \sqrt{s}$ and ω_l , E_l , are the energies of the meson and baryon respectively and m_l , M_l the meson and baryon masses.

Molecular states can be associated with the poles in the scattering amplitudes of Eq. (2.32) in the complex plane of \sqrt{s} . The poles appearing below the threshold in the first Riemann sheet are categorized as bound states, and those found in the second Riemann sheet are considered to be resonances. The loop function, G_l , of a given channel l , will be calculated in the first Riemann sheet for $\text{Re}(\sqrt{s})$ smaller than the threshold of that channel ($\sqrt{s}_{th,l}$), and in the second Riemann sheet for $\text{Re}(\sqrt{s})$ bigger than $\sqrt{s}_{th,l}$. To take this into account, we define a new loop function

$$G_l^{II} = \begin{cases} G_l(s) & \text{for } \text{Re}(\sqrt{s}) < \sqrt{s}_{th,l} \\ G_l(s) + i \frac{2M_l q}{4\pi\sqrt{s}} & \text{for } \text{Re}(\sqrt{s}) \geq \sqrt{s}_{th,l} \end{cases}, \quad (2.34)$$

where q is given by

$$q = \frac{\lambda^{1/2}(s, m_l^2, M_l^2)}{2\sqrt{s}} \quad \text{with } \text{Im}(q) > 0, \quad (2.35)$$

with $\lambda(x, y, z)$ the ordinary Källén function.

After all the poles have been calculated, we can evaluate their coupling constants to various channels. In the vicinity of the poles, the T -matrix can be expressed as

$$T_{ab}(s) = \frac{g_a g_b}{\sqrt{s} - z_R}, \quad (2.36)$$

where $z_R = M_R - i\Gamma_R/2$, which stands for the position of the bound states or resonances found in the complex plane of \sqrt{s} . Therefore, the couplings can be evaluated as the residues at the pole of T_{ab} , which can be written explicitly with the formula

$$g_a^2 = \frac{r}{2\pi} \int_0^{2\pi} T_{aa}(z_R + re^{i\theta}) e^{i\theta} d\theta. \quad (2.37)$$

However, to be consistent with the different complex phases of each coupling, we choose to calculate the biggest coupling (call it j) for each resonance as in Eq. (2.37), and then calculate the remaining couplings in relation to this one:

$$g_a = g_j \lim_{\sqrt{s} \rightarrow z_R} \frac{T_{ja}(s)}{T_{jj}(s)}. \quad (2.38)$$

Meanwhile, with the couplings obtained, we can also evaluate $g_i G_i^{II}$ which can give us the strength of the wave function of the i -channel at the origin [2.24].

2.2 Molecular Ω_c states

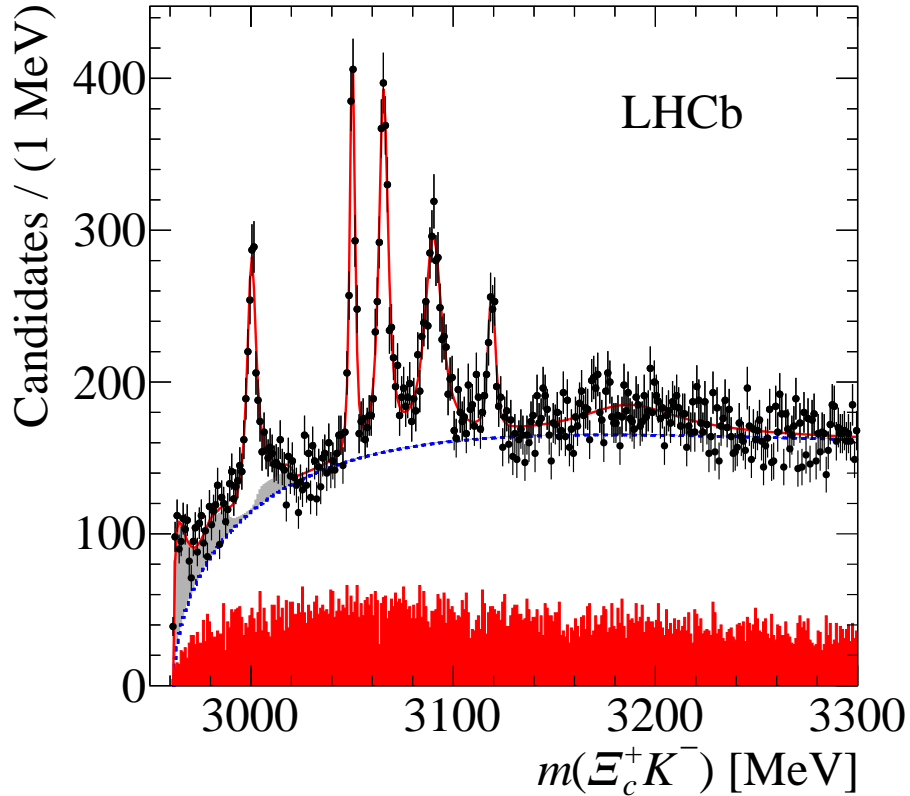


Figure 2.3: New Ω_c states reported by the LHCb collaboration in Ref. [2.2].

2.2.1 Introduction

In Ref. [2.2] the LHCb collaboration reported five new narrow Ω_c^0 states studying the $\Xi_c^+ K^-$ mass spectrum produced in high energy pp collisions: $\Omega_c(3000)$, $\Omega_c(3050)$, $\Omega_c(3066)$, $\Omega_c(3090)$ and $\Omega_c(3119)$. Predictions for such states and related ones had been done within quark model in Refs. [2.25–2.37]. Molecular states had also been used to make predictions in Refs. [2.16, 2.38] studying the interaction of coupled channels, one of them the $\Xi_c^+ K^-$ where the recent LHCb states were found. A more updated study along these lines was done in Ref. [2.39], where predictions for charmed and strange baryons are done using an interaction based on $SU(6)$ flavor-spin symmetry in the light quark sector and $SU(2)$ spin symmetry in the heavy quark sector, extending the $SU(3)$ Weinberg-Tomozawa interaction. All these works take the coupled channels of meson-baryon that couple to the desired baryon quantum numbers and use a unitary scheme to obtain the scattering matrix between the channels, looking for poles of this matrix. The differences come from the input interaction and the way that loops are regularized.

The experimental findings of Ref. [2.2] have brought a new wave of theoretical activity with many suggestions to explain the new states. Different versions of quark models have been proposed in Refs. [2.40–2.43]. Pentaquark options have been suggested in Refs. [2.44–2.49]. QCD sum rules were used to describe these states in Refs. [2.50–2.56]. Lattice QCD has also brought some light into the problem [2.57]. Some works have emphasized the value of decay properties to obtain information on the nature of these states [2.58–2.60] and a discussion on the possible quantum numbers was done in Ref. [2.61].

In the molecular picture, an update of the work of Ref. [2.38] was done in Ref. [2.62] using some information from the experimental spectrum to regularize the loops and then giving a description of the mass and width of two states of Ref. [2.2] as $J^P = 1/2^-$ meson-baryon molecular states.

In the present work we shall follow Refs. [2.39, 2.62] for the coupled channels and the unitarization procedure. We differ in the input for the interaction, which in our case is based on the local hidden gauge approach, exchanging vector mesons [2.9–2.13] as we presented in section 2.1.2.

The extrapolation of the local hidden gauge approach to $SU(4)$ to incorporate c quarks, or even higher with b quarks, is not straightforward, as one cannot invoke the Goldstone boson character for D or B mesons. Yet, what one does is the following: think of the DN interaction for instance. In the $D^0 p \rightarrow D^0 p$ transition we have $c\bar{u}$ in the D^0 and uud quarks in the p , then we can only exchange ρ^0 , ω vector mesons and the c quark of the D^0 is a spectator. In this case the situation is the same as in $\bar{K}^0 p \rightarrow \bar{K}^0 p$. The s quark of the \bar{K}^0 ($s\bar{d}$) is also a spectator and only ρ , ω vector mesons are exchanged. In as much as the c quark in $D^0 p \rightarrow D^0 p$ is a spectator, the dynamics is the same as in the $\bar{K}^0 p \rightarrow \bar{K}^0 p$ transition, and for this we can use the local hidden gauge approach. We find thus a way to obtain the $D^0 p \rightarrow D^0 p$ interaction using the dynamics of the light quark sector, since only these quarks are also involved in this case. Hence, in the diagonal channels the interaction is well controlled.

However, assume the coupled channel $\pi \Sigma_c$, then in the transition $D^0 p \rightarrow \pi^0 \Sigma_c^+$, if we extrapolate the local hidden gauge approach to $SU(4)$, we would be exchanging

a D^* and the c quarks are now involved. This is an extrapolation of the local hidden gauge approach which is model dependent. Fortunately, the exchange of D^* is penalized with respect to the exchange of light vector mesons by a factor of $\left(\frac{m_\rho}{m_{D^*}}\right)^2$, which is a small factor and then one is only introducing uncertainties in some non-diagonal terms which are very small. Formally one can use the $SU(4)$ extrapolation of the local hidden gauge approach and for the diagonal terms the framework automatically filters the exchange of light vectors, providing the results that one obtains from the mapping explained before. This is what is done in Ref. [2.62].

In the present work the diagonal terms that we evaluate coincide with those of Ref. [2.62] where the model of Ref. [2.16] is used implementing also the exchange of vector mesons and $SU(4)$ symmetry for mesons and baryons. We, instead, use explicit wave functions for the baryon states imposing flavor-spin symmetry on the light quark sector and singling out the heavy quarks. Hence, in the baryon sector we are not using $SU(4)$ symmetry. For the diagonal terms we also show that one is exchanging light vectors and the heavy quarks are spectators. In this case we obtain the same matrix elements as in Ref. [2.62], but there are differences in the non-diagonal ones. Since in the dominant terms we are exchanging only light vectors and the heavy quarks are spectators, the interaction automatically respects heavy quark symmetry [2.63–2.65]. The non-diagonal terms which exchange heavy vectors do not fulfill heavy quark symmetry, but neither should they since these are terms of order $O(m_{\bar{Q}}^{-2})$ in the heavy quark mass counting. In addition to the work of Ref. [2.62] we also include pseudoscalar-baryon($3/2^+$) components and we obtain two more states. We can identify two states of $J^P = 1/2^-$ and one of $J^P = 3/2^-$ with the states found in Ref. [2.2]. We also look for vector-baryon states and find three states at higher energies.

2.2.2 Formalism

Following Ref. [2.39] we distinguish the cases with $J^P = 1/2^-$ and $J^P = 3/2^-$ and write the coupled channels. In Ref. [2.39] 12 coupled channels are used ranging from thresholds 2965 MeV to 3655 MeV. The experimental states of Ref. [2.2] range from 3000 MeV to about 3120 MeV. Hence we restrict our space of meson-baryon states up to the $\Omega_c \omega$ with mass 3478 MeV. Yet, the diagonal matrix element in this channel is zero and we can also eliminate it. The energy ranged by the channels chosen widely covers the range of energies of Ref. [2.2] and it is a sufficiently general basis of states. We show in Tables 2.1 and 2.2 these states together with their threshold masses.

Table 2.1: $J = 1/2$ states chosen and threshold mass in MeV.

States	$\Xi_c \bar{K}$	$\Xi'_c \bar{K}$	ΞD	$\Omega_c \eta$	ΞD^*	$\Xi_c \bar{K}^*$	$\Xi'_c \bar{K}^*$
Threshold	2965	3074	3185	3243	3327	3363	3472

Now let us see how we can extend the approach presented in section 2.1.2 to the charm sector. The extension of the VPP vertex to the charm sector is easy. We

Table 2.2: $J = 3/2$ states chosen and threshold mass in MeV.

States	$\Xi_c^* K$	$\Omega_c^* \eta$	ΞD^*	$\Xi_c K^*$	$\Xi^* D$	$\Xi_c' K^*$
Threshold	3142	3314	3327	3363	3401	3472

take the same structure as in Eq. (2.9) but now P and V are

$$P = \begin{pmatrix} \frac{1}{\sqrt{2}}\pi^0 + \frac{1}{\sqrt{3}}\eta + \frac{1}{\sqrt{6}}\eta' & \pi^+ & K^+ & \bar{D}^0 \\ \pi^- & -\frac{1}{\sqrt{2}}\pi^0 + \frac{1}{\sqrt{3}}\eta + \frac{1}{\sqrt{6}}\eta' & K^0 & D^- \\ K^- & \bar{K}^0 & -\frac{1}{\sqrt{3}}\eta + \sqrt{\frac{2}{3}}\eta' & D_s^- \\ D^0 & D^+ & D_s^+ & \eta_c \end{pmatrix}, \quad (2.39)$$

where we also include the mixing between η and η' [2.66], and

$$V_\mu = \begin{pmatrix} \frac{1}{\sqrt{2}}\rho^0 + \frac{1}{\sqrt{2}}\omega & \rho^+ & K^{*+} & \bar{D}^{*0} \\ \rho^- & -\frac{1}{\sqrt{2}}\rho^0 + \frac{1}{\sqrt{2}}\omega & K^{*0} & \bar{D}^{*-} \\ K^{*-} & \bar{K}^{*0} & \phi & D_s^{*-} \\ D^{*0} & D^{*+} & D_s^{*+} & J/\psi \end{pmatrix}_\mu. \quad (2.40)$$

Now for the VBB vertex we will use a similar argument at quark level, as presented in section 2.1.2. However, to extend it to the charm sector, we will leave the heavy quark of the baryon as an spectator, and use $SU(3)$ symmetry on the light quarks. It has been shown in Ref. [2.67] (see section IIA of that reference), using similar arguments at the quark level as in Eqs. (2.14) and (2.20), that in the heavy sector the coupling of the light vectors to the charmed mesons leaves the heavy quark as a spectator. Then one can map the matrix elements with light quarks to the equivalent ones in $SU(3)$, with the result that using Eq. (2.9) in $SU(4)$, with the matrices of Eqs. (2.39) and (2.40), the result obtained is the same as using this quark model with the heavy quarks as spectators. In other words, one is making use of the $SU(3)$ content of $SU(4)$. Furthermore, the fact that the heavy quarks are spectators has immediately as a consequence that the interaction complies with the rules of heavy quark spin symmetry (HQSS). However, if we have non-diagonal transitions like $\Xi_c \bar{K} \rightarrow \Xi D$ one must exchange a D_s^* and the heavy quarks are involved. Here $SU(4)$ is used and the result is more model dependent, apart from not satisfying the rules of HQSS. However, in this case HQSS should not be satisfied, because the heavy quark propagator goes as $(1/m_{D_s^*})^2$ and those terms are subleading in the $(1/m_Q)$ counting (m_Q is the mass of the heavy quarks). One should mention that the use of $SU(4)$ in this case is marginal, since the Lagrangian of Eq. (2.9) is basically counting the quarks involved in the process.

That being said, the first step to calculate VBB is to build the proper wave functions for the charmed baryons.

Baryon wave functions

As we saw in Eqs. (2.15) and (2.16) from section 2.1.2, the mixed symmetric and mixed antisymmetric spin wave function for spin 1/2 baryons, now with the sym-

metric/antisymmetric part on the last two quarks, are

$$\chi_{MS} = \frac{1}{\sqrt{6}}(\uparrow\uparrow\downarrow + \uparrow\downarrow\uparrow - 2\downarrow\uparrow\uparrow), \quad \text{for } S_z = 1/2, \quad (2.41)$$

and

$$\chi_{MA} = \frac{1}{\sqrt{2}}\uparrow(\uparrow\downarrow - \downarrow\uparrow), \quad \text{for } S_z = 1/2. \quad (2.42)$$

Now for the flavor part, we will follow Ref. [2.17] using $SU(3)$ symmetry in the light quarks u , d and s while singling out the charm quark as an spectator. We should note that to be consistent with the chiral Lagrangians one has to use a different phase convention with respect to Ref. [2.17], where the Σ^+ , Ξ^0 and Λ change sign with respect to Ref. [2.17]. The correct assignment for the ϕ_{MA} are given in Table III of Ref. [2.68] (the same assignment is also used in Ref. [2.69]).

Below we list the flavor wave function of the baryons involved in the construction of the Ω_c states.

For the baryon states with $J^P = 1/2^+$:

$$\Xi \equiv \frac{1}{\sqrt{2}}(\phi_{MS}\chi_{MS} + \phi_{MA}\chi_{MA}), \quad (2.43)$$

where for Ξ^0

$$\begin{aligned} \phi_{MS} &= \frac{1}{\sqrt{6}}[s(us + su) - 2uss], \\ \phi_{MA} &= -\frac{1}{\sqrt{2}}[s(us - su)], \end{aligned}$$

and for Ξ^-

$$\begin{aligned} \phi_{MS} &= -\frac{1}{\sqrt{6}}[s(ds + sd) - 2dss], \\ \phi_{MA} &= \frac{1}{\sqrt{2}}[s(ds - sd)] \end{aligned}$$

Note how we change $u \rightarrow d$ to get the isospin partner.

Now for Ξ_c we have $\phi_{MA}\chi_{MA}$

$$\begin{aligned} \Xi_c^+ &= c\frac{1}{\sqrt{2}}(us - su)\chi_{MA}, \\ \Xi_c^0 &= c\frac{1}{\sqrt{2}}(ds - sd)\chi_{MA}, \end{aligned} \quad (2.44)$$

and for Ξ_c' we have $\phi_{MS}\chi_{MS}$

$$\begin{aligned} \Xi_c'^+ &= c\frac{1}{\sqrt{2}}(us + su)\chi_{MS}, \\ \Xi_c'^0 &= c\frac{1}{\sqrt{2}}(ds + sd)\chi_{MS}, \end{aligned} \quad (2.45)$$

Also note how the spin wave functions in Eqs. (2.41) and (2.42) are symmetric or antisymmetric in the last two quarks, corresponding to the flavor symmetry of the last two quarks in Eqs. (2.44) (2.45).

Finally,

$$\Omega_c^0 = css \chi_{MS}. \quad (2.46)$$

For the baryon states of spin $J^P = 3/2^+$ we have the fully symmetric spin wave function χ_S

$$\chi_S = \uparrow\uparrow\uparrow, \quad \text{for } S_z = 3/2. \quad (2.47)$$

For Ξ^* we have $\Phi_S \chi_S$, were the flavor part is also fully symmetric in $SU(3)$

$$\begin{aligned} \Xi^{*0} &= \frac{1}{\sqrt{3}}(sus + ssu + uss)\chi_S, \\ \Xi^{*-} &= \frac{1}{\sqrt{3}}(sds + ssd + dss)\chi_S, \end{aligned} \quad (2.48)$$

and for Ξ_c^* we have the symmetric part for the light quarks, as we had for Ξ_c' in Eq. (2.45), but now the spin is $3/2$

$$\begin{aligned} \Xi_c^{*+} &= c \frac{1}{\sqrt{2}}(us + su)\chi_S, \\ \Xi_c^{*0} &= c \frac{1}{\sqrt{2}}(ds + sd)\chi_S, \end{aligned} \quad (2.49)$$

and finally,

$$\Omega_c^{*0} = css \chi_S \quad (2.50)$$

Once we got the wave functions, we have to construct the molecular states with isospin $I = 0$, strangeness $S = -2$ and charm $C = +1$ to match the Ω_c quantum numbers. For that recall that our isospin multiplets are:

$$\begin{aligned} \bar{K} &= \begin{pmatrix} \bar{K}^0 \\ -K^- \end{pmatrix}; \quad D = \begin{pmatrix} D^+ \\ -D^0 \end{pmatrix}; \quad \Xi = \begin{pmatrix} \Xi^0 \\ -\Xi^- \end{pmatrix}; \quad \Xi^* = \begin{pmatrix} \Xi^{*0} \\ \Xi^{*-} \end{pmatrix}; \\ \Xi_c &= \begin{pmatrix} \Xi_c^+ \\ \Xi_c^0 \end{pmatrix}; \quad \Xi_c' = \begin{pmatrix} \Xi_c'^+ \\ \Xi_c'^0 \end{pmatrix}; \quad \Xi_c^* = \begin{pmatrix} \Xi_c^{*+} \\ \Xi_c^{*0} \end{pmatrix}; \end{aligned} \quad (2.51)$$

and thus

$$\begin{aligned} |\Xi_c \bar{K}, I = 0\rangle &= -\frac{1}{\sqrt{2}} |\Xi_c^+ K^- + \Xi_c^0 \bar{K}^0\rangle, \\ |\Xi D, I = 0\rangle &= -\frac{1}{\sqrt{2}} |\Xi^0 D^0 - \Xi^- D^+\rangle, \\ |\Xi_c^* \bar{K}, I = 0\rangle &= -\frac{1}{\sqrt{2}} |\Xi_c^{*+} K^- + \Xi_c^{*0} \bar{K}^0\rangle, \end{aligned}$$

$$|\Xi^* D, I = 0\rangle = -\frac{1}{\sqrt{2}} |\Xi^{*0} D^0 + \Xi^{*-} D^+\rangle. \quad (2.52)$$

And we also have the channels $\Omega_c \eta$ and $\Omega_c^{*0} \eta$ which already have the right quantum numbers. With these wave functions and the prescription to calculate the VPP and VBB vertices we can construct the matrix elements of the transition potential between the states in Table 2.1 and in Table 2.2. Let us show an example evaluating the first diagonal case $\Xi_c \bar{K} \rightarrow \Xi_c \bar{K}$.

Evaluation of the transition matrix elements of $\Xi_c \bar{K} \rightarrow \Xi_c \bar{K}$

Using the $\Xi_c \bar{K}$ wave function from Eq. (2.52) we find four diagrams at lowest order, as depicted in Fig. 2.4.

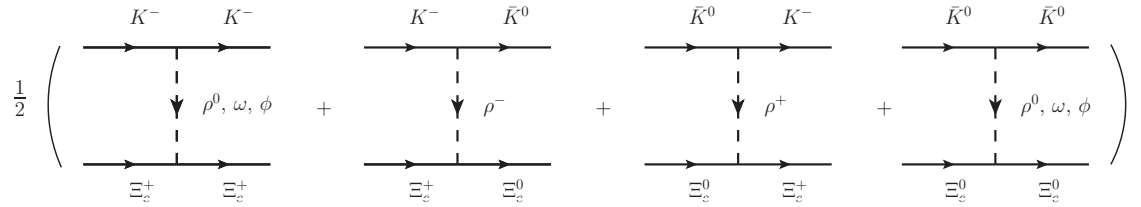


Figure 2.4: Diagrams in the $\Xi_c \bar{K} \rightarrow \Xi_c \bar{K}$ transition.

Let us analyse the upper vertices first. We have four cases: $K^- \rightarrow K^-(\rho^0, \omega, \phi)$, $K^- \rightarrow \bar{K}^0 \rho^-$, $\bar{K}^0 \rightarrow K^- \rho^+$ and $\bar{K}^0 \rightarrow \bar{K}^0(\rho^0, \omega, \phi)$. Using Eq. (2.9) for the VPP vertex we find

$$K^- \rightarrow K^- \begin{pmatrix} \rho^0 \\ \omega \\ \phi \end{pmatrix} : -it_{K^- \rightarrow K^-(\rho^0, \omega, \phi)} = gV_\mu (-ip^\mu - ip'^\mu) \begin{pmatrix} 1/\sqrt{2} \\ 1/\sqrt{2} \\ -1 \end{pmatrix}, \quad (2.53)$$

$$K^- \rightarrow \bar{K}^0 \rho^- : -it_{K^- \rightarrow \bar{K}^0 \rho^-} = g\rho^{+\mu} (-ip^\mu - ip'^\mu), \quad (2.54)$$

$$\bar{K}^0 \rightarrow K^- \rho^+ : -it_{\bar{K}^0 \rightarrow K^- \rho^+} = g\rho^{-\mu} (-ip^\mu - ip'^\mu), \quad (2.55)$$

$$\bar{K}^0 \rightarrow \bar{K}^0 \begin{pmatrix} \rho^0 \\ \omega \\ \phi \end{pmatrix} : -it_{\bar{K}^0 \rightarrow \bar{K}^0(\rho^0, \omega, \phi)} = gV_\mu (-ip^\mu - ip'^\mu) \begin{pmatrix} -1/\sqrt{2} \\ 1/\sqrt{2} \\ -1 \end{pmatrix}, \quad (2.56)$$

with p, p' the momenta of the incoming and outgoing kaons.

The lower vertices are readily calculated using Eq. (2.12), as seen in Fig. 2.5.

For Fig. 2.5(a) we have the matrix elements

$$\frac{1}{\sqrt{2}} \langle (us - su) | \begin{pmatrix} g\frac{1}{\sqrt{2}}(u\bar{u} - d\bar{d}) \\ g\frac{1}{\sqrt{2}}(u\bar{u} + d\bar{d}) \\ gs\bar{s} \end{pmatrix} | \frac{1}{\sqrt{2}}(us - su) \rangle = \begin{pmatrix} \frac{1}{\sqrt{2}}g \\ \frac{1}{\sqrt{2}}g \\ g \end{pmatrix}. \quad (2.57)$$

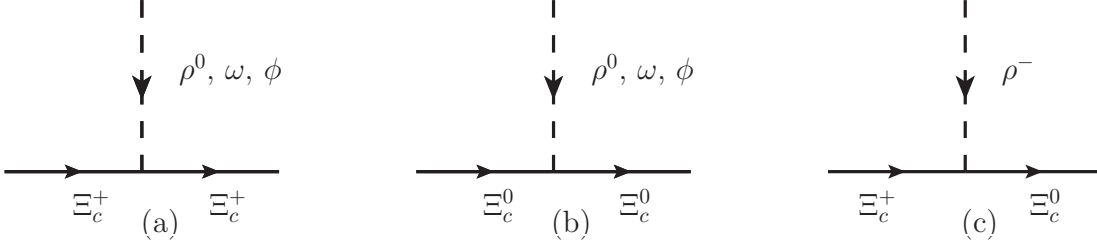


Figure 2.5: Vector-baryon vertex diagrams in the $\bar{K}\Xi_c \rightarrow \bar{K}\Xi_c$ transition.

For Fig. 2.5(b) we have

$$\frac{1}{\sqrt{2}} \langle (ds - sd) | \begin{pmatrix} g \frac{1}{\sqrt{2}} (u\bar{u} - d\bar{d}) \\ g \frac{1}{\sqrt{2}} (u\bar{u} + d\bar{d}) \\ gs\bar{s} \end{pmatrix} | \frac{1}{\sqrt{2}} (ds - sd) \rangle = \begin{pmatrix} -\frac{1}{\sqrt{2}} g \\ \frac{1}{\sqrt{2}} g \\ g \end{pmatrix}. \quad (2.58)$$

The vertex of Fig. 2.5(c) can be evaluated using the operator $g d\bar{u}$ for ρ^- ,

$$\frac{1}{\sqrt{2}} \langle (ds - sd) | g d\bar{u} | \frac{1}{\sqrt{2}} (us - su) \rangle = g \frac{1}{\sqrt{2}} \langle (ds - sd) | \frac{1}{\sqrt{2}} (ds - sd) \rangle = g. \quad (2.59)$$

An alternative method to calculate or double check the result for this vertex is to use Clebsch-Gordan coefficients to relate to another previously calculated one, for example $\rho^0 \Xi_c^+ \Xi_c^+$ from the diagram in Fig. 2.5(a). Let us analyse its isospin content. We had incoming $\rho^0 \Xi_c^+$, and outgoing Ξ_c^+ . Taking into account that Ξ_c has isospin 1/2 and ρ has isospin 1, this vertex corresponds to the Clebsch-Gordan coefficient $1 \times 1/2 \rightarrow 1/2$, i.e., $\mathcal{C}(S_1, S_2, S_T; S_{1z}, S_{2z}, S_{Tz}) = \mathcal{C}(1, 1/2, 1/2; 0, 1/2, 1/2) = -\sqrt{1/3}$, where $|S_1, S_{1z}\rangle = |\rho^0\rangle$, $|S_2, S_{2z}\rangle = |\Xi_c^+\rangle$ (incoming) and $|S_T, S_{Tz}\rangle = |\Xi_c^+\rangle$ (outgoing). On the other hand, for the diagram in Fig. 2.5(c), we have $\mathcal{C}(1, 1/2, 1/2; -1, 1/2, -1/2) = -\sqrt{2/3}$, which means that the vertex $\rho^- \Xi_c^+ \rightarrow \Xi_c^0$ is a factor $\sqrt{2}$ greater than $\rho^0 \Xi_c^+ \rightarrow \Xi_c^+$. Since we had a contribution of $g/\sqrt{2}$ for the first case with ρ^0 , we find that the contribution from $\rho^- \Xi_c^+ \rightarrow \Xi_c^0$ is g , as we had obtained looking at the quark content in Eq. (2.59).

The reverse case for $\Xi_c^0 \rho^+ \rightarrow \Xi_c^+$ also gives the same contribution, so we have $2g$ coming from the ρ^+ and ρ^- exchange.

Altogether, the matrix element for Fig. 2.4 is given by

$$\begin{aligned} -it_{\Xi_c \bar{K} \rightarrow \Xi_c \bar{K}} &= \frac{1}{2} g^2 \left[(-ip^\mu - ip'^\mu)(-g_{\mu 0}) \frac{i}{-m_V^2} \begin{pmatrix} 1/\sqrt{2} \\ 1/\sqrt{2} \\ -1 \end{pmatrix} i \begin{pmatrix} 1/\sqrt{2} \\ 1/\sqrt{2} \\ 1 \end{pmatrix} \right. \\ &+ 2(-ip^\mu - ip'^\mu)(-g_{\mu 0}) \frac{i}{-m_V^2} i \\ &+ \left. (-ip^\mu - ip'^\mu)(-g_{\mu 0}) \frac{i}{-m_V^2} \begin{pmatrix} -1/\sqrt{2} \\ 1/\sqrt{2} \\ -1 \end{pmatrix} i \begin{pmatrix} -1/\sqrt{2} \\ 1/\sqrt{2} \\ 1 \end{pmatrix} \right] \\ &= -1 \frac{1}{4f_\pi^2} (p^0 + p'^0) \equiv D \frac{1}{4f_\pi^2} (p^0 + p'^0), \end{aligned} \quad (2.60)$$

with $D = -1$ (recall that $g = m_V/2f_\pi$).

Following these steps it becomes easy and systematic to evaluate all the matrix elements, which have the general form

$$V_{ij} = D_{ij} \frac{1}{4f_\pi^2} (p^0 + p^0). \quad (2.61)$$

where V_{ij} will be used as the kernel of the Bethe-Salpeter equation from Eq. (2.32).

Alternatively, we can use another expression which includes relativistic correction in s -wave [2.70]

$$V_{ij} = D_{ij} \frac{2\sqrt{s} - M_{B_i} - M_{B_j}}{4f_\pi^2} \sqrt{\frac{M_{B_i} + E_{B_i}}{2M_{B_i}}} \sqrt{\frac{M_{B_j} + E_{B_j}}{2M_{B_j}}}, \quad (2.62)$$

where M_{B_i, B_j} and E_{B_i, B_j} stand for the mass and the center-of-mass energy of the baryons, respectively.

The matrix D_{ij} for the channels from Table 2.1 are given in Table 2.3.

Table 2.3: D_{ij} coefficients of Eq. (2.62) for the meson-baryon states coupling to $J^P = 1/2^-$ in s -wave.

$J = 1/2$	$\Xi_c K$	$\Xi'_c K$	ΞD	$\Omega_c \eta$	ΞD^*	$\Xi_c \bar{K}^*$	$\Xi'_c \bar{K}^*$
$\Xi_c \bar{K}$	-1	0	$-\frac{1}{\sqrt{2}}\lambda$	0	0	0	0
$\Xi'_c \bar{K}$		-1	$\frac{1}{\sqrt{6}}\lambda$	$-\frac{4}{\sqrt{3}}$	0	0	0
ΞD			-2	$\frac{\sqrt{2}}{3}\lambda$	0	0	0
$\Omega_c \eta$				0	0	0	0
ΞD^*					-2	$-\frac{1}{\sqrt{2}}\lambda$	$\frac{1}{\sqrt{6}}\lambda$
$\Xi_c \bar{K}^*$						-1	0
$\Xi'_c \bar{K}^*$							-1

In Table 2.3 we have the parameter λ in some non-diagonal matrix elements, which involve transitions from one meson without charm to one with charm, like $\bar{K} \rightarrow D$. In this case we have for the propagator of the exchanged vector

$$\frac{1}{(q^0)^2 - |\mathbf{q}|^2 - m_{D_s^*}^2} \approx \frac{1}{(m_D - m_K)^2 - m_{D_s^*}^2}, \quad (2.63)$$

and the ratio to the propagator of the light vectors is

$$\lambda \equiv \frac{-m_V^2}{(m_D - m_K)^2 - m_{D_s^*}^2} \approx 0.25. \quad (2.64)$$

We take $\lambda = 1/4$ in all these matrix elements, as it was done in Ref. [2.7].

The diagonal matrix elements of Table 2.3 coincide with those of Ref. [2.62], but not all the non-diagonal. This is not surprising. $SU(4)$ symmetry is used in Ref. [2.62], but only $SU(3)$ is effectively used in the diagonal terms, as we have argued. Then we should note that the heavy baryons that we have constructed are

not eigenstates of $SU(4)$ since we have singled out the heavy quarks and used symmetrized wave functions for the light quarks. This induces a spin-flavor dependence different from the one of pure $SU(4)$ symmetry.

With respect to Ref. [2.39], we have some diagonal matrix elements equal but not all of them, and there are also differences in the non-diagonal terms. These matrix elements are also different from those of Ref. [2.62].

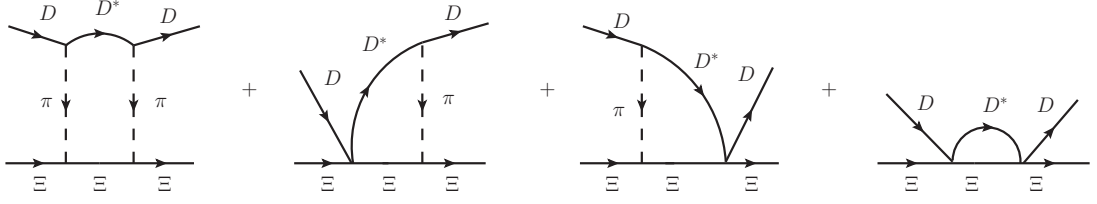
Table 2.4: D_{ij} coefficients of Eq. (2.62) for the meson-baryon states coupling to $J^P = 3/2^-$.

$J = 3/2$	$\Xi_c^* \bar{K}$	$\Omega_c^* \eta$	ΞD^*	$\Xi_c \bar{K}^*$	$\Xi^* D$	$\Xi'_c \bar{K}^*$
$\Xi_c^* \bar{K}$	-1	$-\frac{4}{\sqrt{3}}$	0	0	$\frac{2}{\sqrt{6}}\lambda$	0
$\Omega_c^* \eta$		0	0	0	$-\frac{\sqrt{2}}{3}\lambda$	0
ΞD^*			-2	$-\frac{1}{\sqrt{2}}\lambda$	0	$\frac{1}{\sqrt{6}}\lambda$
$\Xi_c \bar{K}^*$				-1	0	0
$\Xi^* D$					-2	0
$\Xi'_c \bar{K}^*$						-1

To calculate the matrix elements for the states that couple to $J^P = 3/2^-$ of Table 2.2 we proceed in the same way. We must take into account that the VVV_{ex} are like those of PPV_{ex} under the approximation of neglecting $(\mathbf{p}/m_V)^2$, where \mathbf{p} is the momentum of the external vector. In addition one has for the factor $\vec{\epsilon} \cdot \vec{\epsilon}'$ for the vector polarization, which makes these terms to contribute to $J = 1/2$ and $J = 3/2$ with degeneracy. The terms connecting P and V like $\Xi_c^* \bar{K} \rightarrow \Xi D^*$ require exchange of pseudoscalars, which go with the momentum and are small compared to the exchange of vectors [2.71]. In the $\Xi_c^* \bar{K} \rightarrow \Xi D^*$ one would have to exchange a D_s and it would be doubly suppressed. In the $\Xi_c^* \bar{K} \rightarrow \Xi_c \bar{K}^*$ one would exchange a pion, but the K and K^* states are quite separated in energy and the transition is also not important. In the $D\Xi \rightarrow D^*\Xi$ transitions one has the $\pi\Xi\Xi$ Yukawa vertex that goes like $D - F$ compared to $D + F$ for πPP , with $F = 0.51$, $D = 0.75$ [2.72], which is highly suppressed. Therefore, we neglect all terms which involve transition of a pseudoscalar to a vector and then the matrix elements are again given by Eq. (2.62) with the D_{ij} coefficients given in Table 2.4.

In order to see the relevance of the π exchange discussed above, we take the $D\Xi \rightarrow D^*\Xi$ transition and we evaluate the effect in the $D\Xi \rightarrow D\Xi$ interaction going through the intermediate $D^*\Xi$ state. For this we follow Ref. [2.73] and consider the diagrams of Fig. 2.6.

As discussed in Ref. [2.73], in addition to the π exchange there is a contact term called Kroll-Ruderman in the $\gamma N \rightarrow \pi N$ (or $\rho N \rightarrow \pi N$) transition, then the four diagrams of Fig. 2.6 must be evaluated. They provide a δV potential for $D\Xi \rightarrow D\Xi$ which can be evaluated by means of Eq. (40) of Ref. [2.73], simply changing the masses of B , B^* to D , D^* and N to Ξ . We have performed the calculation and, compared to the potential V_{ij} from Eq. (2.62) and Table 2.3 we find $\delta V/V \approx 0.012$ for the ΞD channel calculated at the energy of the pole around 3090 MeV (which is dominated by this channel, as shown in Table 2.6 of the Results section), a correction of order 1%, which we safely neglect.

Figure 2.6: Box diagrams accounting for the $D\Xi \rightarrow D^*\Xi \rightarrow D\Xi$.

2.2.3 Results

In Table 2.5 we show the poles that we obtain for the $J^P = 1/2^-$ sector for different values of the cutoff q_{max} . We only show the results with the pseudoscalar-baryon interaction. This sector decouples from the vector-baryon one, where the states are obtained degenerate in $J^P = 1/2^-, 3/2^-$. We will come back to this sector later on.

Table 2.5: Poles in $J^P = 1/2^-$ sector from pseudoscalar-baryon interaction. (Units: MeV).

q_{max}	600	650	700	750	800
	3065.4 + $i0.1$	3054.05 + $i0.44$	3038.13 + $i1.78$	3016.21 + $i6.02$	2989.69 + $i16.24$
	3114.22 + $i3.75$	3091.28 + $i5.12$	3067.71 + $i4.12$	3046.24 + $i3.83$	3027.75 + $i2.19$

We can see that we always get two states in the range of the masses observed experimentally. The strategy followed in these calculations is to fine tune the cutoff to adjust the pole position to some experimental data. We see that if we take $q_{max} = 650$ MeV the results agree well with the second and fourth resonances reported in Ref. [2.2], $\Omega_c(3050)$ and $\Omega_c(3090)$. It is interesting to note that cutoff values of this order are used in Ref. [2.6] for $\bar{K}N$ or in Ref. [2.74] for DN . Fitting one resonance is partly merit of fine tuning the cutoff, but then the second resonance and the widths are genuine predictions of the theory. Note that the widths are respectively 0.88 MeV and 10.24 MeV, which agree remarkably well with the experiment, $0.8 \pm 0.2 \pm 0.1$ MeV and $8.7 \pm 1.0 \pm 0.8$ MeV, respectively. It is instructive to see the origin of the widths. For this we look at Table 2.6 for the couplings to the different channels. We can see that for the lower state at 3054 MeV only the $\Xi_c \bar{K}$ state is open for decay, precisely the channel where it has been observed, and the coupling of the state to this channel is very small. However, for the state at 3091 MeV the $\Xi'_c \bar{K}$ channel is also open, and the coupling to this channel is considerable. Furthermore, the coupling to $\Xi_c \bar{K}$ is bigger than before and there is more phase space for decay.

Next we look for the states of $J^P = 3/2^-$ from the pseudoscalar-baryon($3/2^+$) interaction. In Table 2.4 we see that the pseudoscalar-baryon($3/2^+$) states do not couple to vector-baryon and we can separate two blocks, the channels $\Xi_c^* \bar{K}$, $\Omega_c^* \eta$, $\Xi^* D$ and ΞD^* , $\Xi_c \bar{K}^*$, $\Xi'_c \bar{K}^*$. The first three channels in s -wave give rise to $J^P = 3/2^-$, while the other three give rise to $J^P = 1/2^-, 3/2^-$, degenerated in our approach. We then separate these two sets of states.

In Table 2.7 we show the results for $J^P = 3/2^-$ for different values of the cutoff. We see that we get two poles. Yet, if we choose the same cutoff as in the $J^P = 1/2^-$

Table 2.6: The coupling constants to various channels for the poles in the $J^P = 1/2^-$ sector, with $q_{max} = 650$ MeV, and $g_i G_i^{II}$ in MeV.

3054.05 + i0.44	$\Xi_c \bar{K}$	$\Xi'_c \bar{K}$	ΞD	$\Omega_c \eta$	ΞD^*	$\Xi_c \bar{K}^*$	$\Xi'_c \bar{K}^*$
g_i	$-0.06 + i0.14$	1.94 + i0.01	$-2.14 + i0.26$	$1.98 + i0.01$	0	0	0
$g_i G_i^{II}$	$-1.40 - i3.85$	-34.41 - i0.30	$9.33 - i1.10$	$-16.81 - i0.11$	0	0	0
3091.28 + i5.12	$\Xi_c \bar{K}$	$\Xi'_c \bar{K}$	ΞD	$\Omega_c \eta$	ΞD^*	$\Xi_c \bar{K}^*$	$\Xi'_c \bar{K}^*$
g_i	$0.18 - i0.37$	$0.31 + i0.25$	5.83 - i0.20	$0.38 + i0.23$	0	0	0
$g_i G_i^{II}$	$5.05 + i10.19$	$-9.97 - i3.67$	-29.82 + i0.31	$-3.59 - i2.23$	0	0	0

sector we find a mass of 3125 MeV and zero width for the lowest state. As we can see, the mass is smaller than all the thresholds in Table 2.2, hence it does not decay into them. To decay into $\Xi_c \bar{K}$, where it has been observed, we would need the exchange of vector mesons in p -wave, which give rise to a small width. We can clearly associate the state found with the $\Omega_c(3119)$ observed experimentally, which has a width of $1.1 \pm 0.8 \pm 0.4$ MeV. The agreement is also remarkable.

Table 2.7: Poles in $J^P = 3/2^-$ sector from pseudoscalar-baryon($3/2^+$) interaction. (Units: MeV).

q_{max}	600	650	700	750	800
	3134.39	3124.84	3112.83	3099.2	3084.52
	$3316.48 + i0.14$	$3290.31 + i0.03$	$3260.42 + i0.08$	$3227.34 + i0.15$	$3191.13 + i0.22$

In Table 2.8 we show the couplings of the states to the coupled channels of Table 2.2. We can see that the state at 3125 MeV couples strongly to $\Xi_c^* \bar{K}$ and $\Omega_c^* \eta$, more strongly to $\Xi_c^* \bar{K}$. The upper state couples very strongly to $\Xi^* D$.

Table 2.8: The coupling constants to various channels for the poles in the $J^P = 3/2^-$ sector, with $q_{max} = 650$ MeV, and $g_i G_i^{II}$ in MeV.

3124.84	$\Xi_c^* \bar{K}$	$\Omega_c^* \eta$	ΞD^*	$\Xi_c \bar{K}^*$	$\Xi^* D$	$\Xi'_c \bar{K}^*$
g_i	1.95	1.98	0	0	-0.65	0
$g_i G_i^{II}$	-35.65	-16.83	0	0	1.93	0
$3290.31 + i0.03$	$\Xi_c^* \bar{K}$	$\Omega_c^* \eta$	ΞD^*	$\Xi_c \bar{K}^*$	$\Xi^* D$	$\Xi'_c \bar{K}^*$
g_i	$0.01 + i0.02$	$0.31 + i0.01$	0	0	6.22 - i0.04	0
$g_i G_i^{II}$	$-0.62 - i0.18$	$-5.25 - i0.18$	0	0	-31.08 + i0.20	0

For the vector-baryon states with $J^P = 1/2^-, 3/2^-$ we choose the same cutoff $q_{max} = 650$ MeV that we have chosen in the former cases and find three states that we show in Table 2.9 together with the couplings to each channel.

The first state obtained has zero width and couples mostly to ΞD^* while the second and third ones have very small widths and couple mostly to $\Xi_c \bar{K}^*$ and $\Xi'_c \bar{K}^*$, respectively. The widths could be bigger if we had considered vector-baryon transitions to pseudoscalar-baryon but we argued that they were small in any case and neglected them in our study.

It is interesting to compare our results with those of Ref. [2.62]. The main feature is that the results obtained are remarkably similar. In Ref. [2.62] two states of $J^P = 1/2^-$ are also found that compare well with the $\Omega_c(3050)$ and $\Omega_c(3090)$,

Table 2.9: The coupling constants to various channels for the poles in $J^P = 1/2^-, 3/2^-$ stemming from vector-baryon interaction with $q_{max} = 650$ MeV, and $g_i G_i^{II}$ in MeV.

3221.98	ΞD^*	$\Xi_c \bar{K}^*$	$\Xi'_c \bar{K}^*$
g_i	6.37	0.59	-0.28
$g_i G_i^{II}$	-29.29	-4.66	1.62
3360.37 + $i0.20$	ΞD^*	$\Xi_c \bar{K}^*$	$\Xi'_c \bar{K}^*$
g_i	-0.11 - $i0.12$	1.31 - i0.03	0.03 + $i0.01$
$g_i G_i^{II}$	2.12 + $i0.48$	-26.04 + i0.36	-0.26 - $i0.06$
3465.17 + $i0.09$	ΞD^*	$\Xi_c \bar{K}^*$	$\Xi'_c \bar{K}^*$
g_i	-0.01 + $i0.06$	0.01 - $i0.01$	1.75 + i0.01
$g_i G_i^{II}$	-0.84 - $i0.23$	0.17 + $i0.24$	-32.29 - i0.08

as we have found here. The width of the second state is about 17 MeV, while we get 10 MeV, closer to the experimental value. In Ref. [2.62] two sets of subtraction constants (cutoffs) are used and in one of them the width of this state is 12 MeV, at the expense of using a somewhat small cutoff in the $\Xi_c \bar{K}$ decay channel of 320 MeV. Even then, the main channels and the strengths of the couplings are similar to ours.

In Ref. [2.62] the compositeness magnitude $-g^2 \partial G / \partial \sqrt{s}$ is evaluated for all channels. This magnitude provides the probability to find bound channels [2.24, 2.75, 2.76] and for the case of open channels it gives the integral of the wave functions squared with a given prescription of the phase [2.77]. The magnitude gG that we calculate gives the wave function at the origin of each channel the resonance couple to [2.24]. Yet, there is a correspondence in these two magnitudes, and we find that when $-g^2 \partial G / \partial \sqrt{s}$ is large for some channel in Ref. [2.62], so is gG in our case.

The pseudoscalar-baryon($3/2^+$) states are not considered in Ref. [2.62] and, thus, the states that we get in Table 2.7 are new. As to the vector-baryon($1/2^+$) states we obtain three new states, two of them in qualitative agreement with Ref. [2.62]. In Ref. [2.62] two states were found at 3231 MeV and 3419 MeV, that couple mostly to ΞD^* and $\Xi'_c \bar{K}^*$, respectively. We also find two states, at 3222 MeV and 3465 MeV, which also couple mostly to ΞD^* and $\Xi'_c \bar{K}^*$, respectively, as in Ref. [2.62], plus a new intermediate state at 3360 MeV that couples mostly to $\Xi_c \bar{K}^*$.

As to the results of Ref. [2.39], the bindings obtained there, in the absence of any experimental data, gave rise to bound Ω_c states with more binding than here. It would be interesting to have a new look in that framework under the light of the new experimental information ¹.

The basic input of our calculations are the V_{ij} transition potentials of Eq. (2.62), and the terms are proportional to $\frac{1}{f_\pi^2}$. We estimate uncertainties in the following way. We increase f_π^2 by 10% and readjust the cutoff to obtain the same energy of the first state (going from $q_{max} = 650$ MeV to 694 MeV), and then we get the results of Table 2.10. As we can see, the changes in the masses and widths are small. The

¹ After completion of this work, this calculation has been performed [2.82]. The results agree qualitatively with experiment, but not as quantitatively as in our case.

difference in the masses are always smaller than 5 MeV, and for the three states that we compare with experiment the changes are even smaller. The widths also change a bit, but the width of the widest state only changes from 10.24 MeV to 11.82 MeV, and the others are still very small and compatible with experiment within errors.

Table 2.10: Dependence of the results on the value of f_π .

$J = 1/2$	$f_\pi = 93$ MeV and $q_{\max} = 650$ MeV	$f_\pi = 97.6$ MeV and $q_{\max} = 694$ MeV
Pole 1	3054.05 + i0.44	3054.05 + i0.70
Pole 2	3091.28 + i5.12	3087.24 + i5.91
$J = 3/2$	$f_\pi = 93$ MeV and $q_{\max} = 650$ MeV	$f_\pi = 97.6$ MeV and $q_{\max} = 694$ MeV
Pole 1	3124.84	3125.71
Pole 2	3290.31 + i0.03	3284.73.24 + i0.05
$J = 1/2, 3/2$	$f_\pi = 93$ MeV and $q_{\max} = 650$ MeV	$f_\pi = 97.6$ MeV and $q_{\max} = 694$ MeV
Pole 1	3221.98	3216.98
Pole 2	3360.37 + i0.20	3361.28 + i0.18
Pole 3	3465.17 + i0.09	3469.04 + i0.07

2.2.4 Conclusions

We have studied Ω_c states which are dynamically generated from the interaction of meson-baryon in the charm sector. The interaction is obtained using an extension of the local hidden gauge approach with the exchange of vector mesons. We show that the dominant terms come from exchange of light vector mesons, leaving the heavy quarks as spectators. This has two good consequences: first we can map the interaction to what happens in $SU(3)$ using chiral Lagrangians, and second, the fact that the heavy quarks are spectators in the interaction guarantee that the dominant terms in the $(1/m_Q)$ counting fulfill the rules of heavy quark symmetry.

We obtain two states with $J^P = 1/2^-$ which are remarkably close in mass and width to the experimental states $\Omega_c(3050)$, $\Omega_c(3090)$. In addition, we also obtain a $3/2^-$ state with zero width at 3125 MeV, which can be associated to the experimental $\Omega_c(3119)$ that also has a width of the order or smaller than 1 MeV.

The agreement of the results with experiment is remarkable. It would be very interesting to see the next experimental steps to determine the spin-parity of these states, which could serve to discriminate between present models where there are large discrepancies concerning the spin-parity assignment.

2.3 The $\Omega_b \rightarrow \Omega_c$ decay and the molecular Ω_c states

In this section we present the follow up article of Ref. [2.3], which is based on the work presented in the previous section 2.2, from Ref. [2.1]. We discuss the reaction $\Omega_b \rightarrow (\Xi_c \bar{K}) \pi^-$, in which the new Ω_c states [2.2] could be observed. The predictions presented here could be confronted with future experiments from the LHCb and other collaborations.

2.3.1 Introduction

The recent discovery of five narrow Ω_c states by the LHCb collaboration [2.2] in pp collisions, also recently confirmed by the Belle collaboration [2.78] in e^+e^- collisions, motivated an increasing amount of theoretical work with different proposals for their structure. In particular, the correct assignment of quantum numbers J^P remains an open question and it could be the key to understand the nature of these states.

Predictions using quark models for such states and related ones were done in Refs. [2.25–2.37, 2.40–2.42, 2.79, 2.80]. Mostly proposing a diquark-quark structure $(ss)c$. Other methods have also been employed to study these states, as QCD Sum Rules in Refs. [2.50–2.56] and Lattice QCD in Ref. [2.57]. Pentaquark options have been suggested in Refs. [2.44–2.49]. Some works have emphasized the value of decay properties to obtain information on the nature of these states [2.58–2.60] and a discussion on the possible quantum numbers was done in Ref. [2.61].

On the other hand, some of these states could actually be pentaquark-like molecules, dynamically generated from meson-baryon interactions in coupled channels with charm $C = 1$, strangeness $S = -2$ and isospin $I = 0$. Predictions in the molecular picture using coupled channels of meson-baryon interactions were done in Refs. [2.16, 2.38, 2.39]. In this picture the interaction in S -wave of baryons with spin-parity $J^P = 1/2^+$ or $J^P = 3/2^+$ with pseudoscalar mesons leads to meson-baryon systems with $J^P = 1/2^-$ and $J^P = 3/2^-$, respectively. Channels with vector mesons instead of pseudoscalars can also be included resulting in $J^P = 1/2^-, 3/2^-$ and $5/2^-$. However, most of the recent works adopting this picture manage to relate two or three of the new Ω_c states to meson-baryon systems with $J^P = 1/2^-$ and $J^P = 3/2^-$, dominated by the pseudoscalar-baryon channels.

In Ref. [2.39] an $SU(6)_{lsf} \times HQSS$ model (HQSS stands for heavy quark spin symmetry) extending the Weinberg-Tomozawa πN interaction was employed to make a systematic study of many possible meson-baryon systems. In Ref. [2.82] the renormalization scheme of Ref. [2.39] was reviewed, performing an update of the results of the $C = 1$, $S = -2$ and $I = 0$ sector in view of the new experimental data. The updated results indicate that one can relate the $\Omega_c(3000)$ to a state with $J^P = 1/2^-$ and the $\Omega_c(3050)$ to another state with $J^P = 3/2^-$, with hints that the $\Omega_c(3090)$ or $\Omega_c(3119)$ could also have $J^P = 1/2^-$.

In Ref. [2.38] the molecular picture was developed using $SU(4)$ symmetry to extend the interaction described by vector meson exchange in the local hidden gauge approach. This work was also reviewed under the light of the new experimental data and an updated study was made in Ref. [2.62], where it was shown that the $\Omega_c(3050)$ and $\Omega_c(3090)$ can be both related to meson-baryon resonances with $J^P = 1/2^-$, stemming from pseudoscalar-baryon($1/2^+$) interaction.

A similar approach which also describes the meson-baryon interaction through vector meson exchange was recently developed in Ref. [2.1], using an extension of the local hidden gauge approach [2.9–2.13] and taking into account the spin-flavor wave functions of the baryons, which was presented on the previous section 2.2. In the present work we will follow this description of the Ω_c states. In section 2.2.3 we saw that a remarkable agreement of both masses and widths of the $\Omega_c(3050)$ and $\Omega_c(3090)$ was obtained from the pseudoscalar-baryon($1/2^+$) interaction, in accordance with results of Ref. [2.62]; also an extra state in the sector of pseudoscalar-baryon($3/2^+$)

could be related to the $\Omega_c(3119)$, therefore assigning to it the quantum numbers $J^P = 3/2^-$.

Other works on the molecular picture followed [2.83–2.85]. In Ref. [2.83] the authors propose that the broad structure found around 3188 MeV [2.2, 2.78] could be related with a molecular ΞD state due to the proximity of its threshold around 3185 MeV. As we saw in the previous section 2.2.3, in our approach [2.1] the molecular state dominated by the ΞD channel corresponds to the $\Omega_c(3090)$.

In the present work we propose the experimental study of these new states through the decay of Ω_b^- baryons, as suggested in Ref. [2.86]. The mass and lifetime of the Ω_b^- were recently measured by the LHCb collaboration [2.87], obtaining results compatible with the previous measurements of the same collaboration [2.88] and also with the ones of the CDF collaboration [2.89], but not with the results of the D0 collaboration [2.90]. We shall adopt the mass value listed by the Particle Data Group [2.91], which is quite close to the most recent measurement of LHCb.

We will discuss the $\Omega_b^- \rightarrow (\Xi_c^+ K^-)\pi^-$ decay and how the coupled channels approach naturally account for the dynamical generation of the Ω_c states from the hadronization that takes place after the conversion of the b quark into a c quark. Then we show the results of how these two states would be seen in the Ω_b^- decay if the molecular picture of Ref. [2.1] is correct, providing solid predictions for the experimental measurements that could be performed by the LHCb collaboration [2.86] in the future, which would provide useful information to distinguish states with different structures and quantum numbers.

2.3.2 The $\Omega_c(3050)$ and $\Omega_c(3090)$ in the molecular picture

In the previous section 2.2 a thorough discussion of the work of Ref. [2.1] was made about the meson-baryon interaction due to the exchange of vector mesons.

While vector-baryon contributions were also considered, it was shown there that these states decouple to a good degree of approximation from pseudoscalar-baryon(1/2) states, and using the channels $\Xi_c \bar{K}$, $\Xi'_c \bar{K}$, ΞD , $\Omega_c \eta$ the states $\Omega_c(3050)$ and $\Omega_c(3090)$ could be reproduced, both the mass and width.

A third state, the $\Omega_c(3119)$, could also be related with another pseudoscalar-baryon(3/2) system. However, since in our approach this state does not mix with the channels of $J = 1/2$, its decay into $\Xi_c \bar{K}$ calls for additional mechanisms with the exchange of pseudoscalars, which go beyond the scope of our approach here.

On the present work we will study the mechanism where these two states, the $\Omega_c(3050)$ and $\Omega_c(3090)$, can be generated in the Ω_b decay. In Table 2.11 we show the main results we will need.

2.3.3 The $\Omega_b^- \rightarrow (\Xi_c \bar{K} / \Xi'_c \bar{K} / \Xi D) \pi^-$ decays

Let us see how the $\Omega_c(3050)$ and $\Omega_c(3090)$ are produced in this reaction within our picture. Since the resonances come from the interaction of pseudoscalar-baryon states shown in Table 2.11, one has to hadronize the three quarks which come from the $b \rightarrow c$ transition and the spectator ss quarks (see Fig. 2.7). In the hadronization we introduce $\bar{q}q$ with the quantum numbers of the vacuum, and two options are

Table 2.11: Pole position [MeV], couplings g_i [dimensionless] and wave functions at the origin $g_i G_i^{II}$ [MeV] from pseudoscalar(0^-)-baryon($1/2^+$) interaction describing the $\Omega_c(3050)$ and $\Omega_c(3090)$.

3054.05 + i0.44	$\Xi_c \bar{K}$	$\Xi_c' \bar{K}$	ΞD	$\Omega_c \eta$
g_i	$-0.06 + i0.14$	1.94 + i0.01	$-2.14 + i0.26$	$1.98 + i0.01$
$g_i G_i^{II}$	$-1.40 - i3.85$	-34.41 - i0.30	$9.33 - i1.10$	$-16.81 - i0.11$
3091.28 + i5.12	$\Xi_c \bar{K}$	$\Xi_c' \bar{K}$	ΞD	$\Omega_c \eta$
g_i	$0.18 - i0.37$	$0.31 + i0.25$	5.83 - i0.20	$0.38 + i0.23$
$g_i G_i^{II}$	$5.05 + i10.19$	$-9.97 - i3.67$	-29.82 + i0.31	$-3.59 - i2.23$

possible: insertion of $\bar{q}q$ between the c and one s -quark, as shown in the figure, or insertion between the two s -quarks. In this latter case the three final quarks (leaving the π^- apart) have $J^P = 1/2^+$ and hence the state has positive parity. With one pseudoscalar, $J^P = 0^-$, and a baryon of $J^P = 1/2^+$ in the final state, this requires a P -wave, but the molecules are produced in S -wave and this mechanism is hence inoperative to produce these resonances. In the case of hadronization between the c - and s -quarks, the c quark can be produced in $L = 1$ after the weak vertex and the negative parity is restored. Then, the $L = 1$ excited c -quark is deexcited via hadronization, where the $\bar{q}q$ is produced in a 3P_0 state [2.92–2.94].

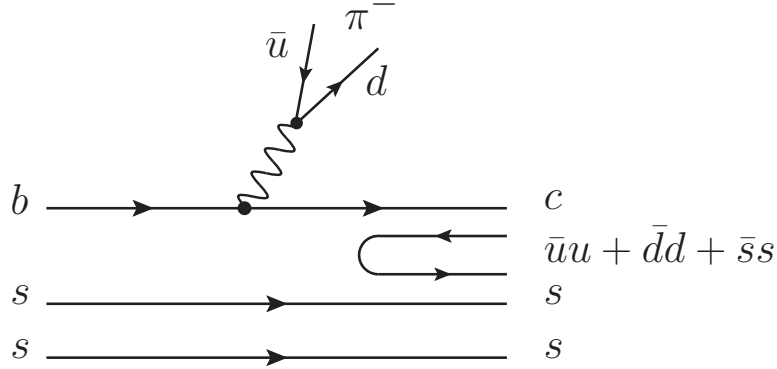


Figure 2.7: Ω_b^- decay at quark level with emission of a π^- and subsequent hadronization.

Looking at the flavor of the quarks, the hadronization proceeds as follows:

$$css \rightarrow c(\bar{u}u + \bar{d}d + \bar{s}s)ss \equiv H, \quad (2.65)$$

$$H = \sum_i c \bar{q}_i q_i ss \equiv \sum_i \Phi_{4i} q_i ss, \quad (2.66)$$

where in the last step we have written the $(q\bar{q})$ matrix

$$(q\bar{q}) = \begin{pmatrix} u\bar{u} & u\bar{d} & u\bar{s} & u\bar{c} \\ d\bar{u} & d\bar{d} & d\bar{s} & d\bar{c} \\ s\bar{u} & s\bar{d} & s\bar{s} & s\bar{c} \\ c\bar{u} & c\bar{d} & c\bar{s} & c\bar{c} \end{pmatrix} \quad (2.67)$$

in terms of their meson components by means of the matrix Φ in Eq. (2.39),

Then replacing the $c\bar{q}$ meson terms we get

$$H = D^0 uss + D^+ dss + \dots \quad (2.68)$$

where we have already neglected the heavy combination of $D_s^+ sss$ which could only contribute to states with $J^P = 3/2^-$ since sss corresponds to the Ω^- , and furthermore its mass is far away from the range of energies studied here.

It is easy to see that, since ss has isospin zero, the combination $D^0 uss + D^+ dss$ has isospin zero², and uss , dss have only overlap with Ξ^0 and Ξ^- , respectively. Hence the combination of Eq. (2.68) can be written up to a global factor by

$$H = |\Xi D, I = 0\rangle = -\frac{1}{\sqrt{2}} |\Xi^0 D^0 - \Xi^- D^+\rangle, \quad (2.69)$$

where we have absorbed the global minus sign when we changed to the isospin zero combination in the order baryon-meson.

Now we proceed to construct the amplitude of the process $\Omega_b^- \rightarrow (\Xi_c \bar{K}) \pi^-$. It is instructive to first look at the process $\Omega_b^- \rightarrow (\Xi D) \pi^-$, as depicted in Fig. 2.8. From Eq. (2.69) we see that after the emission of a pion, the hadronization involving the css quarks generates a ΞD pair in isospin zero. Thus we can write this process as the sum of a tree-level contribution and the final state interaction of ΞD going through the molecular states of Table 2.11. This information is contained in the diagonal t matrix element $t_{\Xi D \rightarrow \Xi D}^{I=0}$, the same t matrix from Ref. [2.1] used to search for the poles, as we saw in section 2.1.3 and 2.2.

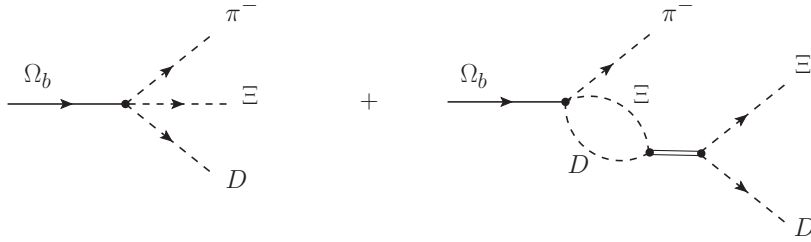


Figure 2.8: $\Omega_b^- \rightarrow \pi^- \Xi D$ process. Tree-level (left) plus ΞD rescattering (right).

Then for the tree-level contribution (left diagram of Fig. 2.8) we simply write $t_{\text{tree}} = V_P$, where V_P contains all information related to the Ω_b^- weak decay and dynamics of the hadronization, a common unknown factor in all process we will investigate. On the other hand, for the ΞD rescattering (right diagram of Fig. 2.8) we will have

$$t_{\text{loop}} = V_P G_{\Xi D} [M_{\text{inv}}(\Xi D)] t_{\Xi D \rightarrow \Xi D}^{I=0} [M_{\text{inv}}(\Xi D)], \quad (2.70)$$

² Recall the isospin doublets:

$$D = \begin{pmatrix} D^+ \\ -D^0 \end{pmatrix}, \quad \Xi = \begin{pmatrix} \Xi^0 \\ -\Xi^- \end{pmatrix}.$$

where $G_{\Xi D}$ is the propagator of the baryon-meson loop used in the Bethe-Salpeter equation, as in Eqs. (2.32) and (2.33), with V the transition potential from Eq. (2.62) as we saw in section 2.2.2, calculated in Ref. [2.1]. Then the amplitude of the process $\Omega_b^- \rightarrow \pi^- \Xi D$ is given by

$$t_{\Omega_b^- \rightarrow \pi^- \Xi D} = V_P \left[1 + G_{\Xi D}(M_{\Xi D}) t_{\Xi D \rightarrow \Xi D}^{I=0}(M_{\Xi D}) \right], \quad (2.71)$$

where we introduced the compact notation $M_{\Xi D}$ for $M_{\text{inv}}(\Xi D)$. With this amplitude we can write the ΞD invariant mass distribution

$$\frac{d\Gamma}{dM_{\text{inv}}(\Xi D)} = \frac{1}{(2\pi)^3} \frac{M_{\Xi}}{M_{\Omega_b^-}} p_{\pi^-} \tilde{p}_D \left| t_{\Omega_b^- \rightarrow \pi^- \Xi D} \right|^2, \quad (2.72)$$

where we adopt the Mandl-Shaw normalization for fermion fields and p_{π^-} is the pion momentum in the Ω_b^- rest frame for the $\Omega_b^- \rightarrow (\Xi D) \pi^-$ decay

$$p_{\pi^-} = \frac{\lambda^{1/2} \left(M_{\Omega_b^-}^2, m_{\pi^-}^2, M_{\text{inv}}^2(\Xi D) \right)}{2M_{\Omega_b^-}}, \quad (2.73)$$

and \tilde{p}_D is the D momentum in the ΞD rest frame

$$\tilde{p}_D = \frac{\lambda^{1/2} \left(M_{\text{inv}}^2(\Xi D), m_D^2, m_{\Xi}^2 \right)}{2M_{\text{inv}}(\Xi D)}. \quad (2.74)$$

For the $\Omega_b^- \rightarrow (\Xi_c \bar{K}) \pi^-$ process there is no tree-level contribution, since the hadronization only produces a ΞD pair, as in Eq. (2.69). Then the only contribution comes from the diagram in Fig. 2.9.

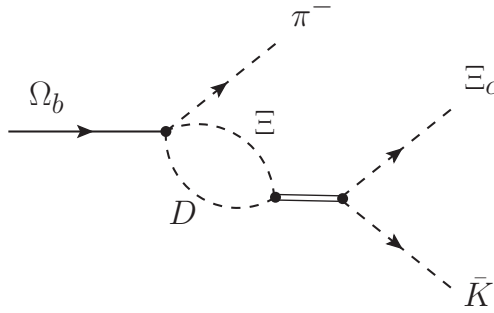


Figure 2.9: $\Omega_b^- \rightarrow \pi^- \Xi_c \bar{K}$ process through ΞD rescattering.

Due to our coupled channels approach, the transition $\Xi D \rightarrow \Xi_c \bar{K}$ is already contained in the t matrix and the production of $\Xi_c \bar{K}$ (also in isospin zero) appears naturally. The corresponding amplitude will be

$$t_{\Omega_b^- \rightarrow \pi^- \Xi_c \bar{K}} = V_P G_{\Xi D}(M_{\Xi_c \bar{K}}) t_{\Xi D \rightarrow \Xi_c \bar{K}}(M_{\Xi_c \bar{K}}), \quad (2.75)$$

where $t_{\Xi D \rightarrow \Xi_c \bar{K}}$ is the transition amplitude of $\Xi D \rightarrow \Xi_c \bar{K}$, from the same t matrix. Then the $\Xi_c \bar{K}$ invariant mass distribution is also analogous,

$$\frac{d\Gamma}{dM_{\text{inv}}(\Xi_c \bar{K})} = \frac{1}{(2\pi)^3} \frac{M_{\Xi_c}}{M_{\Omega_b^-}} p_{\pi^-} \tilde{p}_{\bar{K}} \left| t_{\Omega_b^- \rightarrow \pi^- \Xi_c \bar{K}} \right|^2, \quad (2.76)$$

where p_{π^-} is the pion momentum in the Ω_b^- rest frame (now for $\Omega_b^- \rightarrow (\Xi_c \bar{K}) \pi^-$) and $\tilde{p}_{\bar{K}}$ is the kaon momentum in the $\Xi_c \bar{K}$ rest frame, analogous to Eqs. (2.73) and (2.74).

Analogously, we can also calculate the invariant mass distribution for the final state $\Xi'_c \bar{K}$, replacing Ξ_c by Ξ'_c in the previous equations and taking the matrix element of the t matrix corresponding to the transition $\Xi D \rightarrow \Xi'_c \bar{K}$.

It is also interesting to look at the case of coalescence, where the ΞD pair merges into the resonance regardless of the final decay channel, as depicted in Fig. 2.10.

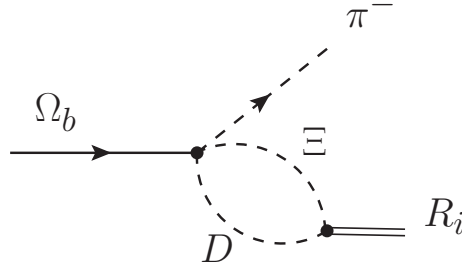


Figure 2.10: Resonance coalescence in the $\Omega_b^- \rightarrow \pi^- R_i$ process through ΞD rescattering, where R_i is the $\Omega_c(3050)$ or $\Omega_c(3090)$.

The value of the amplitude in the process $\Omega_b^- \rightarrow \pi^- R_i$, where R_i is one of the molecular states of Table 2.11, is proportional to the coupling of that resonance to the ΞD channel,

$$t_{\Omega_b^- \rightarrow \pi^- R_i} = V_P G_{\Xi D}(M_{R_i}) g_{R_i, \Xi D}, \quad (2.77)$$

where the propagator is calculated at the resonance mass M_{R_i} . With this quantity we can calculate the equivalent of the integrated mass distribution around the R_i resonance, which does not depend on its decay mode,

$$\Gamma_{\Omega_b^- \rightarrow \pi^- R_i} = \frac{1}{2\pi} \frac{M_{R_i}}{M_{\Omega_b^-}} p'_{\pi^-} \left| t_{\Omega_b^- \rightarrow \pi^- R_i}(M_{R_i}) \right|^2, \quad (2.78)$$

where p'_{π^-} is the pion momentum in the Ω_b^- rest frame for $\Omega_b^- \rightarrow \pi^- R_i$.

Let us make some further remarks concerning the Ω_b decay process. As we have discussed, the mechanism of Figs. 2.8 or 2.9 produces the resonances $\Omega_c(3050)$ and $\Omega_c(3090)$. These resonances are generated in Ref. [2.1], as discussed in section 2.2, through the interaction of the coupled channels $\Xi_c \bar{K}$, $\Xi'_c \bar{K}$, ΞD and $\Omega_c \eta$. This approach takes into account the transition from one channel to another, and all of them participate in the generation of the resonances. In principle one could create

these resonances initiated by any of the channels. However, the discussion leading to Eq. (2.69) tells us that the weak decay mechanism filters the primary production of the ΞD channel and the resonances are only initiated by this channel. This does not mean that the other channels do not play a role here. Their contribution is implicit in the $t_{\Xi D \rightarrow \text{final}}$ transition amplitudes which contain all channels through the terms $V_{\Xi D \rightarrow i} G_i V_{i \rightarrow \text{final}}$, $V_{\Xi D \rightarrow i} G_i V_{ij} G_j V_{j \rightarrow \text{final}}$, etc, that are summed up by the Bethe-Salpeter equation.

One can, however, see if there is a way to produce, for instance, $\Xi_c \bar{K}$ in the first step of the decay. Topologically this is possible producing the hadronization between the ss quarks in Fig. 2.7. Indeed, taking the $\bar{u}u$ component of the hadronization one obtains the cus baryon, corresponding to Ξ_c and $\bar{u}s$ that corresponds to K^- . However, in the spectator picture of Fig. 2.7 this is not possible for other reasons, as we pointed above. Indeed, since the c quark is not affected by the hadronization and belongs to Ξ_c at the end, it is a state $1/2^+$ in its ground state. But the initial ss component is a spectator in the weak decay and both quarks are in $1/2^+$ and ground state. After the weak decay and prior to the hadronization we have c, s, s all in $1/2^+$ and in their ground state, and have total positive parity. This state cannot lead to the $1/2^-$ $\Omega_c(3050)$, $\Omega_c(3090)$ resonances, or equivalently meson-baryon in S -wave.

2.3.4 Results

It is interesting to see how these processes show the importance of the coupled channels. The decay of the Ω_c states into ΞD is kinematically forbidden below the corresponding threshold at 3185 MeV, then we cannot see the corresponding peaks in the ΞD invariant mass distribution, but we can see their indirect effect, both from the meson-baryon loop in Eq. (2.71) and from the amplitude $t_{\Xi D \rightarrow \Xi D}^{I=0}$. The corresponding invariant mass distribution, Eq. (2.72), is shown in Fig. 2.11 by the solid line. To compare with the case where only the tree-level contributes, we remove t_{loop} and keep only t_{tree} (keeping only the term 1 in the bracket of Eq. (2.71)), normalizing the curve such that it has the same area as the solid curve in the energy range shown, which is plotted as the dashed line in Fig. 2.11. We should note that, should we have produced the ΞD in P -wave at tree-level, hadronizing with $\bar{q}q$ within the two s -quarks, we would find a contribution to $d\Gamma/dM_{\text{inv}}(\Xi D)$ in Eq. (2.72) with an extra \tilde{p}_D^2 factor, which changes the shape of the dashed line in Fig. 2.11 drastically and is easily distinguishable from an S -wave.

If we look at $\pi^- \Xi_c \bar{K}$ in the final state, the $\Xi_c \bar{K}$ threshold is at 2965 MeV, and then we can see clearly the peaks of the Ω_c states in the $\Xi_c \bar{K}$ invariant mass distribution. According to Eq. (2.69), we expect only ΞD production from the hadronization that occurs right after the Ω_b^- decay, which means we have no tree-level contribution for $\Xi_c \bar{K}$ production. However, the transition to $\Xi_c \bar{K}$ through off-shell ΞD loops arises naturally from the coupled channels approach. In fact, both the $\Omega_c(3050)$ and $\Omega_c(3090)$ couple strongly to ΞD (see Table 2.11), and their formation from the ΞD state formed in the first step of the Ω_b^- decay with subsequent transition to $\Xi_c \bar{K}$ (going through the ΞD virtual state) is not only possible, but expected.

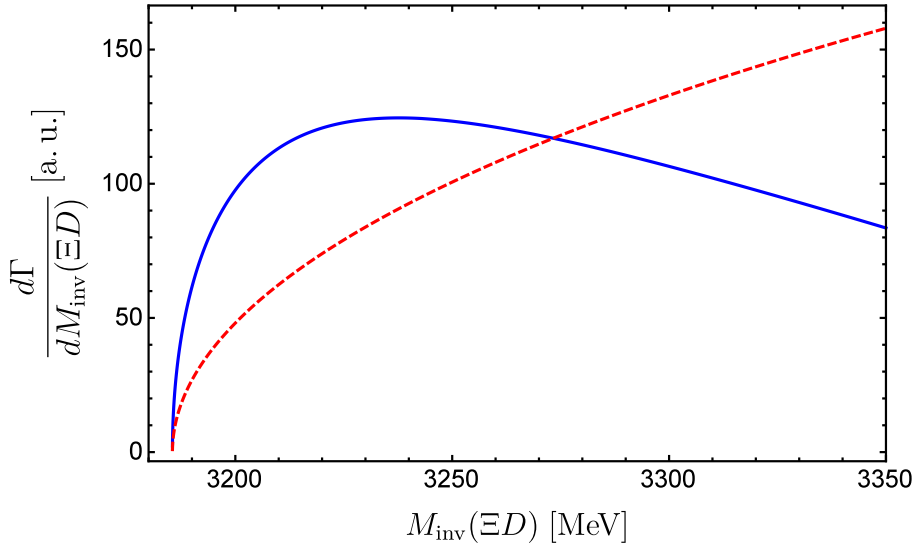


Figure 2.11: ΞD invariant mass distribution from Eq. (2.72). Solid line: using the complete amplitude of Eq. (2.71). Dashed line: removing the $G_{\Xi D} t_{\Xi D \rightarrow \Xi D}^{I=0}$ term (only tree-level contribution) and normalizing such that both curves have the same area.

In Fig. 2.12 we show the $\Xi_c \bar{K}$ invariant mass distribution. The only unknown quantity is the global factor V_P , common to all amplitudes we investigate here. The ratio between the intensity of each peak does not depend on V_P , so all ratios are predictions that could be confronted with future experiments. We can see that the intensity of the $\Omega_c(3050)$ peak is about 65% higher than for the $\Omega_c(3090)$ peak.

The width of the states in Fig. 2.12 is an output of the coupled channels dynamics in Ref. [2.1] to generate the Ω_c states. However, as seen in Fig. 2.9, the strength of these peaks is related to the product of the couplings of the resonances to ΞD and $\Xi_c \bar{K}$ and hence a direct consequence of the way in which the reaction proceeds according to our picture.

Note that we are using the same normalization for all the reactions, hence the ratio of the strength at the peaks in Fig. 2.12 to the strength of the ΞD mass distribution (solid line) in Fig. 2.11 is also a prediction. In arbitrary units, the ΞD distribution has a maximum of about 125 around 3240 MeV, whereas in the $\Xi_c \bar{K}$ distribution the $\Omega_c(3050)$ and $\Omega_c(3090)$ peaks have an intensity of about 15.50×10^3 and 9.45×10^3 , respectively, therefore we predict that the $\Xi_c \bar{K}$ distribution in the vicinity of the resonances peaks is roughly two orders of magnitude higher than that of the ΞD distribution.

Cusp effects in the $\Xi_c \bar{K}$ distribution also appear at the $\Xi'_c \bar{K}$ and ΞD thresholds at 3074 MeV and 3185 MeV, respectively, but their intensity is very small compared to the peaks of the resonances and cannot be seen clearly in Fig. 2.12. Then, according to our predictions they should not be seen in experiment.

We also notice that apparently no significant interference pattern is seen between the two states in Fig. 2.12, even though they have the same quantum numbers, a feature that also agrees with the fit performed by the LHCb collaboration [2.2, 2.40].

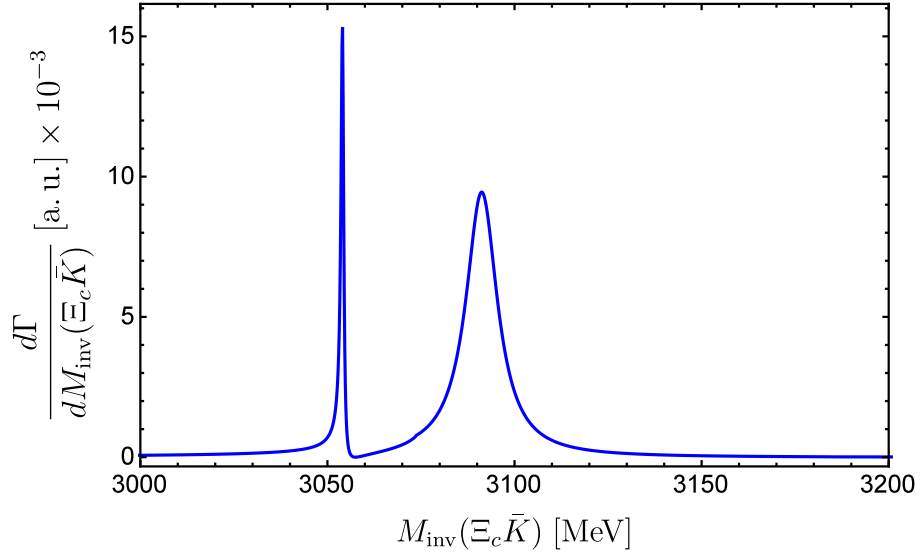


Figure 2.12: $\Xi_c \bar{K}$ invariant mass distribution from Eq. (2.76).

As for the $\Xi'_c \bar{K}$ invariant mass distribution, only the $\Omega_c(3090)$ can be seen, as shown in Fig. 2.13, since this channel is also open for the decay of this state, whereas the $\Omega_c(3050)$ is below the threshold of $\Xi'_c \bar{K}$.

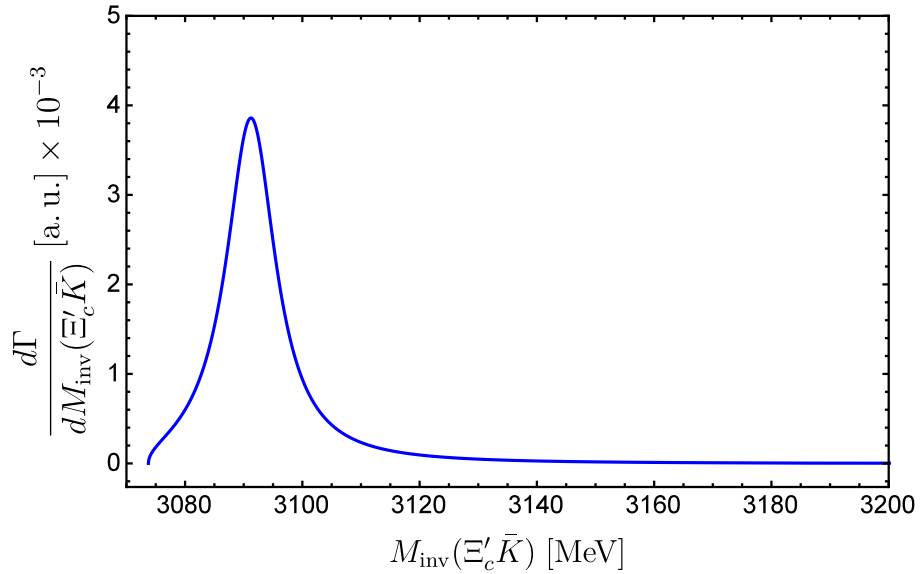


Figure 2.13: $\Xi'_c \bar{K}$ invariant mass distribution from Eq. (2.76), replacing Ξ_c by Ξ'_c and taking $t_{\Xi D \rightarrow \Xi'_c \bar{K}}$.

Again we can compare the intensity of the peaks. In the $\Xi'_c \bar{K}$ distribution the $\Omega_c(3090)$ peak has an intensity of 3.86×10^3 , which is about 40% of the intensity it has in the $\Xi_c \bar{K}$.

Finally, it is interesting to compare the results of $\Gamma_{\Omega_b^- \rightarrow \pi^- R_i}$, given by Eq. (2.78), with the integrated invariant mass distribution of Eq. (2.76) around the peak of each

resonance,

$$\int_{R_i} \frac{d\Gamma}{dM_{\text{inv}}(\Xi_c \bar{K})} dM_{\text{inv}}(\Xi_c \bar{K}). \quad (2.79)$$

In Table 2.12 we show the results of Eqs. (2.78) and (2.79) for the $\Omega_c(3050)$ and $\Omega_c(3090)$, and for the latter we also show the integrated $\Xi'_c \bar{K}$ distribution.

Table 2.12: Comparison between integrated invariant mass distributions around each resonance and the corresponding coalescence (arbitrary units).

State	$\Omega_c(3050)$	$\Omega_c(3090)$	
Pole [MeV]	3054.05 + i0.44	3091.28 + i5.12	
Coalescence Eq. (2.78)	21289	215237	
Channel	$\Xi_c \bar{K}$	$\Xi_c \bar{K}$	$\Xi'_c \bar{K}$
Interval [MeV]	[3049, 3057]	[3057, 3120]	[3074, 3120]
Integral Eq. (2.79)	21344	133482	51074

From these results we can draw some interesting conclusions. Let us look first at the $\Omega_c(3050)$. In Table 2.11 we can see that this state is dominated by the $\Xi'_c \bar{K}$ channel, and also has sizable contributions from the higher channels ΞD and $\Omega_c \eta$. However, the pole is at 3054 MeV, which is 20 MeV below the $\Xi'_c \bar{K}$ threshold, so the only open channel is $\Xi_c \bar{K}$, to which the resonance couples very weakly and the phase space available is only about 90 MeV. This feature explains two points: 1) The narrowness of the state, whose upper limit of the width reported by the LHCb collaboration is $0.8 \pm 0.2 \pm 0.1$ MeV [2.2], in excellent agreement with the result of Ref. [2.1] with $\Gamma = 2 \times \text{Im}(R_i) = 0.88$ MeV; 2) The good agreement of $\Gamma_{\Omega_b^- \rightarrow \pi^- R_i}$, 21289, given by Eq. (2.78), with the integrated invariant mass distribution around the resonance peak, 21344, given by Eq. (2.79) (the small difference is irrelevant and comes essentially from the choice of the interval of integration). This happens because the state is very narrow and the only channel open for decay is the $\Xi_c \bar{K}$, so the value we obtain from the coalescence, which is independent of the decay channel, matches the value obtained from the integration over the only channel available ($\Xi_c \bar{K}$), as it should be.

On the other hand, the $\Omega_c(3090)$ is dominated by the ΞD channel, with some contribution from the other channels. Even though this state couples very strongly to ΞD , it is almost 100 MeV below the respective threshold. It can only decay to $\Xi_c \bar{K}$ and $\Xi'_c \bar{K}$. In both cases the coupling is small, and in the latter channel the phase space available is less than 20 MeV (see Table 2.11). This again, explains two main features: 1) The narrowness, with a width not so small as in the case of the $\Omega_c(3050)$, but still very narrow, since the decay into $\Xi_c \bar{K}$ is reasonable, with more than 120 MeV of phase space available, although the coupling to that channel is weak. The LHCb reports a width of $8.7 \pm 1.0 \pm 0.8$ MeV [2.2], in fair agreement with the result of Ref. [2.1] of 10.24 MeV; 2) The fact that the integrated invariant mass distribution around the peak, 133482 in the $\Xi_c \bar{K}$ distribution, is about 2/3 of the total given by the coalescence, 215237, which is also expected, since in Eq. (2.79) we are integrating only in the $\Xi_c \bar{K}$ channel, whereas this state can also decay into $\Xi'_c \bar{K}$. The sum of both integrals, in $\Xi_c \bar{K}$ and $\Xi'_c \bar{K}$, is 184556, close to the total given by the coalescence, but still below. This is also expected since Eq. (2.78) is actually an

approximation that is valid in the limit of zero width, which works pretty well for the $\Omega_c(3050)$ but is not so good for the $\Omega_c(3090)$, with already 10 MeV of width.

As a prediction we can also state, based on the coalescence results, that the ratio of the $\Omega_c(3050)$ over the $\Omega_c(3090)$ production is about 10% in the Ω_b^- decay:

$$\frac{\Gamma_{\Omega_b^- \rightarrow \pi^- \Omega_c(3050)}}{\Gamma_{\Omega_b^- \rightarrow \pi^- \Omega_c(3090)}} \approx 10\%. \quad (2.80)$$

Another point worth discussing is the possibility to have some component of these resonances of the $3q$ type and not molecular. We have considered Ω_c states of pure molecular nature. In the real world, if allowed by quantum numbers, the mixing with $3q$ components with the same quantum numbers is unavoidable. The question is how large these components are. In our work we are implicitly assuming that they are negligible. The issue of the mixing of $3q$ and molecular components has received some attention [2.95–2.97], and present lattice results [2.98] are helping in these studies through proper analysis, as done in Ref. [2.97]. These studies show that in cases where the dynamical coupled channels unitary approach leads to molecular states, the $3q$ components are indeed small. Yet, the question here is whether we can show how the present results are stable under the assumption of small $3q$ components for the Ω_c states. An answer for this problem is already available in the thorough study carried out in Ref. [2.99].

In that work a study similar to the present one is carried out for the $B_s^0 \rightarrow J/\Psi f_1(1285)$ decay. The J/Ψ plays the role of the pion here and the $f_1(1285)$ state, assumed to be a $K^* \bar{K}$ molecule, plays the role of the Ω_c resonances here. In Ref. [2.99] a study was done taking into account the $f_1(1285)$ as a pure molecule or having a probability z to be a $q\bar{q}$ state. The details of the issue are shown in section IX of Ref. [2.99] where one can see that for values of $z \approx 0.2$ the changes in ratios of magnitudes are smaller than 20% and they are also moderate for values of $z \approx 0.4$. These results tell us that the results obtained here are solid in this respect, since changes of 20% in the results obtained are not relevant for the prospective work carried out here.

2.3.5 Conclusions

We have studied the weak decay $\Omega_b^- \rightarrow (\Xi_c^+ K^-) \pi^-$, in view of the narrow Ω_c states recently measured by the LHCb collaboration and later confirmed by the Belle collaboration. Based on the previous work where the $\Omega_c(3050)$ and $\Omega_c(3090)$ are described as meson-baryon molecular states, using an extension of the local hidden gauge approach in coupled channels, with results in remarkable agreement with experiment, we have investigated the ΞD , $\Xi_c \bar{K}$ and $\Xi'_c \bar{K}$ invariant mass distributions, and discussed the role of coupled channels in the process. Predictions that could be confronted with future experiments are presented, providing useful information that could help to determine the quantum numbers and nature of these states. Since Ω_b^- baryons have already been observed in several experiments, two of them performed by the LHCb collaboration, the present work should encourage such study in the near future, which would certainly bring novel key information for the understanding of these new states.

2.4 Predictions for molecular Ω_b states

In this section we present the work of Ref. [2.4] with predictions for molecular Ω_b states using the same approach of Ref. [2.1] in section 2.2 for the Ω_c states.

2.4.1 Introduction

The study of baryon states with charm or beauty is capturing much attention in hadron physics recently [2.48, 2.100–2.104]. The finding of baryon states of hidden charm (pentaquarks) in Refs. [2.105, 2.106] certainly stimulated this field, but this was followed by another relevant discovery, with the observation of five new Ω_c states [2.2]. This discovery stimulated much theoretical work trying to describe these states, as we saw in section 2.2 and Ref. [2.1]. From these we specially refer to Ref. [2.62] which uses a dynamics closely related to ours.

The Ω_b states have not been the subject of much study. Experimentally the PDG [2.91] quotes the ground state $J^P = \frac{1}{2}^+$ and no more states. The $J^P = \frac{3}{2}^+$ excited state has not yet been observed. Theoretical work is also scarce, but there are predictions for $\frac{1}{2}^-$, $\frac{3}{2}^-$, $\frac{5}{2}^-$, $\frac{1}{2}^+$, $\frac{3}{2}^+$, $\frac{5}{2}^+$, $\frac{7}{2}^+$ states in different quark models, relativistic quark model [2.29], non-relativistic quark model [2.26] and QCD sum rules [2.35, 2.107–2.109]. In this latter line, some recent works make predictions for the Ω_b ground state and the first orbitally and radially excited states, with spin $J = 1/2$ and $3/2$ [2.50, 2.110].

Unlike in the charm sector, no work on Ω_b molecular states has been done. The recent finding of the Ω_c states by the LHCb collaboration [2.2], and the steady work in the search of new states, makes the study of Ω_b molecular states relevant and opportune. The opportunity is even more apparent after the realization in the works of Refs. [2.1, 2.62] that several of the observed states can be well described in the molecular picture. In Ref. [2.62] the local hidden gauge formalism is used to obtain the interaction between mesons and baryons in the charm sector, with the quantum number of Ω_c . The channels considered are $\Xi_c \bar{K}$, $\Xi'_c \bar{K}$, ΞD , $\Omega_c \eta$, $\Omega_c \eta'$ and the interaction proceeds via the exchange of vector mesons, extending the local hidden gauge Lagrangian [2.11–2.13] to $SU(4)$. Two states of $\frac{1}{2}^-$ could be associated to the $\Omega_c(3050)$ and $\Omega_c(3090)$ states of Ref. [2.2], both in energy and approximately width.

As presented in section 2.2, the work of Ref. [2.1] continues with this line but does not assume $SU(4)$ for the interaction. Instead, the wave functions of the charmed baryons in the coupled channels isolate the charm quark and symmetrize the spin-flavor wave function of the light quarks. The diagonal terms in the transition potentials between the coupled channels coincide in Ref. [2.62] and Ref. [2.1], but there are differences in the non-diagonal ones. In addition in Ref. [2.1] the states $\Xi_c^* \bar{K}$, $\Omega_c^* \eta$, $\Xi^* D$ are considered from where another state of $\frac{3}{2}^-$ emerges that can also be associated to a third state of Ref. [2.2].

In Ref. [2.1] one obtains three states, which can be associated to three states of Ref. [2.2], and the agreement of masses and widths is good. The success of this approach to get some of the observed Ω_c states stimulates us to use the same idea and make predictions for Ω_b states. The work is simple because all one must do is

to change a c quark by a b quark, and the matrix elements of the interaction are formally the same, although some differences appear in the non-diagonal terms due to the different masses of the hadrons. On the other hand, we can also benefit from the works of Refs. [2.15, 2.22] which show that to preserve heavy quark symmetry in the molecular states one should use a common cutoff in the regularization of the meson-baryon loop functions in the heavy quark sector. An alternative method to preserve this symmetry is provided in Ref. [2.23]. Given these two ingredients, we feel confident that the two $\frac{1}{2}^-$ states and the $\frac{3}{2}^-$ state that come from our approach for the Ω_b should be realistic. We also predict other states at higher masses, analogous to some states predicted for Ω_c which lie in a region of large background and are more difficult to identify. Ω_b states are produced with smaller statistics in LHCb but they are subject of investigation. With increased luminosity in the next LHCb runs, the observation of Ω_b states will become a state of the art and the comparison with the predictions done here will shed light on hadron dynamics and the nature of some hadronic states.

2.4.2 Formalism

We follow closely the formalism of section 2.2.2 by changing a c quark by a b quark. For the case of Ω_c we took the coupled channels from Ref. [2.39] up to an energy of 3470 MeV, far above the energy of the states seen in Ref. [2.2]. In the present case we take the corresponding states changing the quark c by the b quark. We take into account the S -wave interaction of these coupled channels and hence we can have states with $J^P = \frac{1}{2}^-, \frac{3}{2}^-$. In Tables 2.13, 2.14 and 2.15 we show these coupled channels and the corresponding threshold masses ³.

Table 2.13: The pseudoscalar-baryon states with $J^P = \frac{1}{2}^-$ and their threshold masses in MeV.

States	$\Xi_b \bar{K}$	$\Xi'_b \bar{K}$	$\Omega_b \eta$	$\Xi \bar{B}$
Threshold	6289	6431	6594	6598

Table 2.14: The pseudoscalar-baryon states with $J^P = \frac{3}{2}^-$ and their threshold masses in MeV.

States	$\Xi_b^* \bar{K}$	$\Omega_b^* \eta$	$\Xi^* \bar{B}$
Threshold	6451	6619	6813

³The Ω_b^* state has not yet been observed. We estimate its mass as follows. In the charm sector, we have $m_{D^*} - m_D = 142$ MeV, $m_{\Omega_c^*} - m_{\Omega_c} = 71$ MeV. Hence the difference of masses between Ω_c^* and Ω_c is about one half the one between D^* and D . We apply the same rule in the b sector and take $m_{\Omega_b^*} - m_{\Omega_b} \simeq \frac{1}{2}(m_{B^*} - m_B) \simeq 23$ MeV. If we assume, following the rules of heavy quark spin symmetry, that $m_{\Omega_b^*} - m_{\Omega_b}$ goes as $\frac{1}{m_b}$ and $m_{\Omega_c^*} - m_{\Omega_c} \sim \frac{1}{m_c}$, then we get $m_{\Omega_b^*} - m_{\Omega_b} \simeq 28$ MeV. We take the average value 25 MeV, hence $m_{\Omega_b^*} = 6071$ MeV.

Table 2.15: The vector-baryon states with $J^P = \frac{1}{2}^-, \frac{3}{2}^-$ and their threshold masses in MeV.

States	ΞB^*	$\Xi_b K^*$	$\Xi'_b K^*$
Threshold	6643	6687	6829

The interaction between these channels at tree level is obtained using the local hidden gauge (LHG) approach [2.11–2.13] extended to the beauty sector. The interaction is mediated by the exchange of vector mesons, as shown in Fig. 2.14 for two cases.

The upper vertex in Fig. 2.14 for vector(V)-pseudoscalar(P)-pseudoscalar(P) is given in terms of the VPV Lagrangian of Eq. (2.9) we saw in section 2.1.2, with Φ, V the $SU(4)$ matrices for pseudoscalar mesons and the vector mesons with the quarks u, d, s, b .

$$P = \begin{pmatrix} \frac{1}{\sqrt{2}}\pi^0 + \frac{1}{\sqrt{3}}\eta + \frac{1}{\sqrt{6}}\eta' & \pi^+ & K^+ & B^+ \\ \pi^- & -\frac{1}{\sqrt{2}}\pi^0 + \frac{1}{\sqrt{3}}\eta + \frac{1}{\sqrt{6}}\eta' & K^0 & B^0 \\ K^- & \bar{K}^0 & -\frac{1}{\sqrt{3}}\eta + \sqrt{\frac{2}{3}}\eta' & B_s^0 \\ B^- & \bar{B}^0 & \bar{B}_s^0 & \eta_b \end{pmatrix}, \quad (2.81)$$

where we also include the mixing between η and η' [2.66], and

$$V = \begin{pmatrix} \frac{1}{\sqrt{2}}\rho^0 + \frac{1}{\sqrt{2}}\omega & \rho^+ & K^{*+} & B^{*+} \\ \rho^- & -\frac{1}{\sqrt{2}}\rho^0 + \frac{1}{\sqrt{2}}\omega & K^{*0} & B^{*0} \\ K^{*-} & \bar{K}^{*0} & \phi & B_s^{*0} \\ B^{*-} & \bar{B}^{*0} & \bar{B}_s^{*0} & \Upsilon \end{pmatrix}. \quad (2.82)$$

The change of the c quark by the b quark, with the same structure of the wave functions, has as a consequence that the matrix elements of the transitions are formally the same up to some small change in the non-diagonal terms that we discuss below.

As we had for the Ω_c states, in the diagonal terms one exchanges light vectors and the heavy quark (b quark here) is a spectator. In the non-diagonal transitions, sometimes a B_s^* vector is exchanged, instead of ρ, ω, ϕ in the diagonal terms. Then these terms are very much suppressed by the mass of the B_s^* . In Ref. [2.1], a D_s^* was

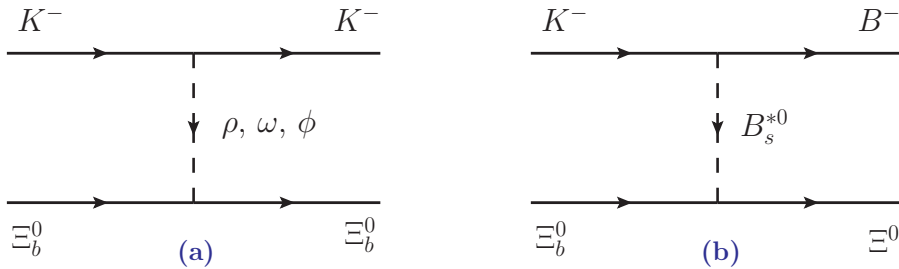


Figure 2.14: Vector mesons exchanged in the diagonal transition of $K^- \Xi_b^0 \rightarrow K^- \Xi_b^0$ (a) and non-diagonal one of $K^- \Xi_b^0 \rightarrow B^- \Xi_b^0$ (b).

exchanged, and both in Ref. [2.62] and Ref. [2.1] it was found that this was penalized by a factor about 1/4, as we saw in Eq. (2.64). We follow the same argumentation and write for the heavy propagator compared with the diagonal case

$$\lambda = \frac{-M_V^2}{q^{02} - |\vec{q}|^2 - m_{B_s^*}^2} \simeq \frac{-M_V^2}{(m_K - m_B)^2 - m_{B_s^*}^2} \approx 0.1. \quad (2.83)$$

The lower vertices in Fig. 2.14 for the vector(V)-baryon(B)-baryon(B) couplings are obtained by writing explicitly the vector mesons and the baryons in terms of quarks, as it is done in Ref. [2.1]. The wave functions for the baryons are identical to those used in section 2.2.2 changing the c quark by a b quark. As to the isospin states (we need only $I = 0$ to construct Ω_b state), we have the isospin multiplets

$$\begin{aligned} \bar{K} &= \begin{pmatrix} \bar{K}^0 \\ -K^- \end{pmatrix}; & \bar{B} &= \begin{pmatrix} \bar{B}^0 \\ -B^- \end{pmatrix}; & \Xi &= \begin{pmatrix} \Xi^0 \\ -\Xi^- \end{pmatrix}; & \Xi^* &= \begin{pmatrix} \Xi^{*0} \\ \Xi^{*-} \end{pmatrix}; \\ \Xi_b &= \begin{pmatrix} \Xi_b^0 \\ \Xi_b^- \end{pmatrix}; & \Xi'_b &= \begin{pmatrix} \Xi_b'^0 \\ \Xi_b'^- \end{pmatrix}; & \Xi_b^* &= \begin{pmatrix} \Xi_b^{*0} \\ \Xi_b^{*-} \end{pmatrix}; \end{aligned}$$

and the isospin $I = 0$ states are easily obtained from those and have the same relative signs as in the charm sector in Eq. (2.52).

Then the transition potentials are given by Eq. (2.62) with the D_{ij} coefficients given in Tables 2.16, 2.17 and 2.18.

Table 2.16: D_{ij} coefficients for the PB channels with $J^P = \frac{1}{2}^-$.

$J^P = 1/2^-$	$\Xi_b \bar{K}$	$\Xi'_b \bar{K}$	$\Xi \bar{B}$	$\Omega_b \eta$
$\Xi_b \bar{K}$	-1	0	$-\frac{1}{\sqrt{2}}\lambda$	0
$\Xi'_b \bar{K}$		-1	$\frac{1}{\sqrt{6}}\lambda$	$-\frac{4}{\sqrt{3}}$
$\Xi \bar{B}$			-2	$\frac{\sqrt{2}}{3}\lambda$
$\Omega_b \eta$				0

Table 2.17: D_{ij} coefficients for the PB channels with $J^P = \frac{3}{2}^-$.

$J^P = 3/2^-$	$\Xi_b^* \bar{K}$	$\Omega_b^* \eta$	$\Xi^* \bar{B}$
$\Xi_b^* \bar{K}$	-1	$-\frac{4}{\sqrt{3}}$	$\frac{2}{\sqrt{6}}\lambda$
$\Omega_b^* \eta$		0	$-\frac{\sqrt{2}}{3}\lambda$
$\Xi^* \bar{B}$			-2

From the potential we construct the t -matrix using the Bethe-Salpeter equation in coupled channels in the on-shell factorized form of Eq. (2.32). As in section 2.2.3 we take the cutoff regularization and use here the same cutoff for every channel, in order to respect rules of heavy quark symmetry, as discussed in Refs. [2.15, 2.22]. We take $q_{max} = 650$ MeV, which was the cutoff providing good agreement with the experimental states in Ref. [2.1]. The poles of the amplitudes provide the states and they are searched in the second Riemann sheet of the complex energy plane as discussed in section 2.1.3.

Table 2.18: D_{ij} coefficients for the VB channels with $J^P = \frac{1}{2}^-, \frac{3}{2}^-$.

$J^P = 1/2^-, 3/2^-$	$\Xi\bar{B}^*$	$\Xi_b\bar{K}^*$	$\Xi'_b\bar{K}^*$
$\Xi\bar{B}^*$	-2	$-\frac{1}{\sqrt{2}}\lambda$	$\frac{1}{\sqrt{6}}\lambda$
$\Xi_b\bar{K}^*$		-1	0
$\Xi'_b\bar{K}^*$			-1

It should be noted that in the case of vector-baryon interaction, V_{ij} of Eq. (2.62) has the extra factor $\vec{\epsilon}\cdot\vec{\epsilon}'$, where $\vec{\epsilon}$ and $\vec{\epsilon}'$ are the polarization vectors of the initial and final vector mesons, stemming from the $V(\vec{\epsilon})$ - $V(\vec{\epsilon}')$ - V (virtual) vertex in the limit of small three momenta compared to the vector meson masses [2.1, 2.18]. This factor induces degeneracy in $J^P = \frac{1}{2}^-, \frac{3}{2}^-$ vector-baryon($\frac{1}{2}^+$) states in S -wave. This factor does not appear for pseudoscalar mesons and, hence, for pseudoscalar-baryon($\frac{1}{2}^+$) we only obtain $J^P = \frac{1}{2}^-$ states and for the pseudoscalar-baryon($\frac{3}{2}^+$) we only obtain $J^P = \frac{3}{2}^-$ states. For the case of vector-baryon we predict states both in $\frac{1}{2}^-$ and $\frac{3}{2}^-$, which in our approach have the same energy. The degeneracy can be broken by mixing the pseudoscalar-baryon and vector-baryon channels, which is done through pion exchange [2.111], but in our case pion exchange is found to be small.

2.4.3 Results

In Tables 2.19, 2.20 and 2.21, we show the results. In Table 2.19 we see that we obtain two states with $J^P = \frac{1}{2}^-$ at 6405 MeV and 6465 MeV. The widths are given by twice the imaginary part of the pole position, and they are small in all cases. We also show the couplings of the states obtained to the different coupled channels, as well as the product $g_i G_i^{II}$ (G_i^{II} is the G function calculated at the pole in the second Riemann sheet), which as shown in Ref. [2.24] is proportional to the wave function at the origin. By looking at the couplings and the wave function at the origin we can see that the first state, at 6405 MeV, couples strongly to $\Xi'_b\bar{K}$ and next to $\Omega_b\eta$. The second state, at 6465 MeV, couples most strongly to $\Xi\bar{B}$ and little to the other channels, and hence it qualifies as mostly a $\Xi\bar{B}$ bound state.

Table 2.19: The poles, and coupling constants of the poles to various channels in the PB sector with $J^P = 1/2^-$, taking $q_{max} = 650$ MeV. g_i has no dimension and $g_i G_i^{II}$ has dimension of MeV.

6405.2	$\Xi_b\bar{K}$	$\Xi'_b\bar{K}$	$\Xi\bar{B}$	$\Omega_b\eta$
g_i	$-0.01 + i0.02$	2.04 + i0.01	$-1.62 + i0.02$	2.08 + i0.01
$g_i G_i^{II}$	$-0.34 - i0.47$	-37.31 - i0.18	$2.27 - i0.02$	-18.28 - i0.09
6465.3 + i1.2	$\Xi_b\bar{K}$	$\Xi'_b\bar{K}$	$\Xi\bar{B}$	$\Omega_b\eta$
g_i	$0.07 - i0.15$	$0.11 + i0.125$	10.70 - i0.10	$0.15 + i0.11$
$g_i G_i^{II}$	$3.92 + i3.91$	$-4.53 - i1.66$	-18.89 + i0.08	$-1.55 - i1.14$

In Table 2.20, we show the states that appear exclusively in $J^P = \frac{3}{2}^-$. They are obtained from a pseudoscalar meson (η , \bar{K} or \bar{B}) and a baryon of spin-parity $\frac{3}{2}^+$

Table 2.20: The poles, and coupling constants of the poles to various channels in the PB sector with $J^P = 3/2^-$, taking $q_{max} = 650$ MeV. g_i has no dimension and $g_i G_i^{II}$ has dimension of MeV.

6427.1	$\Xi_b^* \bar{K}$	$\Omega_b^* \eta$	$\Xi_b^* \bar{B}$
g_i	2.01	2.05	-0.60
$g_i G_i^{II}$	-37.17	-17.86	0.53
6664.8 + i0.2	$\Xi_b^* \bar{K}$	$\Omega_b^* \eta$	$\Xi_b^* \bar{B}$
g_i	-0.02 - i0.01	0.10 + i0.05	11.06 + i0.01
$g_i G_i^{II}$	0.59 - i0.53	-3.07 + i0.41	-19.31 - i0.02

Table 2.21: The poles, and coupling constants of the poles to various channels in the VB sector with $J^P = 1/2^-, 3/2^-$, taking $q_{max} = 650$ MeV. g_i has no dimension and $g_i G_i^{II}$ has dimension of MeV.

6508.0	$\Xi \bar{B}^*$	$\Xi_b \bar{K}^*$	$\Xi_b' \bar{K}^*$
g_i	10.88	0.32	-0.15
$g_i G_i^{II}$	-18.86	-2.37	0.77
6676.1 + i0.1	$\Xi \bar{B}^*$	$\Xi_b \bar{K}^*$	$\Xi_b' \bar{K}^*$
g_i	-0.05 - i0.09	1.78 - i0.10	0.01 + i0.01
$g_i G_i^{II}$	0.68 + i0.27	-35.16 + i1.90	-0.07 - i0.01
6817.5	$\Xi \bar{B}^*$	$\Xi_b \bar{K}^*$	$\Xi_b' \bar{K}^*$
g_i	-0.01 + i0.02	0.01 - i0.01	1.77 + i0.01
$g_i G_i^{II}$	-0.26 - i0.01	0.05 + i0.03	-34.71 - i0.18

(Ξ_b^* , Ω_b^* or Ξ^*). We also find two states, one at 6427 MeV and the other one at 6665 MeV. The first one couples mostly to $\Xi_b^* \bar{K}$ but also to $\Omega_b^* \eta$, while the second one couples mostly to $\Xi_b^* \bar{B}$ and little to the other channels and would qualify as mostly a $\Xi_b^* \bar{B}$ bound state. We can see here a qualitative difference with the results obtained for the Ω_c states. There the first $\frac{3}{2}^-$ state had bigger energy than the two $\frac{1}{2}^-$ states. Here it is in the middle. The reason is simple because the difference between Ξ_b^* and Ξ_b , Ω_b^* and Ω_b are now smaller than between Ξ_c^* and Ξ_c , Ω_c^* and Ω_c . Confirmation of this feature by future experiments would already provide support to the molecular picture that we discuss here.

Finally we also show in Table 2.21 the three states that we obtain from the vector-baryon channels. Here the spin-parity can be $\frac{1}{2}^-$, $\frac{3}{2}^-$, since in our approach these spin states are degenerate. One can break the degeneracy allowing pion exchange between the pseudoscalar-baryon and vector-baryon states as done in Refs. [2.73, 2.74], but as shown in the end of section 2.2.2 for the Ω_c states, the pion exchange was very small in this case. We obtain three states at 6508 MeV, 6676 MeV and 6818 MeV with very small width. The first state couples mostly to $\Xi \bar{B}^*$, the second one to $\Xi_b \bar{K}^*$ and the third one to $\Xi_b' \bar{K}^*$ with small coupling to the other channels, which make them qualify as bound states of these channels. The last state would correspond to a bound $\Xi_b' \bar{K}^*$ state, with a binding of barely 11 MeV.

In Ref. [2.1] we had also found three states of vector-baryon nature, but they appear in a region where the experimental background is large. In any case our approach does not tell the strength at which the states are produced in the partic-

ular LHCb reaction. Yet, other more selective methods to produce the states like $\Omega_b \rightarrow (\Xi_c^+ K^-)\pi^-$ suggested in Refs. [2.3, 2.86] and section 2.3, in the case of Ω_c states, would allow theoretical approaches to predict the relative strength at which every state is produced. In the present case we cannot rely on the weak decay of heavier resonances, but it would be convenient to search for the Ω_b states in different reactions where the strength for the production of the different states would be different, and one would have more chances to find them. The analogy of the Ω_b states with the Ω_c ones, suggest that three of the states predicted by us could be easily seen using a similar reaction.

2.4.4 Conclusions

Motivated by the recent experimental finding of five Ω_c states and the successful reproduction of three of these states in the molecular model for Ω_c states, we have used the same formalism used to obtain the Ω_c states to make predictions for Ω_b states, just changing one c quark by a b quark. The only freedom in the approach is the regulator in the loop function of the meson-baryon states, but for this we used a cutoff regularization with the same cutoff as in the charm sector, which has been shown in different approaches to respect the rules of heavy quark symmetry. In this way, the predictions of the model should be very accurate. Since we study only the interaction of meson-baryon in S -wave, we predict states of pseudoscalar-baryon nature with $J^P = \frac{1}{2}^-$ and $\frac{3}{2}^-$, and we find two states of $\frac{1}{2}^-$, two states of $\frac{3}{2}^-$ and three more states, degenerate in our approach in $\frac{1}{2}^-$, $\frac{3}{2}^-$, that stem from the interaction of vector mesons with baryons.

Although the production of Ω_b states is done with less statistics than the Ω_c states in LHCb, with increased luminosity in future runs the access to these states will become a state of the art. Predictions done before the experiment are very useful, and comparison of the results obtained here with experimental measurements in the future will help us understand better hadron dynamics and the nature of some of the states found. ⁴

⁴ After the production of this work a new article from the LHCb collaboration appeared [2.112], announcing the discovery of new Ω_b states. In a recent article [2.113] it is shown that some narrow peaks seen in the experiment, between 6400 MeV and 6500 MeV, are in fair agreement with our predictions.

Bibliography

- [2.1] V. R. Debastiani, J. M. Dias, W. H. Liang and E. Oset, “*Molecular Ω_c states generated from coupled meson-baryon channels,*” Phys. Rev. D **97**, 094035 (2018).
- [2.2] R. Aaij *et al.* [LHCb Collaboration], “*Observation of five new narrow Ω_c^0 states decaying to $\Xi_c^+ K^-$,*” Phys. Rev. Lett. **118**, 182001 (2017).
- [2.3] V. R. Debastiani, J. M. Dias, W. H. Liang and E. Oset, “ *$\Omega_b^- \rightarrow (\Xi_c^+ K^-) \pi^-$ and the Ω_c states,*” Phys. Rev. D **98**, 094022 (2018).
- [2.4] W. H. Liang, J. M. Dias, V. R. Debastiani and E. Oset, “*Molecular Ω_b states,*” Nucl. Phys. B **930**, 524 (2018).
- [2.5] G. Ecker, “*Chiral perturbation theory,*” Prog. Part. Nucl. Phys. **35**, 1 (1995).
- [2.6] E. Oset and A. Ramos, “*Nonperturbative chiral approach to s wave anti- $K N$ interactions,*” Nucl. Phys. A **635**, 99 (1998).
- [2.7] T. Mizutani and A. Ramos, “ *D mesons in nuclear matter: A DN coupled-channel equations approach,*” Phys. Rev. C **74**, 065201 (2006).
- [2.8] J. A. Oller, E. Oset and A. Ramos, “*Chiral unitary approach to meson meson and meson - baryon interactions and nuclear applications,*” Prog. Part. Nucl. Phys. **45**, 157 (2000).
- [2.9] M. Harada and K. Yamawaki, “*Hidden local symmetry at loop: A New perspective of composite gauge boson and chiral phase transition,*” Phys. Rept. **381**, 1 (2003).
- [2.10] H. Nagahiro, L. Roca, A. Hosaka and E. Oset, “*Hidden gauge formalism for the radiative decays of axial-vector mesons,*” Phys. Rev. D **79**, 014015 (2009).
- [2.11] M. Bando, T. Kugo, S. Uehara, K. Yamawaki and T. Yanagida, “*Is rho Meson a Dynamical Gauge Boson of Hidden Local Symmetry?,*” Phys. Rev. Lett. **54**, 1215 (1985).
- [2.12] M. Bando, T. Kugo and K. Yamawaki, “*Nonlinear Realization and Hidden Local Symmetries,*” Phys. Rept. **164**, 217 (1988).
- [2.13] U. G. Meißner, “*Low-Energy Hadron Physics from Effective Chiral Lagrangians with Vector Mesons,*” Phys. Rept. **161**, 213 (1988).
- [2.14] G. Ecker, J. Gasser, H. Leutwyler, A. Pich and E. de Rafael, “*Chiral Lagrangians for Massive Spin 1 Fields,*” Phys. Lett. B **223**, 425 (1989).
- [2.15] A. Ozpineci, C. W. Xiao and E. Oset, “*Hidden beauty molecules within the local hidden gauge approach and heavy quark spin symmetry,*” Phys. Rev. D **88**, 034018 (2013).

- [2.16] J. Hofmann and M. F. M. Lutz, “*Coupled-channel study of crypto-exotic baryons with charm,*” Nucl. Phys. A **763**, 90 (2005).
- [2.17] F. E. Close, “*An Introduction to Quarks and Partons,*” Academic Press/London 1979, 481p.
- [2.18] E. Oset and A. Ramos, “*Dynamically generated resonances from the vector octet-baryon octet interaction,*” Eur. Phys. J. A **44**, 445 (2010).
- [2.19] J. A. Oller and E. Oset, “*N/D description of two meson amplitudes and chiral symmetry,*” Phys. Rev. D **60**, 074023 (1999).
- [2.20] J. A. Oller and U. G. Meißner, “*Chiral dynamics in the presence of bound states: Kaon nucleon interactions revisited,*” Phys. Lett. B **500**, 263 (2001).
- [2.21] J. J. Wu and B. S. Zou, “*Prediction of super-heavy N^* and Λ^* resonances with hidden beauty,*” Phys. Lett. B **709**, 70 (2012).
- [2.22] J. X. Lu, Y. Zhou, H. X. Chen, J. J. Xie and L. S. Geng, “*Dynamically generated $J^P = 1/2^-(3/2^-)$ singly charmed and bottom heavy baryons,*” Phys. Rev. D **92**, 014036 (2015).
- [2.23] M. Altenbuchinger, L.-S. Geng and W. Weise, “*Scattering lengths of Nambu-Goldstone bosons off D mesons and dynamically generated heavy-light mesons,*” Phys. Rev. D **89**, 014026 (2014).
- [2.24] D. Gamermann, J. Nieves, E. Oset and E. Ruiz Arriola, “*Couplings in coupled channels versus wave functions: application to the $X(3872)$ resonance,*” Phys. Rev. D **81**, 014029 (2010).
- [2.25] D. Ebert, R. N. Faustov and V. O. Galkin, “*Masses of excited heavy baryons in the relativistic quark model,*” Phys. Lett. B **659**, 612 (2008).
- [2.26] W. Roberts and M. Pervin, “*Heavy baryons in a quark model,*” Int. J. Mod. Phys. A **23**, 2817 (2008).
- [2.27] H. Garcilazo, J. Vijande and A. Valcarce, “*Faddeev study of heavy baryon spectroscopy,*” J. Phys. G **34**, 961 (2007).
- [2.28] S. Migura, D. Merten, B. Metsch and H. R. Petry, “*Charmed baryons in a relativistic quark model,*” Eur. Phys. J. A **28**, 41 (2006).
- [2.29] D. Ebert, R. N. Faustov and V. O. Galkin, “*Spectroscopy and Regge trajectories of heavy baryons in the relativistic quark-diquark picture,*” Phys. Rev. D **84**, 014025 (2011).
- [2.30] A. Valcarce, H. Garcilazo and J. Vijande, “*Towards an understanding of heavy baryon spectroscopy,*” Eur. Phys. J. A **37**, 217 (2008).
- [2.31] Z. Shah, K. Thakkar, A. K. Rai and P. C. Vinodkumar, “*Mass spectra and Regge trajectories of Λ_c^+ , Σ_c^0 , Ξ_c^0 and Ω_c^0 baryons,*” Chin. Phys. C **40**, 123102 (2016).

- [2.32] J. Vijande, A. Valcarce, T. F. Carames and H. Garcilazo, “*Heavy hadron spectroscopy: a quark model perspective*,” Int. J. Mod. Phys. E **22**, 1330011 (2013).
- [2.33] T. Yoshida, E. Hiyama, A. Hosaka, M. Oka and K. Sadato, “*Spectrum of heavy baryons in the quark model*,” Phys. Rev. D **92**, 114029 (2015).
- [2.34] H. X. Chen, W. Chen, Q. Mao, A. Hosaka, X. Liu and S. L. Zhu, “*P-wave charmed baryons from QCD sum rules*,” Phys. Rev. D **91**, 054034 (2015).
- [2.35] H. X. Chen, Q. Mao, A. Hosaka, X. Liu and S. L. Zhu, “*D-wave charmed and bottomed baryons from QCD sum rules*,” Phys. Rev. D **94**, 114016 (2016).
- [2.36] G. Chiladze and A. F. Falk, “*Phenomenology of new baryons with charm and strangeness*,” Phys. Rev. D **56**, R6738 (1997).
- [2.37] A. Manohar and H. Georgi, “*Chiral Quarks and the Nonrelativistic Quark Model*,” Nucl. Phys. B **234**, 189 (1984).
- [2.38] C. E. Jimenez-Tejero, A. Ramos and I. Vidana, “*Dynamically generated open charmed baryons beyond the zero range approximation*,” Phys. Rev. C **80**, 055206 (2009).
- [2.39] O. Romanets, L. Tolos, C. Garcia-Recio, J. Nieves, L. L. Salcedo and R. G. E. Timmermans, “*Charmed and strange baryon resonances with heavy-quark spin symmetry*,” Phys. Rev. D **85**, 114032 (2012).
- [2.40] M. Karliner and J. L. Rosner, “*Very narrow excited Ω_c baryons*,” Phys. Rev. D **95**, 114012 (2017).
- [2.41] K. L. Wang, L. Y. Xiao, X. H. Zhong and Q. Zhao, “*Understanding the newly observed Ω_c states through their decays*,” Phys. Rev. D **95**, 116010 (2017).
- [2.42] W. Wang and R. L. Zhu, “*Interpretation of the newly observed Ω_c^0 resonances*,” Phys. Rev. D **96**, 014024 (2017).
- [2.43] B. Chen and X. Liu, “*Six Ω_c^0 states discovered by LHCb as new members of 1P and 2S charmed baryons*,” Phys. Rev. D **96**, 094015 (2017).
- [2.44] G. Yang and J. Ping, “*The structure of pentaquarks Ω_c^0 in the chiral quark model*,” Phys. Rev. D **97**, 034023 (2018).
- [2.45] H. Huang, J. Ping and F. Wang, “*Investigating the excited Ω_c^0 states through $\Xi_c K$ and $\Xi_c' K$ decay channels*,” Phys. Rev. D **97**, 034027 (2018).
- [2.46] H. C. Kim, M. V. Polyakov and M. Praszalowicz, “*Possibility of the existence of charmed exotica*,” Phys. Rev. D **96**, 014009 (2017); Addendum: [Phys. Rev. D **96**, 039902 (2017)].
- [2.47] C. S. An and H. Chen, “*Observed Ω_c^0 resonances as pentaquark states*,” Phys. Rev. D **96**, 034012 (2017).

- [2.48] A. Ali, J. S. Lange and S. Stone, *Exotics: Heavy Pentaquarks and Tetraquarks*, Prog. Part. Nucl. Phys. **97**, 123 (2017).
- [2.49] V. V. Anisovich, M. A. Matveev, J. Nyiri and A. N. Semenova, “Narrow pentaquarks as diquark-diquark-antiquark systems,” Mod. Phys. Lett. A **32**, 1750154 (2017).
- [2.50] S. S. Agaev, K. Azizi and H. Sundu, “On the nature of the newly discovered Ω states,” EPL **118**, 61001 (2017).
- [2.51] H. X. Chen, Q. Mao, W. Chen, A. Hosaka, X. Liu and S. L. Zhu, “Decay properties of P -wave charmed baryons from light-cone QCD sum rules,” Phys. Rev. D **95**, 094008 (2017).
- [2.52] Z. G. Wang, “Analysis of $\Omega_c(3000)$, $\Omega_c(3050)$, $\Omega_c(3066)$, $\Omega_c(3090)$ and $\Omega_c(3119)$ with QCD sum rules,” Eur. Phys. J. C **77**, 325 (2017).
- [2.53] T. M. Aliev, S. Bilmis and M. Savci, “Are the new excited Ω_c baryons negative parity states?,” arXiv:1704.03439 [hep-ph].
- [2.54] S. S. Agaev, K. Azizi and H. Sundu, “Interpretation of the new Ω_c^0 states via their mass and width,” Eur. Phys. J. C **77**, 395 (2017).
- [2.55] Q. Mao, H. X. Chen, A. Hosaka, X. Liu and S. L. Zhu, “ D -wave heavy baryons of the $SU(3)$ flavor $\mathbf{6}_F$,” Phys. Rev. D **96**, 074021 (2017).
- [2.56] Z. G. Wang, X. N. Wei and Z. H. Yan, “Revisit assignments of the new excited Ω_c states with QCD sum rules,” Eur. Phys. J. C **77**, 832 (2017).
- [2.57] M. Padmanath and N. Mathur, “Quantum Numbers of Recently Discovered Ω_c^0 Baryons from Lattice QCD,” Phys. Rev. Lett. **119**, 042001 (2017).
- [2.58] Z. Zhao, D. D. Ye and A. Zhang, “Hadronic decay properties of newly observed Ω_c baryons,” Phys. Rev. D **95**, 114024 (2017).
- [2.59] K. L. Wang, Y. X. Yao, X. H. Zhong and Q. Zhao, “Strong and radiative decays of the low-lying S - and P -wave singly heavy baryons,” Phys. Rev. D **96**, 116016 (2017).
- [2.60] H. C. Kim, M. V. Polyakov, M. Praszalowicz and G. S. Yang, “Strong decays of exotic and non-exotic heavy baryons in the chiral quark-soliton model,” Phys. Rev. D **96**, 094021 (2017).
- [2.61] H. Y. Cheng and C. W. Chiang, “Quantum numbers of Ω_c states and other charmed baryons,” Phys. Rev. D **95**, 094018 (2017).
- [2.62] G. Montaña, A. Feijoo and A. Ramos, “A meson-baryon molecular interpretation for some Ω_c excited baryons,” Eur. Phys. J. A **54**, 64 (2018).
- [2.63] N. Isgur and M. B. Wise, “Weak Decays of Heavy Mesons in the Static Quark Approximation,” Phys. Lett. B **232**, 113 (1989).

- [2.64] M. Neubert, “*Heavy-Quark Symmetry*” Phys. Rept. **245**, 259 (1994).
- [2.65] A. V. Manohar and M. B. Wise, “*Heavy quark physics*,” Camb. Monogr. Part. Phys. Nucl. Phys. Cosmol. **10**, 1 (2000).
- [2.66] A. Bramon, A. Grau and G. Pancheri, “*Intermediate vector meson contributions to $V0 \rightarrow P0 P0$ gamma decays*,” Phys. Lett. B **283**, 416 (1992).
- [2.67] S. Sakai, L. Roca and E. Oset, “*Charm-beauty meson bound states from $B(B^*)D(D^*)$ and $B(B^*)\bar{D}(\bar{D}^*)$ interaction*,” Phys. Rev. D **96**, 054023 (2017).
- [2.68] K. Miyahara, T. Hyodo, M. Oka, J. Nieves and E. Oset, “*Theoretical study of the $\Xi(1620)$ and $\Xi(1690)$ resonances in $\Xi_c \rightarrow \pi + MB$ decays*,” Phys. Rev. C **95**, 035212 (2017).
- [2.69] R. P. Pavao, W. H. Liang, J. Nieves and E. Oset, “*Predictions for $\Xi_b^- \rightarrow \pi^- (D_s^-) \Xi_c^0(2790) (\Xi_c^0(2815))$ and $\Xi_b^- \rightarrow \bar{\nu}_l l \Xi_c^0(2790) (\Xi_c^0(2815))$* ,” Eur. Phys. J. C **77**, 265 (2017).
- [2.70] E. Oset, A. Ramos and C. Bennhold, “*Low lying $S = -1$ excited baryons and chiral symmetry*,” Phys. Lett. B **527**, 99 (2002); Erratum: [Phys. Lett. B **530**, 260 (2002)].
- [2.71] C. W. Xiao, J. Nieves and E. Oset, “*Combining heavy quark spin and local hidden gauge symmetries in the dynamical generation of hidden charm baryons*,” Phys. Rev. D **88**, 056012 (2013).
- [2.72] B. Borasoy, “*Baryon axial currents*,” Phys. Rev. D **59**, 054021 (1999).
- [2.73] W. H. Liang, C. W. Xiao and E. Oset, “*Baryon states with open beauty in the extended local hidden gauge approach*,” Phys. Rev. D **89**, 054023 (2014).
- [2.74] W. H. Liang, T. Uchino, C. W. Xiao and E. Oset, “*Baryon states with open charm in the extended local hidden gauge approach*,” Eur. Phys. J. A **51**, 16 (2015).
- [2.75] T. Sekihara, T. Hyodo and D. Jido, “*Comprehensive analysis of the wave function of a hadronic resonance and its compositeness*,” PTEP **2015**, 063D04 (2015).
- [2.76] Y. Kamiya and T. Hyodo, “*Structure of near-threshold quasibound states*,” Phys. Rev. C **93**, 035203 (2016).
- [2.77] F. Aceti and E. Oset, “*Wave functions of composite hadron states and relationship to couplings of scattering amplitudes for general partial waves*,” Phys. Rev. D **86**, 014012 (2012).
- [2.78] J. Yelton *et al.* [Belle Collaboration], “*Observation of Excited Ω_c Charmed Baryons in e^+e^- Collisions*,” Phys. Rev. D **97**, 051102 (2018).
- [2.79] B. Chen and X. Liu, “*New Ω_c^0 baryons discovered by LHCb as the members of $1P$ and $2S$ states*,” Phys. Rev. D **96**, 094015 (2017).

- [2.80] A. Ali, L. Maiani, A. V. Borisov, I. Ahmed, M. Jamil Aslam, A. Y. Parkhomenko, A. D. Polosa and A. Rehman, “A new look at the Y tetraquarks and Ω_c baryons in the diquark model,” *Eur. Phys. J. C* **78**, 29 (2018).
- [2.81] G. Yang and J. Ping, “Dynamical study of Ω_c^0 in the chiral quark model,” *Phys. Rev. D* **97**, 034023 (2018).
- [2.82] J. Nieves, R. Pavao and L. Tolos, “ Ω_c excited states within a $SU(6)_{\text{lsf}} \times HQSS$ model,” *Eur. Phys. J. C* **78**, 114 (2018).
- [2.83] C. Wang, L. L. Liu, X. W. Kang, X. H. Guo and R. W. Wang, “Possible open-charmed pentaquark molecule $\Omega_c(3188)$ - the $D\Xi$ bound state - in the Bethe-Salpeter formalism,” *Eur. Phys. J. C* **78**, 407 (2018).
- [2.84] R. Chen, A. Hosaka and X. Liu, “Searching for possible Ω_c -like molecular states from meson-baryon interaction,” *Phys. Rev. D* **97**, 036016 (2018).
- [2.85] Y. Huang, C. j. Xiao, Q. F. Lü, R. Wang, J. He and L. Geng, “Strong and radiative decays of $D\Xi$ molecular state and newly observed Ω_c states,” *Phys. Rev. D* **97**, 094013 (2018).
- [2.86] I. Belyaev, “Spectroscopy of charm baryons at LHCb”, talk presented at the Hadron 2017 Conference, Salamanca, September 2017. <https://indico.cern.ch/event/578804/contributions/2636994/>
- [2.87] R. Aaij *et al.* [LHCb Collaboration], “Measurement of the mass and lifetime of the Ω_b^- baryon,” *Phys. Rev. D* **93**, 092007 (2016).
- [2.88] R. Aaij *et al.* [LHCb Collaboration], “Measurement of the Λ_b^0 , Ξ_b^- and Ω_b^- baryon masses,” *Phys. Rev. Lett.* **110**, 182001 (2013).
- [2.89] T. A. Aaltonen *et al.* [CDF Collaboration], “Mass and lifetime measurements of bottom and charm baryons in $p\bar{p}$ collisions at $\sqrt{s} = 1.96$ TeV,” *Phys. Rev. D* **89**, 072014 (2014).
- [2.90] V. M. Abazov *et al.* [D0 Collaboration], “Observation of the doubly strange baryon Ω_b^- ,” *Phys. Rev. Lett.* **101**, 232002 (2008).
- [2.91] C. Patrignani *et al.* (Particle Data Group), “Review of Particle Physics,” (with 2017 update), *Chin. Phys. C* **40**, 100001 (2016).
- [2.92] L. Micu, “Decay rates of meson resonances in a quark model,” *Nucl. Phys. B* **10**, 521 (1969).
- [2.93] A. Le Yaouanc, L. Oliver, O. Pene and J. C. Raynal, “Naive quark pair creation model of strong interaction vertices,” *Phys. Rev. D* **8**, 2223 (1973).
- [2.94] W. H. Liang, M. Bayar and E. Oset, “ $\Lambda_b \rightarrow \pi^-(D_s^-)\Lambda_c(2595)$, $\pi^-(D_s^-)\Lambda_c(2625)$ decays and DN , D^*N molecular components,” *Eur. Phys. J. C* **77**, 39 (2017).

- [2.95] A. Martínez Torres, E. Oset, S. Prelovsek and A. Ramos, “*Reanalysis of lattice QCD spectra leading to the $D_{s0}^*(2317)$ and $D_{s1}^*(2460)$,*” JHEP **1505**, 153 (2015).
- [2.96] P. G. Ortega, J. Segovia, D. R. Entem and F. Fernandez, “*Molecular components in P-wave charmed-strange mesons,*” Phys. Rev. D **94**, 074037 (2016).
- [2.97] M. Albaladejo, P. Fernandez-Soler, J. Nieves and P. G. Ortega, “*Contribution of constituent quark model $c\bar{s}$ states to the dynamics of the $D_{s0}^*(2317)$ and $D_{s1}^*(2460)$ resonances,*” Eur. Phys. J. C **78**, 722 (2018).
- [2.98] G. S. Bali, S. Collins, A. Cox and A. Schäfer, “*Masses and decay constants of the $D_{s0}^*(2317)$ and $D_{s1}^*(2460)$ from $N_f = 2$ lattice QCD close to the physical point,*” Phys. Rev. D **96**, 074501 (2017).
- [2.99] R. Molina, M. Döring and E. Oset, “*Determination of the compositeness of resonances from decays: the case of the $B_s^0 \rightarrow J/\psi f_1(1285)$,*” Phys. Rev. D **93**, 114004 (2016).
- [2.100] H. X. Chen, W. Chen, X. Liu, Y. R. Liu and S. L. Zhu, “*A review of the open charm and open bottom systems,*” Rept. Prog. Phys. **80**, 076201 (2017).
- [2.101] H. X. Chen, W. Chen, X. Liu and S. L. Zhu, “*The hidden-charm pentaquark and tetraquark states,*” Phys. Rept. **639**, 1 (2016).
- [2.102] P. Zhou, Y. K. Hsiao and C. Q. Geng, “*Pentaquarks in semileptonic Λ_b decays,*” Annals Phys. **383**, 278 (2017).
- [2.103] J. X. Lu, L. S. Geng and M. P. Valderrama, “*Heavy baryon-antibaryon molecules in effective field theory,*” Phys. Rev. D **99**, 074026 (2019).
- [2.104] S. L. Olsen, T. Skwarnicki and D. Zieminska, “*Non-Standard Heavy Mesons and Baryons, an Experimental Review,*” Rev. Mod. Phys. **90**, 015003 (2018).
- [2.105] R. Aaij *et al.* [LHCb Collaboration], “*Observation of $J/\psi p$ Resonances Consistent with Pentaquark States in $\Lambda_b^0 \rightarrow J/\psi K^- p$ Decays,*” Phys. Rev. Lett. **115**, 072001 (2015).
- [2.106] R. Aaij *et al.* [LHCb Collaboration], “*Study of the production of Λ_b^0 and \bar{B}^0 hadrons in pp collisions and first measurement of the $\Lambda_b^0 \rightarrow J/\psi p K^-$ branching fraction,*” Chin. Phys. C **40**, 011001 (2016).
- [2.107] X. Liu, H. X. Chen, Y. R. Liu, A. Hosaka and S. L. Zhu, “*Bottom baryons,*” Phys. Rev. D **77**, 014031 (2008).
- [2.108] Q. Mao, H. X. Chen, W. Chen, A. Hosaka, X. Liu and S. L. Zhu, “*QCD sum rule calculation for P-wave bottom baryons,*” Phys. Rev. D **92**, 114007 (2015).
- [2.109] R. M. Albuquerque, S. Narison and M. Nielsen, “ *$SU(3)$ mass-splittings of the heavy-baryons octet in QCD,*” Phys. Lett. B **684**, 236 (2010).
- [2.110] S. S. Agaev, K. Azizi and H. Sundu, “*Decay widths of the excited Ω_b baryons,*” Phys. Rev. D **96**, 094011 (2017).

-
- [2.111] E. J. Garzon and E. Oset, “*Effects of pseudoscalar-baryon channels in the dynamically generated vector-baryon resonances,*” *Eur. Phys. J. A* **48**, 5 (2012).
- [2.112] R. Aaij *et al.* [LHCb Collaboration], “*First observation of excited Ω_b^- states,*” *Phys. Rev. Lett.* **124**, 082002 (2020).
- [2.113] W. H. Liang and E. Oset, “*Observed Ω_b spectrum and meson-baryon molecular states,*” arXiv:2001.02929 [hep-ph].

3 Triangle Singularities

In this chapter we will present three works on triangle singularities.

First we introduce basic concepts of triangle singularities and the general features of our framework in section 3.1.

Next, in section 3.2, we present the work of Ref. [3.1] where we discuss how the $f_1(1420)$ can be explained as a manifestation of the $K^*\bar{K}$ and $\pi a_0(980)$ decay modes of the $f_1(1285)$. In particular, we show that the shoulder on the $\pi a_0(980)$ decay mode in the data of Ref. [3.2] is related to a triangle singularity.

After that, we present in section 3.3 the work of Ref. [3.3], where we have studied the $\gamma p \rightarrow p\pi^0\eta$ reaction paying attention to the two main mechanisms at low energies, the $\gamma p \rightarrow \Delta(1700) \rightarrow \eta\Delta(1232)$ and the $\gamma p \rightarrow \Delta(1700) \rightarrow \pi N(1535)$, showing that the second one involves a mechanism that leads to a triangle singularity. We are able to evaluate quantitatively the cross section for this process and show that it agrees with the experimental determination from Ref. [3.4].

Finally, in section 3.4 we present the work of Ref. [3.5] where we study the relative contributions and singularities of the tree level and triangle diagrams, discussing the Schmid theorem¹ [3.6]. We investigate the process in terms of the width of the unstable particle produced in the first decay and determine the limits of validity and violation of the Schmid theorem, with the particular interest in the case where a resonance is formed from the rescattering on the triangle diagram.

3.1 Introduction

The systematic study of triangle singularities was done by Landau [3.7]. Later S. Coleman and R. E. Norton showed the conditions for the singularity to be physically observable, into what is known as the Coleman-Norton theorem [3.8].

Let us look at a process proceeding at tree level, depicted in Fig. 3.1, in which particle A decays into R and 1, and R further decays into particles 2 and 3. Triangle singularities stem from the related reaction mechanism, which is depicted in Fig. 3.2, where the particle A decays into R and 1, posteriorly R decays into 2 and 3, and then 1 and 2 fuse to give a new particle or simply rescatter to give the same state (or another one if there are inelasticities).

¹ The Schmid theorem states that if one has a tree level mechanism with a particle A decaying into two particles 1 and R , with a posterior decay of R into particles 2 and 3, the possible triangle singularity developed by the mechanism of elastic rescattering of two of the three decay particles does not change the cross section provided by the tree level.

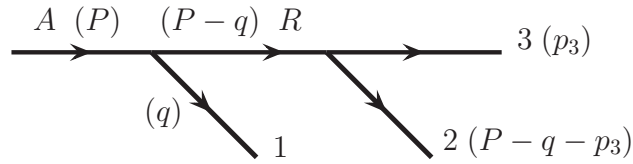


Figure 3.1: Tree level diagram for the process $A \rightarrow 1+2+3$ mediated by a resonance R that decays into particles 2 and 3. In brackets the momenta of the particles.

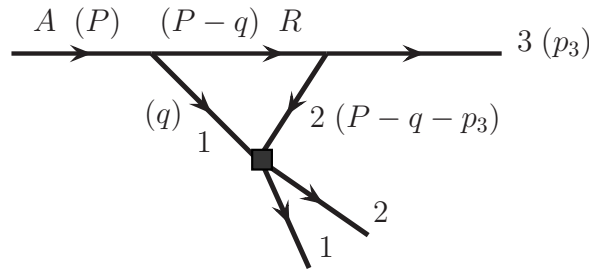


Figure 3.2: Triangle mechanism emerging from the mechanism of Fig. 3.1, with final state interaction of particles 1 and 2. The vertex with particles 1 and 2 symbolizes the $1+2 \rightarrow 1+2$ scattering matrix. In brackets the momenta of the particles.

The loop function containing particles 1, 2 and R as intermediate states can lead to some singularities (in the limit of zero width of the R particle) when all the particles inside the loop in Fig. 3.2 are placed on shell in the integration and the particles R and 3 go parallel in the A rest frame (then particle 1 and 3 are antiparallel). It is interesting to note that if particles R and 3 go in the same direction, then both particles 1 and 2 go in the opposite direction to them in the A and R rest frames, respectively. According to the Coleman-Norton theorem [3.8] the singularity appears when the classical process of particle 2, moving in the same direction as particle 1, but produced later, catches up with particle 1 and scatters (or fuses to produce another particle).

One should note that in the situation where the R resonance is placed on shell in the triangle loop, as well as particles 1 and 2, the tree level mechanism of Fig. 3.1 will also have a singularity in the limit of zero width for the resonance R , since the amplitude goes as $(M_{\text{inv}}(R) - M_R + i\Gamma_R/2)^{-1}$. However, the tree diagram does not have the restriction that particles R and 3 should be parallel and hence the region where R can be placed on shell is much wider than for the triangle singularity. In section 3.4 we will study the relation of the tree level and triangle diagrams regarding their singularity when we discuss the Schmid theorem [3.6].

First, let us study the generic case depicted in Fig. 3.2. The conditions for the triangle singularity to occur, relating the invariant mass of particles 1, 2 with the mass of A , can be seen in a pedagogical description of the process in Ref. [3.9], which we will follow closely in this section since it will be the framework we will adopt throughout this chapter.

The Coleman-Norton theorem [3.8] we have mentioned will determine the conditions for the solutions to be located on the physical boundary, i.e., whether they can produce a prominent effect on the amplitude in the physically allowed region. Note that the intermediate R particle has a finite width, it has to decay into particle 2 and 3, and 2 also must be able to catch up with particle 1. If we fix the masses of the particles 1 and 2, only when the R mass is located in a small range there is a triangle singularity on the physical boundary. Since the mass region is small, the singularity is also close to the R -1 threshold (see, e.g., Refs. [3.10–3.13]).

The position of the singularities in the amplitude of the triangle diagram can be obtained by solving the Landau equation [3.7], as done in Ref. [3.10], for example. However, it can be very instructive to perform the loop integration of the three propagators explicitly. Let us consider the scalar three-point loop integral

$$I_1 = i \int \frac{d^4q}{(2\pi)^4} \frac{1}{(q^2 - m_1^2 + i\epsilon) [(P - q)^2 - m_R^2 + i\epsilon] [(P - q - k)^2 - m_2^2 + i\epsilon]}. \quad (3.1)$$

A simpler expression can be obtained if we neglect the negative energy part of the particle 1 propagator. This is

$$\begin{aligned} \frac{1}{q^2 - m_1^2 + i\epsilon} &= \frac{1}{2\omega_1(q)} \left(\frac{1}{q^0 - \omega_1(q) + i\epsilon} - \frac{1}{q^0 + \omega_1(q) + i\epsilon} \right) \\ &\rightarrow \frac{1}{2\omega_1(q)} \frac{1}{q^0 - \omega_1(q) + i\epsilon}. \end{aligned} \quad (3.2)$$

Since we are interested in the region where the R may be treated nonrelativistically, we can safely neglect the negative energy pole from the R propagator. The integral over q^0 can be done analytically using the residue theorem and we are left with the integral in the 3-momentum \vec{q} . Taking particle A at rest we obtain

$$\begin{aligned} I_1 &= \int \frac{d^3q}{(2\pi)^3} \frac{1}{8 \omega_1(\vec{q}) \omega_R(\vec{q}) \omega_2(\vec{k} + \vec{q})} \\ &\times \frac{1}{k^0 - \omega_2(\vec{k} + \vec{q}) - \omega_R(\vec{q})} \frac{1}{P^0 + \omega_1(\vec{q}) + \omega_2(\vec{k} + \vec{q}) - k^0} \\ &\times \frac{2P^0\omega_1(\vec{q}) + 2k^0\omega_2(\vec{k} + \vec{q}) - 2[\omega_1(\vec{q}) + \omega_2(\vec{k} + \vec{q})][\omega_1(\vec{q}) + \omega_2(\vec{k} + \vec{q}) + \omega_R(\vec{q})]}{[P^0 - \omega_1(\vec{q}) - \omega_2(\vec{k} + \vec{q}) - k^0 + i\epsilon][P^0 - \omega_R(\vec{q}) - \omega_1(\vec{q}) + i\epsilon]}, \end{aligned} \quad (3.3)$$

where $\omega_1(\vec{q}) = \sqrt{m_1^2 + \vec{q}^2}$, $\omega_R(\vec{q}) = \sqrt{m_R^2 + \vec{q}^2}$, $\omega_2(\vec{k} + \vec{q}) = \sqrt{m_2^2 + (\vec{k} + \vec{q})^2}$, $P^0 = M_A$, and $k^0 = \sqrt{m_3^2 + \vec{k}^2}$.

We immediately observe that the poles of the propagators correspond to having pairs of intermediate particles on shell. The conditions for all the three intermediate particles to be on shell are

$$P^0 - \omega_R(\vec{q}) - \omega_1(\vec{q}) = 0, \quad (3.4)$$

$$P^0 - k^0 - \omega_1(\vec{q}) - \omega_2(\vec{k} + \vec{q}) = 0. \quad (3.5)$$

The other propagators do not lead to singularities, since particle 3 cannot decay into $2 + R$ and $P^0 + \omega_1 + \omega_2$ is always larger than k^0 , we have dropped the corresponding $i\epsilon$.

From Eqs. (3.4) and (3.5) we have

$$q_{\text{on}} = \frac{\lambda^{1/2}(M_A^2, m_R^2, m_1^2)}{2M_A}, \quad (3.6)$$

$$\omega_1(q_{\text{on}}) = \frac{M_A^2 + m_1^2 - m_R^2}{2M_A}, \quad (3.7)$$

$$\omega_R(q_{\text{on}}) = \frac{M_A^2 + m_R^2 - m_1^2}{2M_A}, \quad (3.8)$$

where we have defined the Källén function $\lambda(x, y, z) = x^2 + y^2 + z^2 - 2xy - 2yz - 2xz$.

In addition, from energy conservation in the process $A \rightarrow 123$, we have

$$k^0 = \frac{M_A^2 + m_3^2 - m_{12}^2}{2M_A}, \quad k = \frac{\lambda^{1/2}(M_A^2, m_3^2, m_{12}^2)}{2M_A}, \quad (3.9)$$

with m_{12} the invariant mass of the $(1, 2)$ system.

Then Eq. (3.5) leads immediately to

$$\frac{m_{12}^2 + m_R^2 - m_3^2 - m_1^2}{2M_A} - \sqrt{m_2^2 + (\vec{q} + \vec{k})^2} = 0, \quad (3.10)$$

which is the equation providing the singularities of the integrand of the loop integral in Eq. (3.4). However, a singularity of the integrand is not necessarily the singularity of the integral. If we can deform the integration contour in the complex plane to avoid the singularity, the integral would be regular. In the following two cases we cannot deform the contour and a singularity develops: 1) when the singularity of the integrand is located at the endpoint of the integration, 2) two or more singularities of the integrand pinch the contour. They correspond to the cases of endpoint and pinch singularities, respectively.

With that in mind, we notice that, in order to analyze the singularity structure, it is sufficient to focus on the following integral:

$$\begin{aligned} I(m_{12}) &= \int d^3q \frac{1}{[P^0 - \omega_R(\vec{q}) - \omega_1(\vec{q}) + i\epsilon] [E_{12} - \omega_1(\vec{q}) - \omega_2(\vec{k} + \vec{q}) + i\epsilon]} \\ &= 2\pi \int_0^\infty dq \frac{q^2}{P^0 - \omega_R(q) - \omega_1(q) + i\epsilon} f(q), \end{aligned} \quad (3.11)$$

where, in the rest frame of the decaying particle and with the more general notation as labelled in Fig. 3.3 (note that $\vec{p}_{R2} = \vec{k}$) $\omega_R(q) = \sqrt{m_R^2 + q^2}$, $\omega_1(q) = \sqrt{m_1^2 + q^2}$, $\omega_2(\vec{q} + \vec{p}_{R2}) = \sqrt{m_2^2 + (\vec{q} + \vec{p}_{R2})^2}$, $E_{12} = P^0 - p_{R2}^0$, and

$$f(q) = \int_{-1}^1 dz \frac{1}{E_{12} - \omega_1(q) - \sqrt{m_2^2 + q^2 + k^2 + 2qkz} + i\epsilon}, \quad (3.12)$$

where

$$k = |\vec{p}_{R2}| = \frac{\lambda^{1/2}(M_A^2, m_{R2}^2, m_{12}^2)}{2M_A}, \quad (3.13)$$

with $M_A = \sqrt{P^2}$ and $m_{R2} = \sqrt{p_{R2}^2}$, $m_{12} = \sqrt{p_{12}^2}$ and $q = |\vec{q}|$. The integral $I(m_{12})$ is in fact a function of all involved masses and external momenta, and here we only show m_{12} since we will discuss the singularities in this variable.

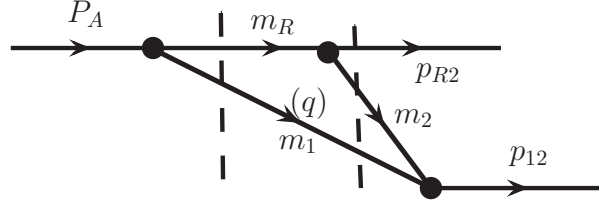


Figure 3.3: A triangle diagram showing the notations used in the general discussion of triangle singularities, where m_i 's denote the masses of the intermediate particles, and P , p_{R2} , p_{12} correspond to the four-momenta of the external particles. Note that $\vec{p}_{R2} = \vec{k}$. The two dashed vertical lines correspond to the two relevant cuts.

It becomes clear that we need to analyze the singularity structure of a double integration: one over q and one angular integration over z . The two factors in the denominator of the integrand of $I(m_{12})$ correspond to the two cuts depicted in Fig. 3.3. The cut crossing particles 1 and R provides a pole of the integrand of $I(m_{12})$ given by

$$P^0 - \omega_R(\vec{q}) - \omega_1(\vec{q}) + i\epsilon = 0, \quad (3.14)$$

which is like Eq. (3.4). However, we have kept the $i\epsilon$ here explicitly, which is important to determine the singularity locations in the complex- q plane. The pertinent solution is

$$q_{\text{on}+} = q_{\text{on}} + i\epsilon \quad \text{with} \quad q_{\text{on}} = \frac{1}{2M_A} \sqrt{\lambda(M_A^2, m_R^2, m_1^2)}. \quad (3.15)$$

The function $f(q)$ has endpoint singularities, which are logarithmic branch points, given when the denominator of the integrand vanishes for z taking the endpoint values ± 1 , i.e., the solutions of

$$E_{12} - \omega_1(q) - \sqrt{m_2^2 + q^2 + k^2 \pm 2qk} + i\epsilon = 0, \quad (3.16)$$

which is like Eq. (3.5). The $+$ and $-$ signs correspond to $z = +1$ and -1 , i.e., the situations for the momentum of particle 1 to be anti-parallel and parallel to the momentum of the $(1, 2)$ system in the frame with $\vec{P} = 0$, respectively. These endpoint singularities of $f(q)$ provide logarithmic branch point singularities to the integrand of $I(m_{12})$, in addition to the pole given by the first cut. Intuitively, we can envisage that when $z = +1, -1$ the principal part of the integration does not cancel the infinities of the denominators because one branch is outside the integration interval $z \in [-1, 1]$. To see if the end points induce singularities in $I(m_{12})$ we need to analyze each possibility.

For $z = -1$, Eq. (3.16) has two solutions:

$$q_{a+} = \gamma(v E_1^* + p_1^*) + i\epsilon, \quad q_{a-} = \gamma(v E_1^* - p_1^*) - i\epsilon, \quad (3.17)$$

where we have defined

$$\begin{aligned} v &= \frac{k}{E_{12}}, & \gamma &= \frac{1}{\sqrt{1-v^2}} = \frac{E_{12}}{m_{12}}, \\ E_1^* &= \frac{1}{2m_{12}} (m_{12}^2 + m_1^2 - m_2^2), & p_1^* &= \frac{1}{2m_{12}} \sqrt{\lambda(m_{12}^2, m_1^2, m_2^2)}. \end{aligned} \quad (3.18)$$

Note that E_1^* and p_1^* are the energy and the magnitude of the 3-momentum of particle 1 in the center-of-mass frame of the (1,2) system, v is the magnitude of the velocity of the (1,2) system in the rest frame of the decaying particle and γ is the Lorentz boost factor. Therefore, the two solutions given above correspond to the momentum of particle 1 in the rest frame of the decaying particle in different kinematic regions, which will be discussed later.

For $z = 1$, the two solutions of Eq. (3.16) are:

$$q_{b+} = \gamma(-v E_1^* + p_1^*) + i\epsilon, \quad q_{b-} = -\gamma(v E_1^* + p_1^*) - i\epsilon. \quad (3.19)$$

The second one, q_{b-} is irrelevant since it is always negative when $\epsilon = 0$, and is never realized in the integral on the momentum modulus in Eq. (3.11). It might be worthwhile to emphasize that all of $q_{a\pm}$ and $q_{b\pm}$ are singularities of the integrand of $I(m_{12})$ simultaneously. However, depending on the value of m_{12} (for real m_{12}), either $\lim_{\epsilon \rightarrow 0}(q_{a-})$ or $\lim_{\epsilon \rightarrow 0}(q_{b+})$, but not both, is positive and appears in the relevant integration range of q from 0 to $+\infty$. These two cases are shown in Fig. 3.4 and Fig. 3.5, respectively.

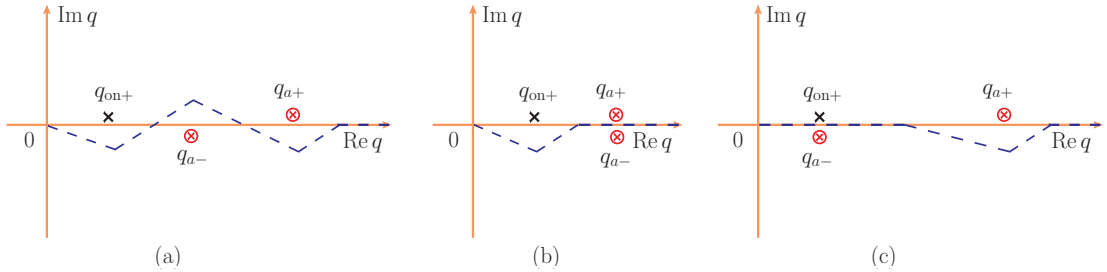


Figure 3.4: Pertinent singularities of the integrand of $I(m_{12})$ when $\lim_{\epsilon \rightarrow 0}(q_{a-})$ is positive. (a) is for the case without any pinching, (b) shows the case when the integration path is pinched between q_{a+} and q_{a-} , which gives the two-body threshold singularity, and (c) is for the case when the pinching happens between q_{on+} and q_{a-} , which gives the triangle singularity. The dashed lines correspond to possible integration paths. (Figure from Ref. [3.9]).

Let us discuss Fig. 3.4 first. In the integration range of q , the integrand has three relevant singularities: a pole q_{on+} and two logarithmic branch points $q_{a\pm}$. Their locations are determined by kinematics. It can happen that all of them are located at different positions, and one can deform the integration path freely as long as it does not hit any singularity of the integrand. One such path is shown as the dashed line segments in Fig. 3.4 (a). In such a kinematic region, $I(m_{12})$ is analytic. Since q_{a-} is in the lower half of the complex- q plane while q_{on+} and q_{a+}

are in the upper half plane, it could happen that the integration path is pinched between q_{a-} and one of q_{on+} and q_{a+} or even both of them. Then one cannot deform the integration path away from the singularities of the integrand and $I(m_{12})$ will be nonanalytic as well. If the integration path is pinched between q_{a-} and q_{a+} , as shown in Fig. 3.4 (b), which happens when $m_{12} = m_1 + m_2$ or $p_1^* = 0$, one gets the normal two-body threshold singularity which is a square-root branch point. If the integration path is pinched between q_{a-} and q_{on+} , as shown in Fig. 3.4 (c), one gets the triangle singularity or anomalous threshold which is a logarithmic branch point. Therefore, the condition for a triangle singularity to emerge is given mathematically by

$$\lim_{\epsilon \rightarrow 0} (q_{on+} - q_{a-}) = 0. \quad (3.20)$$

It could also happen that both q_{on+} and q_{a+} pinch the integration path with q_{a-} at the same time, and then the triangle singularity coincides with the normal threshold at $m_{12} = m_1 + m_2$. The location of the triangle singularity in the variable m_{12} is found by solving Eq. (3.20), which is the main result we later use when searching for possible triangle singularities in experimental data.

It is important to understand the kinematic region where the triangle singularity can occur. Since q_{a-} is the singularity of $f(q)$ at the endpoint $z = -1$, the momentum of particle 2 in the rest frame of the decaying particle is thus $\vec{p}_2 = -\vec{q} - \vec{p}_{R2} = (k - q)\hat{q}$, where \hat{q} stands for the unit vector along the direction of \vec{q} . From Eqs. (3.17) and (3.18), it is easy to see that $k > \lim_{\epsilon \rightarrow 0}(q_{a-})$ for $m_{12} \geq m_1 + m_2$. Thus, particles 1 and 2 move in the same direction in this reference frame. Another condition for q_{a-} to be relevant becomes clear by checking the expression of q_{a-} in Eq. (3.17), which is the Lorentz boost of the momentum of particle 1 from the center-of-mass frame of the (1,2) system to the rest frame of the decaying particle. The negative sign in front of p_1^* in Eq. (3.17) means that the direction of motion of particle 1 in the center-of-mass frame of the (1,2) system is opposite to the one in the rest frame of the decaying particle, while the direction of motion of particle 2 is the same in both reference frames. This implies that particle 2 moves faster than particle 1 in the latter reference frame. Therefore, the triangle singularity happens only when particle 2 moves along the same direction as particle 1, and has a larger velocity in the rest frame of the decaying particle. This, together with having all intermediate particles on their mass shells, gives the condition for having a triangle singularity. One can realize that this is in fact the Coleman-Norton theorem [3.8]: the singularity is on the physical boundary if and only if the diagram can be interpreted as a classical process in space-time.

For given m_1, m_2 and invariant masses for external particles, one can also work out the range of m_R where the triangle singularity shows up, as well as the range of the triangle singularity in m_{12} . For q_{on} and q_{a-} (taking $\epsilon = 0$) taking values in their physical regions, one needs to have $m_R \leq M_A - m_1$ and $m_{12} \geq m_1 + m_2$. Using Eq. (3.20), we find that when

$$m_R^2 \in \left[\frac{M_A^2 m_2 + m_{R2}^2 m_1}{m_1 + m_2} - m_1 m_2, (M_A - m_1)^2 \right], \quad (3.21)$$

$I(m_{12})$ has a triangle singularity, and it is within the range

$$m_{12}^2 \in \left[(m_1 + m_2)^2, \frac{M_A m_2^2 - m_{R2}^2 m_1}{M_A - m_1} + M_A m_1 \right]. \quad (3.22)$$

These are in fact the ranges discussed in Refs. [3.10, 3.13] derived from the point of view of the Coleman-Norton theorem.

The kinematic region where particle 1 moves faster than particle 2 but in the same direction corresponds to the case that the three-momentum of the on shell particle 1 takes the value of q_{a+} . One then has $\lim_{\epsilon \rightarrow 0}(q_{a+} - q_{a-}) > 0$ (it would be equal to 0 if the two particles move with the same speed in the rest frame of the decaying particle), and $I(m_{12})$ has no singularity. From the point of view of the Coleman-Norton theorem [3.8], particle 2 emitted from the decay of particle R cannot catch up with particle 1 so that the rescattering between them in the triangle diagram cannot be interpreted as a classical process. This case corresponds to Fig. 3.4 (a).

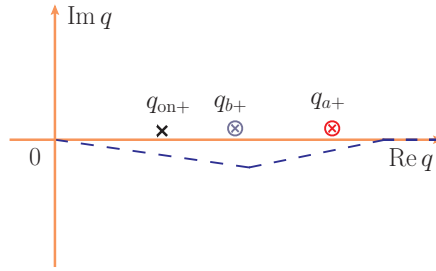


Figure 3.5: Pertinent singularities of the integrand of $I(m_{12})$ when $\lim_{\epsilon \rightarrow 0}(q_{b+})$ is positive. (Figure from Ref. [3.9]).

There is the possibility that $q_{a-} < 0$ (here and in the following when we talk about the sign or relative size of $q_{a\pm}$ and $q_{b\pm}$, ϵ takes the value of 0) and, thus, this solution is unphysical for on-shell intermediate particles. In this case, solving numerically Eq. (3.10) with \vec{q} and \vec{k} in opposite directions will give only one positive q solution, which, by necessity, is q_{a+} . Note that $q_{a-} < 0$ means $q_{b+} = -q_{a-} > 0$, so that q_{b+} is in the physical range of q . We show this case in Fig. 3.5, where only the positive singularities of the integrand, which are the ones in the physical range of q for on-shell intermediate particles, are depicted. Since $q_{a-} < 0$ in this case, and $q_{b-} < 0$, and furthermore q_{on+} , q_{a+} and q_{b+} are on the same side of the $\text{Re } q$ axis, no pinching can occur and, hence, none of these singularities of the integrand turns into a singularity of the integral $I(m_{12})$. The condition for $q_{a-} < 0$ is $p_1^* > v E_1^*$, i.e., the magnitude of velocity of particle 1 in the (1,2) center-of-mass frame (which is equal to the one for particle 2) is larger than the velocity of the (1, 2) system in the rest frame of the initial particle. It implies that particle 1 and particle 2 move in opposite directions in the latter frame and thus particle 2, emitted from the decay of particle R , which moves also opposite to particle 1 in the rest frame of the initial particle, cannot rescatter with particle 1 in a classical picture with energy-momentum conservation, in accordance with the conclusion of Ref. [3.8].

In section 3.4 we will bring back this topic of the singularities of the triangle diagram, and also in the tree level, when we discuss the Schmid theorem [3.6]. In the following sections 3.2 and 3.3 we will see two cases where we applied this framework to study the triangle singularities in experimental data.

3.2 Revising the $f_1(1420)$

In this section we present the work of Ref. [3.1], where we have studied the production and decay of the $f_1(1285)$ into $\pi a_0(980)$ and $K^* \bar{K}$ as a function of the mass of the resonance and find a shoulder around 1400 MeV, tied to a triangle singularity, for the $\pi a_0(980)$ mode, and a peak around 1420 MeV with about 60 MeV width for the $K^* \bar{K}$ mode. Both these features agree with the experimental information on which the $f_1(1420)$ resonance is based. In addition, we find that if the $f_1(1420)$ is a genuine resonance, coupling mostly to $K^* \bar{K}$ as seen experimentally, one should expect about a 20% fraction for $\pi a_0(980)$ decay of this resonance, in contradiction with all experiments. Altogether, we conclude that the $f_1(1420)$ is not a genuine resonance, but the manifestation of the $\pi a_0(980)$ and $K^* \bar{K}$ decay modes of the $f_1(1285)$ at higher energies than the nominal one. We also compare our results with the experimental data from Ref. [3.2].

3.2.1 Introduction

The $f_1(1420)$ resonance is catalogued in the Particle data book [3.14] as an $I^G(J^{PC}) = 0^+(1^{++})$ state and has been observed in over 20 experiments. Its mass is $M = 1426.4 \pm 0.9$ MeV and its width $\Gamma = 54.9 \pm 2.6$ MeV. Its dominant decay mode is $K \bar{K}^*$. In Ref. [3.15] 100% of the width is associated to the $K \bar{K}^* + \text{c.c.}$ mode. In Ref. [3.16] other modes are also searched for, with negative results, concluding again that the $K \bar{K}^* + \text{c.c.}$ channel exhausts the decay width. In Ref. [3.17] the authors also conclude that the $f_1(1420)$ decays into $K \bar{K}^* + \text{c.c.}$ 100%. In Ref. [3.2] the decay mode $\pi a_0(980)$ is reported with $\Gamma(\pi a_0(980))/\Gamma(K \bar{K}^* + \text{c.c.}) = 0.04 \pm 0.01 \pm 0.01$. In this latter paper a clean peak is seen for the $f_1(1285)$ in the $\pi a_0(980)$ mode, followed by a broader structure around 1400 MeV with much smaller strength, that is tentatively associated to the $f_1(1420)$, with the comment “The shoulder at 1.4 GeV can be interpreted as an $a_0(980)\pi$ decay mode of the $f_1(1420)$ ” with no devoted work to support this assertion. A discussion on mesons in the 1400 MeV region can be seen in the PDG review [3.18].

In the present work we shall provide a different explanation of the experimental findings, showing that the $K^* \bar{K}$ peak associated to the $f_1(1420)$ is the manifestation of the $K \bar{K}^* + \text{c.c.}$ decay mode of the $f_1(1285)$. On the other hand, the broad peak for $\pi a_0(980)$ decay in the region of 1400 MeV will be explained as a consequence of a triangle singularity, due to $f_1(1285) \rightarrow K^* \bar{K}$, $K^* \rightarrow \pi K$, $K \bar{K} \rightarrow a_0(980)$. The $K^* \bar{K}$ decay mode of the $f_1(1285)$ appears as “not seen” in the PDG [3.14]. Indeed the $f_1(1285)$ is 100 MeV below the $K^* \bar{K}$ threshold. However, the $K \bar{K} \pi$ mode is reported with a branching fraction of 9%. These features found an adequate answer in several works [3.19, 3.20], where the $f_1(1285)$ was considered as a dynamically generated resonance. This state, together with all the low-lying axial vector resonances, were

obtained in Refs. [3.21, 3.22] as dynamically generated states from the interaction of pseudoscalar mesons with vector mesons, using a coupled channels unitary scheme with chiral dynamics for the meson interaction [3.23]. In the particular case of the $f_1(1285)$, the $K\bar{K}^* + \text{c.c.}$ is the single channel in the coupled channel approach [3.22]. The work in Refs. [3.21, 3.22], using the lowest order chiral Lagrangian, has been extended in Ref. [3.24] including higher order terms, but in the case of the $f_1(1285)$ the higher order terms were found essentially negligible.

In this picture for the $f_1(1285)$, a good description of $\pi a_0(980)$ and the isospin forbidden $\pi f_0(980)$ decay modes were well reproduced [3.20]. Actually the $\pi f_0(980)$ decay mode was first predicted in Ref. [3.20] and corroborated later experimentally by a BESIII experiment [3.25]. Similarly, in Ref. [3.19] the $K\bar{K}\pi$ decay mode was studied and also found consistent with experiment [3.2, 3.26]. In the present work, we shall see that, as a consequence of the $K^*\bar{K}$ nature of the $f_1(1285)$, if we excite that state and go to higher energies where the $K^*\bar{K}$ can be produced, the tail of the $f_1(1285)$ propagator, together with the phase space for $K^*\bar{K}$ production, produce a peak around 1420 MeV with a width of about 60 MeV, that explains the experimental features observed for the $f_1(1420)$ resonance.

One may wonder how much our results are tied to the assumed nature of the $f_1(1285)$ as a dynamically generated resonance. Before we discuss this issue further, let us clarify that for the sake of the present work it is not necessary to assume that this is the nature of the $f_1(1285)$. We only need that it couples to $K\bar{K}^* + \text{c.c.}$ whatever its origin. The fact that with the strength of the coupling to this channel provided by the approach of Ref. [3.22] one obtains a good reproduction of the important partial decay width to $\pi a_0(980)$ [3.20] and the $K\bar{K}\pi$ decay mode [3.19], indicates that the coupling of the $f_1(1285)$ to $K\bar{K}^* + \text{c.c.}$ used here is realistic. In any case, it is interesting to discuss the issue to the light of what a quark structure provides for the axial vector states. The detailed work on relativistic quark models of Ref. [3.27] indicates that masses of the right order of magnitude can be obtained for the axial vector meson states within the scheme of Ref. [3.27], which is very successful to describe the bulk of the meson properties.

Yet, most of the axial vector mesons have large decay widths and couple to pseudoscalar-vector components. Some, as the $f_1(1285)$ have a relatively small width, but can equally couple to pseudoscalar-vector bound components, like $K\bar{K}^*$. The need to consider these meson-meson components for the structure of some mesons became apparent and studies were done in Refs. [3.28–3.31] starting with a seed of $q\bar{q}$ and unitarizing the model with the meson-meson components. For the case of the low lying scalar mesons the result is that, as a consequence of the unitarization, the original $q\bar{q}$ seed is dressed with meson-meson components to the point that the latter become the most important ingredient in low energy reactions. Even in the work of Ref. [3.27] the $f_0(980)$ was hinted as a $K\bar{K}$ bound state, which was more substantiated in Ref. [3.32], and more recently by the framework of the chiral unitary approach [3.33–3.36]. This latter approach is the one used to describe also the low lying axial vectors, with energies below 1.4 GeV, as being largely made of pseudoscalar-vector components in Refs. [3.21, 3.22] and much present phenomenology supports this picture as discussed above. From this perspective, it is then not surprising that other works concentrate on the nature of these states

as tetraquarks [3.37, 3.38]. In the real world a mixture of $q\bar{q}$ and molecular components (or tetraquarks, for this purpose) would appear [3.39], but the molecular components are very important and play a dominant role in low energy reactions as phenomenology is telling us (see Refs. [3.40–3.43] in addition to the works cited above).

On the other hand, the triangle diagram with $K^*\bar{K}K$ intermediate states, with π and $f_0(980)$ or $a_0(980)$ external products, develops a singularity at 1420 MeV, which is seen as a peak for $\pi f_0(980)$ or $\pi a_0(980)$ production. This was already suggested in Ref. [3.12] and shown explicitly in Refs. [3.44, 3.45], and provided a natural explanation of the COMPASS observation [3.46] of a peak in the $\pi f_0(980)$ mode around 1420 MeV, which was interpreted as a new resonance, the “ $a_1(1420)$ ” in Ref. [3.46]. In Refs. [3.44, 3.45] the peak was interpreted as a consequence of a triangle singularity associated to the decay mode of the $a_1(1260)$ into $K^*\bar{K}$, followed by $K^* \rightarrow K\pi$ and fusion of the $K\bar{K}$ to give the $f_0(980)$. The mechanism to produce the $\pi a_0(980)$ from the decay of the $f_1(1285)$ is identical to the one used in Ref. [3.45] to produce the $\pi f_0(980)$ from the decay of the $a_1(1260)$. Only the isospin combinations are different, but the singularity is tied to the masses of the particles and is independent of the internal degrees of freedom like the isospin. We shall see that, also in this case, a peak is produced around 1420 MeV in the $\pi a_0(980)$ decay mode of the $f_1(1285)$ which explains the features of the experiment of Ref. [3.2]. The conclusion of all these observations is that the $f_1(1420)$ is not a genuine resonance, but the manifestation of the $K^*\bar{K}$ and $\pi a_0(980)$ decay modes of the $f_1(1285)$ resonance. This would go in line with the conclusions of Refs. [3.44, 3.45] that the “ $a_1(1420)$ ” is not a genuine resonance, but the manifestation of the $\pi f_0(980)$ decay mode of the $a_1(1260)$ resonance.

3.2.2 Formalism

The resonance $f_1(1420)$ is observed in very high energy collisions, which we depict in Fig. 3.6, and the resonance is observed in the invariant mass of particles 2 and 3.

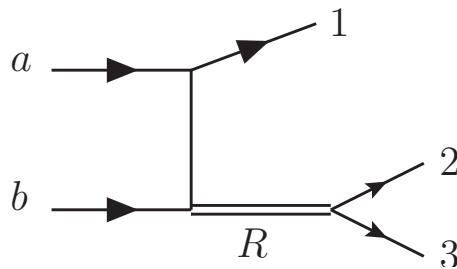


Figure 3.6: Diagrammatic representation of the process producing the resonance, observed in the decay channel 2 + 3.

In the Mandl and Shaw normalization of fermion fields [3.47] we have for this process with three particles in the final state

$$\frac{d^2\sigma}{dt dM_{23}} = \frac{1}{32 p_a^2 s} \prod (2m_F) \frac{1}{(2\pi)^3} \tilde{p}_2 \overline{\sum} \sum |T|^2, \quad (3.23)$$

where m_F refers to the masses of the fermions, and the sum and average of $|T|^2$ is done over the polarizations of all particles involved. In Eq. (3.23) \tilde{p}_2 is the momentum of particle 2 in the rest frame of the 2 + 3 system,

$$\tilde{p}_2 = \frac{\lambda^{1/2}(M_{23}^2, m_2^2, m_3^2)}{2M_{23}}, \quad (3.24)$$

and M_{23} is the invariant mass of the 2 + 3 system. Fixing the Mandelstam variables s and t , $s = (p_a + p_b)^2$, $t = (p_a - p_1)^2$, the T matrix in Eq. (3.23) will be of the type ($M_{\text{inv}} \equiv M_{23}$):

$$T \equiv C \frac{1}{M_{\text{inv}}^2 - M_R^2 + iM_R\Gamma_R} g_{R,23}, \quad (3.25)$$

where we have put a coupling $g_{R,23}$ for the resonance R to the 2 + 3 system. The width for the resonance going to 2 + 3 is given in this case by

$$\Gamma_{R,23} = \frac{1}{8\pi} \frac{1}{M_{\text{inv}}^2} \tilde{p}_2 g_{R,23}^2, \quad (3.26)$$

which allows one to write Eq. (3.23) as

$$\frac{d^2\sigma}{dt dM_{\text{inv}}} = \frac{\prod(2m_F)}{32 p_a^2 s} \frac{1}{(2\pi)^3} C^2 \frac{8\pi M_{\text{inv}}^2 \Gamma_{R,23}}{|M_{\text{inv}}^2 - M_R^2 + iM_R\Gamma_R|^2}. \quad (3.27)$$

This equation is also good when we sum and average over polarizations of the particles in a more general case of $|T|^2$. The sum over polarizations of 2 and 3 will go into $\Gamma_{R,23}$ and the sum and average over polarizations of the other particles can be absorbed in the constant C (for fixed s and t). Eq. (3.27) can also be used for any decay channel of the resonance, substituting $\Gamma_{R,23}$ by Γ_i of the particular decay channel. Since $\sum \Gamma_i = \Gamma_R$, the total width of the resonance, the sum of Eq. (3.27) over all decay channels, can be cast in terms of $\text{Im}[1/(M_{\text{inv}}^2 - M_R^2 + iM_R\Gamma_R)]$, which is a variant of the optical theorem.

3.2.3 The $K^*\bar{K}$ channel

Let us look at the process depicted in Fig. 3.6 with 2, 3 being $K^*\bar{K}$. We shall investigate what happens when the resonance R is the $f_1(1285)$. We can use directly Eq. (3.27) replacing the coupling $g_{R,23}$ in Eq. (3.26) by the $f_1, K^*\bar{K}$ coupling

$$g_{R,23} \rightarrow g_{f_1, K^*\bar{K}} \vec{\epsilon}_{f_1} \cdot \vec{\epsilon}_{K^*}, \quad (3.28)$$

and summing and averaging over polarizations, and we use $g_{f_1, K^*\bar{K}} = 7555$ MeV, from Ref. [3.22], ignoring for the moment the isospin and C -parity structure. The $\Gamma_{f_1, K^*\bar{K}}$ width is then given by

$$\Gamma_{f_1, K^*\bar{K}} = \frac{1}{8\pi} \frac{1}{M_{\text{inv}}^2} g_{f_1, K^*\bar{K}}^2 \tilde{p}_{\bar{K}} \theta(M_{\text{inv}} - m_{K^*} - m_K). \quad (3.29)$$

The $K^*\bar{K}$ production will begin at a threshold of 1383 MeV, 100 MeV above the nominal mass of the $f_1(1285)$. The results of Eq. (3.27) are depicted in Fig. 3.7,

where in addition we plot also the result using in the numerator the nominal width of the $f_1(1285)$, $\Gamma_{f_1} = 24.1$ MeV, which will account for the decays of the $f_1(1285)$ into other channels. In the denominator of Eq. (3.27) we use

$$\Gamma_R = \Gamma_{f_1} + \Gamma_{f_1, K^* \bar{K}}. \quad (3.30)$$

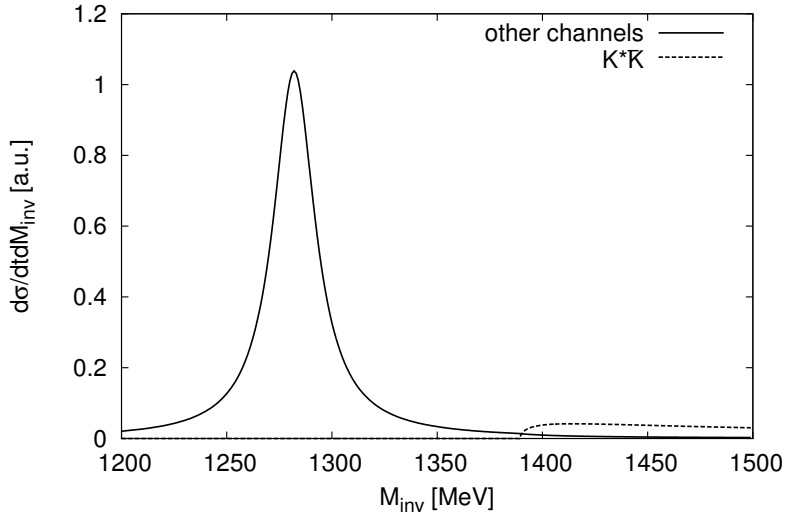


Figure 3.7: Production of $K^* \bar{K}$ induced by the excitation of the $f_1(1285)$ resonance. Dashed line: production of $f_1(1285)$ through the decay of $f_1(1285)$ into $K^* \bar{K}$. Solid line: through the decay of the $f_1(1285)$ into other channels.

We observe in Fig. 3.7 the typical threshold production of a channel. However, since the production is driven by the excitation of the $f_1(1285)$, one has two factors competing, a decreasing strength of the resonance as the energy increases, and an increasing phase space for the $K^* \bar{K}$ production, and the product of these two factors confers the cross section a particular shape. Yet, we want to be more accurate here by taking into account that the K^* will decay into $K\pi$ and the experimentalist will observe $K\pi \bar{K}$ at the end. This will also allow us to go below the threshold of $K^* \bar{K}$ production.

To account for the decay, we look into the diagram of Fig. 3.8.

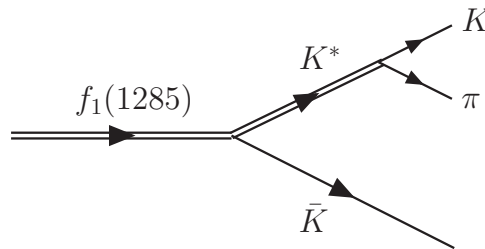


Figure 3.8: Decay diagram for $f_1(1285) \rightarrow K^* \bar{K}$ considering the $K\pi$ decay channel of the K^* .

The decay width of the $f_1(1285)$ for Fig. 3.8 is given by

$$\Gamma_{f_1, K^* \bar{K} \rightarrow K \pi \bar{K}} \equiv \int \frac{d\Gamma_{f_1, K \pi \bar{K}}}{dm_{\text{inv}}} dm_{\text{inv}}, \quad (3.31)$$

where m_{inv} stands for the $K\pi$ invariant mass, and

$$\frac{d\Gamma_{f_1, K \pi \bar{K}}}{dm_{\text{inv}}} = \frac{1}{(2\pi)^3} \frac{1}{4M_{\text{inv}}^2} p_{\bar{K}} \tilde{p}_\pi \overline{\sum} \sum |t'|^2, \quad (3.32)$$

where $p_{\bar{K}}$ is the \bar{K} momentum in the $f_1(1285)$ rest frame and \tilde{p}_π the π momentum in the $K\pi$ rest frame, and t' contains now the K^* propagator, the $f_1(1285) \rightarrow K^* K$ and $K^* \rightarrow K\pi$ couplings. There is no need to evaluate t' explicitly since we can use the same step that led us from Eq. (3.23) to Eq. (3.27) and we can write

$$\begin{aligned} \frac{d\Gamma_{f_1, K \pi \bar{K}}}{dm_{\text{inv}}} &= \frac{1}{(2\pi)^3} \frac{1}{4M_{\text{inv}}^2} g_{f_1, K^* \bar{K}}^2 p_{\bar{K}} \\ &\times \frac{8\pi m_{\text{inv}}^2 \Gamma_{K^*}(m_{\text{inv}})}{|m_{\text{inv}}^2 - m_{K^*}^2 + im_{K^*} \Gamma_{K^*}(m_{\text{inv}})|^2}, \end{aligned} \quad (3.33)$$

where

$$\Gamma_{K^*}(m_{\text{inv}}) = \frac{m_{K^*}^2}{m_{\text{inv}}^2} \frac{\tilde{p}_\pi^3}{\tilde{p}_\pi^3|_{\text{on}}} \Gamma_{K^*}|_{\text{on}}, \quad (3.34)$$

with $\Gamma_{K^*}|_{\text{on}} = 49.1$ MeV the nominal width for the K^* , and $\tilde{p}_\pi, \tilde{p}_\pi|_{\text{on}}$ the pion momenta in the K^* rest frame with K^* mass m_{inv} or m_{K^*} respectively,

$$\tilde{p}_\pi = \frac{\lambda^{1/2}(m_{\text{inv}}^2, m_K^2, m_\pi^2)}{2m_{\text{inv}}}. \quad (3.35)$$

In Eq. (3.34) we have taken into account that the $K^* \rightarrow K\pi$ proceeds in P -wave.

In Fig. 3.9 we plot the results for Eq. (3.27) with $\Gamma_{R,23}$ replaced by Eqs. (3.31) and (3.33), and also when $\Gamma_{R,23}$ is replaced by Γ_{f_1} . Fig. 3.9 is very intuitive, we see a double peak structure. The first peak accounts for the standard $f_1(1285)$ decay into $K\pi\bar{K}$ observed with the shape of the $f_1(1285)$. The ratio of strengths at the peak of the dashed and solid lines provides the branching ratio of the $f_1(1285)$ into $K\pi\bar{K}$ channel. As we see, it is of the order of 8%, the same value obtained in Ref. [3.19] with a more elaborate model that we shall discuss below, and in agreement with experiment [3.14].

Yet, what concerns us here is that the same mechanism produces a second peak around 1420 MeV as a consequence of the influence of the tail of the $f_1(1285)$ resonance and the increasing phase space for $K^*\bar{K}$ production. In Fig. 3.10 we can see in more detail the two peaks corresponding to $K\pi\bar{K}$ production. By assuming a smooth background below the second peak, as an experimental analysis would do, we induce that there is a resonant-like structure peaking around 1420 MeV with a width of about 60 MeV, the features observed in experiment when talking about the $f_1(1420)$ resonance. Yet, we did not have to invoke a new resonance for this structure, which appears naturally and unavoidably from the decay of $f_1(1285)$ into $K^*\bar{K} \rightarrow K\pi\bar{K}$. This also explains why the $f_1(1420)$ resonance is seen in the $K^*\bar{K}$ (or $K\pi\bar{K}$) channel alone. In the next section we address the production of the $\pi a_0(980)$ channel.

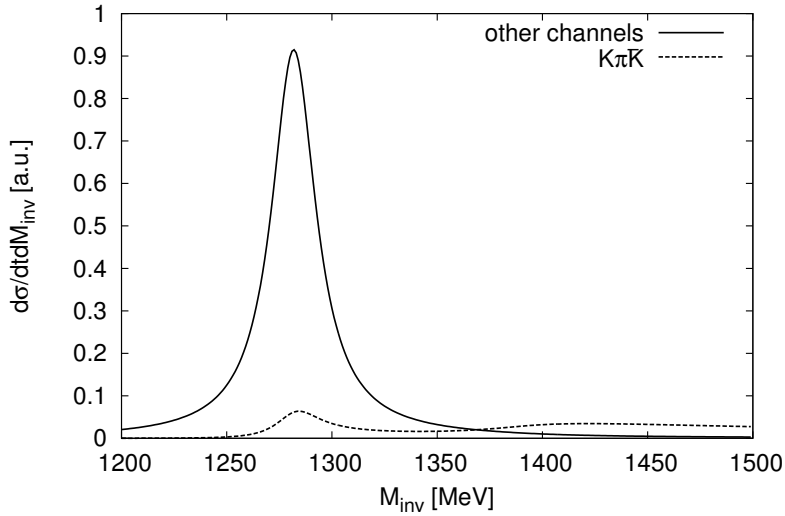


Figure 3.9: Production of $K\pi\bar{K}$ coming from $K^*\bar{K}$ decay of the $f_1(1285)$ considering the decay of K^* into $K\pi$. The dashed line accounts for $K\pi\bar{K}$ production and the solid line accounts for the decay of the $f_1(1285)$ into other channels.

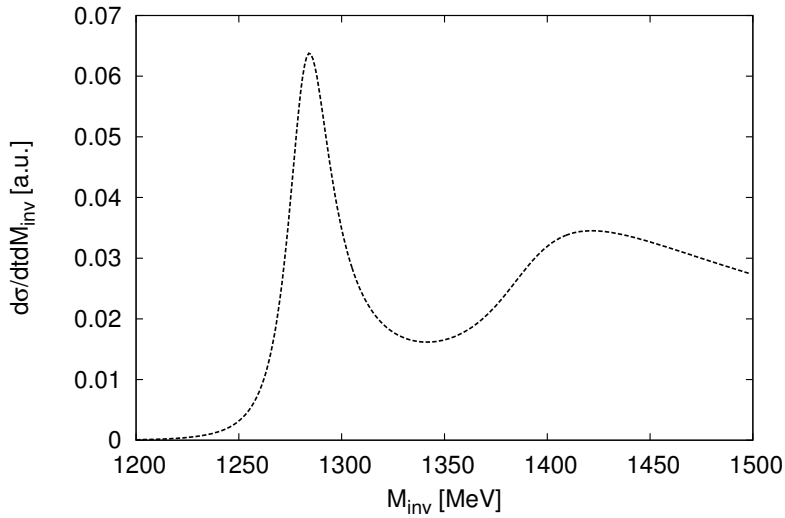


Figure 3.10: The $K\pi\bar{K}$ production cross section from Eq. (3.27) showing detail of the dashed line in Fig. 3.9.

3.2.4 The $\pi a_0(980)$ decay mode of the $f_1(1285)$

This problem was also addressed in Ref. [3.20] but at the peak of the $f_1(1285)$. Now we extend it to higher energies according to Eq. (3.27), but replacing the width $\Gamma_{R,23}$ by $\Gamma_{f_1(1285),\pi a_0(980)}$. Following Ref. [3.20] and sticking to the simplified $K^*\bar{K}$ decay of the former section, we have to look at the diagram of Fig. 3.11, where we consider the $a_0(980)$ decay into the $\pi^0\eta$ channel.

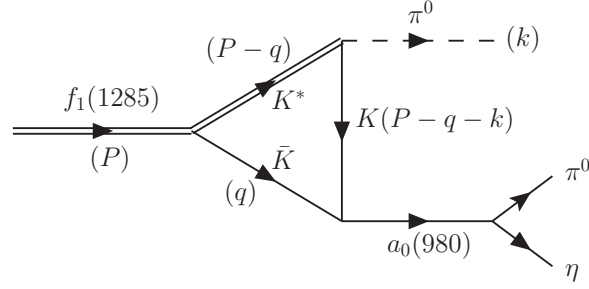


Figure 3.11: Triangle diagram leading to the production of $\pi a_0(980)$, the latter is observed in $\pi^0\eta$. In brackets the momenta of the particles.

The amplitude for the diagram of Fig. 3.11 for the $f_1(1285)$ at rest ($\vec{P} = 0$) is given by

$$t_{f_1, \pi\pi^0\eta} = g_{f_1, K^* \bar{K}} g_{K^*, K\pi} t_T t_{K\bar{K} \rightarrow \pi^0\eta}(\tilde{m}_{\text{inv}}), \quad (3.36)$$

with \tilde{m}_{inv} the $\pi^0\eta$ invariant mass, and where t_T stands for the triangle loop integral with three propagators,

$$t_T = i \int \frac{d^4q}{(2\pi)^4} \vec{\epsilon}_{f_1} \cdot \vec{\epsilon}_{K^*} \vec{\epsilon}_{K^*} \cdot (2\vec{k} + \vec{q}) \frac{1}{q^2 - m_K^2 + i\epsilon} \frac{1}{(P-q)^2 - m_{K^*}^2 + im_{K^*}\Gamma_{K^*}} \times \frac{1}{(P-q-k)^2 - m_K^2 + i\epsilon}, \quad (3.37)$$

and $t_{K\bar{K} \rightarrow \pi^0\eta}$ is evaluated using the chiral unitary approach of Ref. [3.33], with the input used in the study of weak decays of B and D mesons in Refs. [3.48, 3.49].

The integral of q^0 in Eq. (3.37) can be done analytically and it is done in Ref. [3.20] with the result

$$t_T = \tilde{t}_T \vec{\epsilon}_{f_1} \cdot \vec{k}, \quad (3.38)$$

and

$$\tilde{t}_T = \int \frac{d^3q}{(2\pi)^3} \left(2 + \frac{\vec{k} \cdot \vec{q}}{k^2} \right) \times \frac{1}{8\omega(q)\omega'(q)\omega^*(q)} \frac{1}{k^0 - \omega'(q) - \omega^*(q) + i\epsilon} \frac{1}{P^0 - \omega^*(q) - \omega(q) + i\epsilon} \times \frac{2P^0\omega(q) + 2k^0\omega'(q) - 2(\omega(q) + \omega'(q))(\omega(q) + \omega'(q) + \omega^*(q))}{(P^0 - \omega(q) - \omega'(q) - k^0 + i\epsilon)(P^0 + \omega(q) + \omega'(q) - k^0 - i\epsilon)}, \quad (3.39)$$

with $\omega(q) = \sqrt{\vec{q}^2 + m_K^2}$, $\omega'(q) = \sqrt{(\vec{q} + \vec{k})^2 + m_K^2}$, $\omega^*(q) = \sqrt{\vec{q}^2 + m_{K^*}^2}$, (or $\sqrt{\vec{q}^2 + m_{K^*}^2} - i\Gamma_{K^*}/2$ if the K^* width is considered as in Eq. (3.37)).

The width $\Gamma_{f_1(1285), \pi\pi^0\eta}$ is given by

$$\Gamma_{f_1, \pi\pi^0\eta} = \int \frac{d\Gamma_{f_1, \pi\pi^0\eta}}{d\tilde{m}_{\text{inv}}} d\tilde{m}_{\text{inv}}, \quad (3.40)$$

with $d\Gamma_{f_1, \pi\pi^0\eta}/d\tilde{m}_{\text{inv}}$ obtained using Eq. (3.32) with $m_{\text{inv}} \rightarrow \tilde{m}_{\text{inv}}$ (of $\pi^0\eta$), $p_{\bar{K}} \rightarrow p_\pi$, $\tilde{p}_\pi \rightarrow \tilde{p}_\eta$ and

$$\overline{\sum} \sum |t_{f_1, \pi\pi^0\eta}|^2 = \frac{1}{3} \vec{k}^2 |\tilde{t}_T|^2 g_{f_1, K^* \bar{K}}^2 g_{K^*, K\pi}^2 |t_{K\bar{K}, \pi^0\eta}|^2. \quad (3.41)$$

The value of $g_{K^*, K\pi}$ is taken such that

$$\Gamma_{K^*} = \frac{4}{3} \frac{1}{8\pi} \frac{1}{m_{K^*}^2} \tilde{p}_\pi^2 g_{K^*, K\pi}^2 \quad (3.42)$$

gives the width of the K^* , $\Gamma_{K^*} = 49.1$ MeV ($g_{K^*, K\pi} = 5.5$ MeV).

We should note a small modification in the integral with respect to Ref. [3.20]. In this latter work a cutoff $\theta(q_{\text{max}} - q)$ originated in the chiral unitary approach in the study of the $K\bar{K} \rightarrow \pi\eta$ amplitude was implemented, with $q_{\text{max}} = 600$ MeV [3.48, 3.49]. Since in those works the cutoff is implemented in the center of mass (CM) frame, we make a boost of q to the rest frame of the $\pi\eta$ system and implement the cutoff $\theta(q_{\text{max}} - q_{\text{CM}})$. We show the results obtained in Fig. 3.12.

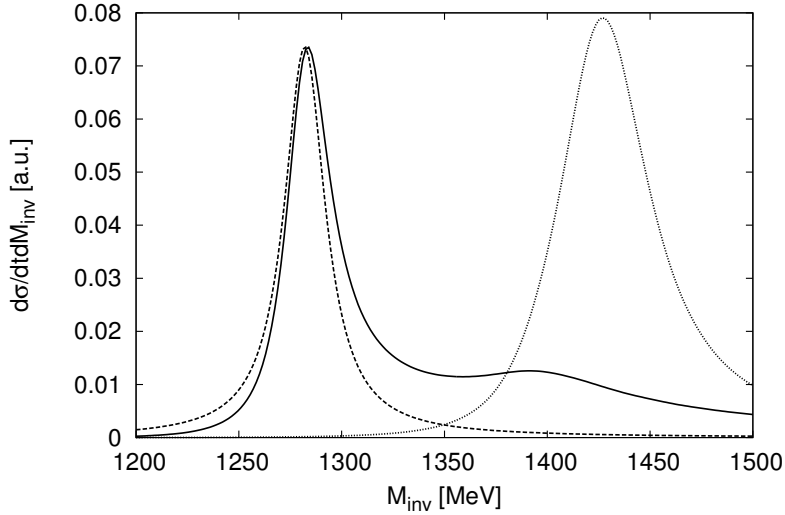


Figure 3.12: Differential cross section for $\pi a_0(980) \rightarrow \pi\pi^0\eta$ production induced by $f_1(1285)$ excitation. Solid line: considering the triangle diagram of Fig. 3.11. Dashed line: using Eq. (3.27) with $\Gamma_R = \Gamma_{f_1(1285)} = 24.1$ MeV, $\Gamma_{R,23}$ a constant and normalizing the curves to the peak of the $f_1(1285)$ (this reflects the shape of the modulus square of the $f_1(1285)$ propagator). The dotted curve is what we would expect for $\pi a_0(980) \rightarrow \pi\pi^0\eta$ production from $f_1(1420)$ excitation assuming that the production rate of the $f_1(1285)$ and $f_1(1420)$ are the same.

As we can see in Fig. 3.12, there is a large strength in the cross section built around 1400 MeV induced by the $f_1(1285)$ excitation, which makes it very distinct from the usual shape of the Breit-Wigner distribution for the $f_1(1285)$. It is interesting to see that this cross section is remarkably similar to the one found in Ref. [3.2] (we shall come back to it in the next section to do a comparison with the data). In Ref. [3.2] no explanation was found for this extra strength and it was suggested that

it should be the $\pi a_0(980)$ decay mode of the $f_1(1420)$. What we see here is that the peculiar shape of the cross section for this particular channel is a consequence of the triangle diagram of Fig. 3.11, the mechanism for $\pi a_0(980)$ production from a resonance (the $f_1(1285)$) that is a bound state of $K^*\bar{K}$, or that couples strongly to $K^*\bar{K}$ for the purpose (the $f_1(1285)$). The unexpected large strength around 1400 MeV comes from a singularity in the triangle diagram as we discuss in the next section. From that we can conclude that the strength found in this channel around 1400 MeV is not tied to the $f_1(1420)$ resonance but to the $f_1(1285)$.

There is one more argument that we can bring in favour of the former interpretation. Indeed, let us assume that the $f_1(1420)$ is a genuine resonance. If it decays into $K^*\bar{K}$ and this channel exhausts the width as found experimentally, we can get the coupling $g_{f_1(1420),K^*\bar{K}}$ by means of Eq. (3.26) and we find

$$g_{f_1(1420),K^*\bar{K}} = 4256 \text{ MeV} . \quad (3.43)$$

With this coupling we can reevaluate the triangle diagram of Fig. 3.11, simply replacing the coupling $g_{f_1(1285),K^*\bar{K}}$ with the new one. Then we would use Eq. (3.27) to get the cross section for $f_1(1420) \rightarrow \pi a_0(980)$, replacing the $f_1(1285)$ propagator by the one of the $f_1(1420)$. The other change might be the constant C , but this constant, appearing in the $a + b \rightarrow 1 + R$ vertex (see Fig. 3.6) is related to the resonance production (irrespective of the decay channels). Since one is dealing with high energies of the order of hundreds of GeV in these reactions, and the masses of the $f_1(1285)$ and $f_1(1420)$ are similar, on statistical grounds we should expect similar production rates for both resonances, and hence C should be similar in the two cases. Assuming C is the same for both resonances, what we see in Fig. 3.12 is a shape for $f_1(1420) \rightarrow \pi a_0(980)$ production very different from the one coming from the $f_1(1285)$ decay, which reflects a $f_1(1420)$ Breit-Wigner structure, and most importantly, with a very large strength, which is not seen in any experiment. Even this signal reduced by a factor five should be clearly seen experimentally, and on statistical grounds it is not easy to justify that the production of the $f_1(1420)$ should be reduced by a factor five with respect to that of the $f_1(1285)$.

There is yet another factor to note. When performing the previous calculation that involves the $f_1(1420)$ propagator, we had to calculate the width of the $f_1(1420)$ into $\pi a_0(980)$. We find that (see next section for a more detailed evaluation)

$$\frac{BR(f_1(1420) \rightarrow \pi a_0(980))}{BR(f_1(1420) \rightarrow K^*\bar{K})} \simeq 0.17 . \quad (3.44)$$

This is a fraction that could not be missed and has not been found in any experiment where this decay mode has been searched for. Only in Ref. [3.2] a 5% ratio was invoked by guessing that the shoulder seen in that decay mode around 1400 MeV was due to this resonance, but we have given a different interpretation for this feature.

It is interesting to recall here that the triangle singularity of Fig. 3.11 also shows up in the decay of the $\eta(1405) \rightarrow \pi a_0(980)$ which was studied in Refs. [3.50, 3.51], together with the isospin violating $\eta(1405) \rightarrow \pi f_0(980)$ decay. This latter decay was abnormally enhanced due to the triangle singularity. In a follow up of Ref. [3.50] in Ref. [3.52] the idea is retaken and applied to study the BESIII decay of

$J/\psi \rightarrow \gamma\eta(1405)(\eta(1475))$ with $\eta(1405) \rightarrow K\bar{K}\pi$, $\eta\pi\pi$ and 3π . In this work the possible contribution of the $f_1(1420)$ in addition to the $\eta(1405)$ was discussed. The $f_1(1420)$ was assumed to be a regular resonance and the triangle singularity enhanced some decay modes, in spite of which its contribution relative to that of the $\eta(1405)$ was found small in the radiative J/ψ decay. Although we find that the $f_1(1420)$ is not a genuine resonance, we have seen that there is indeed strength in the $K\pi\bar{K}$ and $\pi a_0(980)$ channels in the 1420 MeV region from the decay of the $f_1(1285)$. A reanalysis of the BESIII experimental data [3.53] from this new perspective would be most interesting.

It is interesting to evaluate uncertainties of the results obtained. We have used a coupling of $f_1(1285)$ to $K^*\bar{K}$, $g_{f_1, K^*\bar{K}} = 7555$ MeV. In Ref. [3.22] the value is 7230 MeV, but the binding appeared at 1288 MeV. Imposing the binding at 1282 MeV, as in the PDG [3.14], leads to this small change in the coupling. We can take this difference in the couplings as a measure of uncertainties in this magnitude. This will affect the rate for $K^*\bar{K}$ production ($K\pi\bar{K}$ in our approach) of Fig. 3.10, related to the diagram of Fig. 3.8. This means we have a 10% difference between the results with these couplings, or the centroid $\pm 5\%$. We should note that this process is related to the tree-level amplitude of Fig. 3.10 and, thus, it is not tied to the cutoff used, which appears only in the loops.

Similarly, we can estimate the uncertainty in the ratio of Eq. (3.44). Let us recall that here the coupling of $f_1(1285)$ to $K^*\bar{K}$ does not enter, because we took the coupling of $f_1(1420)$ to $K^*\bar{K}$ from the width of that state, Eq. (3.43). Hence, the uncertainties here come from the cutoff used in the loop of Fig. 3.11, replacing the $f_1(1285)$ by $f_1(1420)$. The cutoff affects both the loop function and the $K\bar{K} \rightarrow \pi^0\eta$ amplitude (via $a_0(980)$), since as argued before, one has the same cutoff in the loop of Fig. 3.11 and in the loops of the t -matrix that generates the $a_0(980)$. In order to estimate the uncertainties in the cutoff we have taken a recent experiment where the rate of $a_0(980)$ production is large and the signal is very clean [3.54], and a theoretical calculation that agrees well with the data is available [3.55, 3.56]. We have looked at the data in Fig. 6 of Ref. [3.55], which is calculated with $q_{\max} = 600$ MeV, 580 MeV and 630 MeV. We have redone the calculations and found that by using 550 MeV and 650 MeV, the differences with experiment become already obvious. Then, we redo our calculation of the loop of Fig. 3.11 and then the ratio of Eq. (3.44) becomes $(17.0 \pm 1.5)\%$.

3.2.5 The singularity of the triangle diagram

The shoulder for the $f_1(1285)$ decay to $\pi\pi^0\eta$ around 1400 MeV has its origin in the singularity that the triangle diagram of Fig. 3.11 develops at 1420 MeV. As discussed in section 3.1, triangular singularities stem from triangle diagrams when the intermediate particles are all placed on-shell and the momenta are parallel ($-\vec{q}$ and \vec{k} of Fig. 3.11 go in the same direction). There is also a further constraint which is that the mechanism can lead to a classical process with $R \rightarrow K^*\bar{K}$; $K^* \rightarrow K\pi$; $K\bar{K} \rightarrow a_0(980)$, which is stated by the Coleman-Norton theorem [3.8]. A practical way to see where the singularity appears is to use Eq. (3.20) from section 3.1.

In the present case we can see the origin of the singularities by looking at the expression of Eq. (3.39). The two factors in the denominator that develop singularities are

$$D_1 = P^0 - \omega^*(\vec{q}) - \omega(\vec{q}) + i\epsilon \quad (3.45)$$

and

$$D_2 = P^0 - k^0 - \omega(\vec{q}) - \omega'(\vec{q} + \vec{k}) + i\epsilon. \quad (3.46)$$

When they are zero with \vec{q} and \vec{k} in opposite directions, one gets a pole when $D_1 = 0$ at $q_{\text{on}} + i\epsilon$ and two poles when $D_2 = 0$, at $q_{a+} + i\epsilon$ and $q_{a-} - i\epsilon$. Then, when $q_{\text{on}} = q_{a-}$ two poles appear in opposite sides of the real axis at the same energy and the integral path cannot be deformed to avoid the singularity, which thus shows up in the result of the integral. If the width of the K^* is considered, then $q_{\text{on}} + i\epsilon \rightarrow q_{\text{on}} + i\Gamma_{K^*}/2$ and the singularity turns into a peak. If we apply $q_{\text{on}} = q_{a-}$, as in Eq. (3.20) from section 3.1, we find the singularity when the incoming energy in the triangle diagram is 1420 MeV. To show it, we plot in Fig. 3.13 the result for $|\tilde{t}_T|^2$ of Eq. (3.39). In Fig. 3.13 we see how an original singularity becomes a broad peak when $\Gamma_{K^*} \neq 0$. This softened singularity, together with the propagator of the

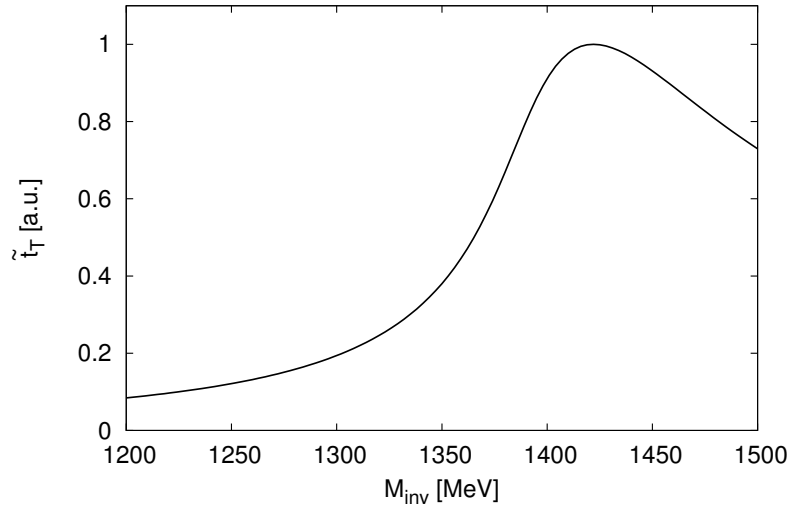


Figure 3.13: Results for the singular diagram, $|\tilde{t}_T|^2$, of Eq. (3.39).

$f_1(1285)$, is what gives rise to the broad shoulder of the $f_1(1285) \rightarrow \pi a_0(980)$ in Fig. 3.12.

3.2.6 Detailed evaluation with the $I = 0$ and $C = +$ parity of the $f_1(1285)$

So far we did not pay attention to the isospin and C -parity structure of the $f_1(1285)$ and $f_1(1420)$, but the shapes and relative weights of the cross sections are well evaluated with the previous formalism. The wave function for the $f_1(1285)$ is given by

$$|f_1(1285)\rangle = -\frac{1}{2}(K^{*+}K^- + K^{*0}\bar{K}^0 - K^{*-}K^+ - \bar{K}^{*0}K^0) \quad (3.47)$$

and then everything is identical to what has been done so far, except that one has four diagrams. The evaluation of the widths for $f_1(1285) \rightarrow \pi a_0(980)$ and $f_1(1285) \rightarrow \pi K \bar{K}$ at the peak of the $f_1(1285)$ are done in Refs. [3.20] and [3.19], respectively. All that must be done is to perform the same evaluation as a function of M_{inv} (for the $f_1(1285)$ at higher energies), and implement the $f_1(1285)$ propagator in Eq. (3.27). The results are shown in Figs. 3.14, 3.15 and 3.16, which should be compared with Figs. 3.12, 3.9 and 3.10, respectively. As we can see, not only the shapes but the absolute numbers are about the same as with the simplified wave function. Moreover, in Fig. 3.15 a peak develops for the $f_1(1285) \rightarrow \pi K \bar{K}$ decay around 1400 MeV (see Fig. 3.16 for more details). The peak and width of the distribution around this energy are in fair agreement with the mass of 1420 MeV and width of about 55 MeV quoted in the PDG [3.14].

We have taken advantage to make a more refined evaluation. Indeed, in Eq. (3.27) we have $\Gamma_R \equiv \Gamma_{f_1(1285)}$ in the denominator. Since we are evaluating the partial decay width into $K\pi\bar{K}$ and $\pi a_0(980)$ we write

$$\begin{aligned} \Gamma_R = & \Gamma_{f_1(1285)} - \Gamma_{f_1(1285) \rightarrow K\pi\bar{K}}|_{\text{on}} - \Gamma_{f_1(1285) \rightarrow \pi a_0(980)}|_{\text{on}} \\ & + \Gamma_{f_1(1285) \rightarrow K\pi\bar{K}}(M_{\text{inv}}) + \Gamma_{f_1(1285) \rightarrow \pi a_0(980)}(M_{\text{inv}}), \end{aligned} \quad (3.48)$$

which guarantees that on shell, $M_{\text{inv}} = 1285$ MeV, $\Gamma_R = 24.1$ MeV. The values that we obtain are $\Gamma_{f_1(1285) \rightarrow K\pi\bar{K}}|_{\text{on}}/\Gamma_{f_1(1285)} = 0.095$, $\Gamma_{f_1(1285) \rightarrow \pi a_0(980)}|_{\text{on}}/\Gamma_{f_1(1285)} = 0.275$.

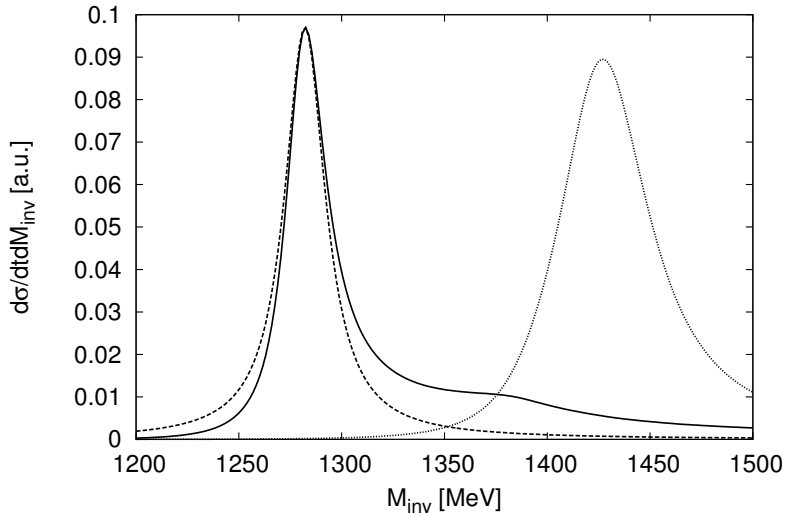


Figure 3.14: The differential cross section for the decay $f_1(1285) \rightarrow \pi a_0(980)$ as in Fig. 3.12, here with the full wave function of Eq. (3.47).

We also make a more detailed comparison with the results of Ref. [3.2]. In Fig. 3.17 we show our results folded with a resolution of 20 MeV to facilitate comparison with the experimental numbers. We normalize the results approximately to the peak of the experimental distribution. We can see that the agreement with experiment is fair.

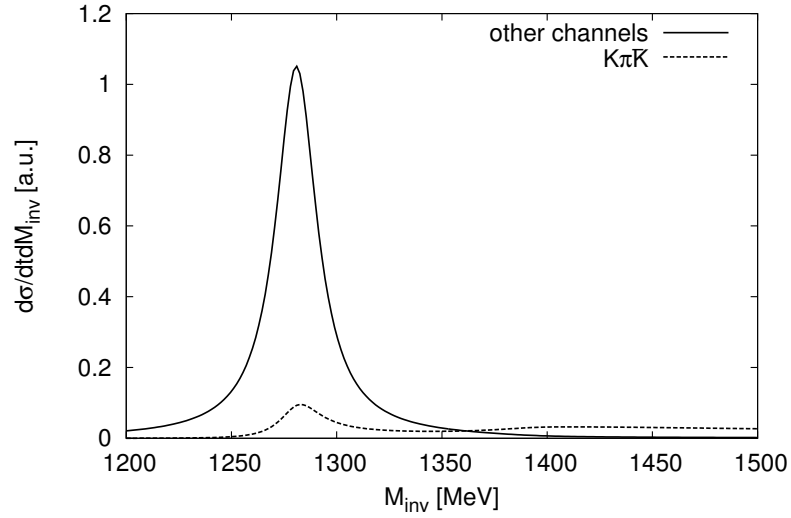


Figure 3.15: The differential cross section for the decay $f_1(1285) \rightarrow K\pi\bar{K}$ as in Fig. 3.9, here with the full wave function of Eq. (3.47).

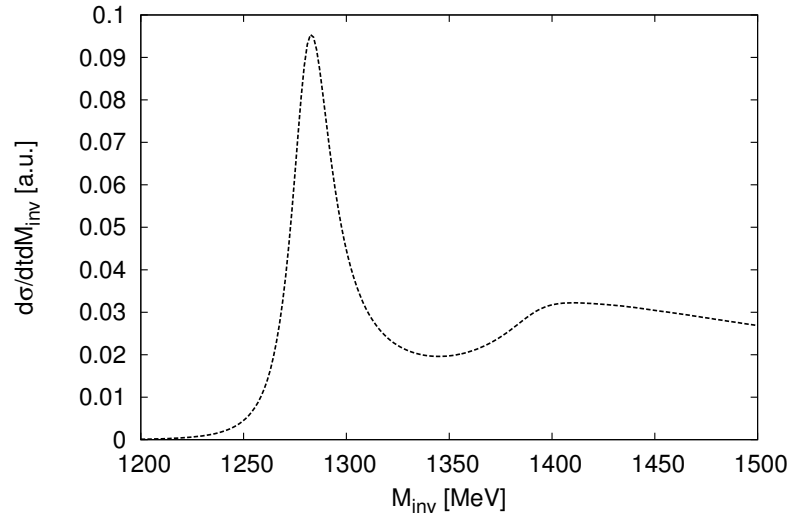


Figure 3.16: Same as Fig. 3.10, here with the complete wave function of Eq. (3.47).

3.2.7 Conclusions

We have carried out a study of the production of the $f_1(1285)$ and decay into $\pi a_0(980)$ and $K^*\bar{K}$ modes. We have studied the cross sections as functions of the $f_1(1285)$ mass, M_{inv} , up to 1500 MeV and we have observed two relevant features:

- 1) The $K^*\bar{K}$ mode (allowing the $K^* \rightarrow K\pi$ decay) has two peaks as a function of M_{inv} , one at the $f_1(1285)$ mass and the other one at about 1420 MeV, this latter one with a width of about 60 MeV.
- 2) The $\pi a_0(980)$ mode has a peak at 1285 MeV and a broad shoulder around 1400 MeV, which comes from a triangle singularity involving $K^*K\bar{K}$ as intermediate

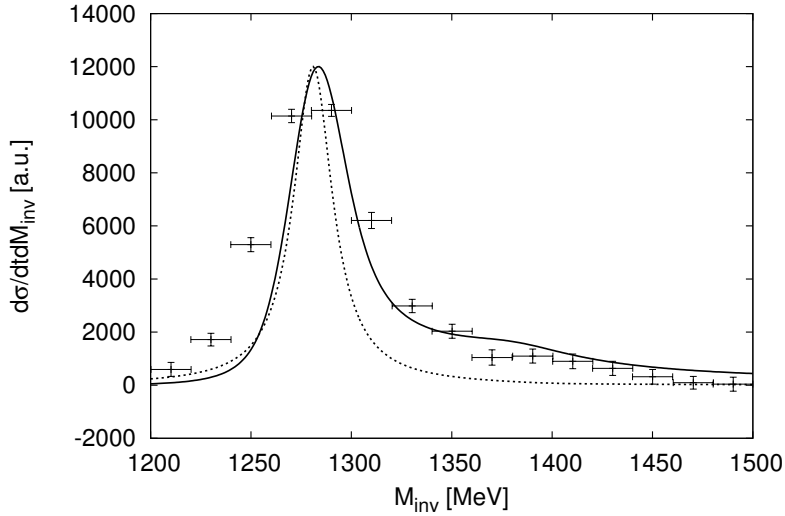


Figure 3.17: Comparison of the results of Fig. 3.14, convoluted with a resolution of 20 MeV, with the experimental results of [3.2].

states, and tied to the nature of the $f_1(1285)$ as a $K^*\bar{K}$ molecule, a sufficient although not necessary condition, since what matters is that the $f_1(1285)$ couples to $K^*\bar{K}$ and this is known experimentally from the $K\pi\bar{K}$ decay mode. The combination of the tail of the $f_1(1285)$ with the increased phase space for the $K^*\bar{K}$ production is the reason for this second peak.

The two features described above are the experimental facts in which the $f_1(1420)$ was accepted as a resonance, but we have shown that they are consequence of the decay modes of the $f_1(1285)$ and one does not have to introduce any new resonance to account for these facts. The absence of the $\pi a_0(980)$ decay mode of the $f_1(1420)$ in all but one experiment [3.2], is a fact that we have exploited here, because if it were a resonance which decays mostly into $K^*\bar{K}$, it would unavoidably have a width into $\pi a_0(980)$ of the order of $(17.0 \pm 1.5)\%$, which has not been observed. The 5% $\pi a_0(980)$ decay mode attributed to the $f_1(1420)$ in Ref. [3.2] was a guess based on the lack of any other interpretation of the shoulder found for this mode around 1400 MeV in the study of the decay of the $f_1(1285)$. We found a natural explanation for this broad peak which then does not require the existence of the $f_1(1420)$.

Altogether, our study leads us to the unavoidable conclusion that the $f_1(1420)$ is not a resonance but simply the manifestation of the $K^*\bar{K}$ and $\pi a_0(980)$ decay modes of the $f_1(1285)$ around 1420 MeV.

3.3 Role of a triangle singularity in the $\pi N(1535)$ contribution to $\gamma p \rightarrow p\pi^0\eta$

In this section we present the work of Ref. [3.3] where we have studied the $\gamma p \rightarrow p\pi^0\eta$ reaction paying attention to the two main mechanisms at low energies, the $\gamma p \rightarrow \Delta(1700) \rightarrow \eta\Delta(1232)$ and the $\gamma p \rightarrow \Delta(1700) \rightarrow \pi N(1535)$. Both of them are driven by the photoexcitation of the $\Delta(1700)$ and the second one involves a mechanism that leads to a triangle singularity. We are able to evaluate quantitatively the cross section for this process and show that it agrees with the experimental determination from Ref. [3.4]. Yet, there are some differences with the standard partial wave analysis which does not include explicitly the triangle singularity. The exercise also shows the convenience to explore possible triangle singularities in other reactions and how a standard partial analysis can be extended to accommodate them.

3.3.1 Introduction

The $\gamma p \rightarrow p\pi^0\eta$ reaction was measured first in Ref. [3.57] up to energies of the photon of $E_\gamma = 1150$ MeV. Early theoretical determinations of the threshold behaviour, with large uncertainties were done in Ref. [3.58]. Some accurate predictions in the range up to $E_\gamma = 1700$ MeV, were done in Ref. [3.59] prior to the measurements done at GRAAL [3.60], CB-ELSA [3.61, 3.62] and MAMI [3.63]. The basic idea of Ref. [3.59] was that the process is dominated by the photoproduction of the $\Delta(1700)(3/2^-)$, which later decays into $\eta\Delta(1232)$ followed by $\Delta(1232) \rightarrow \pi^0 p$. The dominance of this resonance at low energies was also established experimentally [3.60, 3.62, 3.63]. In Ref. [3.63] it is quoted “it is possible to get a reasonable agreement with the data by taking into account only the $D_{33}(1700)$ resonance”. Further support for this idea comes from the correlation of many reactions based upon the dominance of the $\Delta(1700)$. Indeed, in Ref. [3.64] the $\pi^- p \rightarrow K^0\pi^0\Lambda$, $\pi^+ p \rightarrow K^+\pi^+\Lambda$, $K^+\bar{K}^0 p$, $K^+\pi^+\Sigma^0$, $K^+\pi^0\Sigma^+$, $\eta\pi^+ p$ reactions were described successfully based upon the mechanism of $\Delta(1700)$ excitation with subsequent decays into $K\Sigma^*(1385)$ or $\eta\Delta(1232)$. The $p\pi^0$, $p\eta$ and $\eta\pi^0$ mass distributions measured in Ref. [3.60] also give support to this idea, which is further reinforced by the agreement shown in Ref. [3.65] for the polarization observables I^S and I^C , I^θ measured in Refs. [3.66, 3.67].

A high statistics measurement of different observables is done in Ref. [3.4]. In this work a separation of the cross section is made in three main channels, $\eta\Delta$, $\pi N(1535)$ and $a_0(980)p$, and up to E_γ around 1500 MeV the first two channels saturate the cross section. The $\eta\Delta$ channel is dominant, but the $\pi N(1535)$ is also sizable in this region. The experimental results are shown in Fig. 3.18 (the model curves will be explained later). The purpose of the present work is to find a theoretical description of these two channels.

The $\eta\Delta$ channel finds a natural interpretation in the dominance of the $\Delta(1700)$ excitation and provides support for the dynamical generation of this resonance from the interaction of the octet of pseudoscalar mesons with the decuplet of baryons

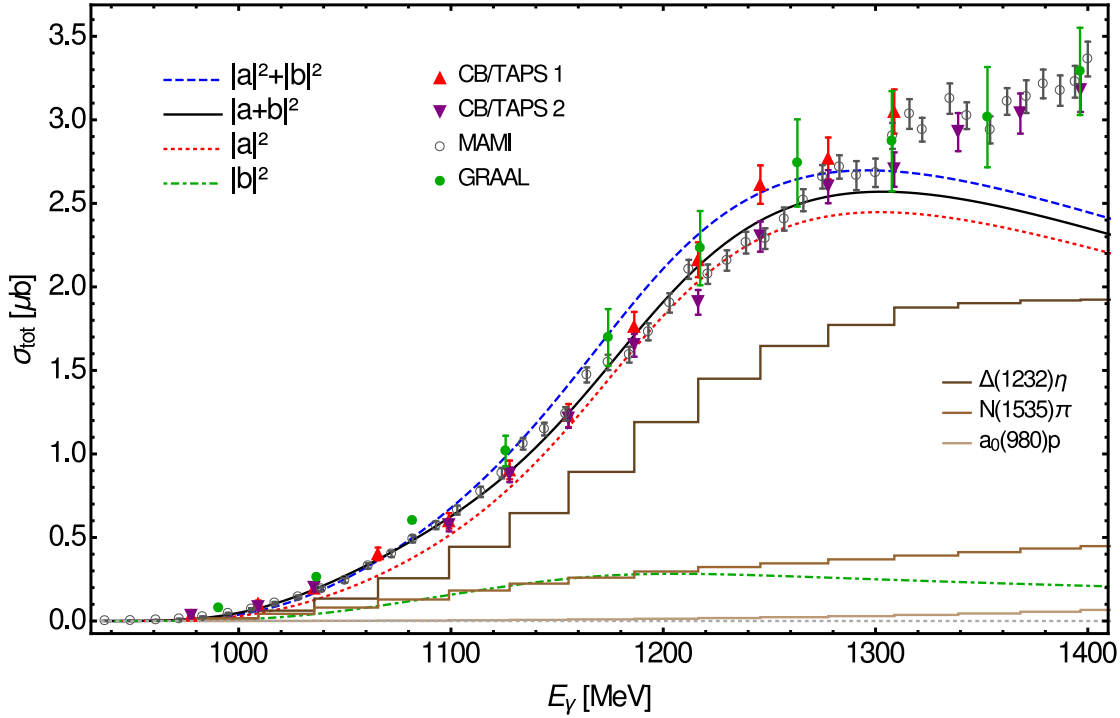


Figure 3.18: Cross section for $\gamma p \rightarrow \pi^0\eta p$. $|a|^2$ stands for the mechanism of Fig. 3.19. $|b|^2$ stands for the triangle mechanism of Fig. 3.20. $|a + b|^2$ stands for the coherent sum of the two former mechanisms and $|a|^2 + |b|^2$ stands for the incoherent sum.

[3.68, 3.69]. Indeed, as shown in Ref. [3.69], the $\Delta(1700)$ is generated from the coupled channels $\Delta\pi$, Σ^*K and $\Delta\eta$, and the scattering matrix leads to a sizable coupling of that resonance to $\Delta\eta$. Hence, the main channel assumed in Ref. [3.59] is photoproduction of the $\Delta(1700)$ followed by the decay of the $\Delta(1700)$ into $\Delta\eta$ and posterior $\Delta \rightarrow \pi N$ decay. In this mechanism there is no direct room for the $\pi N(1535)$ channel, although some terms, with final state interaction of $\pi\eta$, partly incorporated this channel in Ref. [3.59]. In the present work we are going to show that the relatively large weight of the $\pi N(1535)$ channel is tied to a triangular singularity for the process $\gamma p \rightarrow \Delta(1700) \rightarrow \eta\Delta^+$ followed by $\Delta^+ \rightarrow \pi^0 p$ and posterior fusion of the $p\eta$ to produce the $N(1535)$.

Other examples of triangle singularities can be seen in Refs. [3.11, 3.70–3.73]. More closely related to the present problem is the case of the $\eta(1405) \rightarrow \pi a_0(980)$, $\pi f_0(980)$ [3.50–3.52], where in particular, the latter channel violating isospin is enhanced due to a triangle singularity. Another recent example can be seen in the “ $a_1(1420)$ ” peak, originally advocated as a new resonance by the COMPASS collaboration, which hinted in Ref. [3.12] and shown explicitly in Refs. [3.44, 3.45], comes naturally from the $\pi f_0(980)$ decay of the $a_1(1260)$, via a triangular mechanism that develops a singularity when the $a_1(1260)$ decays into K^*K , the $K^* \rightarrow \pi K$ and the $K\bar{K}$ merge to produce the $f_0(980)$. A case similar to this is the recent reanalysis of the $f_1(1420)$, which is shown in Ref. [3.1] and in the former section 3.2 to correspond to two mechanisms: the decay of the $f_1(1285)$ into $\pi a_0(980)$ via a triangular singularity, $f_1(1285) \rightarrow K^*\bar{K}$, $K^* \rightarrow \pi K$, $K\bar{K} \rightarrow a_0(980)$; and decay into $K^*\bar{K}$,

that shows as a pronounced peak above the $K^*\bar{K}$ threshold. Adding to this list of reinterpretation of some accepted resonances is the case of the $f_2(1810)$, also explained in Ref. [3.74] as the production of the $f_2(1650)$ followed by the decay into $K^*\bar{K}^*$, $K^* \rightarrow \pi K$, $K\bar{K}^* \rightarrow a_1(1260)$.

In some cases the singularity helps to explain enhancements in cross sections not attributed to any resonance. This is the case of the $\gamma p \rightarrow K\Lambda(1405)$ reaction, where a triangular singularity stemming from the production of a N^* resonance at 1930 MeV, with $N^* \rightarrow K^*\Sigma$, $K^* \rightarrow K\pi$ and $\pi\Sigma$ merging to give the $\Lambda(1405)$, produces a peak in the cross section around $\sqrt{s} = 2120$ MeV [3.75], that solves a problem in the interpretation of the data [3.76].

Recent interest in triangle singularities was stirred by the suggestion in Refs. [3.10,3.13] that the peak seen in the LHCb collaboration attributed to a pentaquark in Refs. [3.77, 3.78] should be due to a triangle singularity stemming from $A \rightarrow \Lambda(1890)\chi_{c1}$, $\Lambda(1890) \rightarrow K^-p$, $\chi_{c1}p \rightarrow J/\psi p$. However, the $\chi_{c1}p$ system is at threshold for the energy of the peak at 4450 MeV, and if this peak has quantum numbers $3/2^-$ or $5/2^+$ as suggested by the experiment, the $\chi_{c1}p$ system must be in P - or D -wave, which at threshold kills the $\chi_{c1}p \rightarrow J/\psi p$ amplitude. This observation was made in Ref. [3.9] where it was concluded that this mechanism could not be the explanation of the experimental peak if these quantum numbers are confirmed.

In the present work we will show another case of a triangle singularity via $\gamma p \rightarrow \Delta(1700) \rightarrow \eta\Delta \rightarrow \eta\pi^0 p$, with ηp merging into the $N(1535)$, which gives rise to a $\pi N(1535)$ production cross section similar in strength and shape to the experimental one. We will also show that the energy dependence of this cross section is quite different to a standard one proceeding thorough $\gamma p \rightarrow \pi N(1535)$ directly, and it is tied to the structure of the triangle singularity. As we shall see, the $N(1535)$ plays a special role among other possible N^* states, which do not lead to a triangle singularity, or couple weakly to the ηN state.

3.3.2 Formalism

The tree level $\gamma p \rightarrow \Delta(1700) \rightarrow \Delta\eta$

In Fig. 3.19 we depict the mechanism for direct production of the $\Delta(1700)$ followed by the decay into $\Delta(1232)\eta$ and $\Delta(1232) \rightarrow \pi^0 p$.

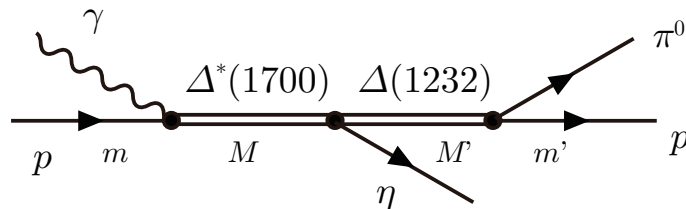


Figure 3.19: Mechanism for $\gamma p \rightarrow \Delta(1700) \rightarrow \eta\Delta(1232) \rightarrow \eta\pi^0 p$ driven by $\Delta(1700)(3/2^-)$ photoproduction.

The first ingredient needed in the evaluation is the $\Delta(1700)\gamma p$ coupling. This proceeds in S -wave and can be taken into account with the amplitude

$$-it_{\Delta^*,\gamma p} = -ig_{\Delta^*,\gamma p} \vec{S} \cdot \vec{\epsilon} \quad (3.49)$$

where $\vec{\epsilon}$ is the polarization of the photon in the Coulomb gauge representation ($\epsilon^0 = 0$) and \vec{S} the spin transition operator from $3/2$ to $1/2$. The width of Δ^* into this channel is given by

$$\Gamma_{\Delta^*,\gamma p} = \frac{1}{2\pi} \frac{M_N}{M_{\Delta^*}} p_\gamma \overline{\sum} \sum |t_{\Delta^*,\gamma p}|^2, \quad (3.50)$$

where

$$\begin{aligned} \overline{\sum} \sum |t_{\Delta^*,\gamma p}|^2 &= |g_{\Delta^*,\gamma p}|^2 \frac{1}{4} \sum_M \sum_m \sum_{\gamma \text{ pol}} \langle m | \vec{S} \cdot \vec{\epsilon} | M \rangle \langle M | \vec{S}^\dagger \cdot \vec{\epsilon} | m \rangle \\ &= |g_{\Delta^*,\gamma p}|^2 \frac{1}{4} \sum_m \sum_{\gamma \text{ pol}} \left\langle m \left| \frac{2}{3} \delta_{ij} - \frac{i}{3} \epsilon_{ijk} \sigma_k \right| m \right\rangle \epsilon_i \epsilon_j \\ &= \frac{1}{3} |g_{\Delta^*,\gamma p}|^2 \sum_{\gamma \text{ pol}} \vec{\epsilon} \cdot \vec{\epsilon} = \frac{2}{3} |g_{\Delta^*,\gamma p}|^2. \end{aligned} \quad (3.51)$$

Experimentally, the branching fraction is $0.22\text{--}0.60\%$ from a Breit-Wigner width $\Gamma_{\Delta^*} = 200 - 400$ MeV and mass $M_{\Delta^*} = 1670 - 1750$ MeV [3.14]. We shall play with the uncertainties for a more accurate fit to the $\gamma p \rightarrow p\pi^0\eta$ data. By taking the central value of the branching fraction, 0.41% , $\Gamma_{\Delta^*} = 300$ MeV and $M_{\Delta^*} = 1700$ MeV, we obtain from Eq. (3.50)

$$g_{\Delta^*,\gamma p} = 0.188. \quad (3.52)$$

The PDG has also data for the helicity amplitudes. It is easy to construct the helicity amplitudes from the coupling of Eq. (3.49), following the steps of Ref. [3.79], and show that both, helicity $1/2$ and $3/2$, are compatible with the structure of Eq. (3.49) and the coupling of Eq. (3.52). On the other hand, the coupling of Δ^* to the channel $\eta\Delta$ is one of the outputs of the chiral unitary approach of Ref. [3.69] where we find

$$g_{\Delta^*,\eta\Delta} = 1.7 - i 1.4, \quad (3.53)$$

and the amplitude $-it_{\Delta^*,\eta\Delta}$ is just $-ig_{\Delta^*,\eta\Delta}$ since the process proceeds via S -wave and has no spin dependence.

The $\Delta(1232)$ decaying to $\pi^0 N$ has a standard coupling as

$$-it_{\Delta,\pi N} = \frac{f_{\pi N\Delta}}{m_\pi} \vec{S} \cdot \vec{k} \mathcal{C}(1, 1/2, 3/2; i_\pi, i_N, i_\Delta), \quad (3.54)$$

with $\mathcal{C}(1, 1/2, 3/2; i_\pi, i_N, i_\Delta)$ the Clebsch-Gordan coefficient, $\sqrt{2/3}$ for $\pi^0 p$, and \vec{k} the pion momentum. From the Δ width, we find

$$\frac{f_{\pi N\Delta}^2}{4\pi} = 0.36; \quad f_{\pi N\Delta} = 2.13. \quad (3.55)$$

The amplitude of Fig. 3.19 can now be constructed with the former ingredients and we have

$$\begin{aligned}
-it_{\gamma p, \eta \pi^0 p} &= \sum_M \sum_{M'} \frac{f_{\pi N \Delta}}{m_\pi} \langle m' | \vec{S} \cdot \vec{k} | M' \rangle \sqrt{\frac{2}{3}} \frac{i}{M_{\text{inv}}(\pi^0 p) - M_\Delta + i\Gamma_\Delta/2} \\
&\quad \times (-i) g_{\Delta^*, \eta \Delta} \delta_{MM'} \frac{i}{\sqrt{s} - M_{\Delta^*} + i\Gamma_{\Delta^*}/2} (-i) g_{\Delta^*, \gamma p} \langle M | \vec{S}^\dagger \cdot \vec{\epsilon} | m \rangle \\
&= g_{\Delta^*, \gamma p} g_{\Delta^*, \eta \Delta} \frac{f_{\pi N \Delta}}{m_\pi} \sqrt{\frac{2}{3}} \frac{1}{M_{\text{inv}}(\pi^0 p) - M_\Delta + i\Gamma_\Delta/2} \\
&\quad \times \frac{1}{\sqrt{s} - M_{\Delta^*} + i\Gamma_{\Delta^*}/2} \sum_M \langle m' | \vec{S} \cdot \vec{k} | M \rangle \langle M | \vec{S}^\dagger \cdot \vec{\epsilon} | m \rangle, \quad (3.56)
\end{aligned}$$

where $M_{\text{inv}}(\pi^0 p)$ is the invariant mass of the $\pi^0 p$ system and s the ordinary Mandelstam variable for the center-of-mass (CM) energy of the γp initial system.

The triangle singularity in $\gamma p \rightarrow \pi^0 N(1535)$

The mechanism that we shall study is depicted in Fig. 3.20. The Δ^* decays into $\Delta \eta$, the Δ decays into $\pi^0 p$ and the ηp merge to produce the $N(1535)$ that subsequently decays into ηp . It is easy to see, by taking Eq. (3.20) from section 3.1, that the diagram of Fig. 3.20 develops a singularity around $\sqrt{s} = 1782$ MeV, which corresponds to E_γ in the laboratory frame at 1220 MeV. One can see in Ref. [3.4] that there is some kind of broad structure around $E_\gamma = 1200$ MeV for the $\pi N(1535)$ part of the cross section in the analysis done there.

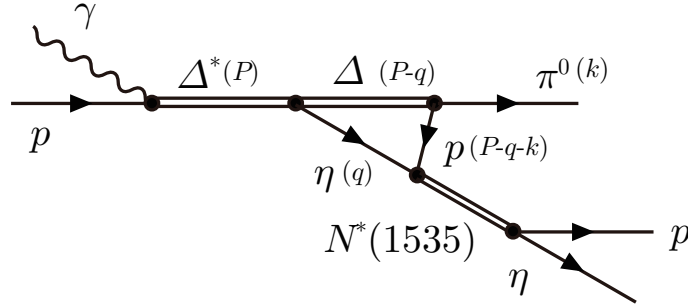


Figure 3.20: Triangle diagram leading to the production of $\pi N(1535)$ (ηp). In parenthesis, the momenta of the particles.

The amplitude for the mechanism of Fig. 3.20 is given by

$$\begin{aligned}
-it &= -it_{\eta p, \eta p} \frac{f_{\pi N \Delta}}{m_\pi} \sqrt{\frac{2}{3}} \vec{S} \cdot \vec{k} (-i) g_{\Delta^*, \eta \Delta} (-i) g_{\Delta^*, \gamma p} \vec{S}^\dagger \cdot \vec{\epsilon} \frac{i}{\sqrt{s} - M_{\Delta^*} + i\Gamma_{\Delta^*}/2} \\
&\quad \times \int \frac{d^4 q}{(2\pi)^4} 2M_\Delta \frac{i}{(P-q)^2 - M_\Delta^2 + i\epsilon} 2M_N \frac{i}{(P-q-k)^2 - M_N^2 + i\epsilon} \frac{i}{q^2 - m_\eta^2 + i\epsilon} \\
&= t_{\eta p, \eta p} g_{\Delta^*, \eta \Delta} g_{\Delta^*, \gamma p} \frac{f_{\pi N \Delta}}{m_\pi} \sqrt{\frac{2}{3}} \vec{S} \cdot \vec{k} \vec{S}^\dagger \cdot \vec{\epsilon} 2M_N 2M_\Delta \frac{1}{\sqrt{s} - M_{\Delta^*} + i\Gamma_{\Delta^*}/2} t_T, \quad (3.57)
\end{aligned}$$

which defines t_T , the triangle amplitude, as $i \int d^4q$ of the product of the three propagators, Δ , η , p . The Mandl-Shaw normalization for fermion fields [3.47], responsible for the factors $2M_N$, $2M_\Delta$ in Eq. (3.57), is used. The q^0 integration in Eq. (3.57) is done analytically and then the t_T amplitude is written as we saw in section 3.1,

$$t_T = \int \frac{d^3q}{(2\pi)^3} \frac{1}{8\omega(q)\omega'(q)\omega^*(q)} \frac{1}{k^0 - \omega'(q) - \omega^*(q) + i\epsilon} \frac{1}{P^0 - \omega^*(q) - \omega(q) + i\epsilon} \frac{1}{2P^0\omega(q) + 2k^0\omega'(q) - 2[\omega(q) + \omega'(q)][\omega(q) + \omega'(q) + \omega^*(q)]} \frac{1}{(P^0 - \omega(q) - \omega'(q) - k^0 + i\epsilon)(P^0 + \omega(q) + \omega'(q) - k^0 - i\epsilon)}, \quad (3.58)$$

where $\omega(q) = \sqrt{m_\eta^2 + \vec{q}^2}$, $\omega'(q) = \sqrt{M_N^2 + (\vec{q} + \vec{k})^2}$, $\omega^*(q) = \sqrt{M_\Delta^2 + \vec{q}^2}$.

To account for the width of the Δ in the loop function we replace $\omega^*(q) \rightarrow \omega^*(q) - i\Gamma_\Delta/2$, where we use an energy-dependent width

$$\Gamma_\Delta(M_{\text{inv}}(q)) = \frac{M_\Delta}{M_{\text{inv}}(q)} \frac{p_\pi^3(M_{\text{inv}}(q))}{p_\pi^3|_{\text{on}}} \Gamma_\Delta|_{\text{on}}, \quad (3.59)$$

with $M_{\text{inv}}(q)$ the $\Delta(1232)$ invariant mass inside the triangular loop, calculated from the second denominator of Eq. (3.58)

$$M_{\text{inv}}(q) = \sqrt{(P^0)^2 + m_\eta^2 - 2P^0\omega(q)}, \quad (3.60)$$

and $\Gamma_\Delta|_{\text{on}} = 117$ MeV, while $p_\pi(M_{\text{inv}}(q))$ is the pion momentum in the $\Delta(1232)$ rest frame

$$p_\pi(M_{\text{inv}}(q)) = \frac{\lambda^{1/2}(M_{\text{inv}}(q)^2, M_N^2, m_\pi^2)}{2M_{\text{inv}}(q)}, \quad (3.61)$$

$$p_\pi|_{\text{on}} = p_\pi(M_{\text{inv}}(q) = M_\Delta), \quad (3.62)$$

where λ is the Källén function, and we set Γ_Δ to zero if $M_{\text{inv}}(q) < M_N + m_\pi$. We have also used the analytical extrapolation of Eq. (3.59) below threshold, but since then the Δ is so far off shell it has a minor relevance in the triangle singularity with changes at the level of less than 2%.

The $\eta p \rightarrow \eta p$ amplitude $t_{\eta p, \eta p}$ is driven by the $N(1535)$, which also shows up as a dynamically generated resonance in Ref. [3.80]. The integral in Eq. (3.58) is convergent. Yet, one must take into account that the chiral unitary approach of Ref. [3.69] can be formally obtained using a Quantum Mechanical formulation with a potential of the type $V(\vec{q}, \vec{q}') = V\theta(q_{\text{max}} - |\vec{q}|)\theta(q_{\text{max}} - |\vec{q}'|)$ [3.81] and this leads to a T -matrix where the two θ functions are also factorized, leading to a q_{max} in the d^3q integration of Eq. (3.58). A value of q_{max} suited for the $\Delta^* \rightarrow \Delta\eta$ as well as for the $t_{\eta p, \eta p}$ that we take from the work of Ref. [3.80] done along similar lines, is $q_{\text{max}} = 800$ MeV in the $N(1535)$ rest frame, that we shall use in our study. We can see that the amplitude of the triangle diagram, Eq. (3.57) and the tree level $\gamma p \rightarrow \Delta^* \rightarrow \Delta\eta$ of Eq. (3.56) have exactly the same spin structure $\vec{S} \cdot \vec{k} \vec{S}^\dagger \cdot \vec{\epsilon}$, and we expect some kind of interference, although the amplitudes are complex and one has to see explicitly how the interference occurs.

The cross section for $\gamma p \rightarrow \eta \pi^0 p$ is given by the standard $a + b \rightarrow 1 + 2 + 3$ formalism, as

$$\begin{aligned} \sigma &= \frac{(2M_N)^2}{4p_\gamma \sqrt{s}} \int \frac{d^3 p_1}{(2\pi)^3} \frac{1}{2E_1} \frac{1}{16\pi^2} \\ &\times \int d\tilde{\Omega}_2 \tilde{p}_2 \frac{1}{M_{\text{inv}}(23)} \overline{\sum \sum} |T|^2, \end{aligned} \quad (3.63)$$

where \tilde{p}_2 is the momentum of particle 2 in the rest frame of 2 + 3 and $\tilde{\Omega}_2$ its solid angle in that frame. Proceeding like in Eq. (3.51), summing over transverse photons

$$\sum_{\gamma \text{ pol}} \epsilon_i \epsilon_j = \delta_{ij} - \frac{p_{\gamma i} p_{\gamma j}}{\vec{p}_\gamma^2}, \quad (3.64)$$

we find that

$$\overline{\sum \sum} |\vec{S} \cdot \vec{k} \vec{S}^\dagger \cdot \vec{\epsilon}|^2 \equiv \frac{1}{2} \left\{ \frac{5}{9} \vec{k}^2 - \frac{1}{3} \vec{k}^2 \cos^2 \theta_1 \right\} \quad (3.65)$$

where θ_1 is the angle between the photon and the π^0 . The variables \tilde{p}_2 , \tilde{p}_3 , defined in the 2 + 3 rest frame, are conveniently boosted to the γp rest frame in order to evaluate the invariant masses entering the evaluation of T . Summing the tree level amplitude and the triangle diagram, T in Eq. (3.63) is given by

$$-iT = (a + b) \vec{S} \cdot \vec{k} \vec{S}^\dagger \cdot \vec{\epsilon}, \quad (3.66)$$

where

$$a = C \frac{1}{M_{\text{inv}}(12) - M_\Delta + i\Gamma_\Delta/2} \quad (3.67)$$

$$b = C 2M_N 2M_\Delta t_T t_{\eta p, \eta p} \quad (3.68)$$

$$C = g_{\Delta^*, \eta \Delta} g_{\Delta^*, \gamma N} \frac{f_{\pi N \Delta}}{m_\pi} \sqrt{\frac{2}{3}} \frac{1}{\sqrt{s} - M_{\Delta^*} + i\Gamma_{\Delta^*}/2}. \quad (3.69)$$

Thus,

$$\overline{\sum \sum} |T|^2 = |a + b|^2 \frac{1}{2} \left\{ \frac{5}{9} \vec{k}^2 - \frac{1}{3} \vec{k}^2 \cos^2 \theta_1 \right\}. \quad (3.70)$$

In Eq. (3.67) we also employ the energy-dependent width of Eq. (3.59), but now as a function of the invariant mass $M_{\text{inv}}(12)$.

We shall also see the contribution of the $\Delta^* \rightarrow \eta \Delta$ alone, just taking $|a|^2$ in Eq. (3.70), and of $\pi N(1535)$, taking $|b|^2$ in Eq. (3.70), instead of $|a + b|^2$, which corresponds to the coherent sum of the two processes.

The singularity that comes out from t_T in Eq. (3.58) leads to a peculiar energy dependence of the cross section for $\pi N(1535)$ production. In order to show it, we also evaluate the $\gamma p \rightarrow \pi N(1535)$ cross section with a standard mechanism that does not involve the triangle singularity, and which we show in Fig. 3.21.

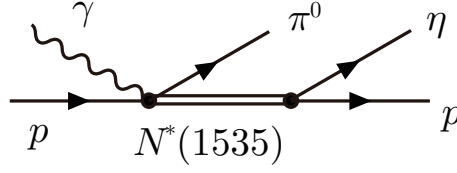


Figure 3.21: Standard mechanism for $\gamma p \rightarrow \pi N(1535)$ production.

The transition from angular momentum $1^- + 1/2^+ \rightarrow 0^- + 1/2^-$ requires P -wave, $L = 1$, to restore the parity. Two structures are possible,

$$\vec{\epsilon} \cdot \vec{k}, \quad (\vec{\sigma} \times \vec{k}) \cdot \vec{\epsilon}. \quad (3.71)$$

Both of them, after squaring and summing over polarizations, taking into account the transversality of the photons, Eq. (3.64), lead to a combination

$$\overline{\sum} \sum |t|^2 \propto c \vec{k}^2 + d \vec{k}^2 \cos^2 \theta_1 \sim (c + \frac{1}{3}d) \vec{k}^2 \quad (3.72)$$

where in the last step we have substituted $\cos^2 \theta_1$ by $1/3$ as it would come by integration over the phase space. Then, the cross section from this mechanism can be obtained from Eq. (3.63) substituting $|T|^2$ by a constant times $\vec{k}^2 |t_{\eta p, \eta p}|^2$

$$|T|^2 \rightarrow D \vec{k}^2 |t_{\eta p, \eta p}|^2. \quad (3.73)$$

At this point we would like to discuss the possibility of having some relevant contribution from other N^* states instead of the $N(1535)$. The $N(1440)$ does not have the ηp channel open for decay and does not develop a triangle singularity. In principle the $N(1520)(3/2^-)$, given the proximity in mass to the $N(1535)$ could also develop a triangle singularity with the same mechanism of Fig. 3.20. However, in Ref. [3.14] we see that the coupling of this resonance to ηp is very small, $BR(\eta p) < 1\%$, while for the $N(1535)$ this mode gives $BR(\eta p) \approx 32 - 52\%$. If we take the $N(1650)$, and other resonances of higher mass, we see that the condition $q_{\text{on}} - q_{a^-} = 0$ from Eq. (3.20) in section 3.1 is far from being fulfilled, and as the mass of the resonance increases $q_{\text{on}} - q_{a^-}$ is even larger, indicating that one never gets a triangle singularity for these resonances. The excitation of the $N(1535)$ has a privileged role as we see.

3.3.3 Results

In Fig. 3.22, we show the result for the amplitude t_T of Eq. (3.58). We can see that $Re(t_T)$ and $Im(t_T)$ have the Breit-Wigner shape like $-BW \equiv -(\sqrt{s} - m_R + i\Gamma_R/2)^{-1}$. However, the real part does not go through zero, so the shape resembles $D - BW(s)$, with D a constant real background. We can see in $|t_T|^2$ a clear peak around $\sqrt{s} = 1770$ MeV, as anticipated by the simple application of the rule of Eq. (3.20).

In Fig. 3.18 we show the results for the cross section. The $t_{\eta p, \eta p}$ amplitude is taken from Ref. [3.80] as a Breit-Wigner amplitude

$$t_{\eta p, \eta p} = \frac{g_{N^*, \eta p}^2}{M_{\text{inv}}(\eta p) - M_{N^*} + i\Gamma_{N^*}/2}, \quad (3.74)$$

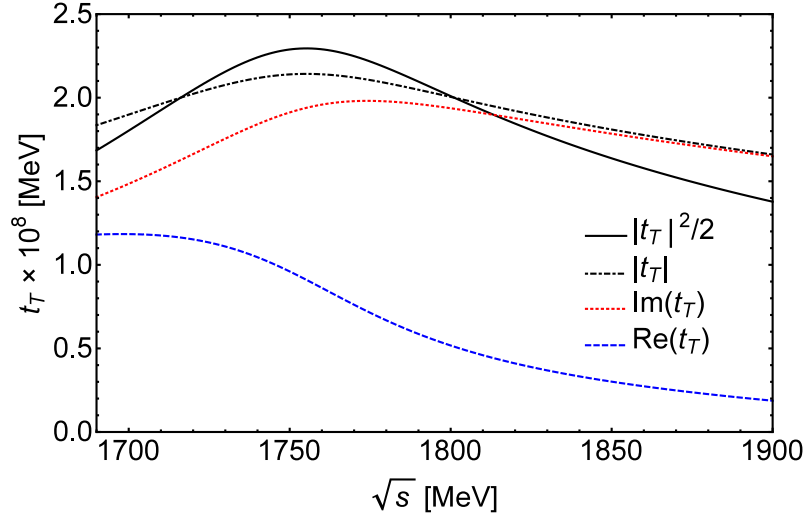


Figure 3.22: $|t_T|^2$, $Re(t_T)$, $Im(t_T)$ and $|t_T|$ as a function of the γp energy, \sqrt{s} . The mass of the ηp system is taken at the $N(1535)$ mass of 1543 MeV determined in [3.80].

and we take the values for M_{N^*} , Γ_{N^*} and $g_{N^*,\eta p}$ from that work, which provides a fair reproduction of the scattering data,

$$\begin{aligned} g_{N^*,\eta p} &= 1.77, \\ M_{N^*} &= 1543 \text{ MeV}, \\ \Gamma_{N^*} &= 92 \text{ MeV}. \end{aligned}$$

The width seems a bit smaller compared to the PDG average 150 MeV, but in agreement with BES data 95 ± 25 MeV [3.82] and not far from the most recent determination of 120 ± 10 MeV in Ref. [3.83].

As shown in the former section, there are uncertainties in the mass, width and radiative decay of the $\Delta(1700)$. Playing with these uncertainties, one obtains a band of allowed cross sections from the dominant $\gamma p \rightarrow \Delta(1700) \rightarrow \eta\Delta \rightarrow \eta\pi^0 p$ mechanism, which is shown in Fig. 2 of Ref. [3.60]. Since we want to see the relative weight of the $\pi N(1535)$ production versus $\eta\Delta(1232)$, we fine tune the values of M_{Δ^*} , Γ_{Δ^*} and $g_{\Delta^*,\gamma p}$ to get a fair agreement with the data for low energies. We find that the values that better fit the curve $|a+b|^2$ to the MAMI data [3.63] up to 1300 MeV are $M_{\Delta^*} = 1663.6$ MeV, $\Gamma_{\Delta^*} = 114.1$ MeV and $g_{\Delta^*,\gamma p} = 0.142$, which corresponds to the branching fraction of 0.60%.

We obtain a fair reproduction of the cross section up to about $p_\gamma = 1300$ MeV. From there on one would be relatively far away from the $\Delta(1700)$ mass and other mechanisms discussed in Ref. [3.4] should come into play. The important finding concerning the triangle singularity is that we obtain a $\pi N(1535)$ contribution in fair agreement with the experimental determination. One should not overstate the agreement, since the methods to obtain it in Ref. [3.4] and here are different. In any case, the approximate agreement is welcome.

It is instructive to see that the cross section for $\pi N(1535)$ production is much wider than one could anticipate from the shape of $|t_T|^2$ in Fig. 3.22. This is because

the $\pi^0\eta p$ production amplitude has an extra factor $|\vec{k}|$ plus phase space factors and the weight of the $\Delta(1700)$ propagator.

In order to see the differences between the approaches followed here and in Ref. [3.4] we show in Fig. 3.18 the contributions of Eq. (3.63) and Eq. (3.70), taking $|a|^2$ (only $\eta\Delta$), $|b|^2$ (only $\pi N(1535)$) and $|a+b|^2$ in the equations. We can see that there is actually not much interference between the two amplitudes. Actually we find a small destructive interference, but this can become slightly constructive with small change of the parameters. The message is small interference, which happens in spite of the same spin structure of the two amplitudes as we have shown in Eqs. (3.56) and (3.57). The reason is that the $N(1535)$ structure provided by the $t_{\eta p, \eta p}$ amplitude is multiplied by t_T , which as seen in Fig. 3.22 has by itself a rich complex structure. This can explain the differences with the analysis of Ref. [3.4], where a more constructive interference between the two mechanisms occurs, as can be seen in Fig. 19 of that paper. In Ref. [3.4] a partial wave analysis is done using a K -matrix approach in which the t -matrix is given $A_{ab} = K_{ac}(1 - \rho K)_{cb}^{-1}$, where ρ is a diagonal matrix that takes into account phase space of the intermediate states, and the kernel K_{ac} is written as background plus a sum of Breit-Wigner amplitudes, $K_{ab} = \sum_{\alpha} \frac{g_a^{\alpha} g_b^{\alpha}}{M_{\alpha}^2 - s} + f_{ab}$. It is clear that in this analysis there is no room for the analytically rich multiplicative structure of the triangle singular mechanism that we have studied here. The reason for the small interference of the tree level and the triangle singularity finds its most clear explanation through the Schmid theorem which we discuss in the following section 3.4.

As commented at the end of the former section, we would like to show the effect of having the $\pi N(1535)$ production from the triangle mechanism. For that purpose, we compare in Fig. 3.23 the results of our approach with the results that we would obtain using the mechanism of Fig. 3.21, for a standard production mechanism.

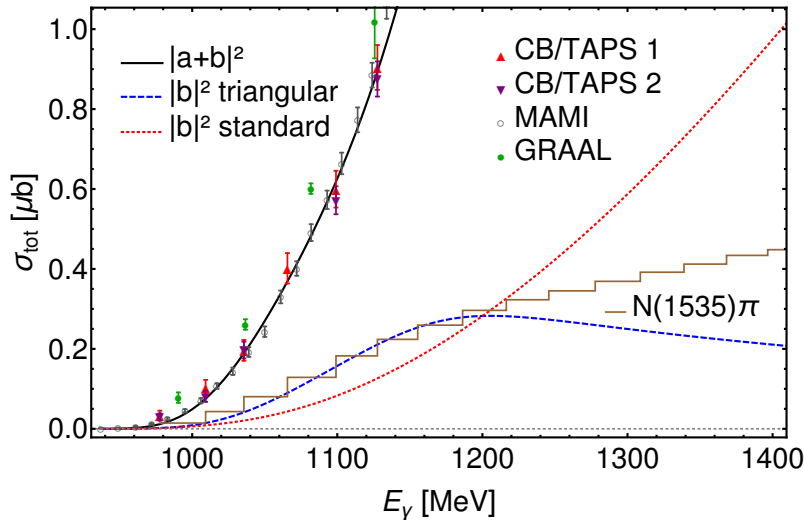


Figure 3.23: Cross section for the $\gamma p \rightarrow \pi N(1535)$ with the triangle mechanism and the standard mechanism of Fig. 3.21.

To facilitate the comparison we have normalized the cross sections at $E_{\gamma} = 1200$ MeV. We can see that the shape of the cross section with the standard mechanism

is quite different, and produces a cross section that keeps rising and has a concave shape. The mechanism that we have produces a different structure and gradually decreases around $E_\gamma = 1300$ MeV, producing a better agreement with the experimental extraction in the range up to about $E_\gamma = 1400$ MeV.

In Ref. [3.4] the data are given up to $E_\gamma = 2500$ MeV, but these are energies too big to be contrasted with our model where only the $\Delta(1700)$ resonance excitation is included, together with a $\Delta(1700)$ induced triangle singularity to account for the $\pi N(1535)$ production. Other resonances and other mechanisms are at play at these energies [3.4]: the $\pi N(1535)$ channel at higher energies would also receive contribution from another triangle singularity involving $\Sigma^{*0}K^+$ in the intermediate state with $\Sigma^{*0} \rightarrow \pi^0\Lambda$ and $K^+\Lambda$ fusing to give the $N(1535)$. Using the method of Eq. (3.20) from section 3.1 the singularity peaks around $E_\gamma = 1410$ MeV, about 200 MeV higher than the one we studied here. We have also evaluated the contribution of this singularity using the couplings from Refs. [3.69,3.80] and we find also a sizeable contribution above $E_\gamma = 1400$ MeV, but for the purpose of the present work, its contribution is very small compared to the one we have calculated up to $E_\gamma = 1300$ MeV, where with the limited information used here we give a fair description of the experimental data.

As we have noted, the dominant mechanism of Fig. 3.19 and the triangle mechanism of Fig. 3.20 have the same spin and angular structure, given by the operator $\vec{S} \cdot \vec{k} \vec{S}^\dagger \cdot \vec{\epsilon}$ of Eq. (3.66). Hence, the angular dependence is given by Eq. (3.65), both in the case of each individual mechanism or the coherent sum of the two. Angular distributions with the dominant mechanism were discussed in Ref. [3.65] and we do not discuss them further here.

3.3.4 Conclusions

We have evaluated the $\gamma p \rightarrow \eta\pi^0 p$ cross section at low energies, up to about 500 MeV above threshold for E_γ , taking into account two mechanisms: the $\gamma p \rightarrow \Delta(1700) \rightarrow \eta\Delta(1232) \rightarrow \eta\pi^0 p$ and the $\gamma p \rightarrow \Delta(1700) \rightarrow \pi N(1535)$. The first mechanism is the one shown to be dominant in the productions of Ref. [3.59] and subsequent papers. The second one is new and involves a triangle singularity in which $\Delta(1700) \rightarrow \eta\Delta(1232)$, $\Delta(1232) \rightarrow \pi^0 p$ and then ηp fuse to produce the $N(1535)$. The latter mechanism gave rise to a peak (broadened by the effect of the $\Delta(1232)$ width) around $E_\gamma = 1220$ MeV ($\sqrt{s} = 1782$ MeV). We have shown that this latter mechanism, which we can evaluate with elements borrowed from the properties of the $\Delta(1700)$ and $N(1535)$ as being dynamically generated resonances, gives rise to a contribution to the cross section in fair agreement with the experimental determination. We showed that the shape produced by the triangle mechanism is quite different from the one we would have assuming a standard P -wave $\pi N(1535)$ production mechanism, and the experimental determination is in better agreement with the triangle mechanism. We also showed that there is some discrepancy in the interference pattern between the two mechanisms with respect to the one obtained in Ref. [3.4], but we argued that this was a consequence of the fact that the analysis of Ref. [3.4] does not include explicitly a triangle singularity in the approach. The triangle amplitude created by itself a kind of a resonance structure which multiplies

(not sums) an amplitude like the one assumed in Ref. [3.63]. As a consequence of this factor we find very small interference between the two mechanisms, while a more constructive interference is seen in the analysis of Ref. [3.4]. This also means that the amount of $\gamma p \rightarrow \eta \Delta(1232)$ in the cross section is somewhat bigger in our approach at energies around $E_\gamma = 1100 - 1400$ MeV.

The exercise made here also has repercussion for other reactions. It has shown that in cases like the present one, where there is an unavoidable triangular singularity, the standard partial wave analyses should be extended to accommodate such a structure. It is not clear a priori that a triangle singularity is going to have a relevance in a given reaction, but, given the simplicity of the rule developed in section 3.1 to find out whether a singularity appears within a certain mechanism, it would be wise to make a general survey of a given reaction to see if such mechanisms can develop. One could easily derive the structure for this singularity, which up to a global factor only depends on the intermediate states of the triangle diagram, and use it as a multiplicative factor on top of the standard amplitude of present partial wave analyses. Future analyses of data along these lines would be most welcome.

3.4 Considerations on the Schmid theorem

In this section we present the work of Ref. [3.5] where we investigate the Schmid theorem [3.6], which states that if one has a tree level mechanism with a particle decaying to two particles and one of them decaying posteriorly to two other particles, the possible triangle singularity developed by the mechanism of elastic rescattering of two of the three decay particles does not change the cross section provided by the tree level. We investigate the process in terms of the width of the unstable particle produced in the first decay and determine the limits of validity and violation of the theorem. One of the conclusions is that the theorem holds in the strict limit of zero width of that resonance, in which case the strength of the triangle diagram becomes negligible compared to the tree level. Another conclusion, on the practical side, is that for realistic values of the width, the triangle singularity can provide a strength comparable or even bigger than the tree level, which indicates that invoking the Schmid theorem to neglect the triangle diagram stemming from elastic rescattering of the tree level should not be done. Even then, we observe that the realistic case keeps some memory of the Schmid theorem, which is visible in a peculiar interference pattern with the tree level.

3.4.1 Introduction

Early studies of triangle singularities were done in Ref. [3.84] but the systematic study was done by Landau [3.7]. Work followed in Refs. [3.85–3.88] and some peaks observed in nuclear reactions [3.89] were suggested as indicative of a triangle singularity [3.90]. A thorough discussion of this early work was done by Schmid in a clarifying article [3.6]. There a surprise appeared, known nowadays as Schmid theorem that states that if the rescattering of particles 1 and 2 occurs, going to the same state $1 + 2$, the triangle singularity does not lead to any observable effect in magnitudes like cross sections or differential widths. It is simply reabsorbed by

the S -wave of the tree level amplitude (the same mechanism without rescattering, see Figs. 3.24 and 3.25) modifying only the phase of this partial amplitude. In angle-integrated cross sections the effect of the triangle singularity disappears.

Some debate originated on the limits to the Schmid theorem and its range of validity [3.73, 3.91–3.93]. In Ref. [3.91], for example, it was shown that if the scattering amplitude of $1 + 2 \rightarrow 1 + 2$ contains inelasticities then the Schmid theorem does not hold.

Recently there has been a renewed interest in triangle singularities because the present wealth of experimental work offers multiple possibilities to study such mechanisms. A topic that stimulated the present interest on the subject was the one of isospin violation in the $\eta(1405)$ decay into $\pi^0 f_0(980)$ versus the isospin allowed decay into $\pi^0 a_0(980)$ [3.50–3.52, 3.94, 3.95]. One interesting work was done in Ref. [3.12], with many suggestions of places and reactions where triangle singularities could be found. One of the most striking examples of this rebirth is the work of Refs. [3.44, 3.96] where a peak observed by the COMPASS collaboration [3.46], and branded as a new resonance $a_1(1420)$, was shown to be actually produced by a triangle singularity. The renewed interest in the issue was also spurred by the work of Ref. [3.10], suggesting that a peak observed by the LHCb collaboration, which has been accepted as a signal of a pentaquark of hidden charm [3.97], was actually due to a triangle singularity. The hypothesis was ruled out in Ref. [3.9] if the present quantum numbers of this peak hold. Yet, given the fact that some uncertainties concerning these quantum numbers still remain, the issue could be reopened in the future.

The work of Ref. [3.9] develops a different formalism than the one usually employed, which is very practical and intuitive, as presented in section 3.1, and we shall also follow these lines in the present work, which offers a quite different formal derivation of the Schmid theorem and allows to see its validity and limitations.

The former recent works on triangle singularities have stimulated many works on the issue [3.1, 3.3, 3.13, 3.98–3.114]. Further information can be found in the report [3.115].

Along the literature on this topic it is customary to find the statement that due to the Schmid theorem, whenever one has rescattering in the loop to go to the same states as inside the loop, there is no need to evaluate the triangle diagram because its contribution is reabsorbed by the tree level. The purpose of the present paper is to get an insight on the theorem and see where it holds exactly, when it fails and when it is just an approximation and how good or bad can it be. For that, a new derivation is carried out, and a study in terms of the width of the intermediate state R is done. The failure of the theorem when the $t_{12,12}$ scattering matrix has inelasticities is also shown in detail, providing the quantitative amount of the breaking of the theorem. Apart from the limit of small Γ_R , where the theorem strictly holds, we study in a particular case what happens for a realistic width, and a typical $1 + 2 \rightarrow 1 + 2$ scattering amplitude, which serves as a guide on how much to trust the theorem to eventually neglect the contribution of the triangle loop.

3.4.2 Formulation

Let us study the decay process of a particle A into two particles 1 and R , with a posterior decay of R into particles 2 and 3, as we saw in Fig. 3.1 in section 3.1, which we repeat here in Fig. 3.24. We shall also assume for simplicity that all

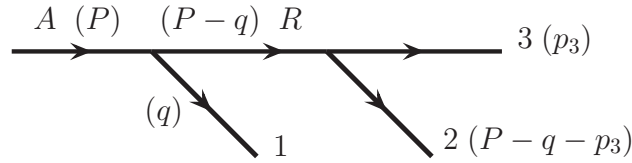


Figure 3.24: Tree level diagram for the process $A \rightarrow 1+2+3$ mediated by a resonance R that decays into particles 2 and 3. In brackets the momenta of the particles.

vertices are scalar, and can be represented by just one coupling in each vertex. The conclusions that we will reach are the same for more elaborate couplings, with spin or momentum dependence.

The next step is to allow particles 1 and 2 to undergo final state interaction, as depicted in Fig. 3.25, which we also saw in Fig. 3.2 in section 3.1.

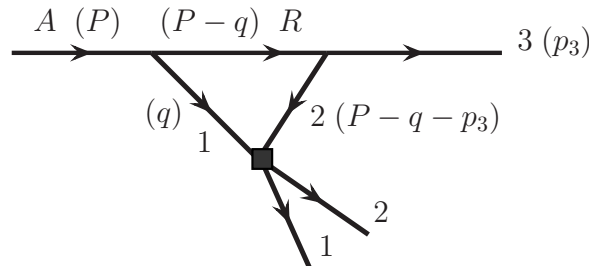


Figure 3.25: Triangle mechanism emerging from the mechanism of Fig. 3.24, with final state interaction of particles 1 and 2. The vertex with particles 1 and 2 symbolizes the $1+2 \rightarrow 1+2$ scattering matrix. In brackets the momenta of the particles.

Let us make a quick recap: we have seen that triangle diagrams can develop a singularity when all the particles inside the loop in Fig. 3.25 are placed on shell and the particles R and 3 go parallel in the A rest frame. In section 3.1 we studied the conditions for this to occur, relating the invariant mass of particles 1,2 with the mass of A . Also recall that if particles R and 3 go in the same direction, then both particles 1 and 2 go in the opposite direction to them in the A and R rest frames, respectively. The last condition for a singularity was given by the Coleman-Norton theorem [3.8], which stated that the classical process of particle 2 catching up with particle 1 should be possible.

We also mentioned that in the situation where the R resonance is placed on shell in the triangle loop, as well as particles 1 and 2, the tree level mechanism of Fig. 3.24 also has a singularity in the limit of zero width for the resonance R , since the amplitude goes as $(M_{\text{inv}}(R) - M_R + i\Gamma_R/2)^{-1}$. Note however, that the

tree diagram does not have the restriction that particles R and 3 should be parallel (as is the case for the triangle singularity) and hence the region where R can be placed on shell is much wider than for the triangle singularity. This relation of the singularities of the tree level and triangle diagram will be the subject of our present study.

Let us come back to the tree level mechanism of Fig. 3.24. Assume for the moment that the decay into $2 + 3$ is the only decay channel of the resonance R . In the limit of $\Gamma_R \rightarrow 0$ one has the decay of A into two elementary particles 1 and R . The width of A can be calculated with the standard formula for decay of two particles or three particles and the results are identical. Intuitively one can say that, once the particle decays into 1 and R , if particle R decays later this does not modify the A width, since this was determined at the moment that A decayed into 1 and R . The same could be said about the triangle mechanism of Fig. 3.25. Once the A particle decays into 1 and R , and R decays into 2 and 3, the probability for this process is established and the posterior interaction of 1 and 2 should not modify this probability. This argument is the intuitive statement of the Schmid theorem, which technically reads as follow: Let $t_t^{(0)}$ be the S -wave projection of the tree level amplitude, t_t , of the diagram of Fig. 3.24, evaluated in the rest frame of $1 + 2$, referred to the angle between the particles 1 and 3. Let t_L be the amplitude corresponding to the triangle loop of Fig. 3.25. The Schmid theorem states that

$$t_t^{(0)} + t_L = t_t^{(0)} e^{2i\delta} \quad (3.75)$$

where δ is the S -wave phase shift of the scattering amplitude $1 + 2 \rightarrow 1 + 2$ (assume also for simplicity that this is the only partial wave in $1 + 2 \rightarrow 1 + 2$). The formula holds for the case that there is only elastic scattering $1 + 2 \rightarrow 1 + 2$. In the case that there can be inelastic channels the formula is modified, as we shall see later on, and the Schmid theorem does not strictly hold.

The interesting thing about Eq. (3.75) is that

$$\left| t_t^{(0)} + t_L \right|^2 = \left| t_t^{(0)} e^{2i\delta} \right|^2 = \left| t_t^{(0)} \right|^2 \quad (3.76)$$

and consequently, since $t_t^{(\ell \neq 0)}$ and $t_t^{(0)}$ do not interfere in the angle integration, then

$$\begin{aligned} \int_{-1}^1 d \cos \theta |t_t + t_L|^2 &= \int_{-1}^1 d \cos \theta \left| t_t^{(\ell \neq 0)} + t_t^{(0)} + t_L \right|^2 \\ &= \int_{-1}^1 d \cos \theta \left| t_t^{(\ell \neq 0)} + t_t^{(0)} e^{2i\delta} \right|^2 \\ &= \int_{-1}^1 d \cos \theta \left(\left| t_t^{(\ell \neq 0)} \right|^2 + \left| t_t^{(0)} \right|^2 \right) \\ &= \int_{-1}^1 d \cos \theta |t_t|^2 \end{aligned} \quad (3.77)$$

and as a consequence the contribution of the triangle diagram does not change the width that one obtains just with the tree level diagram. Note that if we had $1 + 2 \rightarrow 1' + 2'$ or $1 + 2 \rightarrow R'$, where R' is some resonance, the theorem does not hold because there is no contribution of the tree level to these reactions.

Kinematics of $A \rightarrow 1 + 2 + 3$

We assume that all particles are mesons to avoid using different normalization for meson or baryon fields. The width of particle A for this process is given by

$$\Gamma_A = \frac{1}{2M_A} \int \frac{d^3 p_3}{(2\pi)^3} \frac{1}{2\omega_3} \int \frac{d^3 p_2}{(2\pi)^3} \frac{1}{2\omega_2} \int \frac{d^3 p_1}{(2\pi)^3} \frac{1}{2\omega_1} \times (2\pi)^4 \delta^4(P_A - p_1 - p_2 - p_3) |t|^2 \quad (3.78)$$

where P_A is the four-momentum of A and ω_i the on shell energies $\omega_i = \sqrt{m_i^2 + \vec{p}_i^2}$. We perform the integration over particles 1 and 2 in the frame of reference where $\vec{P}_A - \vec{p}_3 = 0$, where the system of 1 + 2 is at rest and the integration over p_3 in the A rest frame. We perform the $d^3 p_2$ integration using the δ function and have in that frame ($\vec{p}_2 = -\vec{p}_1$)

$$\Gamma_A = \frac{1}{2M_A} \int \frac{d^3 p_3}{(2\pi)^3} \frac{1}{2\omega_3} \int \frac{d^3 \tilde{p}_1}{(2\pi)^3} \frac{1}{2\tilde{\omega}_1} \frac{1}{2\tilde{\omega}_2} \times 2\pi \delta\left(\tilde{E}_A - \tilde{\omega}_3 - \tilde{\omega}_1(\tilde{p}_1) - \tilde{\omega}_2(\tilde{p}_1)\right) |t|^2 \quad (3.79)$$

where the tilde refers to variables in the 1 + 2 rest frame, and t is the scattering matrix for the process.

Note that

$$\tilde{E}_A - \tilde{\omega}_3 = \tilde{\omega}_1(\tilde{p}_1) + \tilde{\omega}_2(\tilde{p}_1) = M_{\text{inv}}(12). \quad (3.80)$$

There is no ϕ dependence in that frame if we chose \vec{p}_3 in the z direction and the $d^3 \tilde{p}_1$ integration is done with the result

$$\Gamma_A = \frac{1}{2M_A} \int \frac{d^3 p_3}{(2\pi)^3} \frac{1}{2\omega_3} \frac{1}{8\pi} \int_{-1}^1 d \cos \theta \tilde{p}_1 \frac{1}{M_{\text{inv}}(12)} |t|^2 \quad (3.81)$$

with \tilde{p}_1 the momentum of particle 1 in the 1 + 2 rest frame and θ the angle between \vec{p}_1 and \vec{p}_3 .

Note also that

$$M_{\text{inv}}^2(23) = (P_A - p_1)^2 = M_A^2 + m_1^2 - 2\tilde{E}_A \tilde{E}_1 + 2\tilde{p}_1 \tilde{p}_3 \cos \theta. \quad (3.82)$$

Hence, the integration over $\cos \theta$ is equivalent to an integration over $M_{\text{inv}}(23)$. Similarly we can write

$$M_{\text{inv}}^2(12) = (P_A - p_3)^2 = M_A^2 + m_3^2 - 2M_A \omega_3, \quad (3.83)$$

where the evaluation has been done in the A rest frame. It is also easy to derive

$$\begin{aligned} \tilde{E}_A &= \frac{1}{2M_{\text{inv}}(12)} (M_A^2 + M_{\text{inv}}^2(12) - m_3^2) \\ \tilde{E}_3 &= \frac{1}{2M_{\text{inv}}(12)} (M_A^2 - M_{\text{inv}}^2(12) - m_3^2) \\ \tilde{E}_1 &= \frac{1}{2M_{\text{inv}}(12)} (M_{\text{inv}}^2(12) + m_1^2 - m_2^2) \\ \tilde{p}_1 &= \frac{\lambda^{1/2}(M_{\text{inv}}^2(12), m_1^2, m_2^2)}{2M_{\text{inv}}(12)} \\ \tilde{p}_3 &= \frac{\lambda^{1/2}(M_A^2, m_3^2, M_{\text{inv}}^2(12))}{2M_{\text{inv}}(12)}. \end{aligned} \quad (3.84)$$

The d^3p_3 integration is done in the A rest frame

$$\int \frac{d^3p_3}{(2\pi)^3} \frac{1}{2\omega_3} = \frac{1}{4\pi^2} \int p_3 d\omega_3 \quad (3.85)$$

and using Eqs. (3.82) and (3.83), the ω_3 and $\cos\theta$ integration can be substituted by integrations over $M_{\text{inv}}(12)$ and $M_{\text{inv}}(23)$ and one has the formula given in the PDG [3.14]

$$\frac{d^2\Gamma_A}{dM_{\text{inv}}(12)dM_{\text{inv}}(23)} = \frac{1}{64\pi^3} \frac{1}{M_A^3} M_{\text{inv}}(12)M_{\text{inv}}(23) |t|^2 \quad (3.86)$$

Yet, for the explanation of the Schmid theorem it is better to use Eq. (3.81).

t_t and t_L amplitudes

Since we are concerned only with the situation when the particles are close to on shell we will use

$$\begin{aligned} \frac{1}{q^2 - m^2 + i\epsilon} &= \frac{1}{(q^0)^2 - \vec{q}^2 - m^2 + i\epsilon} \\ &= \frac{1}{2\omega(q)} \left\{ \frac{1}{q^0 - \omega(q) + i\epsilon} - \frac{1}{q^0 + \omega(q) + i\epsilon} \right\} \end{aligned} \quad (3.87)$$

and keep only the term $[2\omega(q)(q^0 - \omega(q) + i\epsilon)]^{-1}$ since this is the term that can be placed on shell.

The amplitude of Fig. 3.24 is given in the $1+2$ rest frame by ($\vec{P}_A = \vec{p}_3$, and we omit the tilde in the momenta)

$$t_t = g_A g_R \frac{1}{2\omega_R(\vec{p}_3 - \vec{q})} \frac{1}{\widetilde{E}_A - \omega_1(q) - \omega_R(\vec{p}_3 - \vec{q}) + i\epsilon} \quad (3.88)$$

where g_A, g_R are the couplings for the decay of A and R . From Eq. (3.88) we get $t_t^{(0)}$ projecting into S -wave

$$\begin{aligned} t_t^{(0)} &= \frac{1}{2} \int_{-1}^1 d\cos\theta \frac{1}{2\omega_R(\vec{p}_3 - \vec{q})} \\ &\quad \times \frac{g_A g_R}{\widetilde{E}_A - \omega_1(q) - \omega_R(\vec{p}_3 - \vec{q}) + i\epsilon} \end{aligned} \quad (3.89)$$

Note that in the realistic situation the $i\epsilon$ in Eqs. (3.88) and (3.89) will be substituted by $i\frac{\Gamma_R}{2}$.

On the other hand, the amplitude of the triangle diagram can be written in the $1+2$ rest frame as

$$\begin{aligned} t_L &= i \int \frac{d^4q}{(2\pi)^4} \frac{1}{2\omega_R(\vec{p}_3 - \vec{q})} \frac{1}{\widetilde{E}_A - q^0 - \omega_R(\vec{p}_3 - \vec{q}) + i\epsilon} \\ &\quad \times \frac{1}{2\omega_1(q)} \frac{1}{q^0 - \omega_1(q) + i\epsilon} \frac{1}{2\omega_2(q)} \end{aligned}$$

$$\times \frac{1}{\tilde{E}_A - q^0 - \tilde{E}_3 - \omega_2(q) + i\epsilon} g_A g_R t_{12,12}, \quad (3.90)$$

where $t_{12,12}$ is the scattering amplitude for $1 + 2 \rightarrow 1 + 2$. The q^0 integration is done immediately using Cauchy's theorem and we obtain

$$t_L = \int \frac{d^3q}{(2\pi)^3} \frac{1}{2\omega_R(\vec{p}_3 - \vec{q})} \frac{1}{\tilde{E}_A - \omega_1(q) - \omega_R(\vec{p}_3 - \vec{q}) + i\epsilon} \\ \times \frac{1}{2\omega_1(q)} \frac{1}{2\omega_2(q)} \frac{g_A g_R t_{12,12}}{\tilde{E}_A - \omega_1(q) - \tilde{E}_3 - \omega_2(q) + i\epsilon}. \quad (3.91)$$

We can see that the R propagator term $\left[2\omega_R(\vec{p}_3 - \vec{q}) \left(\tilde{E}_A - \omega_1(q) - \omega_R(\vec{p}_3 - \vec{q}) + i\epsilon\right)\right]^{-1}$ is common in t_t and t_L of Eqs. (3.88) and (3.91). There is, however, a difference since in the loop function t_L the momentum \vec{q} is an integration variable while, in t_t , \vec{q} is the momentum of the external particle 1. In the loop, after rescattering of particles 1 and 2 the momentum \vec{p}_1 is different than \vec{q} , and only for the situation where all particles in the loop are placed on shell, the moduli of the momenta are equal.

The ϕ integral in Eq. (3.91) is trivially done and we have

$$t_L = \frac{1}{(2\pi)^2} \int_0^\infty q^2 dq \frac{1}{2\omega_1(q)} \frac{1}{2\omega_2(q)} \\ \times \frac{1}{\tilde{E}_A - \tilde{E}_3 - \omega_1(q) - \omega_2(q) + i\epsilon} \\ \times 2 \frac{1}{2} \int_{-1}^1 d \cos \theta \frac{1}{2\omega_R(\vec{p}_3 - \vec{q})} \\ \times \frac{1}{\tilde{E}_A - \omega_1(q) - \omega_R(\vec{p}_3 - \vec{q}) + i\epsilon} g_A g_R t_{12,12}. \quad (3.92)$$

We can see now that the integral over $\cos \theta$ is the same in $t_t^{(0)}$ (Eq. (3.89)) and t_L (Eq. (3.92)).

To find the singularity in t_L let us look for the poles of the two propagators. On the one hand from

$$\tilde{E}_A - \tilde{E}_3 - \omega_1(q) - \omega_2(q) + i\epsilon = 0 \quad (3.93)$$

we obtain

$$q_{\text{on}\pm} = \pm \frac{\lambda^{1/2}(M_{\text{inv}}^2(12), m_1^2, m_2^2)}{2M_{\text{inv}}(12)} \pm i\epsilon \quad (3.94)$$

On the other hand from

$$\tilde{E}_A - \omega_1(q) - \omega_R(\vec{p}_3 - \vec{q}) + i\epsilon = 0 \quad (3.95)$$

we get two solutions which depend on $\cos \theta$. Yet, we are only interested in $\cos \theta = \pm 1$ because it is there that we will not have cancellations in the principal value of $\int_{-1}^1 d \cos \theta$ because we cannot go beyond $|\cos \theta| = 1$ in the integration. In this case

one finds immediately ²

$$\bar{q} = p_3 \cos \theta \frac{E'_1}{M_A} \pm \frac{\tilde{E}_A}{M_A} p'_1 \pm i\epsilon, \quad (\cos \theta = \pm 1) \quad (3.96)$$

where E'_1, p'_1 are the energy and momentum of particle 1 in the A rest frame, while p_3 is the momentum of particle 3 (or A) in the $1+2$ rest frame that we have used before. For $\cos \theta = \pm 1$ this is just a boost from the frame where A is at rest ($\bar{q} = p'_1$) to the one where it has a velocity $v_A = \frac{\tilde{p}_A}{\tilde{E}_A} = \frac{p_3}{E_A}$, but the position in the complex plane is given by the $\pm i\epsilon$.

Take now:

a) $\cos \theta = -1$

The $(-)$ solution in Eq. (3.96),

$$Q_- = -p_3 \frac{E'_1}{M_A} - \frac{\tilde{E}_A}{M_A} p'_1 - i\epsilon, \quad (3.97)$$

gives \bar{q} negative and does not contribute in Eq. (3.92) since q runs from 0 to ∞ . If we take the $(+)$ sign,

$$Q_+ = -p_3 \frac{E'_1}{M_A} + \frac{\tilde{E}_A}{M_A} p'_1 + i\epsilon, \quad (3.98)$$

the pole is in the upper side of the complex plane. This situation corresponds to the one in Fig. 3.26. We can see that in that case one can deform the contour path in the q integration to avoid the poles and one does not have a singularity.

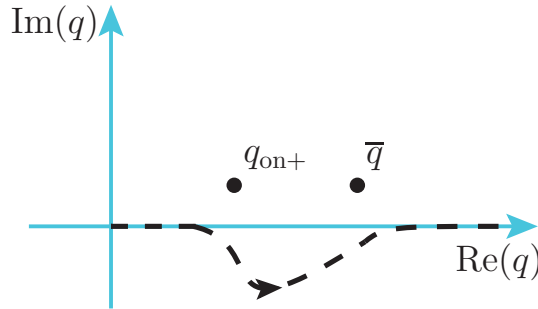


Figure 3.26: Pole positions for the case of $\cos \theta = -1$ when \bar{q} can be positive. The line shows the contour path that one can take to avoid the poles.

b) $\cos \theta = 1$

² Note that Eqs. (3.94) and (3.96) do not coincide with those in section 3.1 because there these momenta are obtained in the A rest frame and here in the $1+2$ rest frame. They can be reached by a boost to the frame where A is at rest.

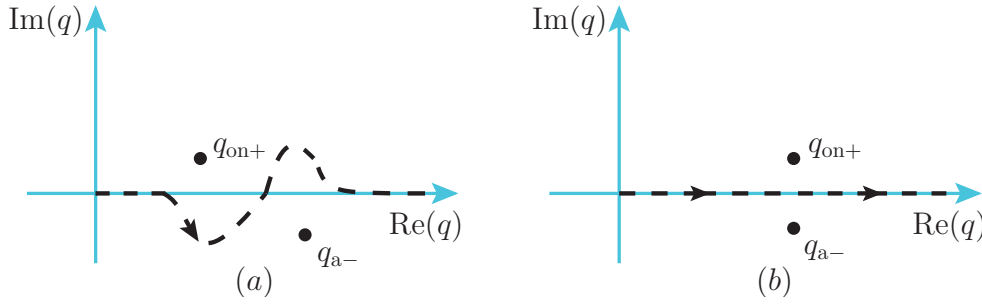


Figure 3.27: Pole positions for q_{on} and q_{a-} for $\cos \theta = 1$. The case (b) leads to the triangle singularity.

The (+) solution,

$$q_{a+} = p_3 \frac{E'_1}{M_A} + \frac{\tilde{E}_A}{M_A} p'_1 + i\epsilon \quad (3.99)$$

corresponds to a pole in the upper part of the complex plane and does not lead to a singularity. The (-) solution, let us call it q_{a-} ,

$$q_{a-} = p_3 \frac{E'_1}{M_A} - \frac{\tilde{E}_A}{M_A} p'_1 - i\epsilon \quad (3.100)$$

lies in the lower side of the complex plane. In this case if q_{a-} is different from q_{on} of Eq. (3.94) we have the situation as in Fig. 3.27(a). In this case we can also deform the contour path to avoid the poles in the q integration of t_L . However in the case that

$$q_{on+} = q_{a-} \quad (\epsilon \rightarrow 0), \quad (3.101)$$

corresponding to Fig. 3.27(b), the path of the integral has to go through the poles q_{on+} and q_{a-} and we cannot deform the contour path to avoid the poles. This is the situation of the triangle singularity³. Note for further discussions that $Q_- = -q_{a+}$ and $Q_+ = -q_{a-}$.

It might be curious to see that we find the singularity for $\cos \theta = 1$, while in section 3.1 it was found for $\cos \theta = -1$. This is a consequence of the different frame of reference. Indeed, we are in the situation of Fig. 3.28. We can make a boost with velocity v_A to bring particle A at rest

$$v_A = \frac{\tilde{p}_A}{\tilde{E}_A} = \frac{p_3}{\tilde{E}_A}. \quad (3.102)$$

The velocity of particle 3 in the 1 + 2 rest frame is

$$v_3 = \frac{p_3}{\tilde{E}_3} > v_A \quad (3.103)$$

but since the mass of particle 3 is smaller than M_A then v_3 is bigger than v_A and in the boost particle 3 still goes in the same direction as before. However p'_1 in that

³Another possibility to have singularities is that $q_{a+} = q_{a-}$ ($\epsilon \rightarrow 0$). This leads to a threshold singularity, discussed in section 3.1 and Ref. [3.9], but which plays no role on the present discussion.

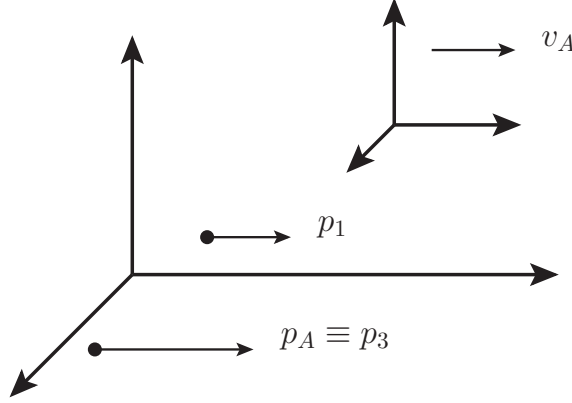


Figure 3.28: Situation of momenta in the 1 + 2 rest frame when $\cos \theta = 1$.

frame has a velocity

$$v_1 = \frac{p'_1}{E'_1} \quad (3.104)$$

and since we are taking the q_{a-} solution positive

$$\begin{aligned} q_{a-} &= p_3 \frac{E'_1}{M_A} - \frac{\tilde{E}_A}{M_A} p'_1 > 0, \\ p_3 E'_1 &> p'_1 \tilde{E}_A; \quad \frac{p_3}{\tilde{E}_A} > \frac{p'_1}{E'_1} \Rightarrow v_A > v_1. \end{aligned} \quad (3.105)$$

Hence particle 1 changes direction under the boost of velocity v_A and in the rest frame \vec{p}'_3 and \vec{p}'_1 have opposite directions, $\cos \theta' = -1$, as it was found in section 3.1.

Formulation of Schmid theorem

Let us perform the $\cos \theta$ integration in t_L of Eq. (3.92).

$$\begin{aligned} I(q) &= \int_{-1}^1 d \cos \theta \frac{1}{2\omega_R(\vec{p}_3 - \vec{q})} \\ &\quad \times \frac{1}{\tilde{E}_A - \omega_1(q) - \omega_R(\vec{p}_3 - \vec{q}) + i\epsilon}. \end{aligned} \quad (3.106)$$

We can introduce the variable x

$$\begin{aligned} x &= \omega_R(\vec{p}_3 - \vec{q}) = \sqrt{m_R^2 + p_3^2 + q^2 - 2p_3q \cos \theta} \\ d \cos \theta &= -\frac{\omega_R}{p_3q} dx \end{aligned} \quad (3.107)$$

$$I(q) = - \int_{\omega_R(p_3+q)}^{\omega_R(p_3-q)} dx \frac{1}{2\omega_R} \frac{\omega_R}{p_3q} \frac{1}{\tilde{E}_A - \omega_1(q) - x + i\epsilon}$$

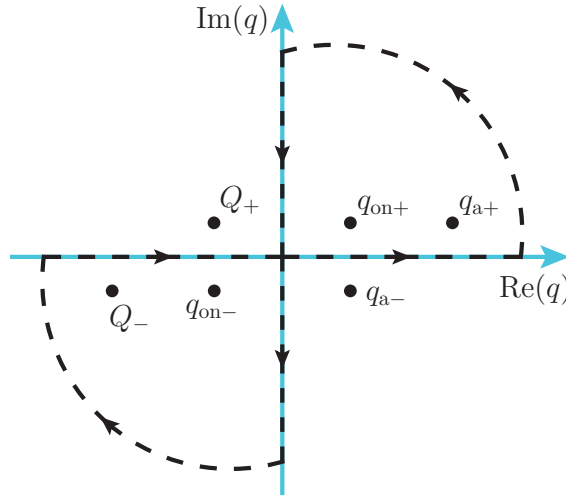


Figure 3.29: Integration path followed to evaluate t_L of Eq. (3.109).

$$\begin{aligned}
 &= \int_{\omega_R(p_3-q)}^{\omega_R(p_3+q)} dx \frac{1}{2p_3q} \frac{1}{\tilde{E}_A - \omega_1(q) - x + i\epsilon} \\
 &= \frac{1}{2p_3q} \ln \left(\frac{\tilde{E}_A - \omega_1(q) - \omega_R(p_3 - q) + i\epsilon}{\tilde{E}_A - \omega_1(q) - \omega_R(p_3 + q) + i\epsilon} \right). \quad (3.108)
 \end{aligned}$$

It is interesting to see that $I(q) = I(-q)$ is an even function of q . Then, since the rest of the integrand of t_L in Eq. (3.92) is also even in q we can write

$$\begin{aligned}
 t_L &= \frac{1}{(2\pi)^2} \frac{1}{2} \int_{-\infty}^{\infty} q^2 dq \frac{1}{2\omega_1(q)} \frac{1}{2\omega_2(q)} \\
 &\quad \times \frac{g_A g_R I(q) t_{12,12}}{\tilde{E}_A - \tilde{E}_3 - \omega_1(q) - \omega_2(q) + i\epsilon}. \quad (3.109)
 \end{aligned}$$

We should note that the singularity that we are evaluating corresponds to the numerator in Eq. (3.108) becoming zero.

Since we have extended the integration to q negative, we must also consider the poles of Q_- and Q_+ of Eqs. (3.97) and (3.98). The situation of the poles is shown in Fig. 3.29. In this figure we also show the contour path followed to perform the integral over q using Cauchy's theorem. We have

$$\begin{aligned}
 &\int_{-\infty}^{\infty} dq \dots + \int_{i\infty}^{-i\infty} dq \dots + \int_{\text{circle}} dq \dots \\
 &= 2\pi i \text{Res}(q_{\text{on}+}) + 2\pi i \text{Res}(q_{\text{a}+}) \quad (3.110)
 \end{aligned}$$

$$- 2\pi i \text{Res}(q_{\text{on}-}) - 2\pi i \text{Res}(Q_-) \quad (3.111)$$

The relevant point now is the fact that the integral over the circle of infinity vanishes and $\int_{i\infty}^{-i\infty} dq$, $\text{Res}(q_{\text{a}+})$ and $\text{Res}(Q_-)$ do not produce any singularity, and thus

$$\int_{-\infty}^{\infty} dq \dots = 2\pi i \text{Res}(q_{\text{on}+}) - 2\pi i \text{Res}(q_{\text{on}-}) \quad (3.112)$$

is the part of the integral that leads to the singularity. We go back to Eq. (3.92) and perform the q integration before $\cos \theta$ is integrated. Since the denominator $(\tilde{E}_A - \tilde{E}_3 - \omega_1(q) - \omega_2(q))$ vanishes for $q_{\text{on}+}$ and $q_{\text{on}-}$, we can apply L'Hôpital rule to calculate the residues ($\tilde{E}_A - \tilde{E}_3 = M_{\text{inv}}(12)$), with q_{on} standing for $q_{\text{on}+}$ or $q_{\text{on}-}$)

$$\begin{aligned} \text{Res}(q_{\text{on}}) &\propto \lim_{q \rightarrow q_{\text{on}}} \frac{q - q_{\text{on}}}{M_{\text{inv}}(12) - \omega_1(q) - \omega_2(q)} \\ &= \frac{1}{\left(\frac{-q}{\omega_1}\right) + \left(\frac{-q}{\omega_2}\right)} \Big|_{q_{\text{on}}} = -\frac{\omega_1 \omega_2}{q_{\text{on}} M_{\text{inv}}(12)}. \end{aligned} \quad (3.113)$$

Thus, the singular part of t_L is contained in

$$\begin{aligned} t_L &= \frac{1}{(2\pi)^2} \frac{1}{4} |q_{\text{on}}| \frac{1}{M_{\text{inv}}(12)} g_A g_R t_{12,12} (-) 4\pi i \\ &\times \frac{1}{2} \int_{-1}^1 d \cos \theta \frac{1}{2\omega_R(\vec{p}_3 - \vec{q})} \\ &\times \frac{1}{\tilde{E}_A - \omega_1(q) - \omega_R(\vec{p}_3 - \vec{q}) + i\epsilon}. \end{aligned} \quad (3.114)$$

Comparing with Eq. (3.89) we find

$$t_L = -i \frac{1}{4\pi} |q_{\text{on}}| \frac{1}{M_{\text{inv}}(12)} t_{12,12} t_t^{(0)}. \quad (3.115)$$

We must now recall the relationship of our t matrix in the field theory formulation with the f matrix of Quantum Mechanics

$$f = -\frac{1}{8\pi} \frac{1}{M_{\text{inv}}} t \quad (3.116)$$

which allows us to reformulate Eq. (3.115) as

$$t_L = 2i |q_{\text{on}}| f t_t^{(0)} \quad (3.117)$$

and since

$$f = \frac{\eta e^{2i\delta} - 1}{2i |q_{\text{on}}|} \quad (3.118)$$

we find that

$$t_t^{(0)} + t_L = t_t^{(0)} (1 + 2i |q_{\text{on}}| f) = \eta e^{2i\delta} t_t^{(0)}, \quad (3.119)$$

also derived in Ref. [3.73]. Eq. (3.119) for the case when there is only the 1, 2 elastic channel ($\eta = 1$) is the expression of the Schmid theorem [3.6]. It was already mentioned in Ref. [3.91] that the Schmid theorem does not hold if $t_{12,12}$ has inelasticities and we can be more quantitative here. Indeed, recalling Eq. (3.77) we have now

$$\int_{-1}^1 d \cos \theta |t_t + t_L|^2 = \int_{-1}^1 d \cos \theta \left\{ \left| t_t^{(\ell \neq 0)} \right|^2 + \eta^2 \left| t_t^{(0)} \right|^2 \right\}$$

$$\begin{aligned}
&= \int_{-1}^1 d \cos \theta \left\{ \left| t_t^{(\ell \neq 0)} \right|^2 + \left| t_t^{(0)} \right|^2 - (1 - \eta^2) \left| t_t^{(0)} \right|^2 \right\} \\
&= \int_{-1}^1 d \cos \theta \left| t_t \right|^2 - (1 - \eta^2) \int_{-1}^1 d \cos \theta \left| t_t^{(0)} \right|^2
\end{aligned} \tag{3.120}$$

and since $t_t^{(0)}$ contains the same singularity as t_L , the singularity of the triangle diagram will show up with a strength of $1 - \eta^2$.

It is interesting to recall at this point that Watson's theorem [3.116] does not hold in this case. We might expect that the sum of the tree level and rescattering would introduce a phase $e^{i\delta}$ in the final state for elastic rescattering, while we see that in the present case one introduces the phase $e^{i2\delta}$ on top of $t_t^{(0)}$, which is itself complex from the structure of the R propagator. A detailed discussion of this issue can be found in Ref. [3.92].

It is also interesting to mention the effects of further rescattering beyond our triangle diagram. Final state interaction with three particles in the final state has been addressed repeatedly. One of the early works on this issue concerns rescattering in the $K \rightarrow 3\pi$ decay [3.117] (for a modern reformulation of this problem one can see the work of Ref. [3.118]). What is relevant for our problem is that further rescattering of particles 1, 2 in Fig. 3.25 is already accounted for by the $t_{12,12}$ scattering matrix that sums all the rescattering loops implicit in the Lippmann-Schwinger equation that generates $t_{12,12}$. However, after the mechanism of Fig. 3.25 one can have for instance, rescattering of particles 2 and 3 which would lead to a new loop with the former external 2 and 3 particles now being intermediate particles. Note that then particles 2 and 3 in the new loop could be off shell, in which case the triangle singularity of the $1R2$ triangle would be destroyed. Even if one concentrates on the contribution of 2 and 3 on shell in the loop, there is an angle integration for p_3 , and p_3 of the new loop and q would no longer be parallel in the whole range of the p_3 integration, which was a necessary condition for the triangle singularity. Hence, this new rescattering term would not have the triangle singularity structure and would be a smooth background term. Nevertheless, the modern techniques [3.118] allow to calculate such terms if precision is desired in a physical process. Yet, these issues go beyond the problem at hand, which is the investigation of the triangle mechanism, to which we come back.

3.4.3 Study of the singular behavior

Let us look at the behavior of t_L around the triangle singularity. For this it is easier to look at $t_t^{(0)}$ which has this same singularity. Let us look at Eq. (3.89). The integral there is $\frac{1}{2}I(q)g_A g_R$, with $I(q)$ from Eq. (3.108). Hence

$$t_t^{(0)} = \frac{g_A g_R}{4p_3 q} \ln \left(\frac{\tilde{E}_A - \omega_1(q) - \omega_R(p_3 - q) + i\epsilon}{\tilde{E}_A - \omega_1(q) - \omega_R(p_3 + q) + i\epsilon} \right) \tag{3.121}$$

and since for the q of the singularity (q positive from now on)

$$\tilde{E}_A - \omega_1(q) - \omega_R(p_3 - q) = 0 \tag{3.122}$$

then

$$\tilde{E}_A - \omega_1(q) = \omega_R(p_3 - q) \quad (3.123)$$

and we can write

$$\begin{aligned} t_t^{(0)} &= \frac{g_A g_R}{4p_3 q} \ln \left(\frac{i \Gamma_R / 2}{\omega_R(p_3 - q) - \omega_R(p_3 + q)} \right) \\ &\sim \frac{g_A g_R}{4p_3 q} \ln \left(\frac{\Gamma_R}{\omega_R(p_3 - q) - \omega_R(p_3 + q)} \right) \end{aligned} \quad (3.124)$$

where we have substituted $i\epsilon$ by $i\frac{\Gamma_R}{2}$ and kept the singular part when $\Gamma_R \rightarrow 0$. In the A decay width we shall have

$$\begin{aligned} \frac{d\Gamma_A^{(L)}}{dM_{\text{inv}}(12)} &\propto \int_{-1}^1 d\cos\theta \left| t_t^{(0)} \right|^2 \\ &\sim 2 \left(\frac{g_A g_R}{4p_3 q} \right)^2 \left| \ln \left(\frac{\Gamma_R}{\omega_R(p_3 - q) - \omega_R(p_3 + q)} \right) \right|^2. \end{aligned} \quad (3.125)$$

On the other hand, we can look at the whole t_t amplitude, and the equivalent part to Eq. (3.125) going into the evaluation of the A width is, using Eq. (3.88),

$$\begin{aligned} \frac{d\Gamma_A^{(t)}}{dM_{\text{inv}}(12)} &\propto \int_{-1}^1 d\cos\theta \frac{g_A^2 g_R^2}{4\omega_R^2(\vec{p}_3 - \vec{q})} \\ &\quad \times \left| \frac{1}{\tilde{E}_A - \omega_1(q) - \omega_R(\vec{p}_3 - \vec{q}) + i\frac{\Gamma_R}{2}} \right|^2. \end{aligned} \quad (3.126)$$

Performing the same change of variable to the variable x of Eq. (3.107) we obtain

$$\begin{aligned} \frac{d\Gamma_A^{(t)}}{dM_{\text{inv}}(12)} &\propto \frac{g_A^2 g_R^2}{4p_3 q} \int_{\omega_R(p_3 - q)}^{\omega_R(p_3 + q)} dx \frac{1}{x} \\ &\quad \times \frac{1}{\left(\tilde{E}_A - \omega_1(q) - x \right)^2 + \left(\frac{\Gamma_R}{2} \right)^2}. \end{aligned} \quad (3.127)$$

By making the change $\tilde{E}_A - \omega_1(q) - x = y$ and substituting $\frac{1}{x}$ by its value in the singularity, $\left[\tilde{E}_A - \omega_1(q) \right]^{-1}$, we get ⁴

$$\begin{aligned} \frac{d\Gamma_A^{(t)}}{dM_{\text{inv}}(12)} &\propto - \frac{1}{4p_3 q} \frac{g_A^2 g_R^2}{\tilde{E}_A - \omega_1(q)} \frac{2}{\Gamma_R} \\ &\quad \times \arctan \frac{2y}{\Gamma_R} \Bigg|_{\tilde{E}_A - \omega_1(q) - \omega_R(p_3 - q)}^{\tilde{E}_A - \omega_1(q) - \omega_R(p_3 + q)} \end{aligned} \quad (3.128)$$

⁴The integral can also be performed analytically, and the most singular term corresponds to the choice made.

where the lower limit in y vanishes. Hence, we get

$$\begin{aligned} \frac{d\Gamma_A^{(t)}}{dM_{\text{inv}}(12)} &\propto -\frac{1}{4p_3 q} \frac{g_A^2 g_R^2}{\tilde{E}_A - \omega_1(q)} \frac{2}{\Gamma_R} \\ &\times \left\{ \arctan \frac{2(\omega_R(p_3 - q) - \omega_R(p_3 + q))}{\Gamma_R} - \arctan \frac{0}{\Gamma_R} \right\} \end{aligned} \quad (3.129)$$

and since $\omega_R(p_3 - q) < \omega_R(p_3 + q)$

$$\lim_{\Gamma_R \rightarrow 0} \arctan \frac{2(\omega_R(p_3 - q) - \omega_R(p_3 + q))}{\Gamma_R} = -\frac{\pi}{2} \quad (3.130)$$

and we get

$$\frac{d\Gamma_A^{(t)}}{dM_{\text{inv}}(12)} \propto \frac{1}{4p_3 q} \frac{g_A^2 g_R^2}{\tilde{E}_A - \omega_1(q)} \frac{\pi}{\Gamma_R}. \quad (3.131)$$

It is interesting to see that when $\Gamma_R \rightarrow 0$, where the Schmid theorem holds, Γ_A from the tree level, Eq. (3.131), grows much faster than Γ_A from the triangle singularity from Eq. (3.125). This means, in a certain sense, that the Schmid theorem, even if true, becomes irrelevant, because in the limit where it holds, the contribution to the A width from the tree level is infinitely much larger than that from the triangle singularity.

Actually, Γ_A from Eqs. (3.125) and (3.131) do not diverge because g_R is related to the width. In fact, assuming $2 + 3$ the only decay channel of R , for the S -wave coupling that we are considering we have

$$\Gamma_R = \frac{1}{8\pi} \frac{g_R^2}{M_R^2} \bar{q} \quad (3.132)$$

with \bar{q} the on shell momentum of particle 2 or 3 in $R \rightarrow 2 + 3$ with R at rest. Then Γ_A from Eq. (3.131) goes to a constant, as it should be. If $2 + 3$ is not the only decay channel then

$$\frac{g_R^2}{8\pi} \frac{1}{M_R^2} \bar{q} = \text{BF}(2 + 3) \Gamma_R \quad (3.133)$$

where $\text{BF}(2+3)$ is the branching fraction of R to the $2+3$ channel, and the conclusion is the same. In fact, in the limit $\Gamma_R \rightarrow 0$, Γ_A calculated with the three body decay is exactly equal to Γ_A calculated from $A \rightarrow R + 1$ times the branching fraction $\text{BF}(2 + 3)$. This means that the contribution of the triangular singularity becomes negligibly small compared to the contribution of the whole tree level. However, if the width Γ_R is different from zero the ratio of contributions of the tree level to the triangle loop becomes finite, and many of the terms that we have been neglecting in the derivation of the Schmid theorem become relevant. Thus, one has to check numerically the contribution of the tree level and the triangle loop, summing them coherently, to see what comes out. This is particularly true when $t_{12,12}$ sits on top of a resonance where the triangle singularity could be very important, or even dominant.

Yet, it is still interesting to note that in the realistic case the reaction studied still has a memory of Schmid theorem, in the sense that the coherent sum of amplitudes gives rise to a width, or cross section, that is even smaller than the incoherent

sum of both contributions. One case where one can already check this is in the study of the $\gamma p \rightarrow \pi^0 \eta p$ reaction in Ref. [3.3], discussed in the former section 3.3. The γp couples to $\Delta(1700)$ which decays to $\eta \Delta(1232)$. The Δ decays into $\pi^0 p$ and ηp fuse to produce the $N^*(1535)$ that subsequently decays into ηp . The contribution of this mechanism is sizable and has been observed experimentally [3.4]. In the study of Ref. [3.3] one compares the loop contribution with the tree level from $\gamma p \rightarrow \Delta(1700) \rightarrow \eta \Delta(1232) \rightarrow \eta \pi^0 p$ and they are of the same order of magnitude. A remarkable feature is that the coherent sum of tree level and loop does not change much the contribution of the tree level, even if the loop contribution is sizable, and is smaller than the incoherent sum of both processes (see Fig. 1 of Ref. [3.3] or Fig. 3.18 in section 3.3). Yet, even then, the $N^*(1535)$ contribution to the $\gamma p \rightarrow \pi^0 \eta p$ gives a distinctive signature, both theoretically and experimentally. The message is clear: one must evaluate both the tree level and the loop contribution for each individual case to assert the relevance of the triangle singularity. Obviously, in the case that the final channel is different from the internal one of the loop there is no tree level contribution and then the triangle singularity shows up clearly.

3.4.4 Considerations on the Dalitz plot

In Fig. 3.30 we show the Dalitz plot for a typical $A \rightarrow 1+2+3$ process, where 1, 2, 3 are final states on shell. Recalling Eq. (3.82) that we reproduce again here

$$M_{\text{inv}}^2(23) = M_A^2 + m_1^2 - 2\tilde{E}_A \tilde{E}_1 + 2\tilde{p}_1 \tilde{p}_3 \cos \theta \quad (3.134)$$

and that $\tilde{E}_A, \tilde{E}_1, \tilde{p}_1, \tilde{p}_3$ all depend on $M_{\text{inv}}(12)$, by fixing $M_{\text{inv}}(12)$ Eq. (3.134) gives the limits of the Dalitz plot. For $\cos \theta = -1$ we have the lower limit and for $\cos \theta = 1$ we have the upper limit of the boundary of the Dalitz region. Let us cut the Dalitz boundary with a line of $M_{\text{inv}}(23) = M_R$. This line cuts the boundary in points A and D . In these points we have all final particles on shell and $M_{\text{inv}}(23) = M_R$. This is the situation of a triangle singularity provided that Eq. (3.101) is fulfilled (note that there are two solutions of q for $\cos \theta = 1$, but only one produces the triangle singularity, where in addition Eq. (3.101) is fulfilled). On the other hand, from point A to D , $M_{\text{inv}}(23) = M_R$ is allowed for some valid $\cos \theta$ and we should expect a singularity (up to the factor g_R^2) of the tree level mechanism. Let us study this in detail.

In Eq. (3.131) we already saw the contribution of t_t to the A width evaluating $\int_{-1}^1 d \cos \theta |t_t|^2$ at the point of the triangle singularity (point D in Fig. 3.30). Let us now evaluate it for an invariant mass $M_{\text{inv}}(12)$ between points A and D in the figure. Close to point A to the left we shall have now

$$\int_{-1}^1 d \cos \theta |t_t|^2 = -\frac{g_A^2 g_R^2}{4p_3 q} \frac{1}{\tilde{E}_A - \omega_1(q)} \frac{2}{\Gamma_R} \arctan \frac{2y}{\Gamma_R} \Bigg|_{y_2}^{y_1} \quad (3.135)$$

with $y_1 < 0$ and $y_2 > 0$, and hence

$$\lim_{\Gamma_R \rightarrow 0} \int_{-1}^1 d \cos \theta |t_t|^2 = -\frac{g_A^2 g_R^2}{4p_3 q} \frac{1}{\tilde{E}_A - \omega_1(q)} \frac{2}{\Gamma_R}$$

$$\times \left(-\frac{\pi}{2} - \frac{\pi}{2} \right) \quad (3.136)$$

which is twice the result of Eq. (3.131). This value stabilizes as we move from A to D , and the interesting thing is that it goes like $(\Gamma_R)^{-1}$ (apart from the factor g_R^2). In addition we can evaluate $\int_{-1}^1 d\cos\theta |t_t|^2$ for $M_{\text{inv}}(12)$ bigger than the one corresponding to point A . In this case R is never on shell and in the limit of small Γ_R we get zero contribution relative to the on shell one. Technically one would find it from Eq. (3.135) since now both y_1 and y_2 would be negative and the upper and lower limits of $\arctan \frac{2y}{\Gamma_R}$ cancel.

3.4.5 Results

We are going to perform calculations with a particular case with the following configuration:

$$\begin{aligned} M_A &= 2154 \text{ MeV} \\ M_R &= 1600 \text{ MeV}, \quad \Gamma_R = 30 \text{ MeV} \\ M_1 &= 500 \text{ MeV} \\ M_2 &= 200 \text{ MeV} \\ M_3 &= 900 \text{ MeV}. \end{aligned} \quad (3.137)$$

In addition we shall take an amplitude $1 + 2 \rightarrow 1 + 2$ parameterized in terms of a Breit-Wigner form

$$t_{12,12} = \frac{g^2}{M_{\text{inv}}^2(12) - M_{\text{BW}}^2 + i\Gamma_{\text{BW}}(M_{\text{inv}}(12))M_{\text{inv}}(12)} \quad (3.138)$$

with $M_{\text{BW}} = 800 \text{ MeV}$, $\Gamma_{\text{BW}} = 20 \text{ MeV}$. We shall use Eq. (3.94) and choose g^2 such that the width is given by Eq. (3.132). In this case we have purely elastic scattering and $g = 1338.7 \text{ MeV}$. We will also consider the case where we take the same value of g and a width double the elastic one to account for inelasticities, to test what happens in the case of inelastic channels.

We will use Eqs. (3.88) and (3.92) and integrate Eq. (3.86) over $M_{\text{inv}}(23)$ to obtain $d\Gamma_A/dM_{\text{inv}}(12)$. Note that according to Eq. (3.82) the integral over $\cos\theta$ that we have done is simply $2M_{\text{inv}}(23)dM_{\text{inv}}(23)/2\tilde{p}_1\tilde{p}_3$. The limits of integration are obtained from Eq. (3.82) for $\cos\theta = \pm 1$, and explicit formulas can be obtained from the PDG [3.14]. In Eq. (3.92) we have used a cutoff in the q integration of 600 MeV, a common value in many of these problems.

The choice of variables in Eqs. (3.137) and (3.138) is done such that Eq. (3.101) is satisfied and we have a triangle singularity for this configuration.

In Fig. 3.30 we show the Dalitz plot for the reaction $A \rightarrow 1 + 2 + 3$. We can indeed see that the triangle singularity point corresponds to point D of Fig. 3.30.

In the first place we evaluate $d\Gamma_A/dM_{\text{inv}}(12)$ for $M_A = 2200 \text{ MeV}$, about 50 MeV above the mass that leads to a triangle singularity at $M_{\text{inv}}(12) = 800 \text{ MeV}$. With

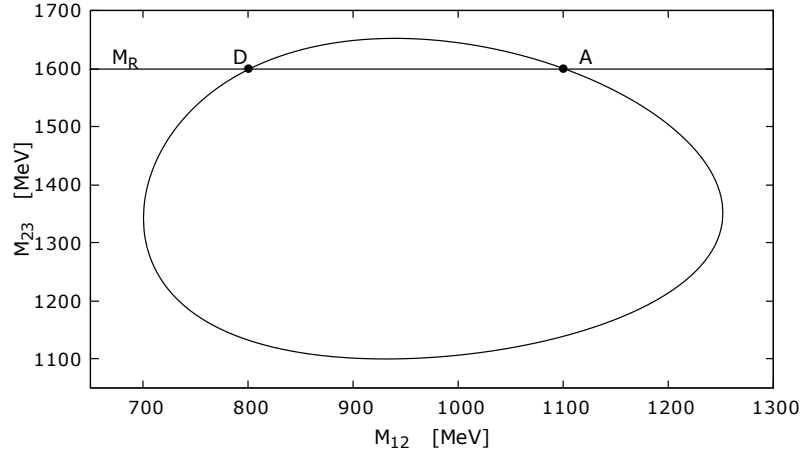


Figure 3.30: Dalitz plot for $A \rightarrow 1 + 2 + 3$ with the parameters of Eqs. (3.137) and (3.138). Point D corresponds to the triangle singularity.

this value of M_A , the triangle singularity appears at $M_{\text{inv}}(12) = 769$ MeV, about 30 MeV below the Breit-Wigner mass. We can expect that the loop function will give a small contribution, since $t_{12,12}$ at this invariant mass is significantly reduced compared to its peak. Yet, this serves us to investigate the points discussed in the former section.

In Fig. 3.31 we show $d\Gamma_A/dM_{\text{inv}}(12)/g_A^2 g_R^2$ as a function of $M_{\text{inv}}(12)$. We show the results for the triangle diagram alone, the tree level alone, and the coherent sum for $\Gamma_R = 30$ MeV. As we have discussed previously, we have proved the Schmid theorem in the limit of $\Gamma_R \rightarrow 0$. Fig. 3.31 gives us the answer of what happens when we look at a realistic case with Γ_R of the order of tens of MeV. As we can see, the triangle loop gives a sizable contribution of the order of the tree level, and the coherent sum of the triangle diagram and the tree level diagram gives rise to a very distinct structure, as a consequence of the resonance in the 1, 2 channel enhanced by the triangle diagram. This already tells us that in a realistic calculation we should not rely on the Schmid theorem to neglect the triangle diagram with elastic rescattering of the internal particles of the loop.

In Fig. 3.32 we show the same results but calculated with $\Gamma_R = 0.5$ MeV. As we can see, the triangle singularity gives a small contribution compared to the tree level, and the coherent sum of the two does not change the contribution of the tree level, as expected from the Schmid theorem. In Fig. 3.33 we show the same results but calculated with $\Gamma_R = 0.1$ MeV. Comparing these results with those of Fig. 3.32, we can see that as Γ_R is made smaller the tree level contribution grows more or less like $1/\Gamma_R$, as expected from Eq. (3.131), while the triangle contribution grows much less.

In Fig. 3.34 we show again the results for the same M_A mass and $\Gamma_R = 0.1$ MeV, but this time we take in Eq. (3.138) $\Gamma_{BW} \rightarrow 2\Gamma_{BW}$ to account for the inelasticities. The contribution of the triangle loop is reduced with respect to the one in the elastic case of Fig. 3.33. Curiously, the relative strength of the singularity (narrow peak in the dotted line) with respect to the resonance peak increases now, as a reminder that according to Eq. (3.120) the Schmid theorem does not hold. Yet, the main

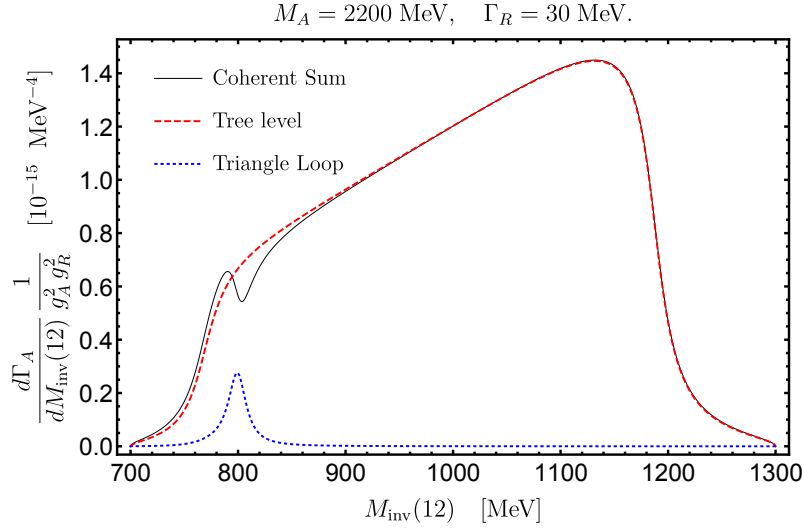


Figure 3.31: $\frac{d\Gamma_A}{dM_{\text{inv}}(12)} \frac{1}{g_A^2 g_R^2}$ as a function of $M_{\text{inv}}(12)$ with $M_A = 2200 \text{ MeV}$ and $\Gamma_R = 30 \text{ MeV}$.

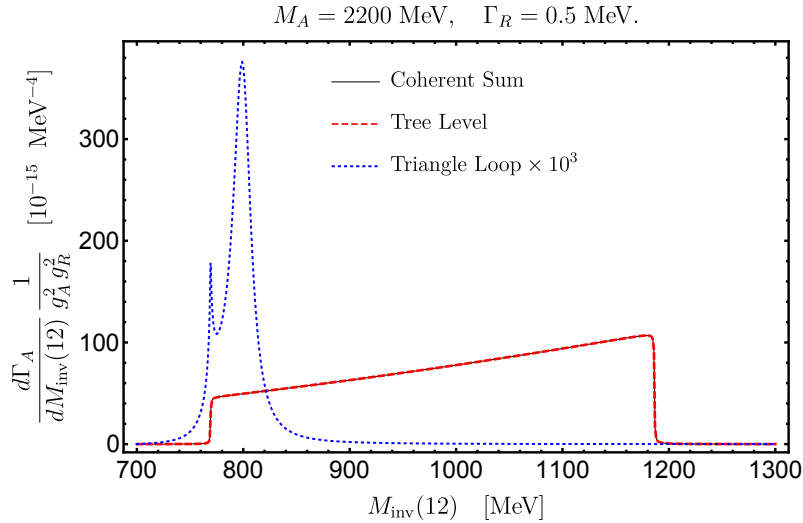


Figure 3.32: $\frac{d\Gamma_A}{dM_{\text{inv}}(12)} \frac{1}{g_A^2 g_R^2}$ as a function of $M_{\text{inv}}(12)$ with $M_A = 2200 \text{ MeV}$ and $\Gamma_R = 0.5 \text{ MeV}$. The dashed and solid lines are indistinguishable in the figure.

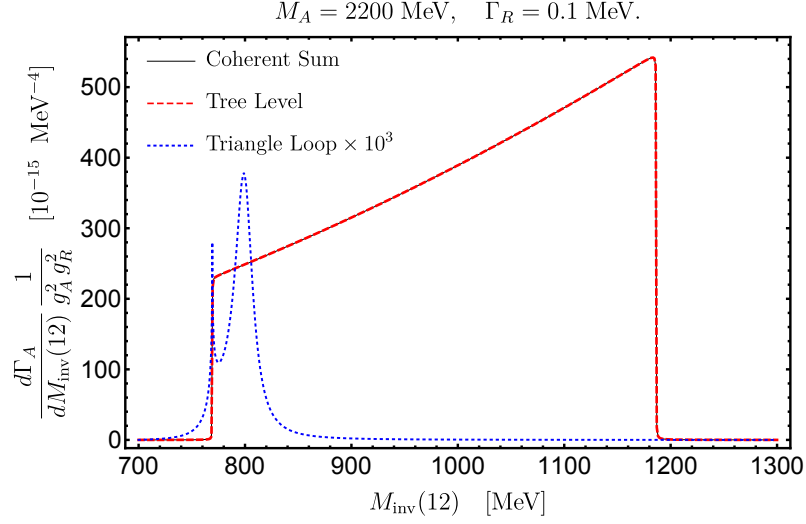


Figure 3.33: $\frac{d\Gamma_A}{dM_{\text{inv}}(12)} \frac{1}{g_A^2 g_R^2}$ as a function of $M_{\text{inv}}(12)$ with $M_A = 2200 \text{ MeV}$ and $\Gamma_R = 0.1 \text{ MeV}$. The dashed and solid lines are indistinguishable in the figure.

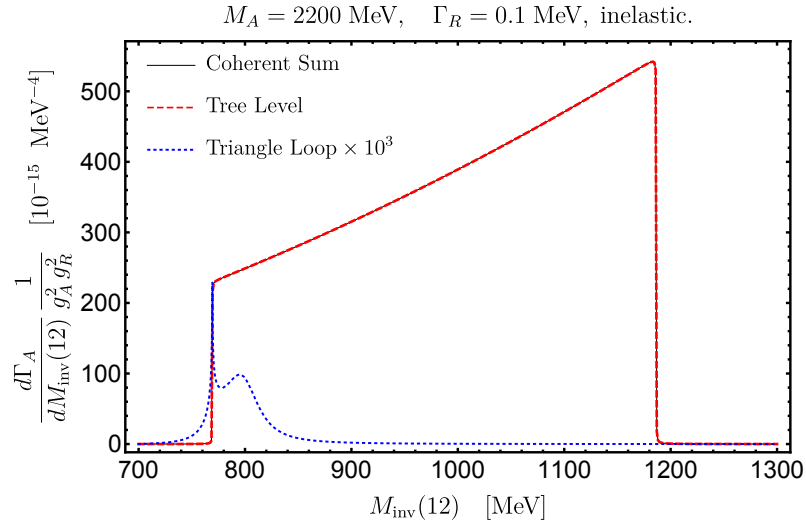


Figure 3.34: $\frac{d\Gamma_A}{dM_{\text{inv}}(12)} \frac{1}{g_A^2 g_R^2}$ as a function of $M_{\text{inv}}(12)$ with $M_A = 2200 \text{ MeV}$ and $\Gamma_R = 0.1 \text{ MeV}$. Here $\Gamma_{BW} \rightarrow 2\Gamma_{BW}$ to account for the inelasticities. The dashed and solid lines are indistinguishable in the figure.

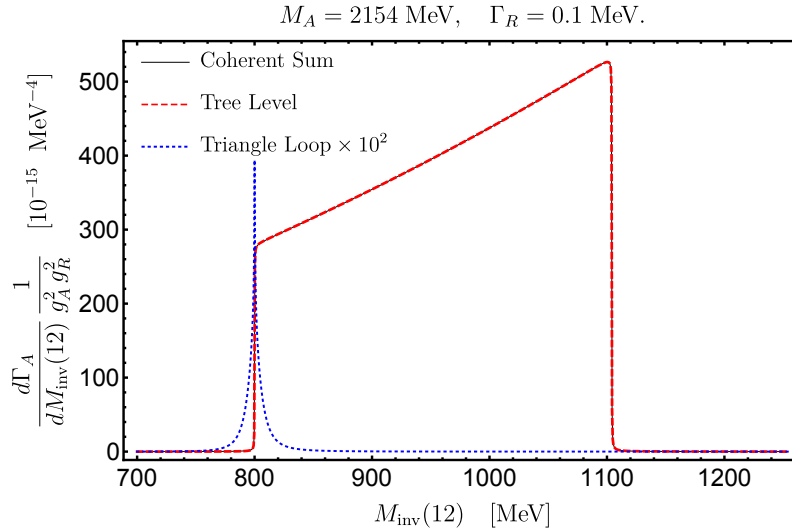


Figure 3.35: $\frac{d\Gamma_A}{dM_{\text{inv}}(12)} \frac{1}{g_A^2 g_R^2}$ as a function of $M_{\text{inv}}(12)$ with $M_A = 2154 \text{ MeV}$ and $\Gamma_R = 0.1 \text{ MeV}$. The dashed and solid lines are indistinguishable in the figure.

message from Figs. 3.32, 3.33 and 3.34 is that in the limit of $\Gamma_R \rightarrow 0$, where the Schmid theorem holds, the relative strength of the triangle diagram versus the tree level becomes negligible.

Next we perform the calculations for $M_A = 2154 \text{ MeV}$, first for $\Gamma_R = 0.1 \text{ MeV}$, and show the results in Fig. 3.35. The novelty in this case is that, since the triangle singularity occurs for $M_{\text{inv}}(12) = 800 \text{ MeV}$, equal to M_{BW} , now the contribution of the triangle mechanism is much bigger than in the former cases. Yet, relative to the tree level its strength is very small and in the coherent sum one does not appreciate its contribution, as was the case of Figs. 3.32 and 3.33, in agreement with the Schmid theorem. Actually this is a good case to show the effects of the Schmid theorem, since the strength of the peak is about 10^{-2} that of the tree level. This implies a factor 10^{-1} in the amplitude, and in an ordinary coherent sum of these two amplitudes one might expect a contribution of about 20% in the differential width, which is not the case in Fig. 3.35. Yet we should stress once more that the triangle mechanism becomes negligible on its own, independently of the Schmid theorem, when $\Gamma_R \rightarrow 0$.

In Fig. 3.36 we show the same results now for $\Gamma_R = 30 \text{ MeV}$. We can see now that the effect of the triangle singularity shows in $\frac{d\Gamma_A}{dM_{\text{inv}}(12)}$. However, it is interesting to see that the coherent sum of the tree level and the triangle singularity is smaller than their incoherent sum, indicating that, although one is in a region where the Schmid theorem does not strictly hold, the process still has some memory of the the absorption of the triangle mechanism by the tree level amplitude that occurs in the limit of small Γ_R . We should also note that if we make Γ_R bigger the relative strength of the loop contribution to the tree level grows and can become dominant at the invariant mass of the triangle singularity.

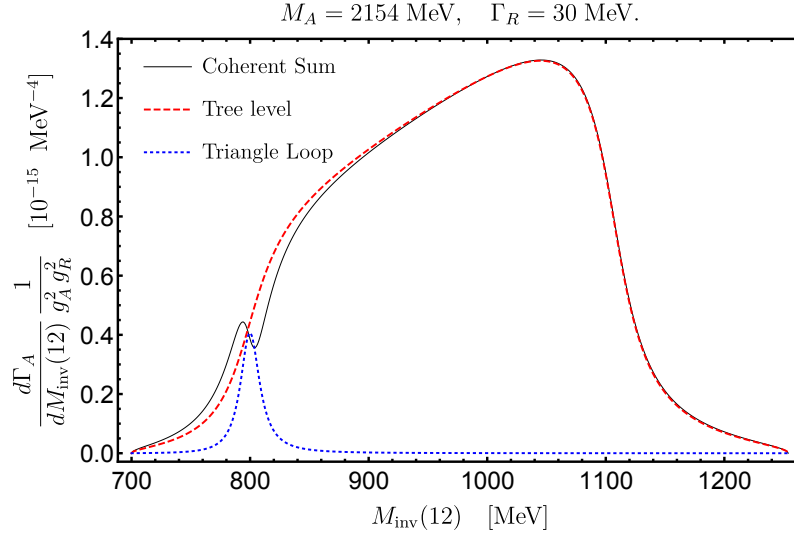


Figure 3.36: $\frac{d\Gamma_A}{dM_{\text{inv}}(12)} \frac{1}{g_A^2 g_R^2}$ as a function of $M_{\text{inv}}(12)$ with $M_A = 2154$ MeV and $\Gamma_R = 30$ MeV.

3.4.6 Conclusions

We have done a new derivation of the Schmid theorem and have studied the results as a function of Γ_R , the width of the intermediate state in the triangle loop that decays into an external particle and an internal one. The Schmid theorem holds strictly in the limit when $\Gamma_R \rightarrow 0$. We show this again and illustrate it with a numerical example.

The first thing that we find is that when $\Gamma_R \rightarrow 0$ the relative weight of the triangle singularity versus the tree level contribution goes to zero. This means that, in a strict sense, the Schmid theorem would be irrelevant because where it holds and shows that the singularity changes only the phase of the S -wave part of the tree level amplitude, $t_t^{(0)}$, the strength of the triangle diagram or of $t_t^{(0)}$ is very small compared with the whole contribution of the full tree level amplitude.

We conducted some tests to see what happens when we have Γ_R finite and also when the scattering amplitude of the two particles that interact in the loop sit on top of a resonance.

In general lines we see that for finite Γ_R widths the Schmid theorem does not strictly hold but the $A \rightarrow 1 + 2 + 3$ process still has some memory of the theorem in the sense that the coherent sum of tree level and triangle singularity gives rise to a differential width where the interference is much smaller than usual, with final results even smaller than the incoherent sum of the two mechanisms.

We also saw that in the case of a $1 + 2 \rightarrow 1 + 2$ scattering amplitude with inelasticities the Schmid theorem does not hold and we could quantify the contribution of the triangle singularity, both analytically and numerically in the example we discussed.

The biggest contribution of the triangle singularity appears when the $1+2 \rightarrow 1+2$ scattering amplitude sits on top of a resonance. In this case, and for finite Γ_R , the

contribution of the triangle singularity shows up clearly and can be even dominant over the tree level in some cases.

The message in general is that for each particular case one has to calculate both the tree level and the triangle mechanism and sum them coherently to see what comes out. Invoking the Schmid theorem to rule out the triangle mechanism in the case that the rescattering of particles 1,2 goes to the same channel should not be done.

Bibliography

- [3.1] V. R. Debastiani, F. Aceti, W. H. Liang and E. Oset, “*Revising the $f_1(1420)$ resonance,*” Phys. Rev. D **95**, 034015 (2017).
- [3.2] D. Barberis *et al.* [WA102 Collaboration], “*A Measurement of the branching fractions of the $f(1)(1285)$ and $f(1)(1420)$ produced in central $p p$ interactions at 450-GeV/c,*” Phys. Lett. B **440**, 225 (1998).
- [3.3] V. R. Debastiani, S. Sakai and E. Oset, “*Role of a triangle singularity in the $\pi N(1535)$ contribution to $\gamma p \rightarrow p\pi^0\eta$,*” Phys. Rev. C **96**, 025201 (2017).
- [3.4] E. Gutz *et al.* [CBELSA/TAPS Collaboration], “*High statistics study of the reaction $\gamma p \rightarrow p\pi^0\eta$,*” Eur. Phys. J. A **50**, 74 (2014).
- [3.5] V. R. Debastiani, S. Sakai and E. Oset, “*Considerations on the Schmid theorem for triangle singularities,*” Eur. Phys. J. C **79**, 69 (2019).
- [3.6] C. Schmid, “*Final-State Interactions and the Simulation of Resonances,*” Phys. Rev. **154**, 1363 (1967).
- [3.7] L. D. Landau, “*On analytic properties of vertex parts in quantum field theory,*” Nucl. Phys. **13**, 181 (1959).
- [3.8] S. Coleman and R. E. Norton, “*Singularities in the physical region,*” Nuovo Cim. **38**, 438 (1965).
- [3.9] M. Bayar, F. Aceti, F. K. Guo and E. Oset, “*A Discussion on Triangle Singularities in the $\Lambda_b \rightarrow J/\psi K^- p$ Reaction,*” Phys. Rev. D **94**, 074039 (2016).
- [3.10] F. K. Guo, U. G. Meißner, W. Wang and Z. Yang, “*How to reveal the exotic nature of the $P_c(4450)$,*” Phys. Rev. D **92**, 071502 (2015).
- [3.11] A. P. Szczepaniak, “*Triangle Singularities and XYZ Quarkonium Peaks,*” Phys. Lett. B **747**, 410 (2015).
- [3.12] X. H. Liu, M. Oka and Q. Zhao, “*Searching for observable effects induced by anomalous triangle singularities,*” Phys. Lett. B **753**, 297 (2016).
- [3.13] F. K. Guo, U. G. Meißner, J. Nieves and Z. Yang, “*Remarks on the P_c structures and triangle singularities,*” Eur. Phys. J. A **52**, 318 (2016).
- [3.14] C. Patrignani *et al.* [Particle Data Group Collaboration], “*Review of Particle Physics,*” Chin. Phys. C **40**, 100001 (2016).
- [3.15] T. A. Armstrong *et al.* [Athens-Bari-Birmingham-CERN Collaboration], “*Spin Parity Analysis of the E Meson Centrally Produced in the Reactions $\pi^+ p \rightarrow \pi^+ (K^0(L) K^+ K^-) p$ and $p p \rightarrow p (K^0(L) K^+ \pi^-) p$ at 85-GeV/c,*” Phys. Lett. **146B**, 273 (1984).

- [3.16] T. A. Armstrong *et al.* [WA76 Collaboration], “Further study of the $E/f_1(1420)$ meson in central production,” *Z. Phys. C* **56**, 29 (1992).
- [3.17] P. Achard *et al.* [L3 Collaboration], “Study of resonance formation in the mass region 1400-MeV to 1500-MeV through the reaction $\gamma\gamma \rightarrow K0(S) K^\pm \pi^\mp$,” *JHEP* **0703**, 018 (2007).
- [3.18] C. Amsler and A. Masoni, “The pseudoscalar and pseudovector mesons in the 1400 MeV region”, review of the PDG [3.14], page 915.
- [3.19] F. Aceti, J. J. Xie and E. Oset, “The $K\bar{K}\pi$ decay of the $f_1(1285)$ and its nature as a $K^*\bar{K} - cc$ molecule,” *Phys. Lett. B* **750**, 609 (2015).
- [3.20] F. Aceti, J. M. Dias and E. Oset, “ $f_1(1285)$ decays into $a_0(980)\pi^0$, $f_0(980)\pi^0$ and isospin breaking,” *Eur. Phys. J. A* **51**, 48 (2015).
- [3.21] M. F. M. Lutz and E. E. Kolomeitsev, “On meson resonances and chiral symmetry,” *Nucl. Phys. A* **730**, 392 (2004).
- [3.22] L. Roca, E. Oset and J. Singh, “Low lying axial-vector mesons as dynamically generated resonances,” *Phys. Rev. D* **72**, 014002 (2005).
- [3.23] M. C. Birse, “Effective chiral Lagrangians for spin 1 mesons,” *Z. Phys. A* **355**, 231 (1996).
- [3.24] Y. Zhou, X. L. Ren, H. X. Chen and L. S. Geng, “Pseudoscalar meson and vector meson interactions and dynamically generated axial-vector mesons,” *Phys. Rev. D* **90**, 014020 (2014).
- [3.25] M. Ablikim *et al.* [BESIII Collaboration], “Observation of the isospin-violating decay $J/\pi \rightarrow \phi\pi^0 f_0(980)$,” *Phys. Rev. D* **92**, 012007 (2015).
- [3.26] D. Barberis *et al.* [WA102 Collaboration], “A Study of the k anti- k π channel produced centrally in $p p$ interactions at 450-GeV/c,” *Phys. Lett. B* **413**, 225 (1997).
- [3.27] S. Godfrey and N. Isgur, “Mesons in a Relativized Quark Model with Chromodynamics,” *Phys. Rev. D* **32**, 189 (1985).
- [3.28] E. van Beveren, T. A. Rijken, K. Metzger, C. Dullemond, G. Rupp and J. E. Ribeiro, “A Low Lying Scalar Meson Nonet in a Unitarized Meson Model,” *Z. Phys. C* **30**, 615 (1986).
- [3.29] N. A. Tornqvist and M. Roos, “Resurrection of the sigma meson,” *Phys. Rev. Lett.* **76**, 1575 (1996).
- [3.30] A. H. Fariborz, R. Jora and J. Schechter, “Global aspects of the scalar meson puzzle,” *Phys. Rev. D* **79**, 074014 (2009).
- [3.31] A. H. Fariborz, N. W. Park, J. Schechter and M. Naeem Shahid, “Gauged linear sigma model and pion-pion scattering,” *Phys. Rev. D* **80**, 113001 (2009).

- [3.32] J. D. Weinstein and N. Isgur, “*K anti-K Molecules*,” Phys. Rev. D **41**, 2236 (1990).
- [3.33] J. A. Oller and E. Oset, “*Chiral symmetry amplitudes in the S wave isoscalar and isovector channels and the σ , $f_0(980)$, $a_0(980)$ scalar mesons*,” Nucl. Phys. A **620**, 438 (1997); Erratum: [Nucl. Phys. A **652**, 407 (1999)].
- [3.34] N. Kaiser, “ *$\pi\pi$ S wave phase shifts and nonperturbative chiral approach*,” Eur. Phys. J. A **3**, 307 (1998).
- [3.35] M. P. Locher, V. E. Markushin and H. Q. Zheng, “*Structure of $f_0(980)$ from a coupled channel analysis of S wave $\pi\pi$ scattering*,” Eur. Phys. J. C **4**, 317 (1998).
- [3.36] J. Nieves and E. Ruiz Arriola, “*Bethe-Salpeter approach for unitarized chiral perturbation theory*,” Nucl. Phys. A **679**, 57 (2000); “*Bethe-Salpeter approach for meson meson scattering in chiral perturbation theory*,” Phys. Lett. B **455**, 30 (1999).
- [3.37] R. L. Jaffe, “*Multi-Quark Hadrons. 1. The Phenomenology of (2 Quark 2 anti-Quark) Mesons*,” Phys. Rev. D **15**, 267 (1977).
- [3.38] E. Santopinto and G. Galata, “*Spectroscopy of tetraquark states*,” Phys. Rev. C **75**, 045206 (2007).
- [3.39] H. Nagahiro, K. Nawa, S. Ozaki, D. Jido and A. Hosaka, “*Composite and elementary natures of $a_1(1260)$ meson*,” Phys. Rev. D **83**, 111504 (2011).
- [3.40] H. Nagahiro, L. Roca, A. Hosaka and E. Oset, “*Hidden gauge formalism for the radiative decays of axial-vector mesons*,” Phys. Rev. D **79**, 014015 (2009).
- [3.41] L. Roca, J. E. Palomar and E. Oset, “*Decay of axial vector mesons into VP and P gamma*,” Phys. Rev. D **70**, 094006 (2004).
- [3.42] L. S. Geng, E. Oset, L. Roca and J. A. Oller, “*Clues for the existence of two $K(1)(1270)$ resonances*,” Phys. Rev. D **75**, 014017 (2007).
- [3.43] L. Roca, A. Hosaka and E. Oset, “*Quantum loops in radiative decays of the $a(1)$ and $b(1)$ axial-vector mesons*,” Phys. Lett. B **658**, 17 (2007).
- [3.44] M. Mikhasenko, B. Ketzer and A. Sarantsev, “*Nature of the $a_1(1420)$* ,” Phys. Rev. D **91**, 094015 (2015).
- [3.45] F. Aceti, L. R. Dai and E. Oset, “*The “ $a_1(1420)$ ” peak as the $\pi f_0(980)$ decay mode of the $a_1(1260)$* ,” Phys. Rev. D **94**, 096015 (2016).
- [3.46] C. Adolph *et al.* [COMPASS Collaboration], “*Observation of a New Narrow Axial-Vector Meson $a_1(1420)$* ,” Phys. Rev. Lett. **115**, 082001 (2015).
- [3.47] F. Mandl and G. Shaw, “*Quantum Field Theory*,” John Wiley and Sons, 2nd Ed. (2010).

- [3.48] W. H. Liang and E. Oset, “ B^0 and B_s^0 decays into $J/\psi f_0(980)$ and $J/\psi f_0(500)$ and the nature of the scalar resonances,” Phys. Lett. B **737**, 70 (2014).
- [3.49] J. J. Xie, L. R. Dai and E. Oset, “The low lying scalar resonances in the D^0 decays into K_s^0 and $f_0(500)$, $f_0(980)$, $a_0(980)$,” Phys. Lett. B **742**, 363 (2015).
- [3.50] J. J. Wu, X. H. Liu, Q. Zhao and B. S. Zou, “The Puzzle of anomalously large isospin violations in $\eta(1405/1475) \rightarrow 3\pi$,” Phys. Rev. Lett. **108**, 081803 (2012).
- [3.51] F. Aceti, W. H. Liang, E. Oset, J. J. Wu and B. S. Zou, “Isospin breaking and $f_0(980)$ - $a_0(980)$ mixing in the $\eta(1405) \rightarrow \pi^0 f_0(980)$ reaction,” Phys. Rev. D **86**, 114007 (2012).
- [3.52] X. G. Wu, J. J. Wu, Q. Zhao and B. S. Zou, “Understanding the property of $\eta(1405/1475)$ in the J/ψ radiative decay,” Phys. Rev. D **87**, 014023 (2013).
- [3.53] M. Ablikim *et al.* [BESIII Collaboration], “First observation of $\eta(1405)$ decays into $f_0(980)\pi^0$,” Phys. Rev. Lett. **108**, 182001 (2012).
- [3.54] M. Ablikim *et al.* [BESIII Collaboration], “Amplitude analysis of the $\chi_{c1} \rightarrow \eta\pi^+\pi^-$ decays,” Phys. Rev. D **95**, 032002 (2017).
- [3.55] W. H. Liang, J. J. Xie and E. Oset, “ $f_0(500)$, $f_0(980)$, and $a_0(980)$ production in the $\chi_{c1} \rightarrow \eta\pi^+\pi^-$ reaction,” Eur. Phys. J. C **76**, 700 (2016).
- [3.56] V. R. Debastiani, W. H. Liang, J. J. Xie and E. Oset, “Predictions for $\eta_c \rightarrow \eta\pi^+\pi^-$ producing $f_0(500)$, $f_0(980)$ and $a_0(980)$,” Phys. Lett. B **766**, 59 (2017).
- [3.57] T. Nakabayashi *et al.*, “Photoproduction of eta mesons off protons for $E_{\text{gamma}} \leq 1.15\text{-GeV}$,” Phys. Rev. C **74**, 035202 (2006).
- [3.58] D. Jido, M. Oka and A. Hosaka, “Chiral symmetry of baryons,” Prog. Theor. Phys. **106**, 873 (2001).
- [3.59] M. Doring, E. Oset and D. Strottman, “Chiral dynamics in the gamma $p \rightarrow \pi^0$ eta p and gamma $p \rightarrow \pi^0 K^0$ Sigma+ reactions,” Phys. Rev. C **73**, 045209 (2006).
- [3.60] J. Ajaka *et al.*, “Simultaneous photoproduction of eta and π^0 mesons on the proton,” Phys. Rev. Lett. **100**, 052003 (2008).
- [3.61] I. Horn *et al.* [CB-ELSA Collaboration], “Evidence for a Parity Doublet Delta (1920) P -33 and Delta (1940) D -33 from gamma $p \rightarrow p \pi^0$ eta,” Phys. Rev. Lett. **101**, 202002 (2008).
- [3.62] I. Horn *et al.* [CB-ELSA Collaboration], “Study of the reaction gamma $p \rightarrow p \pi^0$ eta,” Eur. Phys. J. A **38**, 173 (2008).
- [3.63] V. L. Kashevarov *et al.* [Crystal Ball at MAMI and TAPS and A2 Collaborations], “Photoproduction of π^0 eta on protons and the Delta(1700) $D(33)$ resonance,” Eur. Phys. J. A **42**, 141 (2009).

- [3.64] M. Doring, E. Oset and D. Strottman, “*Clues to the nature of the $\Delta^*(1700)$ resonance from pion- and photon-induced reactions,*” Phys. Lett. B **639**, 59 (2006).
- [3.65] M. Doring, E. Oset and U.-G. Meißner, “*Evaluation of the polarization observables I^S and I^C in the reaction $\gamma p \rightarrow \pi^0 \eta p$,*” Eur. Phys. J. A **46**, 315 (2010).
- [3.66] E. Gutz *et al.* [CBELSA Collaboration], “*Measurement of the beam asymmetry Σ in pi eta: Production off the proton with the CBELSA/TAPS experiment,*” Eur. Phys. J. A **35**, 291 (2008).
- [3.67] E. Gutz *et al.* [CBELSA and TAPS Collaborations], “*Photoproduction of meson pairs: First measurement of the polarization observable I^{**s} ,*” Phys. Lett. B **687**, 11 (2010).
- [3.68] E. E. Kolomeitsev and M. F. M. Lutz, “*On baryon resonances and chiral symmetry,*” Phys. Lett. B **585**, 243 (2004).
- [3.69] S. Sarkar, E. Oset and M. J. Vicente Vacas, “*Baryonic resonances from baryon decuplet-meson octet interaction,*” Nucl. Phys. A **750**, 294 (2005); Erratum: [Nucl. Phys. A **780**, 90 (2006)].
- [3.70] Q. Wang, C. Hanhart and Q. Zhao, “*Systematic study of the singularity mechanism in heavy quarkonium decays,*” Phys. Lett. B **725**, 106 (2013).
- [3.71] N. N. Achasov, A. A. Kozhevnikov and G. N. Shestakov, “*Isospin breaking decay $\eta(1405) \rightarrow f_0(980)\pi^0 \rightarrow 3\pi$,*” Phys. Rev. D **92**, 036003 (2015).
- [3.72] I. T. Lorenz, H. W. Hammer and U. G. Meißner, “*New structures in the proton-antiproton system,*” Phys. Rev. D **92**, 034018 (2015).
- [3.73] A. P. Szczepaniak, “*Dalitz plot distributions in presence of triangle singularities,*” Phys. Lett. B **757**, 61 (2016).
- [3.74] J. J. Xie, L. S. Geng and E. Oset, “ *$f_2(1810)$ as a triangle singularity,*” Phys. Rev. D **95**, 034004 (2017).
- [3.75] E. Wang, J. J. Xie, W. H. Liang, F. K. Guo and E. Oset, “*The role of a triangle singularity in the $\gamma p \rightarrow K^+ \Lambda(1405)$ reaction,*” Phys. Rev. C **95**, 015205 (2017).
- [3.76] K. Moriya *et al.* [CLAS Collaboration], “*Differential Photoproduction Cross Sections of the $\Sigma^0(1385)$, $\Lambda(1405)$, and $\Lambda(1520)$,*” Phys. Rev. C **88**, 045201 (2013); Addendum: [Phys. Rev. C **88**, 049902 (2013)].
- [3.77] R. Aaij *et al.* [LHCb Collaboration], “*Observation of $J/\psi p$ Resonances Consistent with Pentaquark States in $\Lambda_b^0 \rightarrow J/\psi K^- p$ Decays,*” Phys. Rev. Lett. **115**, 072001 (2015).
- [3.78] R. Aaij *et al.* [LHCb Collaboration], “*Study of the production of Λ_b^0 and \bar{B}^0 hadrons in pp collisions and first measurement of the $\Lambda_b^0 \rightarrow J/\psi K^-$ branching fraction,*” Chin. Phys. C **40**, 011001 (2016).

- [3.79] B. X. Sun, E. J. Garzon and E. Oset, “Radiative decay into gamma-baryon of dynamically generated resonances from the vector-baryon interaction,” Phys. Rev. D **82**, 034028 (2010).
- [3.80] T. Inoue, E. Oset and M. J. Vicente Vacas, “Chiral unitary approach to S wave meson baryon scattering in the strangeness $S = 0$ sector,” Phys. Rev. C **65**, 035204 (2002).
- [3.81] D. Gamermann, J. Nieves, E. Oset and E. Ruiz Arriola, “Couplings in coupled channels versus wave functions: application to the $X(3872)$ resonance,” Phys. Rev. D **81**, 014029 (2010).
- [3.82] J. Z. Bai *et al.* [BES Collaboration], “Study of N^* production from $J / \Psi \rightarrow p \text{ anti-}p \text{ eta}$,” Phys. Lett. B **510**, 75 (2001).
- [3.83] V. Sokhoyan *et al.* [CBELSA/TAPS Collaboration], “High-statistics study of the reaction $\gamma p \rightarrow p 2\pi^0$,” Eur. Phys. J. A **51**, 95 (2015); Erratum: [Eur. Phys. J. A **51**, 187 (2015)].
- [3.84] R. Karplus, C. M. Sommerfield and E. H. Wichmann, “Spectral Representations in Perturbation Theory. 1. Vertex Function,” Phys. Rev. **111**, 1187 (1958).
- [3.85] R. F. Peierls, “Possible Mechanism for the Pion-Nucleon Second Resonance,” Phys. Rev. Lett. **6**, 641 (1961).
- [3.86] I. J. R. Aitchison, “Logarithmic Singularities in Processes with Two Final-State Interactions,” Phys. Rev. **133**, B1257 (1964).
- [3.87] Y. F. Chang and S. F. Tuan, “Possible Experimental Consequences of Triangle Singularities in Strange-Particle Production Processes,” Phys. Rev. **136**, B741 (1964).
- [3.88] J. B. Bronzan, “Overlapping Resonances in Dispersion Theory,” Phys. Rev. **134**, B687 (1964).
- [3.89] N. E. Booth, A. Abashian and K. M. Crowe, “Anomaly in Meson Production in $p+d$ Collisions,” Phys. Rev. Lett. **7**, 35 (1961).
- [3.90] V. V. Anisovich and L. G. Dakhno, “Logarithmic singularities in the reactions $\pi^- + p \rightarrow n + \pi^- + \pi^+$ and $p + d \rightarrow \text{He}_3 + 2\pi$,” Phys. Lett. **10**, 221 (1964).
- [3.91] A. V. Anisovich and V. V. Anisovich, “Rescattering effects in three particle states and the Schmid theorem,” Phys. Lett. B **345**, 321 (1995).
- [3.92] I. J. R. Aitchison and C. Kacser, “Watson’s theorem when there are three strongly interacting particles in the final state,” Phys. Rev. **173**, 1700 (1968).
- [3.93] I. J. R. Aitchison and C. Kacser, “Final-State Interactions among Three Particles. 2. Explicit Evaluation of the First Rescattering Correction,” Phys. Rev. **142**, 1104 (1966).

- [3.94] N. N. Achasov, A. A. Kozhevnikov and G. N. Shestakov, “*Isospin breaking decay $\eta(1405) \rightarrow f_0(980)\pi^0 \rightarrow 3\pi$* ,” Phys. Rev. D **92**, 036003 (2015).
- [3.95] N. N. Achasov and G. N. Shestakov, “*Isotopic Symmetry Breaking in the $\eta(1405) \rightarrow f_0(980)\pi^0 \rightarrow \pi^+\pi^-\pi^0$. Decay through a $K\bar{K}$ Loop Diagram and the Role of Anomalous Landau Thresholds*,” JETP Lett. **107**, 276 (2018); [Pisma Zh. Eksp. Teor. Fiz. **107**, 292 (2018)].
- [3.96] F. Aceti, L. R. Dai and E. Oset, “ *$a_1(1420)$ peak as the $\pi f_0(980)$ decay mode of the $a_1(1260)$* ,” Phys. Rev. D **94**, 096015 (2016).
- [3.97] R. Aaij *et al.* [LHCb Collaboration], “*Observation of $J/\psi p$ Resonances Consistent with Pentaquark States in $\Lambda_b^0 \rightarrow J/\psi K^- p$ Decays*,” Phys. Rev. Lett. **115**, 072001 (2015).
- [3.98] E. Wang, J. J. Xie, W. H. Liang, F. K. Guo and E. Oset, “*Role of a triangle singularity in the $\gamma p \rightarrow K^+\Lambda(1405)$ reaction*,” Phys. Rev. C **95**, 015205 (2017).
- [3.99] J. J. Xie, L. S. Geng and E. Oset, “ *$f_2(1810)$ as a triangle singularity*,” Phys. Rev. D **95**, 034004 (2017).
- [3.100] L. Roca and E. Oset, “*Role of a triangle singularity in the $\pi\Delta$ decay of the $N(1700)(3/2^-)$* ,” Phys. Rev. C **95**, 065211 (2017).
- [3.101] D. Samart, W. H. Liang and E. Oset, “*Triangle mechanisms in the build up and decay of the $N^*(1875)$* ,” Phys. Rev. C **96**, 035202 (2017).
- [3.102] S. Sakai, E. Oset and A. Ramos, “*Triangle singularities in $B^- \rightarrow K^-\pi^-D_{s0}^+$ and $B^- \rightarrow K^-\pi^-D_{s1}^+$* ,” Eur. Phys. J. A **54**, 10 (2018).
- [3.103] R. Pavao, S. Sakai and E. Oset, “*Triangle singularities in $B^- \rightarrow D^{*0}\pi^-\pi^0\eta$ and $B^- \rightarrow D^{*0}\pi^-\pi^+\pi^-$* ,” Eur. Phys. J. C **77**, 599 (2017).
- [3.104] S. Sakai, E. Oset and W. H. Liang, “*Abnormal isospin violation and $a_0 - f_0$ mixing in the $D_s^+ \rightarrow \pi^+\pi^0 a_0(980)(f_0(980))$ reactions*,” Phys. Rev. D **96**, 074025 (2017).
- [3.105] M. Bayar, R. Pavao, S. Sakai and E. Oset, “*Role of the triangle singularity in $\Lambda(1405)$ production in the $\pi^- p \rightarrow K^0\pi\Sigma$ and $pp \rightarrow pK^+\pi\Sigma$ processes*,” Phys. Rev. C **97**, 035203 (2018).
- [3.106] W. H. Liang, S. Sakai, J. J. Xie and E. Oset, “*Triangle singularity enhancing isospin violation in $\bar{B}_s^0 \rightarrow J/\psi\pi^0 f_0(980)$* ,” Chin. Phys. C **42**, 044101 (2018).
- [3.107] E. Oset and L. Roca, “*Triangle singularity in $\tau \rightarrow f_1(1285)\pi\nu_\tau$ decay*,” Phys. Lett. B **782**, 332 (2018).
- [3.108] L. R. Dai, R. Pavao, S. Sakai and E. Oset, “*Anomalous enhancement of the isospin-violating $\Lambda(1405)$ production by a triangle singularity in $\Lambda_c \rightarrow \pi^+\pi^0\pi^0\Sigma^0$* ,” Phys. Rev. D **97**, 116004 (2018).

- [3.109] S. R. Xue, H. J. Jing, F. K. Guo and Q. Zhao, “Disentangling the role of the $Y(4260)$ in $e^+e^- \rightarrow D^*\bar{D}^*$ and $D_s^*\bar{D}_s^*$ via line shape studies,” Phys. Lett. B **779**, 402 (2018).
- [3.110] J. J. Xie and F. K. Guo, “Triangular singularity and a possible ϕp resonance in the $\Lambda_c^+ \rightarrow \pi^0 \phi p$ decay,” Phys. Lett. B **774**, 108 (2017).
- [3.111] Z. Cao and Q. Zhao, “The impact of S -wave thresholds $D_{s1}\bar{D}_s + c.c.$ and $D_{s0}\bar{D}_s^* + c.c.$ on vector charmonium spectrum,” Phys. Rev. D **99**, 014016 (2019).
- [3.112] W. Qin, Q. Zhao and X. H. Zhong, “Revisiting the pseudoscalar meson and glueball mixing and key issues in the search for a pseudoscalar glueball state,” Phys. Rev. D **97**, 096002 (2018).
- [3.113] Z. Yang, Q. Wang and U. G. Meißner, “Where does the $X(5568)$ structure come from?,” Phys. Lett. B **767**, 470 (2017).
- [3.114] X. H. Liu and U. G. Meißner, “Generating a resonance-like structure in the reaction $B_c \rightarrow B_s \pi \pi$,” Eur. Phys. J. C **77**, 816 (2017).
- [3.115] F. K. Guo, C. Hanhart, U. G. Meißner, Q. Wang, Q. Zhao and B. S. Zou, “Hadronic molecules,” Rev. Mod. Phys. **90**, 015004 (2018).
- [3.116] K. M. Watson, “The Effect of final state interactions on reaction cross-sections,” Phys. Rev. **88** (1952) 1163.
- [3.117] N. N. Khuri and S. B. Treiman, “Pion-Pion Scattering and $K^\pm \rightarrow 3\pi$ Decay,” Phys. Rev. **119** (1960) 1115.
- [3.118] G. Colangelo, J. Gasser, B. Kubis and A. Rusetsky, “Cusps in $K \rightarrow 3\pi$ decays,” Phys. Lett. B **638** (2006) 187.

Throughout this thesis we saw three main branches of hadron interactions: meson-meson and meson-baryon molecules in chapters one and two, respectively, and triangle singularities in chapter three. Each chapter was based in a selection of published articles sharing a similar framework. Let us go through the main ideas of each work.

In chapter one we first saw how to use elements of $SU(3)$ symmetry to see the weight of different trios of pseudoscalars produced in the charmonium decay $c\bar{c} \rightarrow 123$. The pseudoscalars then would go through final state interaction of pairs of mesons generating the scalar mesons $f_0(500)$, $f_0(980)$ and $a_0(980)$, for which we used the chiral unitary approach.

In our first work we performed calculations for the $\eta_c \rightarrow \eta\pi^+\pi^-$ decay using this approach. After finding the trios of pseudoscalars using $SU(3)$ symmetry, the interaction of pairs of mesons lead to $\eta\pi^+\pi^-$ in the final state. We have evaluated the $\pi^+\pi^-$ and $\pi\eta$ mass distributions and found large and clear signals for $f_0(500)$, $f_0(980)$ and $a_0(980)$ excitation. This reaction is similar to the $\chi_{c1} \rightarrow \eta\pi^+\pi^-$, which has been recently measured at BESIII and its implementation and comparison with our predictions will be very valuable to shed light on the nature of the low mass scalar mesons.

We also used this approach to study the isospin breaking in the reactions $\chi_{c1} \rightarrow \pi^0\pi^+\pi^-$ and $\chi_{c1} \rightarrow \pi^0\pi^0\eta$ and its relation to the $a_0(980) - f_0(980)$ mixing, which was also measured by the BESIII Collaboration, before and after our work. We have shown that the same theoretical model previously developed to study the $\chi_{c1} \rightarrow \eta\pi^+\pi^-$ reaction, and further explored in the predictions to the $\eta_c \rightarrow \eta\pi^+\pi^-$, could be successfully employed in this study. The isospin violation was introduced through the use of different masses for the charged and neutral kaons, either in the propagators of pairs of mesons created in the χ_{c1} decay, or in the propagators inside the T matrix, constructed through the unitarization of the scattering and transition amplitudes of pairs of pseudoscalar mesons. We have found that violating isospin inside the T matrix makes the $\pi^0\eta \rightarrow \pi^+\pi^-$ amplitude nonzero, which gives an important contribution and also enhances the effect of the $K\bar{K}$ term. We also find that the most important effect in the total amplitude is the isospin breaking inside the T matrix, due to the constructive sum of $\pi^0\eta \rightarrow \pi^+\pi^-$ and $K\bar{K} \rightarrow \pi^+\pi^-$, which is essential to get a good agreement with the experimental measurement of the mixing.

Both of our works, the one about the $\eta_c \rightarrow \eta\pi^+\pi^-$ and the one about the $a_0(980) - f_0(980)$ mixing, were cited in the BESIII articles and in other related subsequent works.

In chapter two we saw a method to study meson-baryon interactions and look for new states as poles in the scattering amplitude. In particular, we saw how we can extend the local hidden gauge approach to the heavy quark sector, singling out the heavy quark and assuming $SU(3)$ symmetry in the interaction. We have shown that the dominant terms come from the exchange of light vectors, where the heavy quarks are spectators. This has as a consequence that heavy quark symmetry is preserved for the dominant terms in the $(1/m_Q)$ counting, and also that the interaction in this case can be obtained from the $SU(3)$ chiral Lagrangians.

In the first work on this topic we have investigated Ω_c states, that are dynamically generated from the meson-baryon interaction. We show that for a standard value for the cutoff regulating the loop, we obtain two states with $J^P = 1/2^-$ and two more with $J^P = 3/2^-$, three of them in remarkable agreement with three experimental states, $\Omega_c(3050)$, $\Omega_c(3090)$ and $\Omega_c(3119)$ from the five recently measured by the LHCb collaboration, in mass and width. We also made predictions at higher energies for states of vector-baryon nature, which could be further explored in experiments in the future.

Next, we have studied the weak decay $\Omega_b^- \rightarrow (\Xi_c^+ K^-)\pi^-$, using our approach to describe the Ω_c states. We looked into the particular case where the $\Omega_c(3050)$ and $\Omega_c(3090)$ can be generated from the pseudoscalar-baryon(1/2) interaction. We investigated the ΞD , $\Xi_c \bar{K}$ and $\Xi'_c \bar{K}$ invariant mass distributions making predictions that could be confronted with future experiments, providing useful information that could help determine the quantum numbers and nature of these states.

Finally, we have extended our approach on the Ω_c states and made predictions for the interaction of meson-baryon in the beauty sector, searching for poles in the scattering matrix that correspond to physical states. We have found several Ω_b states: two states with masses 6405 MeV and 6465 MeV for $J^P = \frac{1}{2}^-$; two more states with masses 6427 MeV and 6665 MeV for $\frac{3}{2}^-$; and three states between 6500 and 6820 MeV, degenerate with $J^P = \frac{1}{2}^-, \frac{3}{2}^-$, stemming from the interaction of vector-baryon in the beauty sector, analogous to what we had for the Ω_c states. Future experiment could also search for these states.

Our work on the Ω_c states received many citations, and the predictions about the Ω_b states has also being noted in the report of the LHC for future prospects on the next run after the undergoing upgrade.

In chapter three we showed how triangular singularities can be formed in the decay $A \rightarrow 1 + R$, with subsequent $R \rightarrow 2 + 3$ and rescattering $1 + 2 \rightarrow 1' + 2'$. We showed our approach explicitly doing the loop integral to find the amplitude, and how, studying its poles, we find the conditions for and the position of the singularity. We have seen that specially in the case when there is a resonance from the $(1, 2)$ rescattering at the same energy corresponding to the triangle singularity, its effect can be seen in experiment and even be misunderstood by a new state.

On this topic, we first studied the production and decay of the $f_1(1285)$ into $\pi a_0(980)$ and $K^* \bar{K}$ as a function of the mass of the resonance and found a shoulder around 1400 MeV, tied to a triangle singularity, for the $\pi a_0(980)$ mode, and a

peak around 1420 MeV with about 60 MeV width for the $K^*\bar{K}$ mode. Both these features agree with the experimental information on which the $f_1(1420)$ resonance is based. In addition, we find that if the $f_1(1420)$ is a genuine resonance, coupling mostly to $K^*\bar{K}$ as seen experimentally, one finds unavoidably about a 20% fraction for $\pi a_0(980)$ decay of this resonance, in drastic contradiction with all experiments. Altogether, we have concluded that the $f_1(1420)$ is not a genuine resonance, but the manifestation of the $\pi a_0(980)$ and $K^*\bar{K}$ decay modes of the $f_1(1285)$ at higher energies than the nominal one.

Next, we have studied the $\gamma p \rightarrow p\pi^0\eta$ reaction paying attention to the two main mechanisms at low energies, the $\gamma p \rightarrow \Delta(1700) \rightarrow \eta\Delta(1232)$ and the $\gamma p \rightarrow \Delta(1700) \rightarrow \pi N(1535)$. Both of them are driven by the photoexcitation of the $\Delta(1700)$ and the second one involves a mechanism that leads to a triangle singularity. We are able to evaluate quantitatively the cross section for this process and show that it agrees with the experimental determination. Yet, there are some differences with the standard partial wave analysis which does not include explicitly the triangle singularity. The exercise also shows the convenience to explore possible triangle singularities in other reactions and how a standard partial analysis can be extended to accommodate them.

Finally, we have investigated the Schmid theorem, which states that the possible triangle singularity in a three particle decay developed by the mechanism of elastic rescattering of two of the particles does not change the cross section provided by the tree level. We have investigated the process in terms of the width of the unstable particle produced in the first decay and determined the limits of validity and violation of the theorem. One of the conclusions is that the theorem holds in the strict limit of zero width of that resonance, in which case the strength of the triangle diagram becomes negligible compared to the tree level. Another conclusion, on the practical side, is that for realistic values of the width, the triangle singularity can provide a strength comparable or even bigger than the tree level, which indicates that invoking the Schmid theorem to neglect the triangle diagram stemming from elastic rescattering of the tree level should not be done. Even then, we observe that the realistic case keeps some memory of the Schmid theorem, which is visible in a peculiar interference pattern with the tree level.

Overall, we have seen many examples of the dynamical nature of states emerging from the hadron-hadron interaction, either in the case of the light scalar mesons emerging from meson-meson interactions, or new heavy baryon states from the meson-baryon interaction, or even cases where peaks can be misunderstood as genuine states due to the effects of triangle singularities. In the big picture we have shown, through a series of examples and applications, the importance of the dynamically generated states, and how this description should be part of our understanding of the fundamental interactions of matter.

